CIVIL ENGINEERING STUDIES
Illinois Center for Transportation Series No. 18-014
UILU-ENG-2018-2014
ISSN: 0197-9191

SEISMIC PERFORMANCE OF INTEGRAL ABUTMENT HIGHWAY BRIDGES IN ILLINOIS

Prepared By
James M. LaFave
Larry A. Fahnestock
Derek L. Kozak

University of Illinois at Urbana-Champaign

Research Report No. FHWA-ICT-18-012

A report of the findings of

ICT PROJECT R27-133
Calibration and Refinement of Illinois' Earthquake Resisting System Bridge Design Methodology: Phase II

Illinois Center for Transportation

August 2018

TECHNICAL REPORT DOCUMENTATION PAGE

1. Report No.	2. Government Accession No.	3. Recipient's Catalog No.
FHWA-ICT-18-012	N/A	N/A

4. Title and Subtitle	5. Report Date
Seismic Performance of Integral Abutment Highway Bridges in Illinois	August 2018
	6. Performing Organization Code N/A

7. Author(s)	8. Performing Organization Report No.
James M. LaFave, Larry A. Fahnestock, and Derek L. Kozak	ICT-18-014 UILU-ENG-2018-2014

9. Performing Organization Name and Address	10. Work Unit No.
Illinois Center for Transportation Department of Civil and Environmental Engineering University of Illinois at Urbana-Champaign 205 North Mathews Avenue, MC-250 Urbana, IL 61801	N/A **11. Contract or Grant No.** R27-133

12. Sponsoring Agency Name and Address	13. Type of Report and Period Covered
Illinois Department of Transportation (SPR) Bureau of Research 126 East Ash Street Springfield, IL 62704	Final Report 10/1/2013 – 8/31/2018 **14. Sponsoring Agency Code** FHWA

15. Supplementary Notes

Conducted in cooperation with the U.S. Department of Transportation, Federal Highway Administration.

16. Abstract

The seismic behavior of integral abutment bridges (IABs) is of particular interest in southern Illinois, where proximity to the New Madrid Seismic Zone may create significant ground motion accelerations during an earthquake. IABs are common in modern bridge construction due to their lack of expansion joints between the superstructure and abutment, which leads to decreased environmental damage at the abutment seat when compared to stub abutment bridges. However, elimination of expansion joints can also lead to development of complex soil-structure-interaction limit states at the abutment and its foundation when an IAB is subjected to lateral loads. This report examines the seismic behavior of typical IABs in southern Illinois and develops feedback and recommendations for improving IAB seismic designs. This is accomplished through modeling IABs as a whole bridge system, subjecting the models to representative ground motions, monitoring the behavior of key IAB components, using the monitored results to form a comprehensive view of seismic behavior, and employing the developed knowledge to form recommendations for improving IAB seismic performance. IAB models are developed in OpenSees through nonlinear modeling of multiple components, as well as the connections between components, representing typical IAB designs for Illinois, and are then subjected to 1000-year return period hazard ground motions developed specifically for southern Illinois. Incremental dynamic analyses are also performed. IABs of varying superstructure materials, span configurations, bearing layouts, pier heights, and foundation soil conditions are dynamically analyzed using the sets of developed ground motions. Damage to pier columns is especially prominent in IABs with shorter piers and longer abutment-to-abutment spans, while abutment foundation damage in terms of yielding, local buckling, and rupture of the piles frequently occurs in many IAB variants. Recommendations on design modifications to improve the seismic behavior of IABs by limiting the level of damage to these components are also investigated through modifying elastomeric bearing side retainer strength, fixed bearing strength, pier column size, and backfill contributions.

17. Key Words	18. Distribution Statement
Jointless bridges; abutment pile foundations; multi-column piers; soil structure interaction; earthquake engineering; bridge bearings; quasi-isolation.	No restrictions. This document is available through the National Technical Information Service, Springfield, VA 22161.

19. Security Classif. (of this report)	20. Security Classif. (of this page)	21. No. of Pages	22. Price
Unclassified	Unclassified	85 pp + appendices	N/A

Form DOT F 1700.7 (8-72) **Reproduction of completed page authorized**

ACKNOWLEDGMENT, DISCLAIMER, MANUFACTURERS' NAMES

This publication is based on the results of **ICT-R27-133, Calibration and Refinement of Illinois' Earthquake Resisting System Bridge Design Methodology: Phase II**. ICT-R27-133 was conducted in cooperation with the Illinois Center for Transportation (ICT); the Illinois Department of Transportation (IDOT); and the U.S. Department of Transportation, Federal Highway Administration (FHWA).

Members of the Technical Review panel were the following:

- Mark Shaffer, TRP Chair, IDOT
- Nick Barnett, IDOT
- Justin Belue, IDOT
- Dan Brydl, FHWA
- John Ciccone, IDOT
- Patrik Claussen, IDOT
- Chad Hodel, WHKS
- William Kramer, IDOT
- Carl Puzey, IDOT
- Kevin Riechers, IDOT
- Jayme Schiff, IDOT
- Dan Tobias, IDOT

EXECUTIVE SUMMARY

The increased use of integral abutment bridges (IABs) throughout the United States has led to numerous studies concerning their behavior when subjected to a variety of loads. The seismic behavior of IABs is of particular interest to regions such as southern Illinois, where proximity to the New Madrid Seismic Zone may create significant ground motion accelerations during an earthquake. IABs are common in modern bridge design and construction due to their lack of expansion joints between the superstructure and abutment, which leads to decreased damage at the abutment seat when compared to stub abutment bridges because water, soil, and deicing chemicals are unable to penetrate through a compromised expansion joint in an IAB. However, elimination of expansion joints in IABs can also lead to the development of complex soil-structure-interaction limit states at the abutment and its foundation when an IAB is subjected to lateral loads. Despite this distinct behavior in IABs when subjected to lateral loading, such as seismic loads, there is a lack of comprehensive system-level studies investigating the behavior of IABs subjected to earthquakes.

This report aims to determine the seismic behavior of typical IAB designs in southern Illinois and to develop feedback and recommendations that can improve Illinois IAB seismic designs. This is accomplished through modeling IABs as a whole bridge system, subjecting the IAB models to representative ground motions for southern Illinois, monitoring the behavior of key IAB components, using the monitored results to form a comprehensive view of IAB seismic behavior, and employing the developed knowledge to form recommendations for improving IAB seismic performance. The IAB models are developed in OpenSees through nonlinear modeling of multiple components within an IAB, as well as through connections between the components that allow for their interactions to be observed. The models represent typical IAB designs for Illinois. They are subjected to 1000-year return period hazard ground motions developed specifically for 10 sites within southern Illinois. Incremental dynamic analyses are also performed, by scaling the ground motion accelerations up and down.

IABs of varying superstructure materials, span configurations, bearing layouts, pier heights, and foundation soil conditions are dynamically analyzed using the 10 sets of developed ground motions. The results allow for observations and conclusions to be made concerning the overall seismic performance of current Illinois IAB designs, as well as about which components are the most vulnerable to damage during an earthquake. The abutment foundation piles and the pier columns are identified as most vulnerable and frequently encounter severe damage limit states under design-level shaking. Damage to pier columns is especially prominent in IABs with shorter piers and longer abutment-to-abutment spans, while abutment foundation damage, in terms of the yielding, local buckling, and rupture of the piles, frequently occurs in many IAB variants. Recommendations on design modifications to improve the seismic behavior of IABs by limiting the level of damage to these components are also investigated through modifying elastomeric bearing side retainer strength, fixed bearing strength, pier column size, and backfill contributions.

TABLE OF CONTENTS

LIST OF FIGURES

LIST OF TABLES

CHAPTER 1: BACKGROUND

1.1 MOTIVATION

In 2008 and 2009, the American Association of State Highway Transportation Officials (AASHTO) increased the design seismic hazard level from a 500-year return period event to a 1000-year return period event (AASHTO, 2011). As a result of this increase, many bridge structures in Illinois were affected because seismic design became a requirement at a time when that was not previously the case. The project ICT-R27-070: *Calibration and Refinement of Illinois' Earthquake Resisting System Bridge Design Methodology*, was conducted through the Illinois Center for Transportation (ICT). This research evaluated whether Illinois bridges can withstand the increased seismic hazard when using the Illinois Department of Transportation's (IDOT's) Earthquake Resisting System (ERS) concept. The ERS strategy generally keeps the superstructure and substructure elastic while allowing for the bearings between those two components to act as quasi-isolators by fusing.

The study represented in part by this document continues the line of research and is now associated with the ICT-R27-133 project, *Calibration and Refinement of Illinois' Earthquake Resisting System Bridge Design Methodology: Phase II*. There has already been extensive prior research into the seismic behavior of stub abutment bridges in Illinois during Phase I of the project (Filipov *et al.*, 2013a; Filipov *et al.*, 2013b; LaFave *et al.*, 2013a; LaFave *et al.*, 2013b; Steelman *et al.*, 2013; Steelman *et al.*, 2014; Steelman *et al.*, 2016; Steelman *et al.*, 2018). Therefore, phase II of the project focuses on refining the computational bridge models for stub abutment bridges and expanding the research to integral abutment bridges (IABs). This document presents the results of exploring the latter issue.

The presence of integral abutments in IABs removes the need for expansion joints and bearings between the abutment elements and superstructure, which are typically present in stub abutment bridges. Because they do not allow for individual movement of the superstructure and substructure, using integral abutments can lead to a much stiffer bridge that would behave differently when subjected to earthquake input ground motions. Given this feature of IABs, most aspects of the quasi-isolated behavior, which are relied upon in stub abutment bridges as part of the ERS, are unable to be achieved.

The potential lack of quasi-isolated behavior in IABs has led to the interest in Phase II of this project to study IABs. While there is no information concerning the seismic behavior of IABs in Illinois, there have been previous studies outside of this project focusing on the behavior of IABs when subjected to thermal and live loads (e.g., Olson *et al.*, 2013; LaFave *et al.*, 2016). Thermal and live loads are of great interest due to their applicability to a larger set of regions (*i.e.,* not just in high seismicity regions such as in this study) and because the lack of an expansion joint can lead to larger stresses in abutment foundations (Olson *et al*., 2013). Those projects have also analyzed IABs using numerical models, causing them to be useful resources for seismic IAB modeling.

Another portion of the seismic ICT project work that required refinement in Phase II involved the ground motions used for the dynamic analyses of Phase I. Earthquake time histories are difficult to acquire for Illinois, so the modification of existing ground motions is often necessary. However, the ground motions used in Phase I utilized input ground motions for two sites (Cape Girardeau, MO and Paducah, KY), as taken from Fernandez and Rix (2006), with simple linear scaling of the ground motions to better match the AASHTO design spectrum for Cairo, IL (Filipov *et al.*, 2013b). Both the source ground motions and the modification process in Phase I gave the researchers reasons to believe that changes to the ground motion development procedure were necessary in the future.

Based on the general motivations described above in conjunction with the past research conducted in previous phases of this project, the following research objectives were established:

- Develop horizontal ground motion records with appropriate hazard and site conditions for highway bridge dynamic analysis cases in southern Illinois.
- Develop models for all Illinois IABs using the Open System for Earthquake Engineering Simulation (*OpenSees*) program (McKenna *et al.*, 2006). The models should be developed using numerous individual detailed component models combined into an overall bridge model.
- Identify and monitor critical components in IABs when subjected to static and/or dynamic lateral loading, which may differ from what occurs in stub abutment bridges.
- Develop a more comprehensive view of IAB behavior in conjunction with seismic design by using IAB model results and previous knowledge from existing projects and literature.
- Develop feedback and recommendations that can be used to modify IDOT's IAB design and construction procedures with respect to seismic design.

1.2 REPORT ORGANIZATION

The primary goal of this research was to investigate the seismic behavior of typical IABs in Illinois, assess their performance, and then determine any vulnerabilities in IAB seismic design that should be addressed. This report presents the results of computational modeling for typical IDOT IAB configurations conducted from 2013 through 2018. The computational modeling took place in the Department of Civil & Environmental Engineering at the University of Illinois at Urbana-Champaign. Following is a summary of the contents of this report.

Chapter 1 discusses the motivation for the research and provides an overview of past seismic bridge studies in Illinois as well as IAB studies both in and outside of Illinois.

Chapter 2 presents the parametric variations of the prototype IABs explored in this study. This chapter also details the computational modeling procedures for the IAB models.

Chapter 3 outlines the procedures used to perform dynamic analyses and presents detailed results for one bridge model subjected to ground motions of varying intensities.

Chapter 4 presents overall dynamic analysis results for the 51 IAB variants described in Chapter 2.

Chapter 5 explores potential adjustments and design recommendations to enhance the seismic behavior of IABs.

Chapter 6 summarizes the key results determined through this study, as well as any related IAB design and construction recommendations going forward. Recommendations for further research are also provided.

1.3 LITERATURE REVIEW

1.3.1 Stub Abutment Bridge Seismic Behavior and Models

In the past, there have been studies concerning the seismic behavior of bridges in southern Illinois. The majority of these studies have come from Phases I and II of this project. The modeling of stub abutment bridges and their seismic analysis can be explained in three parts; the physical experiments on highway bridge components, the modeling of stub abutment bridges, and the evaluation of these bridges with related conclusions drawn.

The main bridge component of interest in Phase I was the bearings. Bearings commonly used in Illinois bridge designs were studied by Steelman *et al.* (2013; 2014; 2016; 2018) in order to determine their monotonic and cyclic behavior. The three main types of bearings investigated and tested were Type I elastomeric, Type II elastomeric, and low-profile fixed bearings. The side retainers, which accompany the elastomeric bearings in bridges, were also studied. Type I elastomeric bearings are fabricated using a steel shim reinforced elastomer block, which is fused on top to a steel plate, and in contact with the concrete on the bottom, to allow for movement. Type II elastomeric bearings differ from the Type I bearings by being vulcanized to a steel plate at the bottom and allowing for movement at the top between a steel plate vulcanized to the elastomer with a polytetrafluoroethylene (PTFE) top surface contacting a polished stainless steel top plate. The low-profile fixed bearings are comprised of two steel plates held in place by pintles (IDOT, 2012a).

Results from the physical experiments demonstrated distinct behavior in all four components. Type I and Type II bearings showed an initial static friction force followed by bearing slip and reduced kinetic friction resistance under monotonic loading. Under cyclic loading, the behavior differed slightly in that the Type I bearings needed to reach a post-slip static friction force before sliding again. On the other hand, Type II bearings only needed to reach the kinetic friction resistance upon reloading. Type II bearings also have significantly less friction due to the smaller coefficient of friction between a PTFE surface and steel than the friction between an elastomer and concrete (LaFave *et al.*, 2013b).

The experimental data for the elastomeric bearings, side retainers, and low-profile fixed bearings was used to create simplified structural behavior models that can be used in analysis. The experimental data, which only examined a limited amount of bearing and retainer specimens, has been further extrapolated such that the behavior of all potential IDOT bearings and retainers can be predicted (Filipov *et al.*, 2013a; Filipov *et al.*, 2013b; LaFave *et al.*, 2013a).

Bearings and side retainers are just a few of the components within a complete model for a typical stub abutment bridge. The appropriate model behaviors for the numerous other components not experimented on by Steelman *et al.* (2013; 2014; 2016; 2018) were developed based on information found in the existing literature. These components include the piers, the foundations at the abutment and pier locations, the abutment backwall, and the backfill (Filipov *et al.*, 2013a). Those models were combined with other elements, such as elastic superstructure elements, to form a complete stub abutment bridge model.

The models in Phase I of the project were adequate to obtain many useful findings and conclusions; however, an improvement was desired to the abutment modeling. Luo *et al.* (2016) developed a much more detailed abutment model for use in stub abutment bridges in Illinois. This detailed abutment model expands on the simpler stub abutment model by providing enhanced details for the expansion joint, backfill, foundation, and backwall behavior. In addition, the backfill's effect on the wingwalls, the wingwall connection, and the approach slab friction are all explicitly modeled (Luo *et al.*, 2016).

The combination of all the individual components into a complete bridge model for Illinois allowed previous studies to monitor and evaluate the behavior of each component individually during a global bridge analysis (Filipov *et al.*, 2013a; Filipov *et al.*, 2013b; LaFave *et al.*, 2013a). Key limit states within the bridges were evaluated based on component behavior during an analysis, and they were used to determine the sequence of damage in a bridge as the ground motions become stronger. The sequence of damage in stub abutment bridges allows for observations and conclusions to be made concerning the vulnerability of certain components and whether the desired quasi-isolated behavior is achieved in the bridge (Filipov *et al.*, 2013b; LaFave *et al.*, 2013a).

Results from the Illinois stub abutment bridge seismic analyses indicated a few observations, which can be used to form recommendations for future design. The main observation dealt with the behavior of bridges that employ Type II elastomeric bearings. It was found that unseating can be all too common in these bridges, leading to the recommendation that Type II elastomeric bearings should be limited to use in lower seismic regions (LaFave *et al.*, 2013a). Another observation is the frequent occurrence of yielding of the piers under fixed bearings. This led to a recommendation that fixed bearing anchor bolt sizes should be revised (LaFave *et al.*, 2013a).

1.3.2 Integral Abutment Bridge Studies and Modeling

Conventional stub abutment bridges traditionally accommodate movement of the superstructure caused by thermal, creep, or shrinkage strains by employing expansion joints

and elastomeric bearings at the abutments (Kunin and Alampalli, 1999), as seen in Figure 1.1 (a). While this method is effective at accommodating the superstructure movement, the expansion joints are expensive to buy, install, maintain, and repair. Expansion joints may also cause larger issues if they leak, which allows water, dirt, and deicing chemicals to reach the abutment seat. This is undesirable due to the difficulty in cleaning this location and the increased potential for corrosion of the girders and other related deterioration (Kunin and Alampalli, 1999; Paraschos and Amde, 2011). The use of elastomeric bearings at the abutments of stub abutment bridges also creates issues due to their cost to purchase and install (Paraschos and Amde, 2011).

The advantage of an integral abutment is in the elimination of the issues presented above for stub abutments. Integral abutments remove the expansion joint and elastomeric bearing components at each abutment in favor of creating a continuous superstructure-substructure system that moves together at the abutments. This monolithic design is achieved by embedding the single row of abutment piles (if a pile foundation is used) into the pile cap, resting the superstructure girders on the pile cap, and then placing the deck and abutment concrete at the same time. By pouring the deck and abutment at the same time, the girders end up being embedded approximately 1 ft or more into the abutment (Olson *et al.*, 2009). A diagram of an integral abutment is presented in Figure 1.1 (b). As can be observed, this abutment style eliminates the use of expansion joints and bearings, as well as the expensive costs associated with their installation and maintenance.

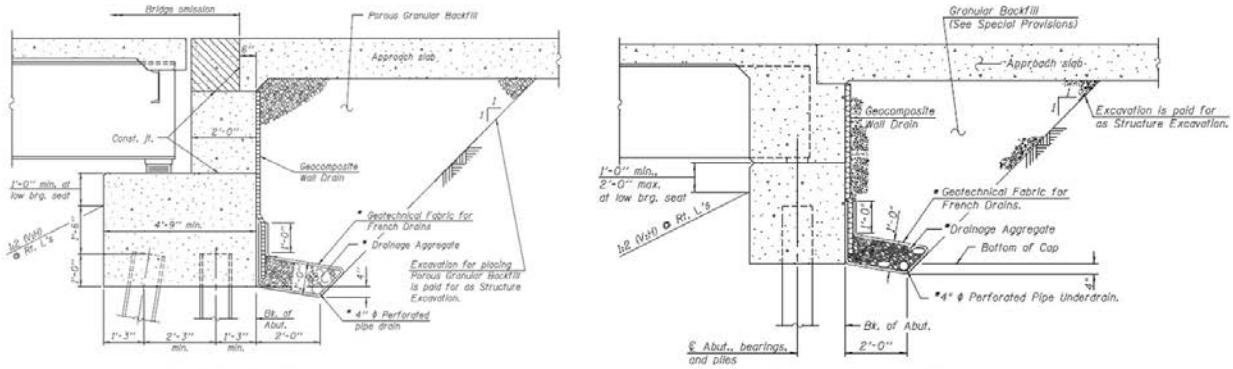

(a) Stub Abutment (b) Integral Abutment

Figure 1.1: Representative diagram of (a) a stub abutment (IDOT, 2012a); (b) an integral abutment (IDOT, 2012b).

While integral abutments provide advantages in the form of reducing potential maintenance costs to the girders and abutment seats, there are also some possible disadvantages and limitations that can present themselves. The major issue with integral abutments stems from the fact that, due to the superstructure and abutment being rigidly connected, both forces and moments are transferred from the superstructure to the abutment and piles, as opposed to just forces in the case of stub abutments. This interaction between the girders and abutments, as well as between the abutment, piles, and the soil surrounding the piles, creates a complex soil-

foundation-structure interaction problem (Olson *et al.*, 2009). The unknown effects from this soil-structure interaction (SSI) problem, and the uncertainties they lead to in terms of pile flexural stresses, has led to some design and construction limitations on IAB span lengths and skew angles (Itani and Pekcan, 2011).

The use of IABs in Illinois has led to studies that assess the behavior of IABs under thermal loads, in order to modify IDOT's IAB design process, as necessary. Studies have included both 2-D and 3-D modeling of IABs (Olson *et al*., 2013; LaFave *et al.*, 2016), as well as the monitoring of IABs in the field (Olson *et al.*, 2009; Olson *et al.*, 2013; LaFave *et al.*, 2017), to determine their behavior when subjected to expected magnitudes of thermal and live loads. These studies have observed how IABs can deal with the expansion and contraction of the superstructure without the use of expansion joints or elastomeric bearings at the abutments.

In addition to these studies of entire IAB non-seismic behavior that have been performed in Illinois, a variety of other studies have also examined the seismic behavior of individual components of IABs. Such component studies include investigating the behavior of the SSI at the abutment (Vasheghani-Farahani *et al*., 2010; Franchin and Pinto, 2014), the pile-pile cap connection (Frosch *et al.*, 2009), and the girder-abutment connection (Itani and Pekcan, 2011). Although the study of individual IAB components has used detailed models in the past, there are typically shortcomings when considering these studies for understanding the overall seismic behavior of IABs. The three main shortcomings of these IAB models concern the overly simplistic approach to overall bridge modeling, the focus on individual components, and/or the use of detailed components for thermal and live load studies only.

Most studies only model the components of interest to study their specific effects (Spyrakos and Ioannidis, 2003; Itani and Pekcan, 2011; Franchin and Pinto, 2014); while these studies are important, they are often unable to capture overall bridge behavior. Component-specific models have been developed for the embankment (Shamsabadi *et al.*, 2005; Shamsabadi *et al.*, 2007; Kotsoglou and Pantazopoulou, 2009) and the pile-pile cap connection (Teguh *et al.*, 2006; Frosch *et al.*, 2009). Models do exist that include all the components known to experience significant nonlinear behavior during earthquakes. However, these models have only been used for thermal behavior assessments in the past (Olson *et al.*, 2009; Olson *et al.*, 2013; LaFave *et al.*, 2016). The presented limitations of the previous models to seismic IAB analysis justifies the work in this project to develop detailed IAB models for assessing seismic behavior.

CHAPTER 2: MODELING OF INTEGRAL ABUTMENT BRIDGES

2.1 OVERVIEW OF PROTOTYPE INTEGRAL ABUTMENT BRIDGES

This section details the prototype IABs included in the parametric study of IAB seismic behavior. The parametric study includes a range of representative IABs that have typically been designed and constructed in Illinois in the past. The parametric study also includes IABs designed for use in the near future, which incorporate newer design properties (such as longer spans) than previously constructed for IABs. The bridges in the parametric study have all been designed using the IDOT Bridge Manual (IDOT, 2012a) and other IDOT references that provide updated information not found in the Bridge Manual. The IABs in the parametric study (see Table 2.1 and Figure 2.1) are designed for the city of Cairo due to its proximity to the New Madrid Seismic Zone (NMSZ), which is responsible for the high seismic hazard in southern Illinois

Table 2.1: Matrix of IABs Analyzed in the Parametric Study

Parameter	Alternatives	IAB Type 1 1-Span Steel	IAB Type 2 3-Span Steel				IAB Type 3 4-Span Steel				IAB Type 4 3-Span Concrete				IAB Type 5 4-Span Concrete			
		1	2	3	4	5	6	7	8	9	10	11	12	13	14	15	16	17
Span Configuration	145' - 160' - 160' - 145'						*	*	*	*					*	*	*	*
	80' - 120' - 80'		*	*	*	*					*	*	*	*				
	160'	*																
Pier Type	Multi-Column	N/A	*	*	*	*	*	*	*	*	*	*	*	*	*	*	*	*
Pier Height	Short - 15'		*	*			*	*			*	*			*	*		
	Tall - 40'				*	*			*	*			*	*			*	*
Bearing Layout	All Fixed		*		*		*		*		*		*		*		*	
	All Type I Elastomeric			*		*		*		*		*		*		*		*
Foundation Soil Condition	Stiff	The above (17) bridges are modeled with all three foundation soil conditions (Stiff, Soft, and Alluvial/Non-Alluvial)																

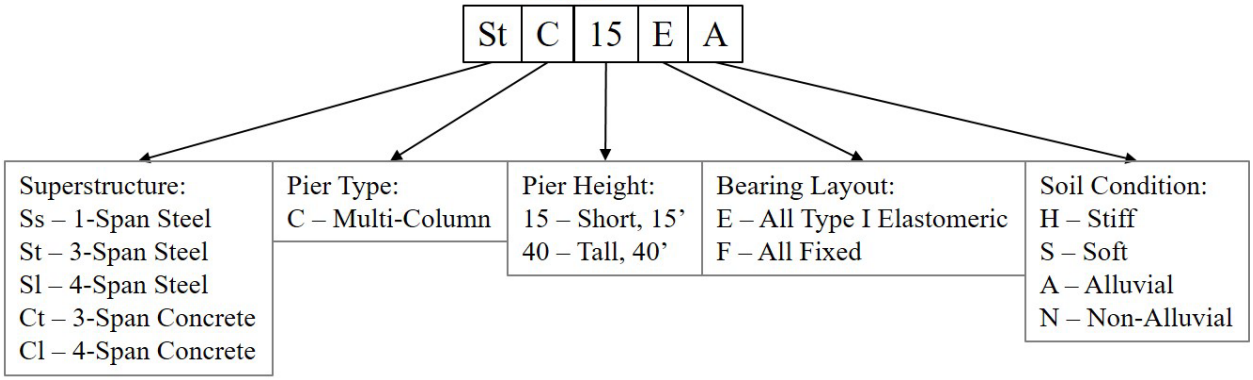

Figure 2.1: Bridge model naming convention.

The 51 parametric study scenarios, described further in Table 2.1, have been developed by varying a bridge's superstructure material and span configuration, height of the piers, layout of bearings at the pier locations, and foundation soil condition. Additionally, variations in seismic hazard are also investigated by varying the site of a bridge throughout southern Illinois. These variations are explored using the bridge analyses described in this report and through the

naming convention provided in Figure 2.1. No skew is considered. Although a number of IABs in Illinois include skew, a fundamental study of IAB seismic behavior without skew is imperative before adding the complexity of skew.

2.1.1 Parametric Variations

2.1.1.1 IAB Superstructure Material and Span Configuration

The parametric study considers five IAB superstructures, and this set contains two superstructure girder materials and three span configurations. The two superstructure girder types are steel plate girders and precast prestressed concrete (PPC) girders. The steel girders are based on typical designs while the PPC girder properties are taken from the IDOT All Bridge Designers Memorandum 15.2 concerning PPC IL-shapes (IDOT 2015). This Memorandum contains information on updated PPC shapes used by IDOT to design for longer spans than previously constructed.

The three different span configurations investigated in the parametric study include single-span (1-span), 3-span, and 4-span IABs. The single-span bridge is only considered with steel girders ("Ss" in the naming convention of Figure 2.1), while the 3- and 4-span IABs are considered for both steel girders ("St" and "Sl" in the naming convention of Figure 2.1, for 3- and 4-span, respectively) and concrete girders ("Ct" and "Cl" in the naming convention of Figure 2.1, for 3- and 4-span, respectively). Only steel girders are considered for single-span bridges since the superstructures are modeled as elastic and the differences in response between concrete and steel single-span bridges are likely minimal. The single-span bridges extend 160-ft between the abutments. The three-span IABs represent typical spans for southern Illinois. These bridges consist of exterior spans of 80-ft between the abutments and piers and a central span of 120-ft between the piers. The four-span IABs consist of exterior spans of 145-ft between the abutments and the piers and two interior spans between piers of 160-ft. The four-span bridges are included in the study as a maximum span that could be encountered with IDOT designs since the overall span of 610-ft is the maximum allowed in the abutment pile selection charts (IDOT, 2012b). A diagram of the three-span IAB configuration is provided in Figure 2.2.

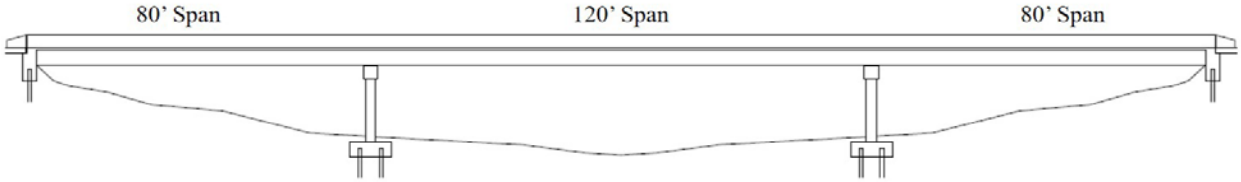

Figure 2.2: Diagram of the three-span IAB configuration considered in the parametric study.

2.1.1.2 Multi-Column Piers

Illinois bridges are typically designed to have either wall piers or multi-column piers. Both of these options have been studied in past Illinois bridge seismic studies, but it has been found that there is little difference between the use of walls or columns at the piers in terms of

seismic performance (LaFave *et al.*, 2013a). For this reason, and to reduce the computational expense of the parametric study, only multi-column piers with four columns ("C" in the naming convention of Fig. 2.1) are considered in the IABs of the parametric study.

Although past Illinois bridge seismic studies have indicated that the type of pier does not have a significant effect on the seismic performance of a bridge, they have indicated that the clear height of the piers can have a significant influence on seismic performance (LaFave *et al.*, 2013a). The clear height of the piers (the height between the top of the pile cap and the bottom of the pier) is varied in the parametric study between a relatively short pier and a taller pier. The short pier clear height is 15 ft ("15" in the naming convention of Fig. 2.1) while the tall pier is represented by a clear height of 40 ft ("40" in the naming convention of Fig. 2.1). The designs of the pier columns vary depending on the specific IAB, as discussed in a later subsection.

2.1.1.3 Bearing Layout

Type I elastomeric bearings and low-profile fixed bearings are considered in the parametric study. While stub abutment bridges typically have bearings at both the abutments and piers, bearings are not needed at the abutments in IABs. Stub abutment bridges require fixed bearings at one pier, whereas IABs are restrained at the ends and may employ elastomeric bearings at all piers. The case of fixed bearings at all piers is also considered, in order to investigate a very stiff bridge scenario.

The elastomeric bearings considered in the parametric study are all Type I elastomeric bearings ("E" in the naming convention of Figure 2.1). Type I elastomeric bearings are accompanied by side retainers in the bridge transverse direction. The fixed bearings considered in the parametric study are low-profile fixed bearings ("F" in the naming convention of Figure 2.1). The size of the elastomeric bearings and the anchor bolts for the retainers and fixed bearings are discussed in a later section.

2.1.1.4 Foundation Soil Conditions

Four foundation soil conditions are considered in the parametric study: stiff soil ("H" in the naming convention of Figure 2.1), soft soil ("S" in the naming convention of Figure 2.1), alluvial soil ("A" in the naming convention of Figure 2.1), and non-alluvial soil ("N" in the naming convention of Figure 2.1). The stiff and soft soil conditions are based on the realistic bounds of soil for southern Illinois (Luo *et al.*, 2016), while the alluvial and non-alluvial soil conditions are based on actual soil data for southern Illinois (Kozak *et al.*, 2017).

The stiff and soft soil conditions are considered for all sites to represent the realistic bounds. However, only one of either the alluvial or non-alluvial soil conditions are considered for each site, equaling three soil conditions per site. The use of either alluvial or non-alluvial soil conditions at a site is based on the local geology of the site. In summary, the three soil conditions considered in the majority of the parametric study for a site in Cairo are the stiff, soft, and alluvial soil conditions.

2.1.1.5 Ground Motion Intensity Variations from Different Site Locations

The majority of the parametric study considers only the soil conditions and seismic hazard for Cairo. This is due to Cairo being the closest location in Illinois to the New Madrid Seismic Zone, which therefore experiences the largest intensity of ground motion shaking and increased seismic hazard. The parametric study also investigates changes in the seismic hazard and the intensity of ground motion shaking by varying the location of the site being investigated. In general, sites further north in Illinois typically have less intense ground motions in terms of spectral acceleration. This is demonstrated by the seismic performance zone designation of sites further north in the state relating to smaller design spectral accelerations at the 1.0 s period than at sites further south. Ten sites are considered, which span across seismic performance zones 2, 3, and 4. The ground motion intensity of each site is varied in the study by using the appropriate ground motions developed for each site.

2.1.2 Integral Abutment Bridge Details

The bridge parameters considered in the parametric study include IAB designs for each of the 51 different variations. The IAB designs are based on the IDOT Bridge Manual (IDOT, 2012a), IDOT All Bridge Designers Memorandum 12.3 concerning IABs (IDOT, 2012b), and input from IDOT engineers to ensure that the designs are typical for the state. The IABs designed for the parametric study represent typical designs of existing single-span and 3-span bridges, as well as designs for a longer 4-span IAB representative of possible future IAB construction. The basic parameters for the 51 distinct IABs are summarized in Table 2.2. Tables containing more detailed information for the 51 IABs and their modeling in *OpenSees* can be found in Appendix A.

2.2 INTEGRAL ABUTMENT BRIDGE MODELING

2.2.1 INTEGRAL ABUTMENT BRIDGE MODEL DESCRIPTION

The goal in the development of the IAB model is to accurately represent an IAB's seismic behavior while still accounting for computational efficiency. This goal is achieved by using experimental data and literature to develop models for individual components, by ensuring that accurate masses are appropriately placed, and by ensuring the model captures the damage found in actual IABs after earthquakes. The model must also account for the bridge parameters of interest, which are varied throughout the parametric study as described earlier. A sample three-span steel IAB is presented alongside its *OpenSees* model in Figure 2.3, to show the similarity in component placement.

Table 2.2: Basic Design Details for the IAB Parametric Study

Superstructure	**1-Span Steel**	**3-Span Steel**		**4-Span Steel**		**3-Span Concrete**		**4-Span Concrete**	
Girder Size	70" Plate Girder	40" Plate Girder		60" Plate Girder		IL54-2438 PPC Girder		IL72-3838 PPC Girder	
Number of Girders	6 @ 7'-0" Spacing	6 @ 7'-3" Spacing		8 @ 5'-6" Spacing		6 @ 7'-3" Spacing		7 @ 6'-2" Spacing	
Deck Width	43'-2"	43'-2"		43'-2"		43'-2"		43'-2"	
Deck Thickness	8"	8"		8"		8"		8"	
Span Lengths	160'	80'-120'-80'		145'-160'-160'-145'		80'-120'-80'		145'-160'-160'-145'	
Pier Bearings									
Type I Bearings	-	15-a		20-d		13-b		18-d	
Retainer Bolt Dia.	-	1.25"		2.00"		1.00"		1.50"	
Fixed Bearing Bolt Dia.	-	1.25"		2.00"		1.00"		1.50"	
Column Piers									
Column Clear Height	-	15'	40'	15'	40'	15'	40'	15'	40'
Column Diameter	-	2'-6"	3'-0"	2'-6"	3'-0"	2'-6"	3'-0"	2'-6"	3'-0"
Reinforcement	-	12 - #10	14 - #11	12 - #10	14 - #11	12 - #10	14 - #11	12 - #10	14 - #11
Reinforcement Ratio	-	2.08 %	2.04 %	2.08 %	2.04 %	2.08%	2.04 %	2.08%	2.04 %
Pier Foundation									
Column Clear Height	-	15'	40'	15'	40'	15'	40'	15'	40'
Pile Section	-	HP10x42		HP10x42		HP10x42		HP12x74	
Number of Pile Rows	-	2	2	3	3	3	3	3	3
Piles per Pile Row	-	7	8	7	8	7	7	6	7
Distance Between Pile Rows	-	5'-0"	5'-0"	5'-0"	5'-0"	4'-0"	4'-0"	4'-0"	4'-0"
Abutment Foundation									
Number of Piles	6	6		8		6		7	
Pile Section	HP12x74	HP10x42		HP14x117		HP10x42		HP14x117	

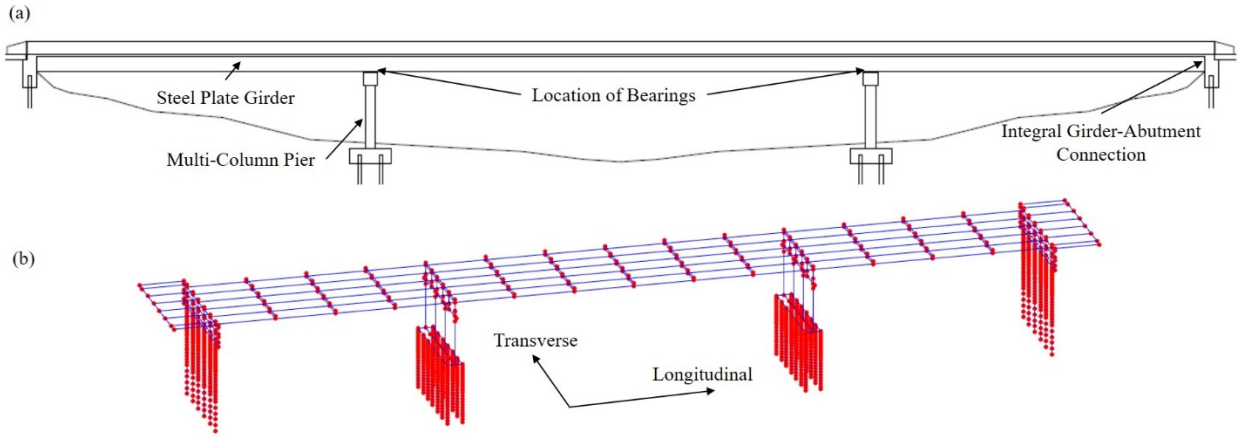

Figure 2.3: (a) Diagram of a typical three-span steel IAB, and (b) The representative *OpenSees* model for that three-span IAB.

The IAB model developed for this study is similar to the models developed to study stub abutment bridge seismic behavior in Illinois (Filipov *et al.*, 2013a; Filipov *et al.*, 2013b; Luo *et al.*, 2016; Luo *et al.*, 2017) using the Open System for Earthquake Engineering Simulation program (*OpenSees*) (McKenna *et al.*, 2006). The prior work to develop stub abutment bridge models established useful component numerical models for simulating the seismic response of highway bridges in Illinois. Full-scale testing was used to validate elastomeric bearing, side retainer, and low-profile fixed bearing models that were implemented in *OpenSees* (Filipov *et al.*, 2013a).

The overall IAB system model, though, cannot be validated with experimental data. However, qualitative validation has been conducted through the comparison of the IAB model behavior to damage found in post-earthquake IAB observation studies. Waldin *et al.* (2012) and Wood (2015) found large amounts of damage to the abutments, abutment piles, and piers in IABs after earthquakes in New Zealand. Significant damage to these same components is also found in the IAB models developed in this study, generally validating the overall behavior of the models to capture actual bridge behavior.

2.2.2 Integral Abutment Component Models

The integral abutment model comprises of ten primary sub-components whose models are described in the following subsections. The representation of the model that is used in *OpenSees* to describe the integral abutment is provided in Figure 2.4.

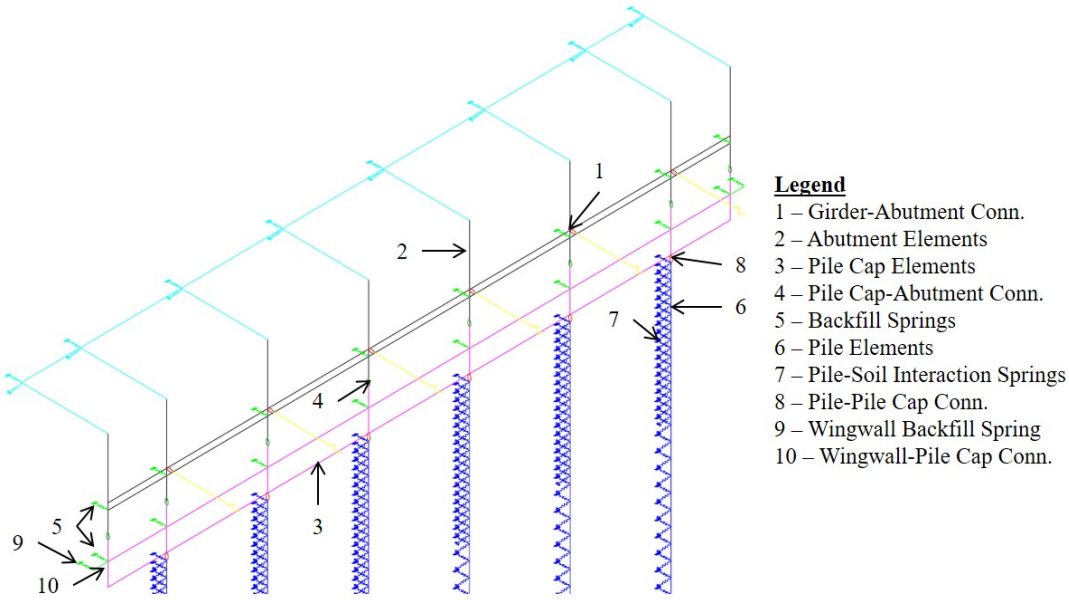

Figure 2.4: Model representation of an integral abutment.

2.2.2.1 Girder-Abutment Connections

The girder-abutment connection (component 1 in Figure 2.4) consists of two primary elements:

1. A direct bearing of the superstructure girder on either a 2-in thick rocker plate or a 1-in thick bearing pad. A rocker plate is used if the girders are steel plate girders, and the bearing pad is used if the girders are prestresed concrete beams (IDOT, 2012b).

2. Concrete is poured such that the girders are cast directly into the abutment, and the deck and abutment are a single monolithic portion of concrete. While the concrete is wet, the girder may still rotate on the rocker plate or bearing pad to accommodate the weight of the concrete deck. However, once the concrete hardens, relative rotation of the girders does not generally occur due to the large section of concrete encasing them in the abutment with a sufficient embedment length.

In the model, the connection is only set to be rigid after the dead load application. To simulate the wet concrete allowing for rotation, and because the wet concrete does not transfer moments from the superstructure to the abutment during the application of dead load, the connection is first modeled to allow for free rotation. The connection model is then set to rigid during the dynamic analysis to simulate the hardened concrete, which does transfer moments and must maintain a consistent rotation.

2.2.2.2 Abutment and Pile Cap

The abutments and pile caps (components 2 and 3, respectively, in Figure 2.4) are both individually poured sections of concrete which are connected through a construction jointThe components themselves are much stronger and stiffer than any of the other components attached to them. Per standard IDOT details, both components are 3-ft 4-in. wide for steel

girders, and they are 3-ft 8-in. wide for prestressed concrete girders. The pile cap is a minimum of 3-ft 6-in. tall, and the height of the abutment varies depending on the girder height and deck thickness (IDOT, 2012b). Given these very large sections, the abutment and pile cap elements are essentially modeled as being rigid elements due to their very large un-cracked elastic stiffness values.

The construction joint between the pile cap and abutment (component 4 in Figure 2.4) is composed of #8 reinforcing steel dowels at the front and back of the abutment with a 12-in. center-to-center spacing (IDOT, 2012b). This construction joint is represented by a connection in *OpenSees* that considers both the dowel shear behavior and the friction between the two concrete surfaces.

Dowel shear behavior is determined using a model based on experimental data by Vintzeleou and Tassios (1986). The concrete-to-concrete friction model is based on equations from Tassios (1983), which can be used to determine the coefficient of friction on the interface as well as the relative displacement to reach maximum shear resistance. The two individual models are combined into the single component model shown in Figure 2.5.

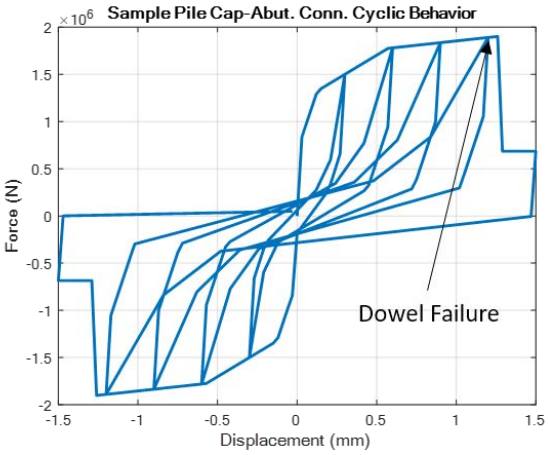

Figure 2.5: Sample cyclic behavior for the overall behavior at the pile cap-abutment interface.

2.2.2.3 Abutment Backfill

Prior numerical studies have shown that the abutment backfill (component 5 in Figure 2.4) is a key component of stub abutment bridge seismic behavior (Luo *et al.*, 2016). The lack of a gap between the superstructure and abutment in IABs means that the backfill is immediately engaged and therefore contributes a significant amount of longitudinal horizontal load resistance. The model simulates the passive backfill pressure against the abutment and pile cap using the force-displacement relationship provided in Shamsabadi *et al.* (2005) and Shamsabadi *et al.* (2007). This relationship is based on soil mobilizing in a logarithmic spiral failure surface and also considers a hyperbolic stress-strain behavior of the soil, which is also known as the LSH model. Soil mobilization indicates the point at which the soil behind the backwall fails along the LSH surface and the passive backfill resistance is at its peak.

A modified *HyperbolicGapMaterial*was developed in *OpenSees* for Luo *et al.* (2016) that accounts for the LSH model. This modified material was used in the IAB model to represent the backfill at various points. The backfill resistance is only experienced when the abutment is compressed into the backfill. When the abutment pulls away from the backfill, there is no resistance from the backfill. Backfill soil properties used to calculate the backfill model behavior are based on typical values used for sandy gravel backfill materials in Illinois.

2.2.2.4 Abutment Foundations

The foundations of the abutments comprise of piles attached to pile caps. The abutment foundations are modeled to account for the pile element behavior (component 6 in Figure 2.4), the behavior of the soil surrounding the piles (component 7 in Figure 2.4), and the behavior of the connection between the piles and the pile cap (component 8 in Figure 2.4). These components are detailed in Figure 2.6, which demonstrates how the elements are represented in the model.

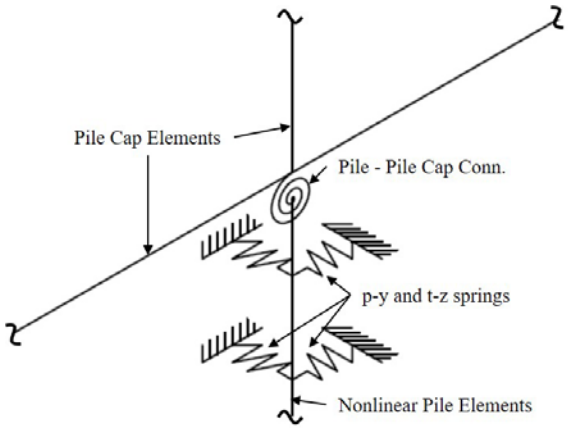

Figure 2.6: Model representation of the components included in the abutment foundations.

The piles are modeled as nonlinear beam-column elements. These elements account for both the nonlinear steel material in the piles as well as the HP-shape of the piles by using fiber sections. The piles are oriented such that weak-axis bending occurs when forces are applied in the bridge longitudinal direction (IDOT, 2012b). This orientation is used to allow for the integral abutments to be more flexible in the longitudinal direction in order to accommodate thermal loads. The sizes of the HP-shapes used for the piles are dictated by pile sizing charts provided by IDOT (2012b).

The HP-shape cross-sections are divided into multiple fibers, each with a defined material behavior. Due to the potentially significant nonlinear behavior in the piles, caused by both axial forces and bending moments, the pile section is discretized into 120 fibers. The 120 fibers are arranged such that each flange and the web contain 20x2 fibers, as shown in Figure 2.7 (a). The steel material used in each fiber follows the Giuffré-Menegotto-Pinto Model along with isotropic strain hardening (*Steel02* in *OpenSees*). The steel parameters used in this study are defined by a Young's modulus of 29,000 ksi, an actual yield strength of 55 ksi (1.1 x 50 ksi), and

an actual ultimate strength of 71.5 ksi (1.1 x 65 ksi), which are based on typical properties of similar A572 Gr. 50 steel (AISC, 2017). The strain hardening ratio was determined as 0.48%, also using A572 Gr. 50 steel data and assuming the ultimate strain occurs at 0.12.

The pile elements are discretized along the length of the pile to account for the larger moments that will be experienced near the abutments. It has been indicated that the critical pile depth is taken to be the top 10 ft of the soil (IDOT, 2012b), so the soil closest to the top contains shorter elements to better capture the behavior. As shown in Figure 2.7 (b), the top 10 ft of the piles are discretized into (20) 6-in. sections, the following 10 ft are discretized into (10) 12-in. sections, and the deepest 10 ft are discretized into (5) 24-in. long sections. At a depth of 30 ft, the pile elements are fixed.

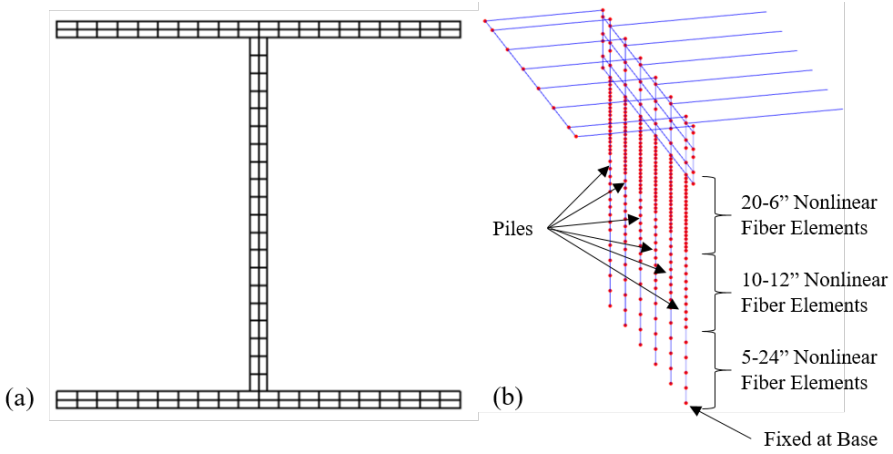

Figure 2.7: (a) Discretization of the pile cross-section, and (b) Discretization of the pile elements along their length.

Attached to the ends of each of the nonlinear pile elements are zero-length elements representing the soil surrounding the piles at that specific depth through p-y and t-z springs. The *OpenSees* built-in material model *PySimple1* is used for the p-y springs in both horizontal directions. This material is based on models from Boulanger *et al.* (1999), using data from Illinois soil profiles. Four Illinois soil conditions with accompanying soil profiles are considered – alluvial, non-alluvial, stiff, and soft. The alluvial and non-alluvial profiles are based on the soil boring data described in Kozak *et al.* (2017), whereas the stiff and soft soil profiles were developed in Luo *et al.* (2016) to describe realistic bounds for soft and stiff soil conditions in southern Illinois.

For p-y springs in a clay layer, the p_{ult} parameter is calculated from equations in Matlock (1970) and Terzaghi *et al.* (1996) by using the soil's undrained shear strength and unit weight. Sand p-y behavior is based on equations and figures from the American Petroleum Institute (API) (2002); p_{ult} can be calculated using coefficients on the effective friction angle of the soil and the depth of the layer.

The t-z springs account for the vertical resistance applied to the piles from the soil and also use soil parameters from the four soil conditions discussed above. Similar to the p-y springs, the t-z springs require t_{ult} and z_{50} values in the *OpenSees* model. The API (2002) provides equations and suggested values for modeling these springs.

Examples of the p-y and t-z spring behavior under cyclic loading conditions are shown in Figure 2.8. The t-z spring resistance is from friction only, leading to a lower capacity at the plateau. In the p-y springs, the effects of drag and re-engagement with soil can be observed through the pinching behavior in the cyclic response.

The final modeled component of the abutment foundations are the pile-pile cap connections. These connections are meant to represent the embedment of the pile into the pile cap and to account for the spiral reinforcement that is present. The piles are embedded 24 in. into the pile cap (IDOT, 2012b), which is sufficient to model this connection as rigid. This assumption is further verified through past studies which observed that there is no decrease in the lateral load capacity of the connection if the piles are embedded 24 in. or more (Frosch *et al.*, 2009).

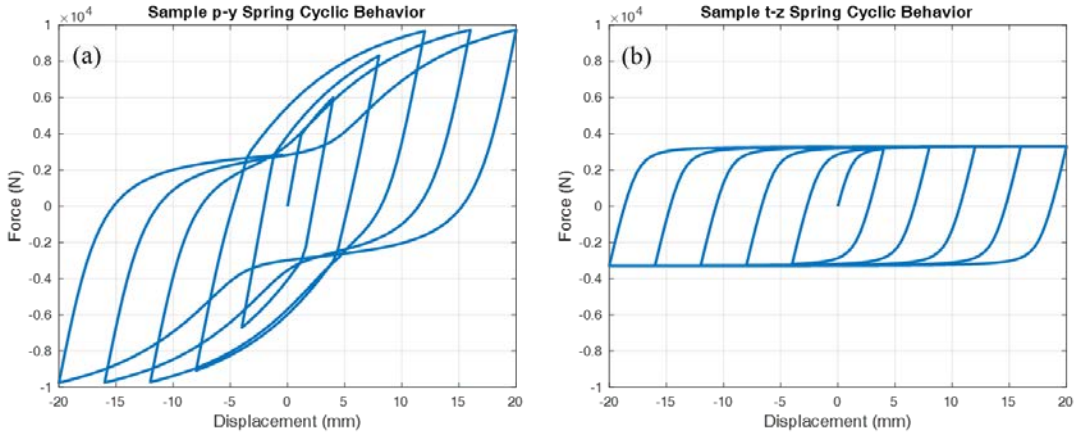

Figure 2.8: Example zero-length spring behavior for (a) cyclic p-y springs, and (b) cyclic t-z springs.

2.2.3 Non-Abutment Component Models

Outside of the abutment, the IAB model includes the superstructure longitudinal and transverse elements, the approach slabs, the fixed and elastomeric bearings found between the piers and superstructure, the pier columns, and the pier foundations. The locations of these components within the IAB model are presented in Figure 2.9. Many of the non-abutment components, such as the bearings and pier columns, are similar to those considered in Filipov *et al.* (2013a; 2013b) for use in stub abutment bridges, so the developed constitutive models are unchanged. Refinements have been made to components such as the pier columns and the superstructure in order to better represent an IAB.

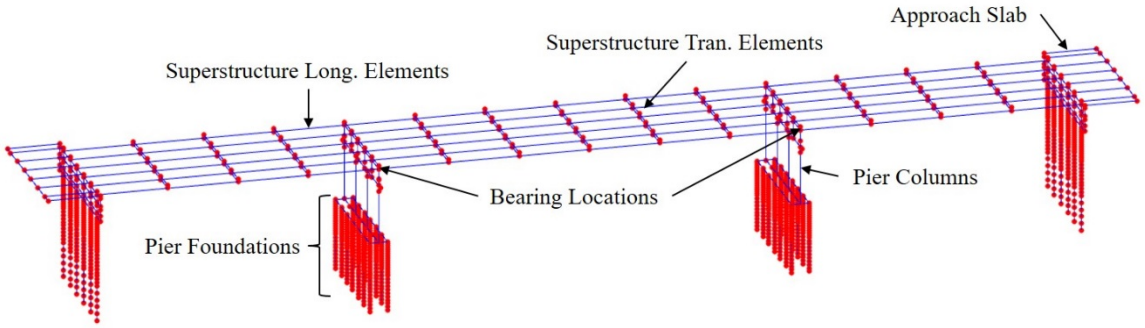

Figure 2.9: Location of non-integral abutment components modeled in an overall IAB model.

2.2.3.1 Superstructure

The bridge superstructure is modeled using the grillage method, which represents the girders, deck, parapets, and transverse diaphragms as beam-column elements in the longitudinal and transverse directions. These elements are illustrated in Figure 2.9. The longitudinal elements represent the composite girder-deck section and are located at the elevation of the centroid of the composite section. The longitudinal elements are spaced according to the girder spacing used in actual bridge designs.

Two transverse elements are defined at different elevations in the superstructure, as presented in Figure 2.10 for the deck and model cross-section. The lower transverse elements are located at the girder-deck composite centroid elevation and represent the diaphragms connecting the girders when steel girders are used. They also represent either the permanent bracing (at non-pier and non-abutment locations) or concrete diaphragms (at pier and abutment locations) when prestressed concrete girders are used. The upper transverse elements are located at the deck centroid's elevation and represent the deck. The transverse elements are spaced according to the diaphragm and permanent bracing spacing limits provided in the IDOT Bridge Design Manual (IDOT, 2012a).

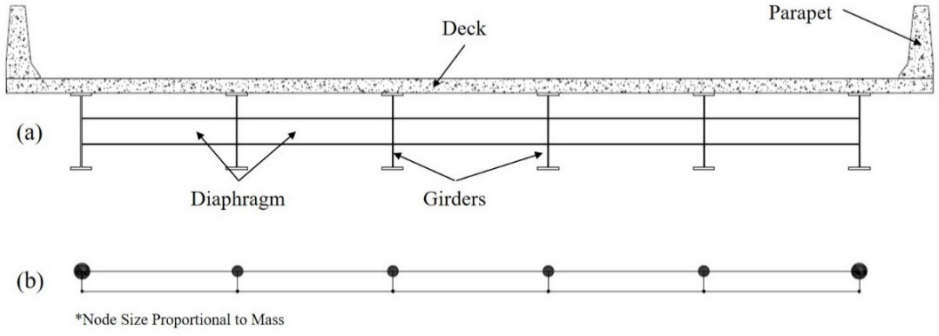

Figure 2.10: (a) Diagram of the superstructure cross-section, and (b) Representative model of the superstructure cross-section with masses.

The mass of the superstructure is also accounted for in the model, as indicated by the circles at the nodes in Figure 2.10 (b). The masses along the upper transverse element represent the

deck and the parapets (only in the exterior nodes, as indicated by the larger circles in those locations). The masses along the lower transverse element represents the mass of the girders.

2.2.3.2 Approach Slabs

The approach slabs are not modeled in detail due to their lack of observed damage in past earthquakes. The important contribution from the approach slabs in the model is the mass of these 30-ft long concrete slabs, which may have significant inertial contributions during dynamic events. Friction between the approach slab and the soil beneath it is not modeled due to an assumption that the soil has settled and there is negligible contact with the slab (Luo *et al.*, 2016). Only 15-ft of the approach slab and its mass contributions are included, as the other half of the mass is expected to be resisted by the approach-transition slab foundation.

2.2.3.3 Elastomeric Bearings, Side Retainers and Fixed Bearings

Type I elastomeric bearings and their side retainers have been experimentally studied in the past (LaFave *et al.*, 2013b; Steelman *et al.*, 2013; Steelman *et al.*, 2018), and numerical models for use in bridge response analysis have been developed based on the experimentally-observed behavior (Filipov *et al.*, 2013b; LaFave *et al.*, 2013a). These previously-developed numerical models are used to represent Type I bearing behavior in the IAB models as well. Samples of these previously-developed numerical models are provided in Figure 2.11.

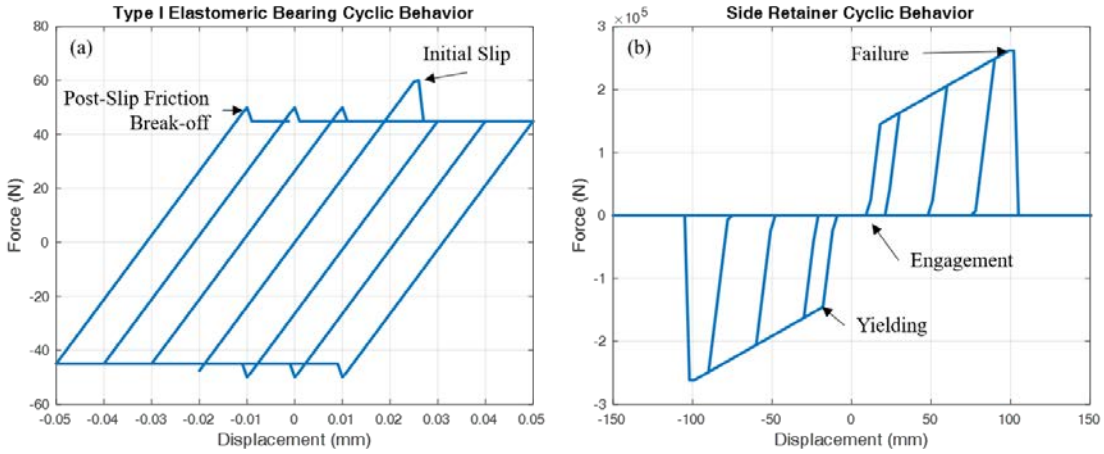

Figure 2.11: Sample (a) Type I elastomeric bearing cyclic behavior, and (b) side retainer cyclic behavior.

Low-profile fixed bearings have also been experimentally studied to determine their monotonic static and cyclic loading behavior (LaFave *et al.*, 2013b; Steelman *et al.*, 2014). The experiments demonstrated that the primary fuse in the fixed bearing (the component that will fail first) is the anchor bolts (LaFave *et al.*, 2013b). Given this, the fixed bearing model accounts for the shear behavior of the steel anchor bolts and also the friction occurring between the plate and concrete after the anchor bolts fracture. The behavior of the steel anchor bolts is shown in Figure 2.12.

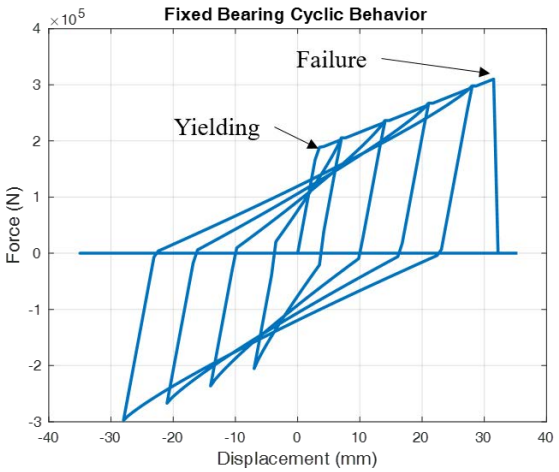

Figure 2.12: Sample cyclic low-profile fixed bearing behavior (not including the frictional contribution) for a bearing using 1.25-in. diameter steel anchor bolts.

2.2.3.4 Pier Columns

There is evidence of the possibility of significant damage to bridge pier columns during earthquake events (Waldin *et al.*, 2012). As such, the four circular pier columns of the IABs are explicitly modeled between the pier cap and pile cap at each pier. The pile caps and pier caps are modeled as rigid since they are much stiffer and stronger than the columns. While the pile and pier caps are modeled as rigid, their masses, along with the column masses, are still accounted for in the IAB model. The distributed plasticity column elements that represent the pier columns are force-based beam-column elements developed by Scott and Fenves (2006).

The nonlinear behavior in the plastic hinge region is accounted for by using a fiber model of the column cross section. The section is modeled with 8 wedges split into 10 rings. The 2 exterior rings represent the unconfined concrete, while the inner 8 rings represent the confined concrete in the column. The steel reinforcing bars in the column are found between the confined and unconfined concrete. The parameters and modeling methods used for the pier columns in the IAB models have been taken from Filipov *et al.* (2013b), who validated them against experiments by Kowalsky *et al.* (1999).

2.2.3.5 Pier Foundations

The pier foundation model is similar to the abutment foundation model. In both cases, the pile caps are modeled as rigid while the individual piles are explicitly modeled along with p-y and t-z springs to represent the effects of the soil surrounding the piles. Unlike the abutment foundations, the pier foundations experience relatively smaller bending stresses and comprise of more than one row of piles.

The relatively lower bending stresses in the pier piles when compared to the abutment piles leads to some changes in the model of the pier piles as well. The discretization of the pier piles, in terms of both the element and the cross-section, varies from the abutment piles. The pile elements are discretized such that they only extend 20 ft below the pile, where they are then

assumed to be fixed. The bottom 10 ft of piles are discretized into (10) 12-in. elastic beam-columns, while the top 10 ft are discretized in (20) 6-in. long nonlinear beam-columns. Additionally, the nonlinear beam-column elements in the top 10 ft have sections composed of only 30 fibers, as opposed to the 120 fibers used in the abutment piles.

The p-y and t-z springs used in the pier foundations are calculated using the same method described for the abutment foundations. There are slight changes between the p-y and t-z curves in the pier and abutment foundations due to the potential differences in pile size (depending on design) and due to the different pile orientations used between the two locations.

2.2.4 Limit States

The IAB seismic damage limit states that track inelastic bridge behavior are divided into three categories based on their desirability; ideal, acceptable, and unacceptable. Ideal limit states act as fuses and protect other more critical bridge components. The ideal limit states typically cause minimal damage or damage to components that are easily replaceable or repairable, so that a bridge can remain functional immediately after an earthquake. Acceptable limit states do not involve severe damage, but the damage occurs in components that are difficult to inspect or replace. Damage from acceptable limit states still allows for immediate use of a bridge after an earthquake for emergency services. Unacceptable limit states are those involving severe damage that renders a bridge unusable for even emergency services immediately after a seismic event. A list of the potential limit states in an IAB model and their associated abbreviations are presented in Table 2.3.

Table 2.3: IAB Model Limit States

Ideal Limit States	Acceptable Limit States	Unacceptable Limit States
Backfill Mobilization – BF	Abut. Pile Yielding – APY	Bearing Unseating – BU
Retainer Engagement – RE	Abut. Pile Local Buckling – APB	Severe Steel Pier Damage – SS
Retainer Yielding – RY	Abut. Pile Soil Mobilization – APS	Severe Concrete Pier Damage - CS
Retainer Fusing – RF	Pile Cap-Abut. Interface Failure – PA	Abut. Pile Rupture – APR
Fixed Bearing Yielding – FY	Pier Pile Yielding – PPY	
Fixed Bearing Fusing – FF	Pier Pile Soil Mobilization– PPS	
Bearing Sliding – BS	Moderate Steel Pier Damage – SM	
Light Steel Pier Damage - SL	Moderate Concrete Pier Damage - CM	
Light Concrete Pier Damage - CL		

The limit states for light, moderate, and severe pier column damage are presented in Table 2.4. Reinforcing steel damage corresponds to the beginning of yielding for light damage, the end of yielding for moderate damage, and rupture for severe damage. Concrete damage is represented by concrete cracking and concrete spalling for light and moderate damage, respectively. Severe concrete damage is defined as strains beyond the limit where the concrete would still be repairable, and so the column would need to be replaced (Kowalsky, 2000).

Table 2.4: Corresponding Strain Values for Pier Column Limit States

Limit State	Concrete (compression)	Reinforcing Steel (Tension)
Light Damage	$-0.005 < \varepsilon_{conc} \leq -0.002$	$0.0021 \leq \varepsilon_{rebar} < 0.015$
Moderate Damage	$-0.018 < \varepsilon_{conc} \leq -0.005$	$0.015 \leq \varepsilon_{rebar} < 0.06$
Severe Damage	$\varepsilon_{conc} \leq -0.018$	$0.06 \leq \varepsilon_{rebar}$

Nine limit states are classified as ideal limit states. Mobilization of the backfill soil at the abutments (BF) is indicated to have occurred when one of the backfill springs achieves its ultimate capacity. Three retainer limit states are included: engagement (RE), yielding (RY), and fusing, which occurs at an anchor bolt fracture (RF). Fixed bearings also experience yielding (FY) followed by fusing, when anchor bolt fracture occurs (FF). Damage to the retainers or fixed bearings leads to the onset of sliding. The bearing sliding limit state (BS) occurs if a bearing reaches the kinetic/sliding portion of bearing friction behavior. Light damage to the reinforcing steel (SL) and unconfined concrete (CL) of the column piers is also classified as ideal. These are not fuse limit states, but indications of minor damage to the pier columns.

Eight limit states are classified as acceptable. Moderate damage to the reinforcing steel (SM) and unconfined concrete (CM) of the pier columns indicates that there is a significant amount of damage in the columns, yet not enough to cause collapse. Yielding of the piles at the abutment (APY) and pier (PPY) foundations is indicated by yielding of the material of any of the fibers in the steel pile cross-section. Local buckling of the abutment piles (APB) is estimated to occur when the strain in any pile fiber reaches 20 times the strain at expected yield (yield strain). This value of 20 times the yield strain has been identified as the onset of local buckling through a combination of cyclic pile loading experiments and analyses (Frosch *et* al., 2009). The soil surrounding the piles may also be mobilized by reaching its capacity in the abutment (APS) and pier (PPS) foundations. The onset of the PA limit state occurs upon failure of the dowels.

Four limit states are classified as unacceptable due to the likelihood of a loss of bridge span should any of them occur. The first limit state is bearing unseating (BU), which occurs if a bearing displaces a distance larger than the seat width. The seat width dimension is calculated per the IDOT Bridge Manual (IDOT, 2012a). A loss of span may also occur if there is severe damage to the pier columns. Severe damage to the reinforcing steel (SS) or unconfined concrete (CS) of the pier columns, as indicated by achieving the strains in Table 2.4, could compromise the vertical load-carrying capacity of the column and make travel on a bridge

dangerous immediately after an earthquake. The occurrence of any of these three unacceptable limit states during an earthquake would result in a dangerous bridge that could not be crossed and would significantly hinder emergency response.

The rupture of the abutment piles (APR) is also identified as an unacceptable limit state due to a bridge becoming dangerous to use once piles have cracked and ruptured. The APR limit state identified in this study is based on judgement and the strain at which the ultimate stress of the steel is expected to occur. APR is estimated to occur when the strain in any pile fiber reaches a value of 40 times the yield strain of the steel.

Most of the ideal and acceptable limit states directly correspond with a change in analytical behavior occurring in the component models. Unlike those limit states, the unacceptable limit states do not correspond to any changes in modeled behavior. Instead, they only identify when certain strain or displacement limits are reached. Given this, the bridge model continues to behave normally once these limit states occur despite severe adverse effects occurring in actual bridges should these strains or displacements be achieved. Any analytical behavior beyond the occurrence of the first unacceptable limit state is therefore not clearly meaningful and subsequently discarded in the analyses.

CHAPTER 3: DYNAMIC ANALYSIS

3.1 DYNAMIC ANALYSIS PROCEDURE

Dynamic analyses were performed on the IABs of the parametric study in order to obtain information concerning the behavior of IABs during design-level seismic events. Analyses were also performed on the sequence of damage occurring during seismic events of varying intensities.

The dynamic analyses were performed through the application of 20 ground motions developed for Cairo, IL. As indicated earlier, the soil properties in Cairo correspond to the alluvial soil condition, so that is used in the analyses as the realistic foundation soil condition. Analyses for the three-span and four-span concrete IABs with 15-ft tall piers and fixed bearings were not able to converge with any soil condition through numerous attempts, and so therefore there are only design-level dynamic analysis results for 45 of the 51 IABs.

Incremental dynamic analyses (IDA) were also performed on the 17 IABs that have alluvial foundation soil conditions, using ground motion scale factor as an intensity measure. These dynamic analyses expose the IAB models to the design-level ground motions scaled up and down to varying degrees. The ground motions are linearly scaled between a scale factor (SF) of 0.5 to 1.75 in 0.25 increments, where a scale factor of 1.00 corresponds to the design-level hazard of a 1000-year return period. Through the comparison of the uniform hazard spectrum (UHS) for the design-level 1000-year return period hazard and the maximum considered earthquake (MCE)-level 2500-year return period hazard, it was determined that a scale factor of 1.75 is a suitable approximation for the MCE across southern Illinois. Similar to how the three-and four-span concrete IABs with 15-ft tall piers and fixed bearings did not yield any analysis results at the design-level, they were also unable to converge during the IDA. The four-span concrete IAB with 40-ft tall piers and fixed bearings was also unable to converge at some larger scale factors, leading to its exclusion from the IDA as well. These non-converged analyses are likely due to the failure of multiple bridge components and the large concrete superstructure masses leading to unrealistically large displacements, which the analysis calculations could not resolve.

The acceleration time history of each ground motion, regardless of site or scale factor, is applied to the model as a uniform horizontal base excitation at all boundary nodes. This means that any potential spatial variation of the ground motion along the length of the bridge is not considered. Spatial variation is not accounted for due to the variability of conditions which may be present between the abutments. These variabilities include whether the bridge is crossing a deep river, a shallow river, or another road, as well as any slight differences between the embankment soil at each abutment. To account for the most general case in this study, these variations are not considered, and the ground motion is assumed to be identical along the length of the bridge.

3.2 GROUND MOTION TIME HISTORIES

The lack of suitable ground motions for a 1000-year return period event in southern Illinois necessitates the development of ground motions for this specific purpose. A process was used to modify existing ground motion records into ground motions, which can be used for seismic bridge assessments in southern Illinois, specifically for Cairo. The process involved the creation and matching of existing ground motions to the conditional mean spectra (CMS) for 10 sites around southern Illinois, which were then propagated through site-appropriate soil profiles to acquire surface ground motions. These surface ground motions are the motions used in the seismic analysis of IAB models and are presented in Figure 3.1.

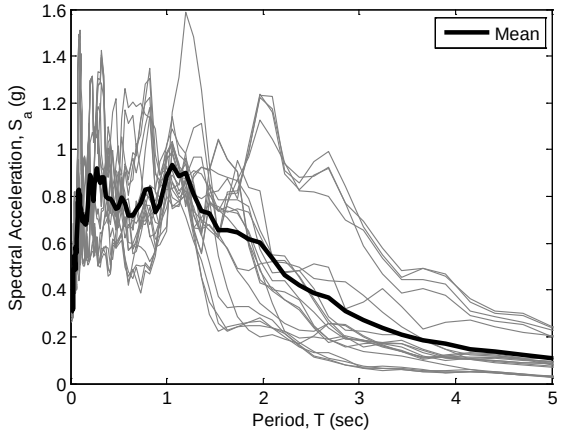

Figure 3.1: Final ground motion spectra for Cairo.

For information concerning the ground motions at southern Illinois sites, and for more detailed explanations of the ground motion development procedure, refer to Appendix B of this report or Kozak *et al.* (2017).

3.3 SAMPLE DESIGN-LEVEL DYNAMIC ANALYSIS RESULTS

The analysis of the 45 IAB models (note that CtC15F_ and ClC15F_ did not yield results) at the 1000-year return period design-level earthquake hazard, provides information concerning the frequency of occurrence of the various limit states within the bridges. By assessing which limit states occur, and how often they occur, the IABs may be deemed ideal, acceptable, or unacceptable designs for the current design-level. This section illustrates the results for StC15EA. Tables are presented that describe the frequency at which each limit state occurs for each IAB out of the 20 ground motions it is subjected to. Additionally, figures presenting typical behavior for the IAB during one of the ground motions are also provided to demonstrate key behavior. The behavior is presented using plots of the center node displacement time history, center node displacement-base shear behavior, overall backfill behavior at one abutment, retainer behavior of all the retainers, stress-strain behavior of the four extreme fibers at the top of one of the abutment piles, and the behavior of the top p-y spring in one of the abutment

piles. The red dashed lines in the backfill behavior and the top p-y spring behavior plots correspond to the load required to mobilize these components.

Table 3.1: Frequency of Limit State Occurrences for StC15EA Under Design-Level Ground Motions

StC15EA			
LS Class	**Limit State**	**Long.**	**Tran.**
Ideal	**BF**	0%	0%
	SL	60%	40%
	CL	35%	10%
	RE	0%	100%
	RY	0%	100%
	RF	0%	0%
Acceptable	**APY**	100%	100%
	APB	0%	0%
	APS	70%	30%
	PA	0%	0%
	PPY	0%	0%
	PPS	0%	0%
	SM	0%	0%
	CM	0%	0%
Unaccept.	**BU**	0%	0%
	SS	0%	0%
	CS	0%	0%
	APR	0%	0%

Table 3.1 provides an example of the tables used to describe the frequency of limit state occurrences for IABs under design-level ground motions. The results presented in Table 3.1 indicate that in the longitudinal direction, there is only light pier column steel and concrete damage (SL and CL), as well as the yielding of the abutment piles (APY) and the mobilization of the soil surrounding the piles (APS). In the transverse direction, SL, CL, APY, and APS also occur, in addition to engagement and fusing of the retainers (RE and RF, respectively).

The table of frequency of limit state occurrences is a useful tool in comparing the severity of damage in an IAB during design-level shaking. StC15EA does not have any unacceptable limit states occur, which is encouraging. However, the table allows for observations to be made indicating that the abutment piles always yield in both directions. Although no unacceptable limit states occur, the consistent occurrence of an acceptable limit state is still an interesting result requiring further investigation. The tables are also handy for determining which

parametric variations aid in the fusing of certain components. An example of this is how the StC15EA results do not indicate any retainer fusing (RF) despite yielding occurring. Comparing the frequency of RF to other IABs allows for conclusions to be made concerning which parameters aid in allowing the retainers to fuse.

Sample figures that summarize the dynamic behavior of StC15EA and its components are provided in Figure 3.2 and Figure 3.3. These figures facilitate observations to be made concerning the individual component behavior during a dynamic analysis. The longitudinal plots include information concerning the center node displacement, overall deck displacement vs. total base shear, backfill behavior, the behavior of the four corners of a critical abutment pile, and the behavior of the p-y spring at the abutment. The transverse plots provide the same information with the exception of the backfill behavior being replaced by the retainer behavior.

The behavior and time history plots allow for observations to be made concerning limit state occurrences beyond the frequency of limit state occurrence tables. For example, APY is shown to always occur in Table 3.1, and APB never occurs. However, the table is incapable of telling us whether the piles barely yield, or yield and then nearly reach local buckling. Figure 3.2 (d) and Figure 3.3 (d) allow for these gaps in knowledge to be filled in by noting that the maximum pile strain is nearly 5 times the yield strain in the longitudinal direction and only about 3 times the yield strain in the transverse direction. Similarly, Figure 3.3 (c) demonstrates that the retainers do experience significant yielding and are close to fusing despite it never occurring. Other interesting behavior can also be observed, such as the effect of backfill re-engagement in the longitudinal direction and retainer re-engagement in the transverse direction. Both of these occurrences result in the overall deck displacement-base shear response to have a noticeable pinching behavior.

Although the plots described in this section may not be present in the summary of the parametric study results found in Chapter 4, the complete set of figures describing the design-level dynamic analyses can be found in Appendix C.

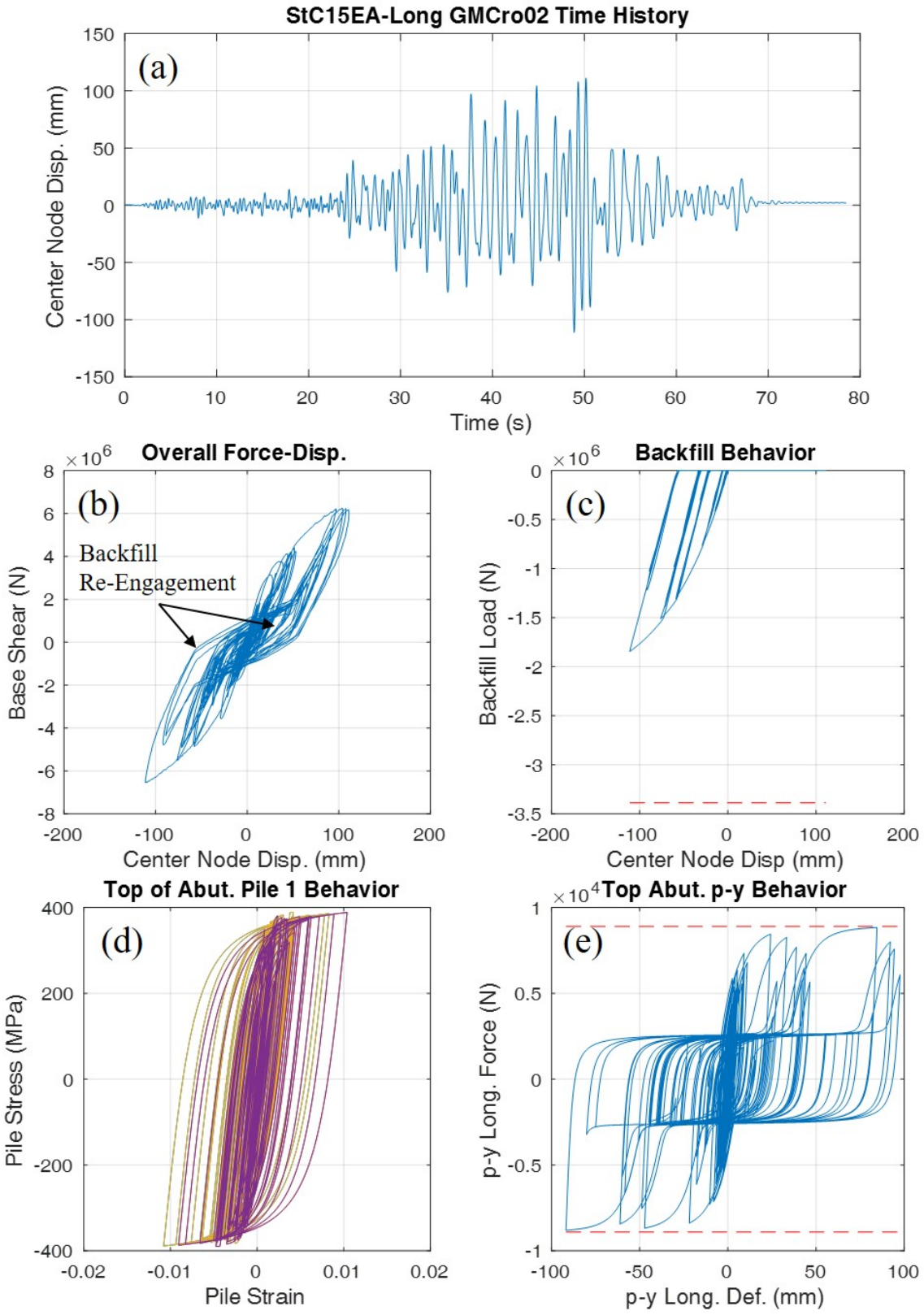

Figure 3.2: Dynamic analysis results for StC15EA subjected to a design-level ground motion in the longitudinal direction.

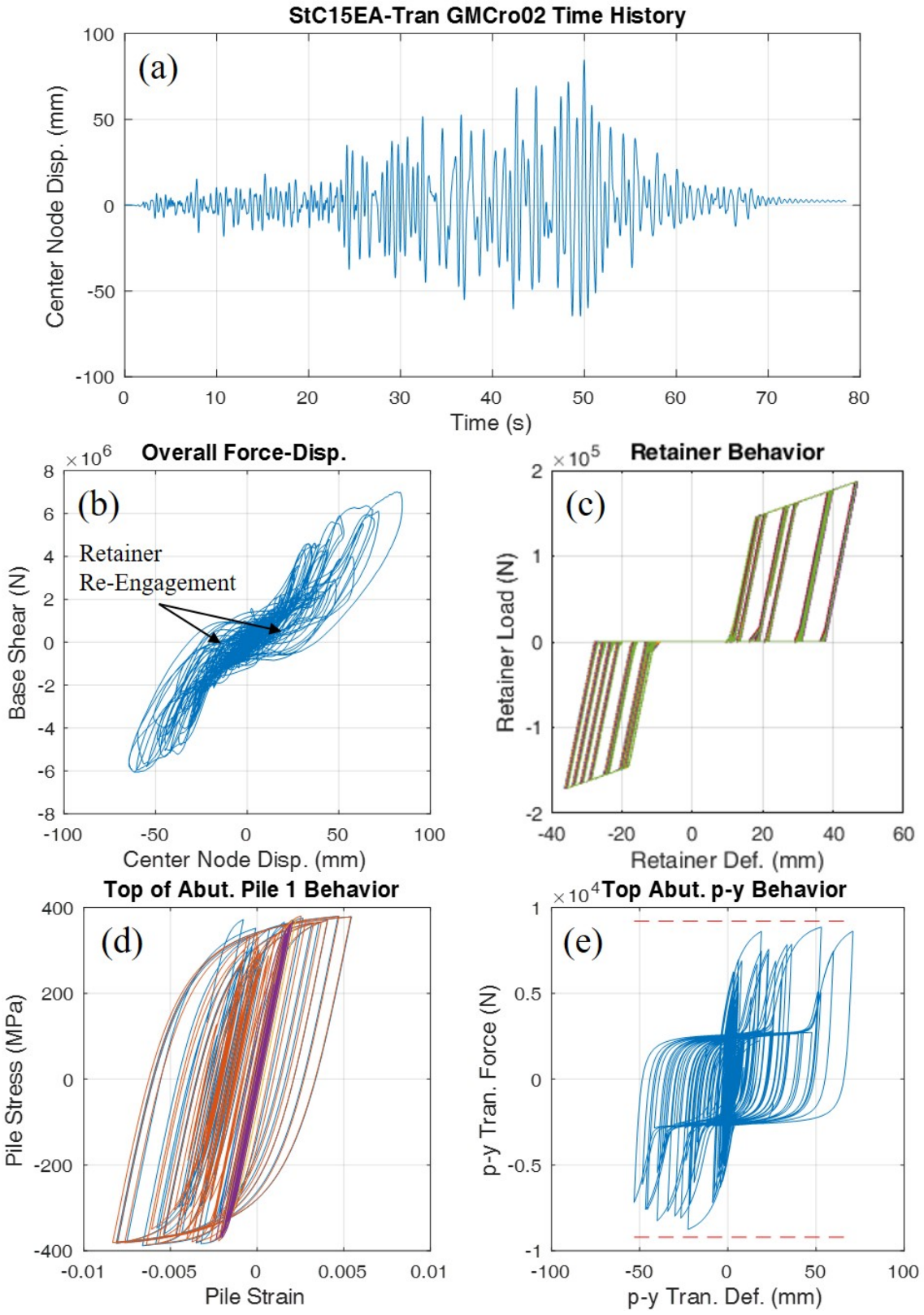

Figure 3.3: Dynamic analysis results for StC15EA subjected to a design-level ground motion in the transverse direction.

3.4 SAMPLE INCREMENTAL DYNAMIC ANALYSIS RESULTS

The IDA results are presented in two fashions. The first is a table, similar to the tables for the design-level analysis results, which provides the percent of analyses at each scale factor that a limit state occurred.

Table 3.2: Frequency of Limit State Occurrences for the IDA of StC15EA in the Transverse Direction, Where a Scale Factor of 1.00 Represents the Design-Level

		StC15EA					
		Transverse Direction					
LS Class	Limit State	SF 0.50	SF 0.75	SF 1.00	SF 1.25	SF 1.50	SF 1.75
Ideal	BF	0%	0%	0%	0%	0%	0%
	SL	0%	10%	40%	80%	100%	100%
	CL	0%	0%	10%	50%	80%	100%
	RE	100%	100%	100%	100%	100%	100%
	RY	25%	95%	100%	100%	100%	100%
	RF	0%	0%	0%	0%	0%	0%
Acceptable	APY	10%	70%	100%	100%	100%	100%
	APB	0%	0%	0%	0%	25%	60%
	APS	0%	10%	30%	30%	80%	90%
	PA	0%	0%	0%	0%	0%	0%
	PPY	0%	0%	0%	0%	10%	15%
	PPS	0%	0%	0%	0%	10%	0%
	SM	0%	0%	0%	0%	40%	80%
	CM	0%	0%	0%	0%	50%	80%
Unaccept.	BU	0%	0%	0%	0%	0%	0%
	SS	0%	0%	0%	0%	0%	5%
	CS	0%	0%	0%	0%	0%	20%
	APR	0%	0%	0%	0%	0%	0%

The second presentation is via the IDA plots themselves, which present component and overall bridge response against ground motion scale factor. These plots help to identify the dispersion of the results by providing the maximum and minimum results from the 20 ground motions at each scale factor, along with the median. They also aid in determining how close components were to the limit states and can better compare damage between bridges than the frequency of limit state occurrence data. The IDA plots are made for several areas. Some of them include center node displacement, base shear, maximum abutment pile strain (normalized to pile yielding, and including lines defining local buckling and rupture in yellow and red, respectively), maximum abutment p-y spring force (normalized to the p-y spring ultimate capacity), and maximum backfill spring force (normalized to each backfill spring's ultimate capacity). Other areas consist of, maximum concrete and steel pier column strain (including lines defining the

light, moderate, and severe limit states in green, yellow, and red, respectively), retainer force (including lines defining retainer engagement, yielding, and fusing in green, yellow, and red, respectively), and fixed bearing force (including lines defining anchor bolt yielding and fusing in yellow and red, respectively). A sample of the IDA plots presenting the difference in retainer force and fixed bearing force in three-span steel bridges under transverse excitation is presented in Figure 3.4

In addition to the two described IDA data presentations, the IDA results may also be presented through sequence of damage plots, which are described and presented in Appendix D.

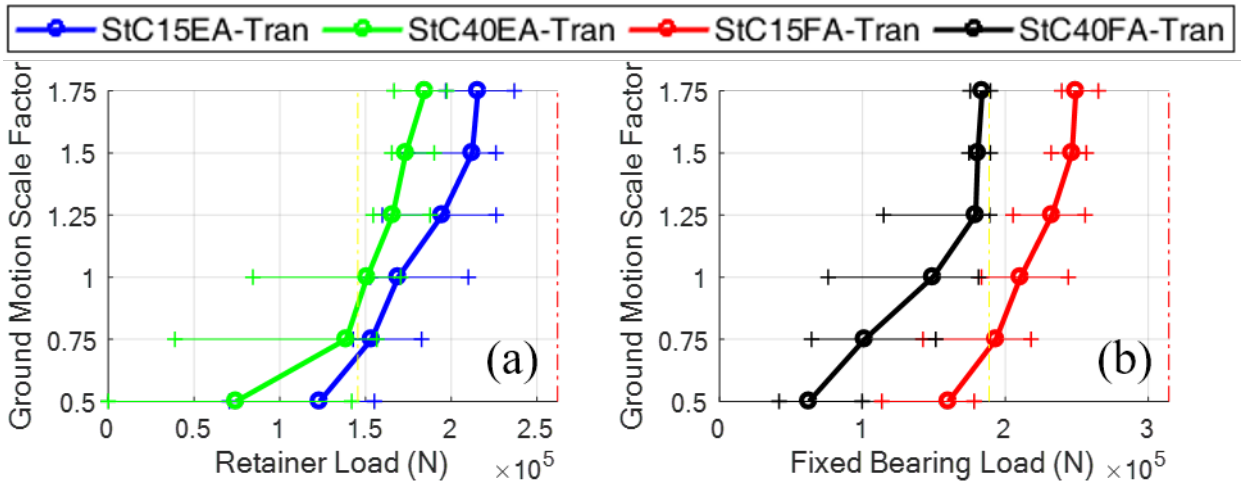

Figure 3.4: IDA plots for three-span steel IABs in the transverse direction, where a scale factor of 1.00 represents the design-level.

CHAPTER 4: PARAMETRIC STUDY RESULTS

4.1 SINGLE-SPAN STEEL INTEGRAL ABUTMENT BRIDGES

4.1.1 Design-Level Dynamic Analysis Results

The design-level dynamic results for the three single-span steel IABs are presented in Table 4.1. Due to the lack of piers, there are only six limit states which could even apply to these bridges, and the only variation is in the foundation soil condition. A few general observations can be made from Table 4.1. One of which is that backfill mobilization and failure at the pile cap-abutment interface does not occur. This leaves the only limit states that occur as being the yielding of the abutment piles (APY) and mobilization of the soil surrounding the abutment piles (APS). Although the piles yield, the strains in the piles are not excessive, as pile local buckling is never reached.

Table 4.1: Frequency of Limit State Occurrences for Single-Span Steel IABs Under the Design-Level Ground Motion Suite

Bridge	Longitudinal Limit State Occurrence					
	Ideal	Acceptable				Unacceptable
	BF	APY	APB	APS	PA	APR
Ss____S	0%	65%	0%	30%	0%	0%
Ss____A	0%	80%	0%	0%	0%	0%
Ss____H	0%	30%	0%	0%	0%	0%
Bridge	**Transverse Limit State Occurrence**					
	Ideal	**Acceptable**				**Unacceptable**
	BF	**APY**	**APB**	**APS**	**PA**	**APR**
Ss____S	0%	80%	0%	65%	0%	0%
Ss____A	0%	10%	0%	5%	0%	0%
Ss____H	0%	0%	0%	0%	0%	0%

In the longitudinal direction, there is more damage to the abutment foundation (both the piles and the surrounding soil) under softer soil conditions. Due to the soft soil condition having the lowest ultimate capacity in the p-y springs, mobilization of the abutment soil (APS) only occurs in Ss____S. However, even when the APS limit state does not occur, the top p-y springs in the piles are still very close to mobilizing. It can also be noted that the piles do not achieve an extreme level of yielding, only reaching a maximum local stress of less than 60 ksi and a strain of about 0.003, which is well short of the pile local buckling strain of 0.04 as determined through estimates based on experimental results (Frosch *et al.*, 2009). Although backfill mobilization does not occur in the analyses, the backfill is still engaged during dynamic loading in the longitudinal direction. However, it is generally not close to mobilizing.

In the transverse direction, there is once again less occurrence of abutment pile yielding (APY) and mobilization of the soil surrounding the abutment piles (APS) as the soil conditions become stiffer. In fact, APY and APS occur most of the time in the soft soil condition, rarely in the alluvial soil condition, and never in the stiff soil condition. Observations concerning the p-y spring behavior are also similar in both the longitudinal and transverse directions, with the p-y spring almost reaching the ultimate capacity. APS occurs more often in the transverse direction with the soft and alluvial soil conditions when compared to the longitudinal direction. However, APS once again never occurs in the stiff soil condition. The increase in APS occurrence is due to the lack of backfill in the transverse direction, requiring all the lateral force to be resisted by the abutment piles and the soil. Due to the arrangement of the piles, which has strong axis bending under transverse excitation, they do not yield as often in the transverse direction, allowing for more force to be taken within the soil.

Overall, the single-span steel IABs have acceptable designs due to the worst limit states being acceptable limit states. The lack of bearings and piers makes it impossible for the superstructure to unseat or piers to fail. While the APY and APS limit states are acceptable, they are still not as ideal as backfill mobilization, which does not occur in any of these analyses. Improvements could perhaps be made by allowing for more backfill engagement and less damage to the abutment foundation.

4.1.2 Incremental Dynamic Analysis Results

As with the design-level response, abutment pile yielding (APY) and mobilization of the soil surrounding the piles (APS) occurs in single-span steel IABs at most scale factors. Additionally, at a scale factor of 1.75 under transverse excitation, abutment pile local buckling (APB) also occurs. This result is shown in Table 4.2, which provides the frequency of limit state occurrences under ground motions at each scale factor. Table 4.2 demonstrates that the APY and APS limit states begin to occur in a majority of the analyses at scale factors of 1.0 and larger, and they rarely occur at smaller scale factors. It can also be seen that in both directions APY occurs in all the analyses when subjected to ground motions with a scale factor of 1.5 and larger.

The IDA for the single-span steel IAB results indicates that backfill is not close to mobilizing at any scale factor. In fact, the backfill force rarely exceeds 50% of the backfill capacity even at the largest scale factor. Also, in the longitudinal IDA, a gradual increase in component response as scale factors increase, indicates there are no major events causing a fusing mechanism in this direction. In the transverse direction IDA, it can be confirmed that there is no backfill force at all, indicating that all the force is taken by the abutment piles and soil.

When observing the sequence of damage for the single-span steel IAB in Figure 4.1, it can be determined that for the most part it is acceptable. The longitudinal sequence does have APY at a slightly smaller scale factor than ideal, but APS is within the ideal region at a scale factor of 1.25. Although APY occurs at slightly smaller scale factors than ideal, there are limited energy dissipating components in the single-span IABs. This means that it is better to have APY occur slightly too easily than have it not occur at all and then have the bridge be extremely stiff. The

transverse sequence is ideal, as both APY and APS occur at the design-level scale factor of 1.0, and APB occurs at a scale factor of 1.75. This leads to the conclusion that the single-span steel IAB designs are in the range of slightly discouraged to ideal. The lack of backfill mobilization at any level is concerning due to its potential help in allowing the APY to occur at a later scale factor, and because backfill mobilization is ideal at low scale factors.

Table 4.2: Frequency of Limit State Occurrences for the IDA of Single-Span Steel IABs, Where a Scale Factor of 1.00 Represents the Design-Level

Bridge	SF	Longitudinal Limit State Occurrence					
		Ideal	Acceptable				Unacc.
		BF	APY	APB	APS	PA	APR
Ss____A	0.50	0%	0%	0%	0%	0%	0%
	0.75	0%	5%	0%	0%	0%	0%
	1.00	0%	80%	0%	0%	0%	0%
	1.25	0%	80%	0%	10%	0%	0%
	1.50	0%	100%	0%	15%	0%	0%
	1.75	0%	100%	0%	45%	0%	0%
Bridge	**SF**	**Transverse Limit State Occurrence**					
		Ideal	**Acceptable**				**Unacc.**
		BF	**APY**	**APB**	**APS**	**PA**	**APR**
Ss____A	0.50	0%	0%	0%	0%	0%	0%
	0.75	0%	0%	0%	0%	0%	0%
	1.00	0%	10%	0%	5%	0%	0%
	1.25	0%	65%	0%	30%	0%	0%
	1.50	0%	100%	0%	65%	0%	0%
	1.75	0%	100%	45%	100%	0%	0%

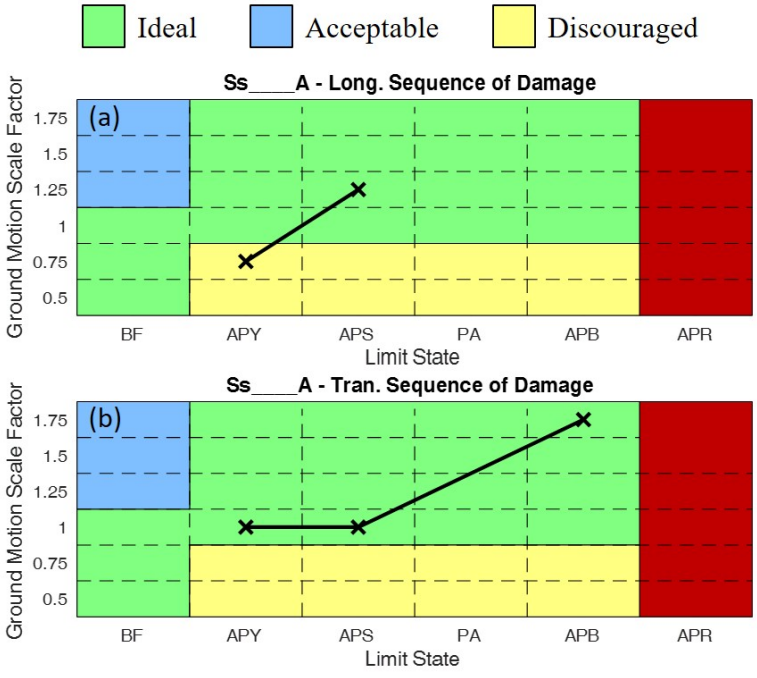

Figure 4.1: Sequences of damage for single-span steel IABs, where a scale factor of 1.00 represents the design-level.

4.2 THREE-SPAN STEEL INTEGRAL ABUTMENT BRIDGES

4.2.1 Design-Level Dynamic Analysis Results

The three-span steel IAB dynamic analysis results are presented in Table 4.3, along with the sample component behavior presented back in Figure 3.2 for longitudinal behavior and Figure 3.3 for transverse behavior. The results from dynamic excitation in the longitudinal direction indicate the occurrence of many limit states. However, backfill mobilization (BF), retainer or fixed bearing damage (RE, RY, RF, FY, and FF), failure of the pile cap-abutment interface (PA), or any of the unacceptable limit states do not occur. The lack of unacceptable limit states is encouraging. However, in the longitudinal direction, backfill mobilization is an ideal limit state that does not occur, although it can be shown to be engaged (see Figure 3.2 (c)). The engagement and compaction of the backfill is the reason for the pinching behavior in the center node displacement-base shear response of Figure 3.2 (b).

The longitudinal results also yield important information concerning the abutment foundation, which has its piles yield (APY) in every analysis of every bridge. The pile behavior is shown to reach nearly 5 times the yield strain in Figure 3.2 (d), which is nowhere near the 20 times yield strain value for pile local buckling (APB). The abutment foundation soil also mobilizes (APS) frequently, especially in soft soil conditions where it always mobilizes, and in alluvial soil conditions where it mobilizes most of the time. It can be observed from Table 4.3 that APB and APS occurs more often in IABs with 40-ft tall piers as opposed to those with 15-ft tall piers. This is caused by the less stiff tall piers requiring the abutments to provide most of the stiffness for the bridge, resulting in larger demands on the abutments.

The pier columns are another location of significant damage in the bridges under longitudinal excitation. Soft soil conditions consistently provide light (SL and CL) and moderate (SM and CM) damage. Moderate damage is rarely observed outside of the soft soil condition, and the amount of light pier damage tends to decrease under stiffer soil conditions. It can also be noted that IABs with 15-ft tall piers experience more light pier damage due to their increased stiffness also increasing the force demand on the piers. Severe (SS and CS) pier column damage is never encountered.

The final set of limit states that commonly occurs under longitudinal excitation is damage to the pier foundations, pier pile yielding (PPY) and mobilization of the soil (PPS). These limit states only tend to occur under the soft soil condition, due to the decreased ultimate capacity of the soil. The only bridge where the majority of analyses experience PPY or PPS is StC40ES, which has PPS occurring in 70% of the analyses.

The transverse dynamic results presented in Table 4.3 and Figure 3.3 provide similar observations to the longitudinal results concerning initial abutment foundation damage (APY and APS). APY occurs most of the time with IABs having 40-ft tall piers, and APB also occurs due to the less stiff piers increasing the demand on the piles. In IABs with 15-ft tall piers, APY occurs most of the time, with strains reaching only about 3 times the yield strain, as seen in Figure 3.3 (d). APS also tends to follow the trends identified in the longitudinal direction, with the soft soil

condition having more APS occurrences and the 40-ft tall pier IABs causing more demand on the abutments, therefore increasing the amount of APS occurrences. Despite StC15EA only having APS occur 30% of the time, Figure 3.3 (e) still shows that there is quite a lot of force on the p-y springs, bringing them close to the ultimate capacity.

The transverse direction results also provide information concerning pier column damage. Once again, there is no severe damage to the piers (SS and CS). In terms of light and moderate damage, there is less in the transverse than in the longitudinal direction, with moderate damage only occurring rarely in IABs with 40-ft piers and soft soil conditions. Light pier damage occurs frequently and is more common in bridges with soft soil and tall piers.

Other damage to the IABs includes that of the pier foundations (PPY and PPS) in soft soil conditions and damage to the elastomeric bearing retainers and fixed bearings. Damage to the backfill is not expected in the transverse direction. The retainers experience significant damage in the form of anchor bolt yielding, as shown in Figure 3.3 (c), which allows for the pinching behavior in Figure 3.3 (b). While retainers yield all of the time in IABs with 15-ft tall piers, and most of the time in IABs with 40-ft tall piers, they never fuse. Similarly, the fixed bearings yield almost all the time in IABs with 15-ft piers, and sometimes in IABs with 40-ft piers, but they never fuse. The reason for IABs with 15-ft piers experiencing more retainer and fixed bearing damage is due to the shorter piers being stiffer and not deforming as much. This causes larger shear displacements and shear forces in the bearings between the superstructure and pier caps.

Overall, the three-span IAB designs are acceptable, as there is no occurrence of unacceptable limit states in any analysis. However, the designs could be improved by engaging the backfill more, as opposed to abutment foundation damage. Also, retainer and fixed bearing fusing should be increased, especially in IABs with 40-ft tall piers.

Table 4.3: Frequency of Limit State Occurrences for Three-Span Steel IABs Under the Design-Level Ground Motion Suite

Bridge	Longitudinal Limit State Occurrence																			
	Ideal								Acceptable								Unacceptable			
	BF	SL	CL	RE	RY	RF	FY	FF	APY	APB	APS	PA	PPY	PPS	SM	CM	BU	SS	CS	APR
StC15ES	0%	100%	100%	0%	0%	0%	-	-	100%	0%	100%	0%	20%	45%	50%	65%	0%	0%	0%	0%
StC15EA	0%	60%	35%	0%	0%	0%	-	-	100%	0%	70%	0%	0%	0%	0%	0%	0%	0%	0%	0%
StC15EH	0%	20%	5%	0%	0%	0%	-	-	100%	0%	30%	0%	0%	0%	0%	0%	0%	0%	0%	0%
StC40ES	0%	80%	25%	0%	0%	0%	-	-	100%	30%	100%	0%	0%	70%	10%	5%	0%	0%	0%	0%
StC40EA	0%	15%	0%	0%	0%	0%	-	-	100%	15%	100%	0%	0%	5%	0%	0%	0%	0%	0%	0%
StC40EH	0%	0%	0%	0%	0%	0%	-	-	100%	0%	60%	0%	0%	0%	0%	0%	0%	0%	0%	0%
StC15FS	0%	100%	90%	-	-	-	0%	0%	100%	0%	95%	0%	5%	20%	50%	60%	0%	0%	0%	0%
StC15FA	0%	80%	60%	-	-	-	0%	0%	100%	0%	55%	0%	0%	0%	10%	20%	0%	0%	0%	0%
StC15FH	0%	35%	25%	-	-	-	0%	0%	100%	0%	30%	0%	0%	0%	0%	0%	0%	0%	0%	0%
StC40FS	0%	70%	35%	-	-	-	0%	0%	100%	30%	100%	0%	0%	35%	10%	10%	0%	0%	0%	0%
StC40FA	0%	15%	0%	-	-	-	0%	0%	100%	15%	100%	0%	0%	0%	0%	0%	0%	0%	0%	0%
StC40FH	0%	0%	0%	-	-	-	0%	0%	100%	0%	55%	0%	0%	0%	0%	0%	0%	0%	0%	0%
Bridge	Transverse Limit State Occurrence																			
	Ideal								Acceptable								Unacceptable			
	BF	SL	CL	RE	RY	RF	FY	FF	APY	APB	APS	PA	PPY	PPS	SM	CM	BU	SS	CS	APR
StC15ES	0%	80%	40%	100%	100%	0%	-	-	80%	0%	75%	0%	75%	35%	0%	0%	0%	0%	0%	0%
StC15EA	0%	40%	10%	100%	100%	0%	-	-	100%	0%	30%	0%	0%	0%	0%	0%	0%	0%	0%	0%
StC15EH	0%	40%	0%	100%	100%	0%	-	-	100%	0%	10%	0%	0%	0%	0%	0%	0%	0%	0%	0%
StC40ES	0%	100%	85%	100%	100%	0%	-	-	100%	50%	100%	0%	0%	20%	10%	10%	0%	0%	0%	0%
StC40EA	0%	65%	20%	100%	80%	0%	-	-	100%	5%	70%	0%	0%	0%	0%	0%	0%	0%	0%	0%
StC40EH	0%	25%	0%	100%	55%	0%	-	-	100%	0%	35%	0%	0%	0%	0%	0%	0%	0%	0%	0%
StC15FS	0%	70%	30%	-	-	-	100%	0%	75%	0%	35%	0%	50%	30%	0%	0%	0%	0%	0%	0%
StC15FA	0%	60%	5%	-	-	-	80%	0%	60%	0%	10%	0%	0%	0%	0%	0%	0%	0%	0%	0%
StC15FH	0%	80%	0%	-	-	-	100%	0%	60%	0%	0%	0%	0%	0%	0%	0%	0%	0%	0%	0%
StC40FS	0%	100%	95%	-	-	-	15%	0%	100%	45%	100%	0%	0%	0%	10%	15%	0%	0%	0%	0%
StC40FA	0%	65%	35%	-	-	-	0%	0%	100%	5%	75%	0%	0%	0%	0%	0%	0%	0%	0%	0%
StC40FH	0%	35%	0%	-	-	-	0%	0%	100%	0%	30%	0%	0%	0%	0%	0%	0%	0%	0%	0%

4.2.2 Incremental Dynamic Analysis Results

Table 4.4 presents the limit state occurrence results for the three-span steel IABs with 15-ft tall piers, while Table 4.5 presents the results for the IABs with 40-ft tall piers. Throughout all the results, it can be observed that there is no backfill mobilization in any bridge at any scale factor. Despite this, the other component damage limit states in the abutments occur quite frequently. APY occurs often for most of the bridges and scale factors, with the exception of the transverse analyses for 15-ft tall IABs. Aside from that situation, APY occurs in all of the analyses with a scale factor of 0.75 and larger, but the piles do not tend to reach larger strain limit states such as APB and APR very often. APS also occurs frequently, and along with APB and APR provides an easier comparison across Tables 4.4 and 4.5. This comparison demonstrates that abutment foundation damage is more frequent in bridges with 40-ft piers, due to the increased flexibility in the piers resulting in a decrease in their demand and an increase in demand on the abutments.

At the pier columns, Tables 4.4 and 4.5 indicate that damage to the pier foundation (PPY and PPS) does not begin to occur until scale factors of at least 1.25, with more damage occurring under longitudinal excitation. While light pier column damage (SL and CL) tends to occur at low scale factors, moderate column damage (SM and CM) typically does not occur in significant amounts until scale factors of at least 1.25. Severe pier column damage (SS and CS) begins to occur much more frequently at scale factors of 1.5 and larger. It can be seen that there is more pier column damage in IABs with shorter piers. This is due to the shorter, stiffer piers increasing the demand on the piers and leading them to damage more often. This trend continues with retainer engagement (RE) and yielding (RY), as well as with fixed bearing yielding (FY). These limit states also occur more often with shorter piers due to the increased forces being distributed to the piers through the bearings. In general, retainer yielding is very common in IABs using retainers. However, fixed bearing yielding rarely occurs in IABs with 40-ft piers, even at large scale factors, while it commonly occurs at scale factors as low as 0.75 in IABs with 15-ft piers. Neither retainer fusing (RF) nor fixed bearing fusing (FF) occurs at any scale factor.

Other general IDA observations in both directions indicate that IABs with 40-ft piers tend to have more deck displacement despite having similar base shears. IABs with 40-ft piers also tend to have more abutment foundation damage in terms of the abutment pile strain and p-y spring force. Both of these observations can be attributed to the increased flexibility of IABs with taller piers.

Other interesting observations from the IDA involve the lack of fixed bearing yielding occurring in StC40FA. StC40FA fixed bearings reach forces close to fixed bearing yielding at scale factors of around 1.25. However, at larger scale factors, the fixed bearings seem unable to achieve yielding, as it rarely occurs in this bridge. Another interesting observation pertains to the strains in the piers. IABs with 15-ft piers experience more damage than those with 40-ft piers in the longitudinal direction. This trend does not hold in the transverse direction. In the transverse direction, while there is a lack of severe pier column damage (indicated by the red dashed line), the pier strains tend to be closer together.

Table 4.4: Frequency of Limit State Occurrences for the IDA of Three-Span Steel IABs With 15-ft Tall Piers, Where a Scale Factor of 1.00 Represents the Design-Level

Bridge	SF	Longitudinal Limit State Occurrence																			
		Ideal								Acceptable								Unacceptable			
		BF	SL	CL	RE	RY	RF	FY	FF	APY	APB	APS	PA	PPY	PPS	SM	CM	BU	SS	CS	APR
StC15EA	0.50	0%	0%	0%	0%	0%	0%	-	-	55%	0%	10%	0%	0%	0%	0%	0%	0%	0%	0%	0%
	0.75	0%	15%	0%	0%	0%	0%	-	-	100%	0%	30%	0%	0%	0%	0%	0%	0%	0%	0%	0%
	1.00	0%	60%	35%	0%	0%	0%	-	-	100%	0%	70%	0%	0%	0%	0%	0%	0%	0%	0%	0%
	1.25	0%	80%	80%	0%	0%	0%	-	-	100%	15%	95%	0%	0%	20%	40%	50%	0%	0%	5%	0%
	1.50	0%	100%	100%	0%	0%	0%	-	-	100%	80%	100%	0%	0%	70%	95%	100%	0%	0%	25%	0%
	1.75	0%	100%	100%	0%	0%	0%	-	-	100%	100%	100%	0%	0%	85%	100%	100%	0%	40%	80%	55%
StC15FA	0.50	0%	0%	0%	-	-	-	0%	0%	55%	0%	10%	0%	0%	0%	0%	0%	0%	0%	0%	0%
	0.75	0%	35%	15%	-	-	-	0%	0%	100%	0%	30%	0%	0%	0%	0%	0%	0%	0%	0%	0%
	1.00	0%	80%	60%	-	-	-	0%	0%	100%	0%	55%	0%	0%	0%	10%	20%	0%	0%	0%	0%
	1.25	0%	85%	80%	-	-	-	0%	0%	100%	5%	80%	0%	0%	10%	55%	65%	0%	0%	5%	0%
	1.50	0%	100%	100%	-	-	-	0%	0%	100%	55%	100%	0%	0%	65%	80%	80%	0%	0%	20%	0%
	1.75	0%	100%	100%	-	-	-	0%	0%	100%	100%	100%	0%	0%	90%	100%	100%	0%	20%	75%	25%
Bridge	SF	Transverse Limit State Occurrence																			
		Ideal								Acceptable								Unacceptable			
		BF	SL	CL	RE	RY	RF	FY	FF	APY	APB	APS	PA	PPY	PPS	SM	CM	BU	SS	CS	APR
StC15EA	0.50	0%	0%	0%	100%	25%	0%	-	-	10%	0%	0%	0%	0%	0%	0%	0%	0%	0%	0%	0%
	0.75	0%	10%	0%	100%	95%	0%	-	-	70%	0%	10%	0%	0%	0%	0%	0%	0%	0%	0%	0%
	1.00	0%	40%	10%	100%	100%	0%	-	-	100%	0%	30%	0%	0%	0%	0%	0%	0%	0%	0%	0%
	1.25	0%	80%	50%	100%	100%	0%	-	-	100%	0%	35%	0%	0%	0%	0%	10%	0%	0%	0%	0%
	1.50	0%	100%	80%	100%	100%	0%	-	-	100%	25%	80%	0%	10%	10%	40%	50%	0%	0%	0%	0%
	1.75	0%	100%	100%	100%	100%	0%	-	-	100%	60%	90%	0%	15%	0%	80%	80%	0%	5%	20%	0%
StC15FA	0.50	0%	0%	0%	-	-	-	0%	0%	0%	0%	0%	0%	0%	0%	0%	0%	0%	0%	0%	0%
	0.75	0%	5%	0%	-	-	-	80%	0%	5%	0%	0%	0%	0%	0%	0%	0%	0%	0%	0%	0%
	1.00	0%	60%	5%	-	-	-	80%	0%	60%	0%	10%	0%	0%	0%	0%	0%	0%	0%	0%	0%
	1.25	0%	100%	35%	-	-	-	100%	0%	100%	0%	15%	0%	0%	0%	0%	5%	0%	0%	0%	0%
	1.50	0%	100%	95%	-	-	-	100%	0%	100%	0%	55%	0%	0%	0%	15%	25%	0%	0%	0%	0%
	1.75	0%	100%	100%	-	-	-	100%	0%	100%	10%	80%	0%	0%	0%	35%	50%	0%	0%	0%	0%

Table 4.5: Frequency of Limit State Occurrences for the IDA of Three-Span Steel IABs With 40-ft Tall Piers, Where a Scale Factor of 1.00 Represents the Design-Level

Bridge	SF	Longitudinal Limit State Occurrence																			
		Ideal								Acceptable								Unacceptable			
		BF	SL	CL	RE	RY	RF	FY	FF	APY	APB	APS	PA	PPY	PPS	SM	CM	BU	SS	CS	APR
StC40EA	0.50	0%	0%	0%	0%	0%	0%	-	-	65%	0%	30%	0%	0%	0%	0%	0%	0%	0%	0%	0%
	0.75	0%	0%	0%	0%	0%	0%	-	-	100%	0%	60%	0%	0%	0%	0%	0%	0%	0%	0%	0%
	1.00	0%	15%	0%	0%	0%	0%	-	-	100%	15%	100%	0%	0%	5%	0%	0%	0%	0%	0%	0%
	1.25	0%	75%	45%	0%	0%	0%	-	-	100%	75%	100%	0%	0%	55%	0%	5%	0%	0%	0%	10%
	1.50	0%	90%	80%	0%	0%	0%	-	-	100%	90%	100%	0%	0%	90%	20%	25%	0%	0%	0%	55%
	1.75	0%	100%	80%	0%	0%	0%	-	-	100%	95%	100%	0%	0%	95%	40%	55%	0%	0%	15%	80%
StC40FA	0.50	0%	0%	0%	-	-	-	0%	0%	70%	0%	30%	0%	0%	0%	0%	0%	0%	0%	0%	0%
	0.75	0%	0%	0%	-	-	-	0%	0%	100%	0%	60%	0%	0%	0%	0%	0%	0%	0%	0%	0%
	1.00	0%	15%	0%	-	-	-	0%	0%	100%	15%	100%	0%	0%	0%	0%	0%	0%	0%	0%	0%
	1.25	0%	75%	40%	-	-	-	0%	0%	100%	75%	100%	0%	0%	5%	0%	0%	0%	0%	0%	5%
	1.50	0%	85%	75%	-	-	-	0%	0%	100%	90%	100%	0%	0%	50%	20%	25%	0%	0%	0%	55%
	1.75	0%	95%	85%	-	-	-	0%	0%	100%	95%	100%	0%	0%	55%	40%	60%	0%	0%	15%	80%
Bridge	SF	Transverse Limit State Occurrence																			
		Ideal								Acceptable								Unacceptable			
		BF	SL	CL	RE	RY	RF	FY	FF	APY	APB	APS	PA	PPY	PPS	SM	CM	BU	SS	CS	APR
StC40EA	0.50	0%	0%	0%	80%	0%	0%	-	-	45%	0%	10%	0%	0%	0%	0%	0%	0%	0%	0%	0%
	0.75	0%	20%	0%	100%	40%	0%	-	-	100%	0%	35%	0%	0%	0%	0%	0%	0%	0%	0%	0%
	1.00	0%	65%	20%	100%	80%	0%	-	-	100%	5%	70%	0%	0%	0%	0%	0%	0%	0%	0%	0%
	1.25	0%	100%	100%	100%	100%	0%	-	-	100%	70%	100%	0%	0%	5%	0%	0%	0%	0%	0%	0%
	1.50	0%	100%	100%	100%	100%	0%	-	-	100%	100%	100%	0%	0%	10%	45%	55%	0%	0%	0%	20%
	1.75	0%	100%	100%	100%	100%	0%	-	-	100%	100%	100%	0%	0%	25%	70%	75%	0%	0%	15%	60%
StC40FA	0.50	0%	0%	0%	-	-	-	0%	0%	45%	0%	10%	0%	0%	0%	0%	0%	0%	0%	0%	0%
	0.75	0%	20%	0%	-	-	-	0%	0%	100%	0%	30%	0%	0%	0%	0%	0%	0%	0%	0%	0%
	1.00	0%	65%	35%	-	-	-	0%	0%	100%	5%	75%	0%	0%	0%	0%	0%	0%	0%	0%	0%
	1.25	0%	85%	80%	-	-	-	10%	0%	100%	55%	100%	0%	0%	0%	5%	0%	0%	0%	0%	0%
	1.50	0%	100%	100%	-	-	-	15%	0%	100%	100%	100%	0%	0%	5%	55%	55%	0%	0%	0%	15%
	1.75	0%	100%	100%	-	-	-	15%	0%	100%	100%	100%	0%	0%	25%	70%	85%	0%	0%	20%	55%

4.3 FOUR-SPAN STEEL INTEGRAL ABUTMENT BRIDGES

4.3.1 Design-Level Dynamic Analysis Results

The four-span steel IAB dynamic analysis results are presented in Table 4.6. The longitudinal direction results are very similar to the longitudinal direction results for the three-span steel IABs. This is demonstrated through the APY limit state virtually always occurring, with the piles reaching large strains of around 5 times the yield strain. This leads to the APB limit state rarely occurring and the APR limit state never occurring. Similar trends are also observed in three-span steel IABs with APS always occurring in soft soil, almost always occurring in alluvial soil, and frequently occurring in stiff soil. It can also be observed that APS occurs more often in IABs with 40-ft tall piers.

The pier columns consistently encounter light damage (SL and CL) in the longitudinal direction, but less frequently encounter moderate damage (SM and CM), and they encounter severe damage (SS and CS) in only a handful of analyses. It was found that pier column damage is more frequent in IABs with 15-ft tall piers. This is due to the stiff, short piers increasing the demand on the columns. The combination of the short piers and the soft soil conditions leads to frequent severe damage in the concrete of the pier columns (CS). Below the columns, in the pier foundation, the damage to the soil (PPS) is kept mainly to the bridges with the soft soil condition.

Once again, there is no mobilization of the backfill (BF) in the longitudinal dynamic analyses. However, backfill engagement is occurring. As stated earlier, the backfill affects the overall bridge behavior due to its engagement and compaction behind each abutment, which creates a pinching effect in the center node displacement-base shear behavior. The similar behavior of the backfill and overall bridge in the longitudinal direction makes sense due to the reliance on backfill and abutment behavior when the bridge is subjected to longitudinal loads.

The four-span IABs in the transverse direction are extremely flexible. Following this, it can be observed that the transverse dynamic results for four-span steel IABs are different from the dynamic results for three-span steel IABs. This is demonstrated by observing that APY, APB and APS occur much less frequently than in the three-span IABs. The abutment piles rarely yield in 15-ft pier IABs and are actually quite far from yielding. On the other hand, due to the decreased pier stiffness in the 40-ft piers causing more demand on the abutments, the abutment piles in IABs with tall piers almost always yield. However, the piles rarely reach strains associated with local buckling. Similar to the taller, less stiff, piers causing more demand in the abutments, it can be observed that APS is much more common in IABs with 40-ft tall piers. IABs with 15-ft tall piers are far from encountering APS, as the p-y behavior is not near mobilization.

Table 4.6: Frequency of Limit State Occurrences for Four-Span Steel IABs Under the Design-Level Ground Motion Suite

Bridge	Longitudinal Limit State Occurrence																			
	Ideal								Acceptable								Unacceptable			
	BF	SL	CL	RE	RY	RF	FY	FF	APY	APB	APS	PA	PPY	PPS	SM	CM	BU	SS	CS	APR
SIC15ES	0%	100%	100%	0%	0%	0%	-	-	100%	15%	100%	0%	0%	0%	85%	85%	0%	5%	45%	0%
SIC15EA	0%	100%	100%	0%	0%	0%	-	-	100%	0%	100%	0%	0%	5%	25%	35%	0%	0%	5%	0%
SIC15EH	0%	35%	25%	0%	0%	0%	-	-	100%	0%	30%	0%	0%	0%	0%	0%	0%	0%	0%	0%
SIC40ES	0%	80%	80%	0%	0%	0%	-	-	100%	35%	100%	0%	0%	25%	15%	20%	0%	0%	0%	0%
SIC40EA	0%	75%	50%	0%	0%	0%	-	-	100%	15%	100%	0%	0%	0%	0%	5%	0%	0%	0%	0%
SIC40EH	0%	5%	0%	0%	0%	0%	-	-	100%	0%	50%	0%	0%	0%	0%	0%	0%	0%	0%	0%
SIC15FS	0%	100%	100%	-	-	-	0%	0%	100%	15%	100%	0%	0%	0%	100%	100%	0%	5%	45%	0%
SIC15FA	0%	90%	85%	-	-	-	0%	0%	90%	0%	75%	0%	0%	0%	60%	80%	0%	0%	0%	0%
SIC15FH	0%	85%	80%	-	-	-	0%	0%	100%	0%	25%	0%	0%	0%	5%	25%	0%	0%	0%	0%
SIC40FS	0%	85%	80%	-	-	-	0%	0%	100%	35%	100%	0%	0%	35%	15%	20%	0%	0%	0%	0%
SIC40FA	0%	75%	50%	-	-	-	0%	0%	100%	15%	100%	0%	0%	5%	0%	0%	0%	0%	0%	0%
SIC40FH	0%	0%	0%	-	-	-	0%	0%	100%	0%	45%	0%	0%	0%	0%	0%	0%	0%	0%	0%
Bridge	Transverse Limit State Occurrence																			
	Ideal								Acceptable								Unacceptable			
	BF	SL	CL	RE	RY	RF	FY	FF	APY	APB	APS	PA	PPY	PPS	SM	CM	BU	SS	CS	APR
SIC15ES	0%	100%	100%	100%	0%	0%	-	-	15%	0%	0%	0%	0%	100%	100%	100%	0%	0%	50%	0%
SIC15EA	0%	100%	100%	100%	0%	0%	-	-	10%	0%	0%	0%	0%	0%	100%	100%	0%	0%	35%	0%
SIC15EH	0%	100%	100%	100%	0%	0%	-	-	20%	0%	0%	0%	0%	0%	100%	100%	0%	0%	35%	0%
SIC40ES	0%	100%	100%	100%	0%	0%	-	-	85%	15%	65%	0%	0%	0%	80%	85%	0%	0%	0%	0%
SIC40EA	0%	100%	100%	100%	0%	0%	-	-	100%	5%	80%	0%	0%	0%	85%	85%	0%	0%	0%	0%
SIC40EH	0%	100%	100%	100%	0%	0%	-	-	100%	0%	5%	0%	0%	0%	85%	90%	0%	0%	0%	0%
SIC15FS	0%	100%	100%	-	-	-	0%	0%	0%	0%	0%	0%	0%	100%	80%	85%	0%	0%	25%	0%
SIC15FA	0%	100%	100%	-	-	-	0%	0%	0%	0%	0%	0%	0%	0%	75%	90%	0%	0%	25%	0%
SIC15FH	0%	100%	100%	-	-	-	0%	0%	5%	0%	0%	0%	0%	0%	70%	90%	0%	0%	25%	0%
SIC40FS	0%	100%	100%	-	-	-	0%	0%	85%	15%	70%	0%	0%	0%	85%	90%	0%	0%	0%	0%
SIC40FA	0%	100%	100%	-	-	-	0%	0%	95%	0%	80%	0%	0%	0%	85%	95%	0%	0%	0%	0%
SIC40FH	0%	100%	100%	-	-	-	0%	0%	100%	0%	5%	0%	0%	0%	85%	95%	0%	0%	0%	0%

The pier columns for the transverse direction always encounter light damage (SL and CL), and almost always encounter moderate damage (SM and CM). The moderate damage is seen in IABs with both short and tall piers, despite short piers being much stiffer and having an increased demand. Moderate damage is frequently encountered in IABs of both pier heights because the span is so long that the lateral force cannot be effectively redistributed to the abutments. The short pier IABs still have more force demand on them and frequently encounter severe damage to the pier column concrete (CS).

Retainer and fixed bearing damage in the transverse direction are minimal, with retainer engagement (RE) occurring whenever possible, but no other limit states. The increased column damage and flexibility of the bridge in general creates a fuse that limits the amount of force transferred through the bearings. Increased pier damage and subsequent lack of damage to the retainers/fixed bearings and abutment foundations in the transverse direction leads the overall behavior of the bridge to be much more linear than in the longitudinal direction. Due to most components that would dissipate energy remaining linear, the overall behavior also largely remains linear, with only a slight pinching behavior due to retainer engagement.

Despite the increased flexibility and forces that come with the four-span bridges, the four-span steel IABs with 40-ft piers remain acceptable designs. The IABs with 15-ft piers are less acceptable due to the frequency of severe pier column damage (SS and CS) in the transverse direction results. The IABs with tall piers seem to avoid severe pier column damage by creating more damage to the abutment foundations, which is not an ideal solution, but still better than the collapse of a pier. In the longitudinal cases, backfill mobilization never occurs, and in the transverse direction, retainer or fixed bearing yielding and fusing do not occur. These limit states would be more ideal ways to dissipate the seismic energy.

4.3.2 Incremental Dynamic Analysis Results

Table 4.7 describes the frequency of limit state occurrences in four-span steel IABs with 15-ft piers during the IDA. Results for the IABs with 40-ft piers are presented in Table 4.8. IABs with both pier heights demonstrate similar behavior concerning the initial abutment foundation damage limit states (APY and APS) in the longitudinal direction. While there are rare occurrences at the 0.5 scale factor, the APY and APS commonly occur in the analyses at scale factors of 0.75 and larger. They also quickly reach 100% occurrence in all the analyses at scale factors of 1.25 and larger. This corresponds to the onset of the APB and APR limit states at scale factors of 1.25 and 1.5, respectively. The APY, APB, APR, and APS occurrences in the transverse direction varies depending on the pier height. As shown in Table 4.7, the IABs with 15-ft piers do not begin to experience APY until the design-level, and it does not occur in 100% of the analyses until the MCE-level. APS occurs even less and never reaches 100% occurrence. APB and APR are rarely experienced, and only at the largest scale factors. This changes for IABs with 40-ft piers in the transverse direction, where damage occurs at much lower scale factors; APY and APS are very common, and APB and APR begin occurring at smaller scale factors. The larger abutment foundation damage in IABs with tall piers can be attributed to the taller, more flexible piers distributing the force such that there is more demand on the abutment.

When using shorter piers, the opposite is true, with an increased demand being on the piers instead of the abutments. This can be seen when comparing the severe pier column damage limit states (SS and CS) in Table 4.7 and Table 4.8. It can be shown that there is much more pier column damage in IABs with 15-ft piers than there is in IABs with 40-ft piers. This culminates in IABs with 15-ft piers commonly having SS and CS occur at scale factors of 1.25 and larger, while IABs with 40-ft piers experience less frequency of SS and CS, and they begin to occur at larger scale factors. In general, across all the IABs, it is shown that there is almost always light pier column damage (SL and CL) at scale factors of at least 1.0. Also, it can be shown that there is more damage at all scale factors in the transverse direction than in the longitudinal direction.

The elastomeric bearing retainers and fixed bearings do not encounter any yielding or fusing at any scale factor, as shown in Table 4.7 and 4.8. However, retainer engagement, which is expected to occur easily in the transverse direction, does occur in every applicable bridge at every scale factor. Other limit states that occur include mobilization of the soil surrounding the pier piles (PPS). PPS rarely occurs, though, and when it does, it is only present in the longitudinal direction at scale factors of at least 1.25.

General IDA observations in both directions conclude that IABs with 40-ft piers encounter more deck displacement, IABs with 15-ft piers tend to have more pier strain leading to more pier damage, and IABs with 40-ft piers have greater abutment pile strain. These conclusions can be attributed to shorter, stiffer piers providing more pier column demand, while taller, less stiff piers decrease the demand on the piers and increase it in the abutments.

As stated, IABs with 40-ft piers tend to have more damage in the abutment piles. However, the effects on the soil surrounding the piles depends on the direction of excitation. In the longitudinal direction, there is not much difference between IABs of different pier heights, as they all tend to reach the p-y spring ultimate capacity at low scale factors. The transverse direction experiences a clear distinction between the short and tall piers, with the taller piers experiencing more damage at lower scale factors.

The retainers and fixed bearings both experience similar behavior. The observed behavior has the force on the retainers and fixed bearings being consistent throughout the IDA. This is likely due to moderate pier damage occurring at low scale factors. The occurrence of moderate pier column damage would act as a fuse and limit the force being transferred across the bearings to the piers.

Table 4.7: Frequency of Limit State Occurrences for the IDA of Four-Span Steel IABs With 15-ft Tall Piers, Where a Scale Factor of 1.00 Represents the Design-Level

Bridge	SF	Longitudinal Limit State Occurrence																			
		Ideal								Acceptable								Unacceptable			
		BF	SL	CL	RE	RY	RF	FY	FF	APY	APB	APS	PA	PPY	PPS	SM	CM	BU	SS	CS	APR
SIC15EA	0.50	0%	0%	0%	0%	0%	0%	-	-	10%	0%	5%	0%	0%	0%	0%	0%	0%	0%	0%	0%
	0.75	0%	40%	10%	0%	0%	0%	-	-	80%	0%	40%	0%	0%	0%	0%	0%	0%	0%	0%	0%
	1.00	0%	100%	100%	0%	0%	0%	-	-	100%	0%	100%	0%	0%	5%	25%	35%	0%	0%	5%	0%
	1.25	0%	100%	100%	0%	0%	0%	-	-	100%	30%	100%	0%	0%	0%	85%	90%	0%	5%	60%	0%
	1.50	0%	100%	100%	0%	0%	0%	-	-	100%	60%	100%	0%	0%	0%	95%	100%	0%	35%	85%	20%
	1.75	0%	100%	100%	0%	0%	0%	-	-	100%	80%	100%	0%	0%	10%	100%	100%	0%	65%	90%	30%
SIC15FA	0.50	0%	20%	5%	-	-	-	0%	0%	5%	0%	0%	0%	0%	0%	0%	0%	0%	0%	0%	0%
	0.75	0%	80%	75%	-	-	-	0%	0%	75%	0%	30%	0%	0%	0%	0%	20%	0%	0%	0%	0%
	1.00	0%	90%	85%	-	-	-	0%	0%	90%	0%	75%	0%	0%	0%	60%	80%	0%	0%	0%	0%
	1.25	0%	100%	100%	-	-	-	0%	0%	100%	5%	100%	0%	0%	0%	100%	100%	0%	0%	55%	0%
	1.50	0%	100%	100%	-	-	-	0%	0%	100%	60%	100%	0%	0%	0%	100%	100%	0%	30%	85%	20%
	1.75	0%	100%	100%	-	-	-	0%	0%	100%	80%	100%	0%	0%	0%	100%	100%	0%	60%	95%	30%
Bridge	SF	Transverse Limit State Occurrence																			
		Ideal								Acceptable								Unacceptable			
		BF	SL	CL	RE	RY	RF	FY	FF	APY	APB	APS	PA	PPY	PPS	SM	CM	BU	SS	CS	APR
SIC15EA	0.50	0%	100%	100%	100%	0%	0%	-	-	0%	0%	0%	0%	0%	0%	30%	65%	0%	0%	0%	0%
	0.75	0%	100%	100%	100%	0%	0%	-	-	0%	0%	0%	0%	0%	0%	80%	85%	0%	0%	0%	0%
	1.00	0%	100%	100%	100%	0%	0%	-	-	10%	0%	0%	0%	0%	0%	100%	100%	0%	0%	35%	0%
	1.25	0%	100%	100%	100%	0%	0%	-	-	75%	0%	20%	0%	0%	0%	100%	100%	0%	30%	100%	0%
	1.50	0%	100%	100%	100%	0%	0%	-	-	90%	10%	50%	0%	0%	0%	100%	100%	0%	75%	100%	0%
	1.75	0%	100%	100%	100%	0%	0%	-	-	100%	20%	75%	0%	0%	0%	100%	100%	0%	85%	100%	15%
SIC15FA	0.50	0%	100%	100%	-	-	-	0%	0%	0%	0%	0%	0%	0%	0%	5%	10%	0%	0%	0%	0%
	0.75	0%	100%	100%	-	-	-	0%	0%	0%	0%	0%	0%	0%	0%	35%	75%	0%	0%	0%	0%
	1.00	0%	100%	100%	-	-	-	0%	0%	0%	0%	0%	0%	0%	0%	75%	90%	0%	0%	25%	0%
	1.25	0%	100%	100%	-	-	-	0%	0%	35%	0%	0%	0%	0%	0%	95%	100%	0%	10%	65%	0%
	1.50	0%	100%	100%	-	-	-	0%	0%	90%	0%	20%	0%	0%	0%	100%	100%	0%	60%	100%	0%
	1.75	0%	100%	100%	-	-	-	0%	0%	100%	15%	55%	0%	0%	0%	100%	100%	0%	85%	100%	5%

Table 4.8: Frequency of Limit State Occurrences for the IDA of Four-Span Steel IABs With 40-ft Tall Piers, Where a Scale Factor of 1.00 Represents the Design-Level

Bridge	SF	Longitudinal Limit State Occurrence																			
		Ideal								Acceptable								Unacceptable			
		BF	SL	CL	RE	RY	RF	FY	FF	APY	APB	APS	PA	PPY	PPS	SM	CM	BU	SS	CS	APR
SIC40EA	0.50	0%	0%	0%	0%	0%	0%	-	-	35%	0%	10%	0%	0%	0%	0%	0%	0%	0%	0%	0%
	0.75	0%	15%	0%	0%	0%	0%	-	-	100%	0%	70%	0%	0%	0%	0%	0%	0%	0%	0%	0%
	1.00	0%	75%	50%	0%	0%	0%	-	-	100%	15%	100%	0%	0%	0%	0%	5%	0%	0%	0%	0%
	1.25	0%	85%	80%	0%	0%	0%	-	-	100%	50%	100%	0%	0%	10%	20%	30%	0%	0%	0%	15%
	1.50	0%	95%	85%	0%	0%	0%	-	-	100%	80%	100%	0%	0%	20%	55%	80%	0%	0%	10%	30%
	1.75	0%	100%	85%	0%	0%	0%	-	-	100%	80%	100%	0%	0%	30%	75%	80%	0%	0%	20%	50%
SIC40FA	0.50	0%	0%	0%	-	-	-	0%	0%	35%	0%	10%	0%	0%	0%	0%	0%	0%	0%	0%	0%
	0.75	0%	0%	0%	-	-	-	0%	0%	100%	0%	70%	0%	0%	0%	0%	0%	0%	0%	0%	0%
	1.00	0%	75%	50%	-	-	-	0%	0%	100%	15%	100%	0%	0%	5%	0%	0%	0%	0%	0%	0%
	1.25	0%	85%	80%	-	-	-	0%	0%	100%	50%	100%	0%	0%	25%	20%	25%	0%	0%	0%	15%
	1.50	0%	95%	85%	-	-	-	0%	0%	100%	80%	100%	0%	0%	35%	40%	65%	0%	0%	5%	30%
	1.75	0%	100%	85%	-	-	-	0%	0%	100%	80%	100%	0%	0%	40%	70%	75%	0%	0%	20%	50%
Bridge	SF	Transverse Limit State Occurrence																			
		Ideal								Acceptable								Unacceptable			
		BF	SL	CL	RE	RY	RF	FY	FF	APY	APB	APS	PA	PPY	PPS	SM	CM	BU	SS	CS	APR
SIC40EA	0.50	0%	100%	100%	100%	0%	0%	-	-	35%	0%	0%	0%	0%	0%	0%	10%	0%	0%	0%	0%
	0.75	0%	100%	100%	100%	0%	0%	-	-	90%	0%	15%	0%	0%	0%	70%	75%	0%	0%	0%	0%
	1.00	0%	100%	100%	100%	0%	0%	-	-	100%	5%	80%	0%	0%	0%	85%	85%	0%	0%	0%	0%
	1.25	0%	100%	100%	100%	0%	0%	-	-	100%	25%	75%	0%	0%	0%	85%	100%	0%	0%	20%	0%
	1.50	0%	100%	100%	100%	0%	0%	-	-	100%	45%	75%	0%	0%	0%	100%	100%	0%	15%	50%	20%
	1.75	0%	100%	100%	100%	0%	0%	-	-	100%	65%	75%	0%	0%	5%	95%	100%	0%	15%	55%	25%
SIC40FA	0.50	0%	100%	100%	-	-	-	0%	0%	20%	0%	0%	0%	0%	0%	0%	15%	0%	0%	0%	0%
	0.75	0%	100%	100%	-	-	-	0%	0%	85%	0%	10%	0%	0%	0%	65%	65%	0%	0%	0%	0%
	1.00	0%	100%	100%	-	-	-	0%	0%	95%	0%	80%	0%	0%	0%	85%	95%	0%	0%	0%	0%
	1.25	0%	100%	100%	-	-	-	0%	0%	100%	25%	75%	0%	0%	0%	95%	100%	0%	0%	30%	0%
	1.50	0%	100%	100%	-	-	-	0%	0%	100%	45%	75%	0%	0%	0%	95%	100%	0%	15%	50%	20%
	1.75	0%	100%	100%	-	-	-	0%	0%	100%	60%	75%	0%	0%	0%	95%	95%	0%	15%	60%	25%

4.4 THREE-SPAN CONCRETE IABS

4.4.1 Design-Level Dynamic Analysis Results

The design-level dynamic analysis results are presented for three-span concrete IABs in Table 4.9. The larger mass present in the three-span concrete IAB superstructure (11.22 kips/ft), as opposed to the three-span steel IAB superstructure (7.019 kips/ft), is shown to have a significant effect by noting the more frequent occurrence of most limit states in Table 4.9 when compared to Table 4.3. The larger masses tend to increase the lateral inertia force produced by the superstructure during ground accelerations, resulting in unacceptable limit states beginning to occur under design-level shaking. As previously pointed out, the three-span concrete IABs with 15-ft tall piers and fixed bearings did not yield results, which is why they are omitted from Table 4.9.

The longitudinal design-level dynamic analysis results show that abutment pile yielding (APY) and mobilization of the soil surrounding the abutment piles (APS) occurs in every analysis. These components tend to encounter large amounts of nonlinear behavior, with the piles reaching strains over 50 times the yield strain and the p-y springs consistently reaching their ultimate capacity. The large strains correspond to frequent occurrences of the abutment pile local buckling (APB) and rupture (APR) limit states. The increased demand in the abutments is expected due to longitudinal loads typically being resisted primarily by the abutments and due to the increased lateral force in concrete IABs. This point is further demonstrated through large backfill contributions, which do not ever mobilize, but do reach levels of backfill contribution larger than experienced in the steel IABs.

In terms of pier column damage in the longitudinal direction, there is frequent light damage (SL and CL) in IABs with 40-ft piers, but moderate damage (SM and CM) is more rare. This is not the case for IABs with 15-ft piers, as they almost always have light damage, frequently have moderate damage, and have severe pier column damage (SS and CS) occurring most of the time in bridges with stiff and alluvial soil conditions. In general, there is more pier column damage in softer soils. The increased occurrence of severe pier column damage in IABs with 15-ft tall piers is due to the increased stiffness of the short piers causing more demand than on the tall piers. Once again, the increased mass of the superstructure increases the number of occurrences of pier damage.

The severe damage to the pier columns has an adverse effect on the overall bridge behavior. As observed in Figure 4.2, this column damage results in a permanent offset to the superstructure of around 16 in. (400 mm).

The design-level dynamic results in the transverse direction also indicate that the APY and APS limit states occur almost all the time. The only exception is the APS limit state in CtC15EH, which still reaches a high frequency with 90% occurrence. The piles reach a lesser state of nonlinear behavior than in the longitudinal direction, by only having strains of around 25 times the yield strain. However, that is still a significant amount of demand placed on the abutment piles, and the APB and APR limit states still do occur often.

Pier column damage in the transverse direction is increased in most cases as compared to the longitudinal results. Light column damage is very frequent across all bridges, while moderate damage is mainly observed in non-stiff soil conditions. Severe pier column damage (SS and CS) is only observed in IABs with 15-ft tall piers. Once again, these results follow the trend of having more pier column damage in bridges with shorter piers. This is due to the increased stiffness of the short piers causing more demand on the piers, which leads to more damage.

Related to the stiffness of the piers is the retainer and fixed bearing behavior. The increased stiffness in the piers allow for more force to be transferred through the bearings (from the superstructure to the pier cap). This is shown with CtC15E always encountering retainer fusing (RF), while CtC40E models only encounter retainer fusing sometimes. This is also observed with the fixed bearings, where the anchor bolts always yield (FY), yet never fuse (FF), due to the 40-ft tall piers limiting the amount of force transferred through the bearings. In general, the occurrences of retainer yielding (RY) and fusing (RF) are increased when compared to the three-span steel IABs, due to the increased superstructure mass creating larger forces in the bridge.

Fusing of the retainers has an interesting effect on overall bridge behavior, as shown in Figure 4.3. Initially, the behavior follows a pattern observed in other bridges, which is mostly linear with a bit of pinching due to retainer engagement. However, upon fusing of the retainers, the stiffness of a bridge decreases due to the lack of retainers for resisting larger displacements.

The IABs with short piers are deemed to have overall unacceptable behavior due to their consistent severe pier column damage. The exception to this is if the foundation soil is extremely stiff, in which case unacceptable limit states do not occur. The IABs with tall piers are generally unacceptable due to large amounts of abutment pile strain (frequent occurrences of APR) and no backfill mobilization (BF). Ideally, the amount of pile strain should be reduced, while backfill contributions could be increased.

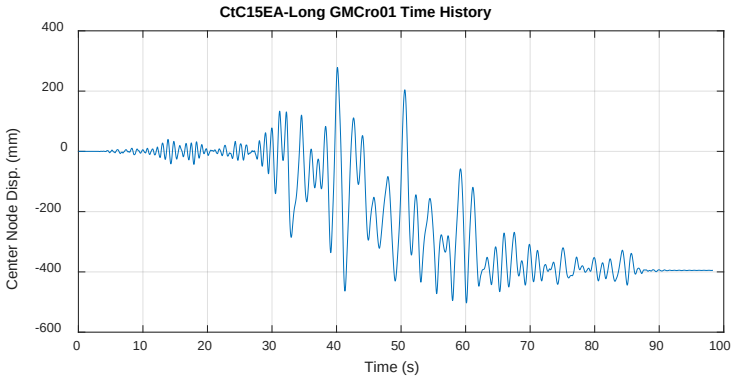

Figure 4.2: Center node displacement time history of CtC15EA subjected to a longitudinal design-level ground motion.

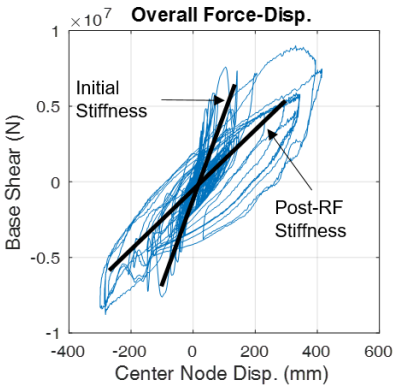

Figure 4.3: Center node displacement-base shear behavior of CtC15EA subjected to a longitudinal design-level ground motion.

Table 4.9: Frequency of Limit State Occurrences for Three-Span Concrete IABs Under the Design-Level Ground Motion Suite

Bridge	Longitudinal Limit State Occurrence																			
	Ideal								Acceptable								Unacceptable			
	BF	SL	CL	RE	RY	RF	FY	FF	APY	APB	APS	PA	PPY	PPS	SM	CM	BU	SS	CS	APR
CtC15ES	0%	100%	100%	0%	0%	0%	-	-	100%	70%	100%	0%	0%	0%	85%	85%	0%	20%	75%	15%
CtC15EA	0%	100%	100%	0%	0%	0%	-	-	100%	75%	100%	0%	0%	0%	75%	85%	0%	5%	50%	20%
CtC15EH	0%	100%	80%	0%	0%	0%	-	-	100%	25%	100%	0%	0%	0%	25%	25%	0%	0%	0%	0%
CtC40ES	0%	75%	70%	0%	0%	0%	-	-	100%	65%	100%	0%	0%	10%	20%	30%	0%	0%	0%	15%
CtC40EA	0%	80%	75%	0%	0%	0%	-	-	100%	80%	100%	0%	0%	0%	20%	20%	0%	0%	0%	30%
CtC40EH	0%	55%	40%	0%	0%	0%	-	-	100%	75%	100%	0%	0%	10%	0%	5%	0%	0%	0%	20%
CtC40FS	0%	75%	70%	-	-	-	0%	0%	100%	70%	100%	0%	0%	15%	25%	30%	0%	0%	0%	15%
CtC40FA	0%	80%	65%	-	-	-	0%	0%	100%	80%	100%	0%	0%	15%	20%	20%	0%	0%	0%	30%
CtC40FH	0%	55%	35%	-	-	-	0%	0%	100%	75%	100%	0%	0%	0%	0%	5%	0%	0%	0%	20%
Bridge	Transverse Limit State Occurrence																			
	Ideal								Acceptable								Unacceptable			
	BF	SL	CL	RE	RY	RF	FY	FF	APY	APB	APS	PA	PPY	PPS	SM	CM	BU	SS	CS	APR
CtC15ES	0%	95%	80%	100%	100%	100%	-	-	100%	80%	100%	0%	0%	0%	65%	65%	0%	25%	50%	15%
CtC15EA	0%	100%	80%	100%	100%	100%	-	-	100%	90%	100%	0%	0%	0%	40%	40%	0%	5%	15%	10%
CtC15EH	0%	70%	45%	100%	100%	100%	-	-	100%	90%	90%	0%	0%	0%	0%	0%	0%	0%	0%	0%
CtC40ES	0%	85%	80%	100%	100%	60%	-	-	100%	75%	100%	0%	0%	0%	40%	50%	0%	0%	0%	15%
CtC40EA	0%	95%	80%	100%	100%	65%	-	-	100%	90%	100%	0%	0%	0%	25%	35%	0%	0%	0%	30%
CtC40EH	0%	90%	70%	100%	100%	20%	-	-	100%	100%	100%	0%	0%	0%	0%	5%	0%	0%	0%	45%
CtC40FS	0%	100%	100%	-	-	-	100%	0%	100%	80%	100%	0%	0%	0%	55%	60%	0%	0%	0%	15%
CtC40FA	0%	100%	95%	-	-	-	100%	0%	100%	90%	100%	0%	0%	0%	30%	55%	0%	0%	0%	25%
CtC40FH	0%	100%	100%	-	-	-	100%	0%	100%	100%	100%	0%	0%	0%	5%	10%	0%	0%	0%	20%

4.4.2 Incremental Dynamic Analysis Results

The frequency of limit state occurrences during the IDA of the three-span concrete IABs is presented in Table 4.10 for IABs with 15-ft piers and in Table 4.11 for IABs with 40-ft piers. The increased superstructure mass in the concrete IABs creates more damage in all the bridge components when compared to the steel IABs. This is exemplified in Tables 4.10 and 4.11 through APY always occurring in every bridge at every scale factor, APB occurring at scale factors of 0.75 and greater, and APR occurring at the design level and greater. In addition, APS is occurring in every bridge with scale factors of 0.75 or greater, along with increased light pier column damage, which occurs most of the time in analyses with scale factors of 0.75 or greater. Backfill mobilization (BF), which is not encountered in any steel IAB, also begins to occur at larger scale factors.

The pier column damage results provided in Table 4.10 and Table 4.11 provide some other interesting observations. The first of which is that pier column damage of any level (light, moderate, or severe) is rare at the 0.5 scale factor level. Light pier column damage (SL and CL) occurs frequently at scale factors greater than and equal to the design level. Similarly, the design-level scale factor of 1.0 is the beginning of significant amounts of moderate pier column damage (SM and CM) in all bridges, and of severe pier column damage (SS and CS) in IABs with 15-ft piers. The increased likelihood of severe damage in IABs with short piers can once again be attributed to the increased stiffness of the piers leading to greater demands on them. There is much more damage to the retainers and fixed bearings in three-span concrete IABs as compared to three-span steel IABs. This is shown by retainer yielding (RY) always occurring at every scale factor and retainer fusing (RF) always occurring at scale factors of 0.75 and larger in IABs with 15-ft piers. In IABs with 40-ft piers, RF frequently occurs at scale factors equal to and larger than 1.0, and always at the 1.5 and larger scale factor. Fixed bearings almost always yield (FY) at every scale factor, with the sole exception being the 80% occurrence at a scale factor of 0.5 in Table 4.10. Despite this, fixed bearing fusing (FF) is still elusive, as it only occurs in 20% of the analyses at the MCE-level scale factor of 1.75. These results once again show the tendency for the shorter, stiffer piers to create more demand on the piers and bearings.

The IDA demonstrates similar deck displacements for IABs of varying pier heights. Common themes in both directions also include that IABs with 15-ft piers have larger pier strains, especially after moderate pier column damage becomes more predominant in the longitudinal direction at a scale factor of 0.75, and in the transverse direction at a scale factor of 1.0. The abutment p-y springs also reach their ultimate capacity at very low scale factors. In the longitudinal direction, IABs with 40-ft piers consistently experience more pile strain, and some results of the backfill force at large scale factors are also seen to reach the ultimate capacity.

IABs with 15-ft piers tend to have more force in the retainers, as expected, due to the increased pier demand with short piers. However, this hardly matters as the retainers for all bridges fuse after scale factors of 1.0. The force in the fixed bearings are limited at scale factors of 0.75 and larger, indicating a fuse is occurring elsewhere in the bridge. The fuse is likely the moderate damage of the pier columns, which begins to occur at scale factors of 0.75 and typically signifies the maximum lateral force that the piers can resist.

Table 4.10: Frequency of Limit State Occurrences for the IDA of Three-Span Concrete IABs With 15-ft Tall Piers, Where a Scale Factor of 1.00 Represents the Design-Level

Bridge	SF	Longitudinal Limit State Occurrence																			
		Ideal								Acceptable								Unacceptable			
		BF	SL	CL	RE	RY	RF	FY	FF	APY	APB	APS	PA	PPY	PPS	SM	CM	BU	SS	CS	APR
CtC15EA	0.50	0%	0%	0%	0%	0%	0%	-	-	100%	0%	55%	0%	0%	0%	0%	0%	0%	0%	0%	0%
	0.75	0%	95%	65%	0%	0%	0%	-	-	100%	5%	100%	0%	0%	0%	15%	20%	0%	0%	0%	0%
	1.00	0%	100%	100%	0%	0%	0%	-	-	100%	75%	100%	0%	0%	0%	75%	85%	0%	5%	50%	20%
	1.25	0%	100%	100%	0%	0%	0%	-	-	100%	85%	100%	0%	0%	0%	85%	90%	0%	35%	80%	60%
	1.50	10%	100%	100%	0%	0%	0%	-	-	100%	90%	100%	0%	10%	5%	90%	100%	0%	50%	75%	70%
	1.75	20%	100%	100%	5%	5%	0%	-	-	100%	100%	100%	0%	25%	15%	100%	100%	10%	70%	80%	70%
Bridge	SF	Transverse Limit State Occurrence																			
		Ideal								Acceptable								Unacceptable			
		BF	SL	CL	RE	RY	RF	FY	FF	APY	APB	APS	PA	PPY	PPS	SM	CM	BU	SS	CS	APR
CtC15EA	0.50	0%	0%	0%	100%	100%	5%	-	-	80%	0%	25%	0%	0%	0%	0%	0%	0%	0%	0%	0%
	0.75	0%	100%	25%	100%	100%	100%	-	-	100%	40%	100%	0%	0%	0%	0%	0%	0%	0%	0%	0%
	1.00	0%	100%	80%	100%	100%	100%	-	-	100%	90%	100%	0%	0%	0%	40%	40%	0%	5%	15%	10%
	1.25	0%	95%	85%	100%	100%	100%	-	-	100%	100%	100%	0%	0%	0%	80%	80%	0%	45%	65%	55%
	1.50	0%	95%	85%	100%	100%	100%	-	-	100%	100%	100%	0%	20%	20%	80%	80%	20%	75%	80%	80%
	1.75	0%	100%	95%	100%	100%	100%	-	-	100%	100%	100%	0%	20%	20%	80%	80%	20%	75%	80%	80%

Table 4.11: Frequency of Limit State Occurrences for the IDA of Three-Span Concrete IABs With 40-ft Tall Piers, Where a Scale Factor of 1.00 Represents the Design-Level

Bridge	SF	Longitudinal Limit State Occurrence																			
		Ideal								Acceptable								Unacceptable			
		BF	SL	CL	RE	RY	RF	FY	FF	APY	APB	APS	PA	PPY	PPS	SM	CM	BU	SS	CS	APR
CtC40EA	0.50	0%	0%	0%	0%	0%	0%	-	-	100%	0%	75%	0%	0%	0%	0%	0%	0%	0%	0%	0%
	0.75	0%	55%	15%	0%	0%	0%	-	-	100%	45%	100%	0%	0%	5%	0%	0%	0%	0%	0%	0%
	1.00	0%	80%	75%	0%	0%	0%	-	-	100%	80%	100%	0%	0%	0%	20%	20%	0%	0%	0%	30%
	1.25	0%	85%	75%	0%	0%	0%	-	-	100%	85%	100%	0%	0%	20%	30%	50%	0%	0%	5%	70%
	1.50	10%	85%	75%	0%	0%	0%	-	-	100%	90%	100%	0%	5%	50%	50%	70%	0%	15%	20%	70%
	1.75	20%	90%	75%	0%	0%	0%	-	-	100%	90%	100%	0%	20%	30%	70%	70%	0%	20%	25%	70%
CtC40FA	0.50	0%	0%	0%	-	-	-	0%	0%	100%	0%	75%	0%	0%	0%	0%	0%	0%	0%	0%	0%
	0.75	0%	45%	20%	-	-	-	0%	0%	100%	45%	100%	0%	0%	0%	0%	0%	0%	0%	0%	0%
	1.00	0%	80%	65%	-	-	-	0%	0%	100%	80%	100%	0%	0%	15%	20%	20%	0%	0%	0%	30%
	1.25	0%	85%	75%	-	-	-	0%	0%	100%	85%	100%	0%	0%	5%	30%	45%	0%	0%	5%	70%
	1.50	10%	85%	75%	-	-	-	0%	0%	100%	90%	100%	0%	0%	20%	45%	70%	0%	10%	20%	70%
	1.75	20%	90%	85%	-	-	-	0%	0%	100%	90%	100%	0%	20%	15%	70%	70%	0%	20%	25%	70%
Bridge	SF	Transverse Limit State Occurrence																			
		Ideal								Acceptable								Unacceptable			
		BF	SL	CL	RE	RY	RF	FY	FF	APY	APB	APS	PA	PPY	PPS	SM	CM	BU	SS	CS	APR
CtC40EA	0.50	0%	5%	0%	100%	100%	0%	-	-	100%	5%	80%	0%	0%	0%	0%	0%	0%	0%	0%	0%
	0.75	0%	85%	60%	100%	100%	0%	-	-	100%	75%	100%	0%	0%	0%	0%	0%	0%	0%	0%	0%
	1.00	0%	95%	80%	100%	100%	65%	-	-	100%	90%	100%	0%	0%	0%	25%	35%	0%	0%	0%	30%
	1.25	0%	100%	85%	100%	100%	85%	-	-	100%	100%	100%	0%	0%	0%	55%	65%	0%	0%	10%	70%
	1.50	0%	100%	90%	100%	100%	100%	-	-	100%	100%	100%	0%	0%	0%	65%	70%	0%	20%	20%	70%
	1.75	0%	100%	95%	100%	100%	100%	-	-	100%	100%	100%	0%	0%	0%	70%	75%	0%	20%	30%	75%
CtC40FA	0.50	0%	15%	5%	-	-	-	80%	0%	100%	5%	70%	0%	0%	0%	0%	0%	0%	0%	0%	0%
	0.75	0%	100%	80%	-	-	-	100%	0%	100%	80%	100%	0%	0%	0%	0%	0%	0%	0%	0%	0%
	1.00	0%	100%	95%	-	-	-	100%	0%	100%	90%	100%	0%	0%	0%	30%	55%	0%	0%	0%	25%
	1.25	0%	100%	100%	-	-	-	100%	0%	100%	100%	100%	0%	0%	0%	70%	80%	0%	0%	15%	65%
	1.50	0%	100%	100%	-	-	-	100%	0%	100%	100%	100%	0%	0%	0%	75%	80%	0%	20%	20%	70%
	1.75	0%	100%	100%	-	-	-	100%	20%	100%	100%	100%	0%	0%	0%	80%	85%	5%	20%	30%	75%

4.5 FOUR-SPAN CONCRETE INTEGRAL ABUTMENT BRIDGES

4.5.1 Design-Level Dynamic Analysis Results

The design-level dynamic analysis results for four-span concrete IABs follows similar trends to the three-span concrete IABs in that they experience more damage than their steel counterparts. The additional occurrence of certain limit states, as presented in Table 4.12, is again due to the increased weight of the concrete superstructure (13.59 kips/ft) as opposed to the steel superstructure (8.204 kips/ft). Additionally, there is a lot of pier column and abutment damage in the transverse direction due to the four-span concrete IABs being extremely flexible in that direction. As previously noted, the ClC15F models were unable to yield results at the design-level, so they are not included in Table 4.12.

Dynamic results in the longitudinal direction indicate that damage to the abutment foundation through abutment pile yielding (APY) and mobilization of the soil surrounding the piles (APS) almost always occurs under design-level shaking. This can be confirmed through the high levels of nonlinearity experienced by the abutment piles and p-y springs. The abutment piles reach a strain of nearly 100 times the yield strain, often triggering the APR limit state, and the p-y springs consistently reach their ultimate capacity. Similar to the three-span concrete IABs, the large amount of lateral force caused by the inertia of the heavy superstructure is mainly resisted by the abutments in the longitudinal direction. This not only explains the frequent damage to the abutment foundation, but it also allows for large amounts of backfill contribution.

Pier column damage in the longitudinal direction indicates that severe damage is common in IABs with 15-ft piers. In IABs with 40-ft tall piers, light pier damage commonly occurs, moderate pier damage occurs often as well, but severe damage is extremely rare. This discrepancy can once again be attributed to the shorter, stiffer piers distributing the lateral force such that they have a higher demand in the columns and therefore suffer more damage. The taller, less stiff piers distribute the force such that there is more demand on the abutments and less on the columns, leading to less pier column damage.

The severe pier column damage observed in ClC15EA is shown to have an adverse effect on overall bridge behavior. Similar to in CtC15EA, the severe pier column damage causes a permanent offset in the IAB superstructure of close to 60 in. (1500 mm).

The transverse direction results provided in Table 4.12 demonstrate that although APY, APB, APR, and APS do occur frequently, it is less frequent than in the longitudinal direction. Another observation is that there are more APY, APB, APR and APS occurrences in IABs with 40-ft tall piers. This follows the trend that IABs with taller, less stiff piers redistribute the force such that there is less force on the piers and more on the abutments. The abutment pile and p-y behavior for ClC15EA indicates that the piles barely yield and p-y springs only briefly reach their ultimate capacity. This follows well with the Table 4.12 observations given the low frequency of APY and APS and the lack of APR occurrences.

Table 4.12: Frequency of Limit State Occurrences for Four-Span Concrete IABs Under the Design-Level Ground Motion Suite

Bridge	Longitudinal Limit State Occurrence																			
	Ideal								Acceptable								Unacceptable			
	BF	SL	CL	RE	RY	RF	FY	FF	APY	APB	APS	PA	PPY	PPS	SM	CM	BU	SS	CS	APR
CIC15ES	0%	93%	93%	0%	0%	0%	-	-	100%	33%	100%	0%	0%	0%	67%	67%	0%	0%	67%	0%
CIC15EA	0%	94%	94%	0%	0%	0%	-	-	100%	59%	100%	0%	0%	0%	76%	76%	0%	6%	76%	6%
CIC15EH	0%	90%	90%	0%	0%	0%	-	-	100%	70%	100%	0%	0%	0%	75%	80%	0%	20%	70%	20%
CIC40ES	0%	75%	70%	0%	0%	0%	-	-	100%	60%	95%	0%	0%	0%	25%	35%	0%	0%	10%	15%
CIC40EA	0%	75%	70%	0%	0%	0%	-	-	100%	60%	100%	0%	0%	0%	20%	35%	0%	0%	0%	10%
CIC40EH	0%	80%	80%	0%	0%	0%	-	-	100%	80%	100%	0%	0%	0%	15%	25%	0%	0%	0%	20%
CIC40FS	0%	70%	70%	-	-	-	0%	0%	100%	60%	95%	0%	0%	0%	25%	45%	0%	0%	0%	15%
CIC40FA	0%	75%	70%	-	-	-	0%	0%	100%	65%	100%	0%	0%	0%	20%	35%	0%	0%	0%	10%
CIC40FH	0%	80%	70%	-	-	-	0%	0%	100%	80%	100%	0%	0%	0%	10%	20%	0%	0%	0%	25%
Bridge	Transverse Limit State Occurrence																			
	Ideal								Acceptable								Unacceptable			
	BF	SL	CL	RE	RY	RF	FY	FF	APY	APB	APS	PA	PPY	PPS	SM	CM	BU	SS	CS	APR
CIC15ES	0%	100%	100%	100%	100%	0%	-	-	75%	20%	40%	0%	0%	100%	100%	100%	0%	40%	95%	0%
CIC15EA	0%	100%	100%	100%	100%	0%	-	-	75%	15%	55%	0%	0%	0%	100%	100%	0%	35%	100%	0%
CIC15EH	0%	100%	100%	100%	100%	0%	-	-	80%	0%	25%	0%	0%	0%	100%	100%	0%	30%	95%	0%
CIC40ES	0%	100%	100%	100%	100%	0%	-	-	94%	22%	78%	0%	0%	0%	72%	89%	0%	6%	22%	11%
CIC40EA	0%	100%	100%	100%	100%	0%	-	-	100%	20%	85%	0%	0%	0%	75%	90%	0%	0%	25%	20%
CIC40EH	0%	100%	100%	100%	100%	0%	-	-	100%	20%	30%	0%	0%	0%	75%	90%	0%	0%	30%	20%
CIC40FS	0%	100%	100%	-	-	-	10%	0%	95%	25%	65%	0%	0%	0%	85%	100%	0%	10%	30%	20%
CIC40FA	0%	100%	100%	-	-	-	0%	0%	95%	20%	85%	0%	0%	0%	75%	100%	0%	0%	30%	15%
CIC40FH	0%	100%	100%	-	-	-	0%	0%	100%	20%	30%	0%	0%	0%	75%	100%	0%	0%	35%	10%

Due to the very flexible nature of the four-span concrete IABs in the transverse direction, there is frequently severe damage to the piers. As expected, the IABs with shorter, stiffer piers experience much more severe pier column damage than those with taller piers. Light pier column damage always occurs, and moderate pier column damage is also very frequent, with IABs having 15-ft tall piers again experiencing more damage. Located on top of the piers are elastomeric bearing retainers and fixed bearings. The retainers always engage and yield, but never fuse. Although they never fuse, they do yield more often than experienced in the four-span steel IAB case, due to the increased superstructure mass causing more force to be transferred through the bearings. Similar to the retainers, the fixed bearings also never fuse. However, the fixed bearings also rarely yield, with the only occurrences happening just twice in ClC40FS.

The unacceptable limit state of either severe steel or concrete pier column damage consistently occurs in the four-span concrete IABs under design-level shaking. This leads to these bridge designs not being acceptable. The frequent occurrence of severe pier column damage is a major problem. However, the lack of backfill mobilization (BF), retainer fusing (RF), or any fixed bearing damage (FY and FF) did not help the situation. Instead of having these ideal limit states occur and then limit forces to components such as the piers and abutment foundation, they do not occur and those other components frequently fail.

4.5.2 Incremental Dynamic Analysis Results

Table 4.13 and Table 4.14 provide the frequency of limit state occurrences during the IDA for four-span concrete IABs with 15-ft and 40-ft piers, respectively. Damage to the abutment foundation (APY, APB, APR and APS) is increased in this IAB as compared to its steel superstructure counterpart. The increase in damage is observed in the longitudinal direction by both abutment pile yielding (APY) and abutment soil mobilization (APS) occurring in almost all of the analyses at all scale factors. Exceptions to this are the rare analyses where APS does not occur at a scale factor of 0.5. Larger levels of pile strain are also demonstrated by abutment pile local buckling (APB) often occurring at scale factors larger than 0.75, and abutment pile rupture (APR) occurring at scale factors of 1.0 and larger.

In the transverse direction, APY and APS damage does not occur at scale factors as low as those found in the longitudinal direction. However, APY is still extremely frequent despite not hitting 100% occurrence until a scale factor of 1.5 in IABs with 15-ft piers, and a scale factor of 1.0 in IABs with 40-ft piers. The amount of abutment pile strain achieved is also reduced when compared to the longitudinal direction, as demonstrated by the APB and APR limit states. The decreased abutment damage in the transverse direction is due to the extreme flexibility of the four-span IAB in that direction. This distributes more force to the piers and decreases the force in the abutments. Once again, there is more pile damage at the abutments in IABs with 40-ft piers due to their flexibility allowing for increased demand on the abutments when compared to the 15-ft pier IABs.

Pier column damage also increases in the transverse direction when compared to the longitudinal direction due to flexibility of the four-span bridge. Additionally, pier height also

plays a part, with IABs having 15-ft piers experiencing severe pier column damage (SS or CS) in the majority of analyses at scale factors of 0.75 and larger. The damage in the 40-ft piers is reduced, with no severe damage occurring in the longitudinal direction at a scale factor of 1.0 and only 25% of analyses experiencing severe pier column damage at the 1.0 scale factor. However, these values increase to 30% in the longitudinal direction and 60% in the transverse direction at the 1.75 scale factor. The retainers on top of the pier columns always yield (RY) at all scale factors, although they never fuse (RF).

The final limit state of interest is the ideal backfill mobilization limit state (BF). Despite being an ideal limit state, it rarely occurs in other IABs. The maximum frequency of occurrence encountered in Table 4.14 is 15%, which is still low. However, BF does begin to occur at a scale factor of 1.75 for IABs with 15-ft piers and 1.25 for IABs with 40-ft piers. Once again, the increased occurrence of abutment limit states like BF in IABs with taller piers is observed.

Deck displacements experience very similar behavior in the longitudinal direction, regardless of pier height, while the transverse displacements are more affected by the pier height, with 40-ft pier IABs producing larger displacements. In terms of base shear, for both directions the base shear reaches a limit when the occurrence of a significant amount of the analyses encounters severe pier column damage

Other general observations from the IDA include increased pier strains in IABs with 15-ft piers and increased abutment pile strains in the transverse direction in IABs with 40-ft piers, while pile strain is about the same in the longitudinal direction regardless of pier height. These observations once again relate to stiffer piers causing more pier demand, and more flexible piers leading to more abutment demand. The p-y spring behavior is difficult to differentiate due to the maximum p-y spring force consistently reaching the ultimate capacity at very low scale factors in both directions.

The increased abutment demand due to taller, more flexible piers is experienced in the backfill behavior as well. There is more backfill engagement in IABs with 40-ft piers. It is necessary to note that the backfill forces are large. However, very few of the analyses produce backfill forces close to the ultimate backfill capacity (indicated by a normalized force of 1.0). It is encouraging that some analyses at scale factors as low as 1.25 provide backfill so close to mobilizing. However, ideally the median (thick line) IDA curve would be closer to the normalized backfill force of 1.0.

As stated previously, the shorter piers produce more demand at the piers, which include the bearings and retainers. IABs with 15-ft tall piers encounter more retainer force than IABs with 40-ft tall piers. It is also interesting to note that the retainers for both heights of IABs always yield but never fuse, even at large scale factors.

The high flexibility of the four-span concrete IAB in the transverse direction leads to a poor seismic performance where every limit state that occurs begins at the lowest scale factor of 0.5. This result indicates that a four-span concrete IAB may not survive an earthquake of even half the intensity of the design-level seismic event.

Table 4.13: Frequency of Limit State Occurrences for the IDA of Four-Span Concrete IABs With 15-ft Tall Piers, Where a Scale Factor of 1.00 Represents the Design-Level

Bridge	SF	Longitudinal Limit State Occurrence																				
		Ideal								Acceptable								Unacceptable			
		BF	SL	CL	RE	RY	RF	FY	FF	APY	APB	APS	PA	PPY	PPS	SM	CM	BU	SS	CS	APR
ClC15EA	0.50	0%	50%	50%	0%	0%	0%	-	-	100%	0%	85%	0%	0%	0%	0%	0%	0%	0%	0%	0%
	0.75	0%	85%	85%	0%	0%	0%	-	-	100%	20%	100%	0%	0%	0%	70%	80%	0%	0%	50%	0%
	1.00	0%	95%	95%	0%	0%	0%	-	-	100%	65%	100%	0%	0%	0%	80%	80%	0%	5%	80%	5%
	1.25	0%	100%	100%	0%	0%	0%	-	-	100%	70%	100%	0%	0%	0%	85%	85%	0%	20%	75%	20%
	1.50	0%	100%	100%	0%	0%	0%	-	-	100%	70%	100%	0%	0%	0%	90%	95%	0%	20%	85%	25%
	1.75	5%	100%	100%	0%	0%	0%	-	-	100%	80%	100%	5%	0%	0%	95%	95%	0%	20%	95%	35%
Bridge	SF	Transverse Limit State Occurrence																				
		Ideal								Acceptable								Unacceptable			
		BF	SL	CL	RE	RY	RF	FY	FF	APY	APB	APS	PA	PPY	PPS	SM	CM	BU	SS	CS	APR
ClC15EA	0.50	0%	100%	100%	100%	100%	0%	-	-	5%	0%	0%	0%	0%	0%	95%	100%	0%	0%	45%	0%
	0.75	0%	100%	100%	100%	100%	0%	-	-	65%	0%	15%	0%	0%	0%	100%	100%	0%	5%	85%	0%
	1.00	0%	100%	100%	100%	100%	0%	-	-	75%	15%	55%	0%	0%	0%	100%	100%	0%	35%	100%	0%
	1.25	0%	100%	100%	100%	100%	0%	-	-	80%	15%	65%	0%	0%	0%	100%	100%	0%	30%	100%	5%
	1.50	0%	100%	100%	100%	100%	0%	-	-	100%	30%	75%	0%	0%	0%	100%	100%	0%	40%	100%	5%
	1.75	0%	100%	100%	100%	100%	0%	-	-	100%	35%	80%	0%	0%	0%	100%	100%	0%	45%	100%	5%

Table 4.14: Frequency of Limit State Occurrences for the IDA of Four-Span Concrete IABs With 40-ft Tall Piers, Where a Scale Factor of 1.00 Represents the Design-Level

Bridge	SF	Longitudinal Limit State Occurrence																			
		Ideal								Acceptable								Unacceptable			
		BF	SL	CL	RE	RY	RF	FY	FF	APY	APB	APS	PA	PPY	PPS	SM	CM	BU	SS	CS	APR
ClC40EA	0.50	0%	5%	0%	0%	0%	0%	-	-	100%	0%	90%	0%	0%	0%	0%	0%	0%	0%	0%	0%
	0.75	0%	75%	60%	0%	0%	0%	-	-	100%	30%	100%	0%	0%	0%	10%	20%	0%	0%	0%	0%
	1.00	0%	75%	70%	0%	0%	0%	-	-	100%	60%	100%	0%	0%	0%	20%	35%	0%	0%	0%	10%
	1.25	10%	80%	75%	0%	0%	0%	-	-	100%	70%	100%	0%	0%	0%	35%	60%	0%	10%	20%	30%
	1.50	15%	85%	80%	0%	0%	0%	-	-	100%	70%	100%	0%	5%	5%	45%	70%	0%	15%	30%	35%
	1.75	15%	90%	90%	0%	0%	0%	-	-	100%	80%	100%	0%	5%	5%	50%	70%	0%	15%	30%	40%
Bridge	SF	Transverse Limit State Occurrence																			
		Ideal								Acceptable								Unacceptable			
		BF	SL	CL	RE	RY	RF	FY	FF	APY	APB	APS	PA	PPY	PPS	SM	CM	BU	SS	CS	APR
ClC40EA	0.50	0%	100%	90%	100%	100%	0%	-	-	55%	0%	20%	0%	0%	0%	40%	55%	0%	0%	5%	0%
	0.75	0%	100%	100%	100%	100%	0%	-	-	75%	20%	55%	0%	0%	0%	65%	75%	0%	0%	10%	0%
	1.00	0%	100%	100%	100%	100%	0%	-	-	100%	20%	85%	0%	0%	0%	75%	90%	0%	0%	25%	20%
	1.25	0%	100%	100%	100%	100%	0%	-	-	100%	30%	90%	0%	0%	0%	95%	100%	0%	20%	35%	20%
	1.50	0%	100%	100%	100%	100%	0%	-	-	100%	35%	95%	0%	0%	0%	100%	100%	0%	20%	50%	20%
	1.75	0%	100%	100%	100%	100%	0%	-	-	100%	50%	100%	0%	0%	0%	100%	100%	0%	20%	60%	30%

4.6 VARIATION OF GROUND MOTION INTENSITY

Bridge designs identical to those described above were also subjected to ground motions at locations in southern Illinois other than Cairo. These locations correspond to ten sites around southern Illinois for which ground motion time histories were developed. The IABs of interest for this portion of the study include only one IAB for each superstructure material and span configuration combination (single-span steel, three-span steel, four-span steel, three-span concrete, and four-span concrete). Each of the five IABs have 15-ft pier heights and realistic soil foundation conditions. Realistic soil foundation conditions consist of alluvial (models ending with A) and non-alluvial (models ending with N) soil conditions. The use of either alluvial or non-alluvial soil conditions varies from site to site depending on the soil conditions found to be most appropriate for the ten actual sites. The sites with alluvial soil conditions are Benton, Cairo, East St. Louis, Mt. Carmel, Salem, and Sparta, and the sites with non-alluvial soil conditions are Anna, Carbondale, Eldorado, and Elizabethtown.

The five IABs at each of the ten sites in southern Illinois are subjected to dynamic analyses using 20 ground motions per site at the design-level 1000-year return period hazard. This allows for a direct comparison to the Cairo design-level results presented earlier. The 20 ground motions used at each site were developed specifically for the site given its geographic hazard and soil conditions. The response spectra for the 20 ground motions used for the design-level dynamic analyses in this chapter can be found in Appendix B. Additionally, Table 4.15 describes the maximum, minimum, and median peak acceleration values for the 20 ground motions. This allows for comparisons and relationships to be made between the sites and the intensity of the ground motions that the IABs are subjected to. From Table 4.15, it can be seen that there is a difference in ground motion intensity between sites at the far south of the state (*i.e.,* Cairo, Anna, Elizabethtown) that have relatively large peak accelerations, and more north in southern Illinois (*i.e.,* Salem, East St. Louis, Mt. Carmel), which have relatively small peak accelerations.

Table 4.15: Statistics for the Peak Acceleration Values, a_{max}, in the Sets of 20 Ground Motions at Each Southern Illinois Site

Site	Peak Acceleration, a_{max} (g)		
	Minimum	Maximum	Median
Anna	0.1924	0.2421	0.2176
Benton	0.1410	0.2102	0.1709
Cairo	0.2601	0.3429	0.3049
Carbondale	0.1655	0.2099	0.1861
East St. Louis	0.0843	0.1650	0.1248
Eldorado	0.1295	0.1914	0.1732
Elizabethtown	0.1489	0.2047	0.1735
Mt. Carmel	0.0930	0.1732	0.1309
Salem	0.0900	0.1752	0.1281
Sparta	0.1203	0.1982	0.1499

The goal of this part of the study is to assess how much the drop in intensity of design-level ground motions affects the behavior of IABs during an earthquake. The results will help determine whether the vulnerabilities in the IABs assessed earlier perhaps warrant some enhancements to IAB designs throughout all of southern Illinois, or maybe just within the region surrounding Cairo. This is assessed by grouping the southern Illinois sites into their appropriate seismic performance zones (SPZs) and then making assessments based on the overall trends within each SPZ. Three SPZs are encountered in southern Illinois: SPZ 4, SPZ 3, and SPZ 2. SPZ 4 is the zone of largest earthquake intensity and encompasses the most southern portion of the state. Slightly further north is SPZ 3, followed by SPZ 2 even further north.

In order to make reading the tables in this chapter easier, the sites are arranged such that SPZ 4 locations are at the top, followed by SPZ 3 and SPZ 2 sites. Within the SPZs themselves, the sites are arranged based on latitude due to SPZ being strongly tied to latitude in southern Illinois. The only exception to the latitude sorting is with respect to Anna and Elizabethtown in SPZ 3. While Anna is further north, it is actually closer to the SPZ 3-4 border, leading it to have larger ground motion intensities than Elizabethtown. The sorting of the ten sites is presented in Table 4.16, along with the SPZ, latitude, and median peak acceleration of the ground motions appropriate for each site. SPZ 4 only comprises of Cairo. However, Anna is extremely close to being in SPZ 4, despite actually being in SPZ 3. In addition to Anna, SPZ 3 also contains Elizabethtown, Carbondale, Eldorado, and Benton. SPZ 2 consists of Sparta, Mt. Carmel, East St. Louis, and Salem.

Table 4.16: Site, Characteristics Related to Seismic Performance Zone, Latitude, and Median Peak Acceleration Values

Site	Seismic Performance Zone	Latitude (°)	Median a_{max} (g)
Cairo	4	37.013	0.3049
Anna	3	37.461	0.2176
Elizabethtown	3	37.449	0.1735
Carbondale	3	37.726	0.1861
Eldorado	3	37.814	0.1732
Benton	3	38.004	0.1709
Sparta	2	38.133	0.1499
Mt. Carmel	2	38.415	0.1309
East St. Louis	2	38.617	0.1248
Salem	2	38.628	0.1281

Describing the IAB seismic vulnerabilities based on SPZ is useful. However, it should be noted that while SPZ 4 has the largest hazard in the state, it also mainly consists of a sparsely populated region in Illinois. This can be observed through noting that between 2005 and 2014 there were at least 114 IABs constructed in SPZs 2, 3, and 4 in Illinois, according to the online

inventory of IDOT bridges (IDOT, 2016). Of these 114 IABs, only 5 were in SPZ 4, while 31 were in SPZ 3 and 78 were in SPZ 2. Given this information, it is important to consider while reviewing this chapter that although SPZ 4 produces the largest seismic hazard in Illinois, there are fewer IABs constructed in SPZ 4 than in other regions of Illinois.

4.6.1 Design-Level Dynamic Analysis Results for ClC15EA

Only one set of design-level dynamic analysis results is provided in the body of this report with respect to variation in ground motion intensity. ClC15EA was selected to demonstrate the behavior, as it had the most unacceptable design-level seismic behavior at Cairo. In general, conclusions drawn from ClC15E_ are also applicable for Ss_____, StC15E_, SlC15E_, and CtC15E_. The tables providing their frequency of limit state occurrences can be found in Appendix C.

The design-level dynamic analysis results for the four-span concrete IAB with 15-ft tall piers and realistic soil conditions are provided in Table 4.17. These results demonstrate the high frequency of damage to the abutment piles leading to yielding (APY), local buckling (APB), and mobilization of the soil (APS), as well as severe damage to the pier columns (SS and CS) at Cairo. These are products of the concrete superstructure being much heavier than steel superstructures, leading to increased lateral inertia forces during excitation, as well as from the increased flexibility of the bridge in the transverse direction. It is necessary to note and observe in Table 4.17 that severe pier column concrete damage (CS) occurs in all of the analyses for Cairo in the transverse direction, leading to a design that performs quite unacceptably.

The longitudinal direction results also contain significant CS occurrences at the SPZ 4 site of Cairo. Damage to the piers decreases in Anna, which is very close to the SPZ 3-4 border, but still contains some CS occurrences. Beyond Anna, no pier column damage (SL, CL, SM, CM, SS, and CS) occurs at any other site in the longitudinal direction. This represents a significant drop off in potential pier damage in the longitudinal direction beyond SPZ 4. In the longitudinal direction, the majority of the damage occurs at the abutment foundations, with abutment pile yielding (APY) occurring quite frequently at the southern SPZ 3 sites. However, APY occurrences dissipate to having none at the northern SPZ 3 site of Benton nor at any SPZ 2 site. APB and APR are frequent occurrences in SPZ 4, but they completely disappear in SPZ 3. Mobilization of the soil surrounding the abutment piles (APS) is also common at southern SPZ 3 sites, but reduces to having no occurrences at northern SPZ 3 sites and at SPZ 2 sites. In general, for the longitudinal direction, SPZ 2 sites experience essentially no damage to any components.

Table 4.17: Frequency of Limit State Occurrences During Dynamic Analyses at the Design-Level for Four-Span Concrete IABs Across the Southern Illinois Sites

SPZ	Site	Bridge	Longitudinal Limit State Occurrence																
			Ideal						Acceptable								Unacceptable			
			BF	SL	CL	RE	RY	RF	APY	APB	APS	PA	PPY	PPS	SM	CM	BU	SS	CS	APR
4	Cairo	ClC15EA	0%	94%	94%	0%	0%	0%	100%	65%	100%	0%	0%	0%	76%	76%	0%	6%	76%	5%
3	Anna	ClC15EN	0%	25%	25%	0%	0%	0%	100%	0%	80%	0%	0%	0%	10%	15%	0%	0%	10%	0%
3	Elizabethtown	ClC15EN	0%	0%	0%	0%	0%	0%	100%	0%	25%	0%	0%	0%	0%	0%	0%	0%	0%	0%
3	Carbondale	ClC15EN	0%	0%	0%	0%	0%	0%	80%	0%	0%	0%	0%	0%	0%	0%	0%	0%	0%	0%
3	Eldorado	ClC15EN	0%	0%	0%	0%	0%	0%	15%	0%	0%	0%	0%	0%	0%	0%	0%	0%	0%	0%
3	Benton	ClC15EA	0%	0%	0%	0%	0%	0%	0%	0%	0%	0%	0%	0%	0%	0%	0%	0%	0%	0%
2	Sparta	ClC15EA	0%	0%	0%	0%	0%	0%	0%	0%	0%	0%	0%	0%	0%	0%	0%	0%	0%	0%
2	Mt. Carmel	ClC15EA	0%	0%	0%	0%	0%	0%	0%	0%	0%	0%	0%	0%	0%	0%	0%	0%	0%	0%
2	East St. Louis	ClC15EA	0%	0%	0%	0%	0%	0%	5%	0%	0%	0%	0%	0%	0%	0%	0%	0%	0%	0%
2	Salem	ClC15EA	0%	0%	0%	0%	0%	0%	0%	0%	0%	0%	0%	0%	0%	0%	0%	0%	0%	0%
SPZ	Site	Bridge	Transverse Limit State Occurrence																
			Ideal						Acceptable								Unacceptable			
			BF	SL	CL	RE	RY	RF	APY	APB	APS	PA	PPY	PPS	SM	CM	BU	SS	CS	APR
4	Cairo	ClC15EA	0%	100%	100%	100%	100%	0%	75%	15%	55%	0%	0%	0%	100%	100%	0%	35%	100%	0%
3	Anna	ClC15EN	0%	100%	100%	100%	100%	0%	10%	0%	0%	0%	0%	0%	70%	90%	0%	0%	45%	0%
3	Elizabethtown	ClC15EN	0%	100%	100%	100%	100%	0%	0%	0%	0%	0%	0%	0%	5%	35%	0%	0%	0%	0%
3	Carbondale	ClC15EN	0%	80%	80%	100%	100%	0%	0%	0%	0%	0%	0%	0%	0%	0%	0%	0%	0%	0%
3	Eldorado	ClC15EN	0%	35%	40%	100%	90%	0%	0%	0%	0%	0%	0%	0%	0%	0%	0%	0%	0%	0%
3	Benton	ClC15EA	0%	20%	20%	100%	85%	0%	0%	0%	0%	0%	0%	0%	0%	0%	0%	0%	0%	0%
2	Sparta	ClC15EA	0%	0%	0%	100%	70%	0%	0%	0%	0%	0%	0%	0%	0%	0%	0%	0%	0%	0%
2	Mt. Carmel	ClC15EA	0%	5%	10%	100%	75%	0%	0%	0%	0%	0%	0%	0%	0%	0%	0%	0%	0%	0%
2	East St. Louis	ClC15EA	0%	15%	15%	100%	70%	0%	0%	0%	0%	0%	0%	0%	0%	0%	0%	0%	0%	0%
2	Salem	ClC15EA	0%	5%	5%	100%	35%	0%	0%	0%	0%	0%	0%	0%	0%	0%	0%	0%	0%	0%

The transverse direction results, also presented in Table 4.17, further show a reduction in pier column damage outside of SPZ 4, but not as large of a reduction as observed in the longitudinal direction. Once again, Anna, which is close to the SPZ 4 border, still experiences significant amounts of severe pier column concrete damage (CS). Additionally, Elizabethtown in SPZ 3 experiences some moderate pier column damage (SM and CM). Beyond these two exceptions, moderate and severe pier column damage is not found at any other sites. Light pier column damage (SL and CL) is present throughout SPZ 3 sites, with the most southern sites experiencing the highest frequencies of occurrence. In SPZ 2 sites, even the light pier column damage rarely occurs. The increased amount of pier damage in the transverse direction, as compared to the longitudinal direction, can be attributed to the increased flexibility of the IAB in this direction. APY and APS experience significant occurrences in SPZ 4, but this quickly reduces to no occurrences in SPZ 3, where it is extremely rare even at Anna. Limit states describing larger abutment pile strains (APB and APR) are rare in SPZ 4 and disappear in SPZ 3. Retainer fusing (RF) does not occur at any site. However, retainer yielding (RY) is frequent throughout all sites, with the frequency of occurrence ranging between 35% and 75% in SPZ 2. As expected, retainer engagement (RE) always occurs due to it ideally occurring under even the smallest amounts of lateral excitation.

By evaluating the limit states reached at the sites in each of the SPZs, it can be determined that in SPZ 2 the performance of the four-span concrete IAB designs are ideal. Relatively northern SPZ 3 sites also tend to have ideal design performance, but as a whole, SPZ 3 is generally acceptable. An exception to this is Anna, where the designs are not acceptable. Given that the designs are not typically acceptable in SPZ 4, and Anna's close proximity to SPZ 4, this observed behavior makes sense.

4.7 OVERALL OBSERVATIONS

General observations and trends can be found through both the design-level and incremental dynamic analysis results. The first observation found across all the analyses is that, in terms of span configuration, the three-span IABs are stiffer than the four-span IABs. In the longitudinal direction, it can be shown that abutment foundation damage (*i.e.,* damage to the abutment piles and their surrounding soil) is about the same regardless of the span configuration. This is due to the entire bridge moving toward one of the abutments in both span configuration cases, leading to similar abutment demands. Additionally, the APY and APS limit states associated with the abutment foundation generally tend to occur relatively frequently at low scale factors, so the contributions are similar due to both the piles yielding and soil mobilizing early in the analyses. Large amounts of abutment pile strains (APB and APR) are generally infrequent in steel IABs, though they are a bit more frequent in concrete IABs. There is a difference between the frequencies of occurrence for pier column damage, though, with four-span IABs producing more pier damage. This is due to the longer spans between piers leading to the piers being required to resist more lateral and axial force.

In the transverse direction, it is shown that there is more abutment foundation damage and less pier column damage in three-span IABs. This is attributed to the shorter, stiffer bridge

allowing for forces to be distributed more evenly, with more force to the abutments and less to the piers than in the four-span bridge. Due to this, the opposite is true for four-span IABs, which experience more pier column damage and less abutment foundation damage. The flexibility of the long-span bridges leads to large pier displacements and large amounts of damage. The four-span IABs perform poorly under transverse excitation, with nearly all the damage limit states occurring under the smallest amount of excitation.

In both directions, damage to the abutment piles is found to be more significant than damage to the pier piles. Strains in the abutment piles frequently reach levels allowing for local buckling and rupture. However, maximum strains in the pier piles rarely cause yielding. In IABs where PPY does occur, the strains rarely become excessively large, with typical maximum strains remaining below 7 times the yield strain. This indicates that local buckling and rupture of the pier piles is likely never encountered.

Trends are also observed when comparing bridges with short (15-ft tall) and tall (40-ft tall) piers. In general, short piers are stiffer than the tall piers and produce similar trends in both directions. With the stiffer short piers, there is an increased demand on the piers, leading to more damage. This increased pier demand decreases the demand on the abutments, and slightly decreases the damage found in the abutment foundations and the strain in the abutment piles. The stiffer piers also lead to more retainer and fixed bearing damage, due to increased forces needing to be transferred through the bearings from the superstructure to the pier caps. This means that that more flexible tall piers experience the opposite behavior, as there is increased abutment foundation damage and decreased pier damage when they are used. This is attributed to the less stiff piers allowing for more force to be distributed to the much stiffer abutments, which increases the demand on the abutments and decreases the demand on the piers.

This trade-off between abutment foundation damage and pier damage is observed numerous times in the analysis results. Ideal IAB seismic behavior would have them both occur under only relatively large earthquakes, so a balance point must be found where neither abutment foundation damage nor pier damage is too frequent. This solution is not ideal, but levels of strain in the abutment piles up to rupture will not lead to unacceptable limit states occurring as is the case with severe pier column damage. There is likely a point where columns are stiff enough and robust enough to accommodate the increased demand, while at the same time sufficiently reducing abutment demand.

As mentioned earlier, there is increased retainer and fixed bearing damage in IABs with shorter piers. There is also a slight trend of having more retainer and fixed bearing damage in three-span IABs. However, the pier height is a much better predictor of retainer and fixed bearing behavior, as some three-span IABs with taller piers do not experience much damage to the retainers and fixed bearings. Pier damage may also play a part, as it has been observed in some cases that the occurrence of moderate pier column damage, which typically coincides with the force capacity of the piers, may act as a fuse and limit further force from being transferred through the bearings. Increased retainer and fixed bearing damage is also observed in concrete

IABs over steel IABs, due to the increased mass of the superstructure causing higher shear forces across the bearings.

Retainer and fixed bearing damage are not the only limit states affected by the superstructure material choice. Concrete IABs are found to produce more damage and/or force in many components such as the backfill, abutment foundation, and pier columns. The extra damage found in these components is attributed to the heavier superstructure, which causes more inertia (lateral) force during an earthquake and therefore leads to more force in most of the components. The added weight of the concrete superstructure also develops larger normal loads in the bearings, which increases the friction force transferred between the superstructure and piers.

Given all these trends, it is found that there are serious seismic design concerns with four-span IABs, especially in the transverse direction and with concrete superstructures. The main components of concern in the IABs are the pier columns and abutment foundations, due to the consistent damage to them. The pier columns often reach severe damage, which could cause failure of the pier and loss of span in a bridge. Severe pier damage usually occurs at earthquake intensities larger than the design-level, but often not too much larger. Abutment foundation damage is a consistent occurrence at the lowest levels of earthquake shaking. Although damage to the abutment foundations may not cause immediate collapse, the amount of strain experienced in the abutment piles can be significant enough to cause pile rupture, and damage to these components is difficult to identify and repair. If left untreated they could have significant negative impacts to a bridge's behavior in future events. Additionally, many components that are desired to fail often do not actually do so. These components include the elastomeric bearing retainers and fixed bearings, whose anchor bolt yielding and fracture could help mitigate the force and damage to other more vulnerable components such as the piers. Damage to the retainers and fixed bearings is easy to identify, and replacement of the components is simple, making them ideal fuses in an IAB.

Results from the design-level dynamic analyses at different sites around southern Illinois with varying ground motion intensity levels indicate that although there are consistent seismic design concerns for IABs at Cairo in SPZ 4, similar IABs are at least acceptable outside of SPZ 4. The only major exception to this is at Anna, where unacceptable designs for four-span concrete IABs are present. However, Anna is extremely close to SPZ 4, further showing that these IAB designs are generally not acceptable in SPZ 4. IAB designs at SPZ 3 sites are generally acceptable, and designs at SPZ 2 sites are frequently ideal, with only light pier damage and retainer damage. As previously noted, while the largest seismic hazard and amount of limit state occurrences is in SPZ 4, the amount of IABs in SPZ4 is relatively sparse in comparison to SPZ 2 and 3. This sparsity of IABs in SPZ 4 reduces the potential risk to the overall inventory of IABs in southern Illinois, although their increased demands certainly should not be ignored in design.

As bridge sites become further north and there is a change in SPZ, certain trends seem to emerge throughout the IABs analyzed. The first observed trend is the relatively small effect that

location has on the occurrence of retainer engagement, yielding, and fusing. Retainer engagement tends to always occur, while there is a slight decrease in retainer yielding and fusing occurrences as the sites become further away from Cairo and the ground motion intensity decreases. However, this decrease in retainer damage is relatively gradual when compared to abutment foundation and pier column damage changes, which decrease rapidly once the site is not in SPZ 4. Across all the IABs analyzed above, the change in limit state occurrences between SPZ 4 and SPZ 3 is a drop to occurring 0% of the time in SPZ 3 if the frequency of occurrence is less than 60% in SPZ 4 (*i.e.*, Cairo). The decrease in pier column damage is especially noticeable in four-span IABs, where the designs typically change from unacceptable due to severe pier column damage in SPZ 4 to acceptable outside of SPZ 4. The reason why the four-span IABs significantly benefit is due to their large spans, which lead to larger superstructure masses when compared to the three-span IABs. The reduction in ground motion accelerations across the sites, as shown in Table 4.15 and Table 4.16, causes a greater reduction in lateral inertia forces in long-span bridges. The four-span concrete IAB especially benefits from this severe decrease in lateral force, due to it being the heaviest bridge analyzed.

Results for the limit state occurrence frequencies at various sites can impact potential IAB designs by ensuring that unnecessary enhancements are not made to designs which already behave ideally during design-level seismic events. Any design enhancements addressing the concerns above are applicable to sites within SPZ 4, such as Cairo. Sites in SPZ 3 are usually acceptable, indicating that they may potentially require enhancements using similar theories, but to a much lesser extent, as those utilized for SPZ 4 sites. This is to ensure the IABs in SPZ 3 have closer to ideal seismic performance. The ideal designs, typically in SPZ 2, require no enhancements as their current designs already yield ideal seismic performance. These results may of course vary slightly with different soil conditions, as liquefaction and significant clay softening due to shaking is not accounted for in these analyses.

CHAPTER 5: RECOMMENDATIONS FOR DESIGN ENHANCEMENTS

The seismic assessment of current integral abutment bridge (IAB) designs in Illinois demonstrated consistent vulnerabilities in the pier columns and abutment foundations. Additionally, the fusing of ideal components, such as the side retainers and fixed bearings, does not necessarily occur in many analyses, leading to increased load in the pier columns. The analyses revealed four areas of concern: the lack of elastomeric bearing side retainer fusing, the lack of fixed bearing fusing, the abundance of pier column damage, and the abundance of abutment foundation damage. This chapter aims to address these concerns by exploring enhancement of IABs, with the objectives of increasing retainer and fixed bearing fusing and reducing damage in the pier columns and abutment foundations. These objectives can be accomplished by reducing the number of retainers in the IAB, reducing the size of the fixed bearing anchor bolts, increasing the size of the pier columns, and/or increasing the backfill contribution at the abutments. The effectiveness of these enhancements is then discussed.

Enhancements are made to separately address the four areas of concern. The enhanced IABs are analyzed using an IDA for the site of Cairo since it has the highest seismic hazard in the state of Illinois, within seismic performance zone (SPZ) 4. As discussed earlier, recommendations that are developed in this chapter may not apply or may only partially apply to sites in SPZs 2 or 3. Many sites in SPZ 3 demonstrate IAB damage to a lesser extent and may still benefit from some of the recommendations presented, but may not require the full spectrum of design enhancements proposed for IABs in SPZ 4. IABs in SPZ 2 typically already exhibit ideal seismic behavior and would most likely not require any of the enhancements described in this chapter.

The full set of IDA results and limit state occurrences comparing the original and enhanced IAB designs are presented in Appendix E.

5.1 REDUCTION IN RETAINER USE

Reducing the number of elastomeric bearing side retainers to two retainers per pier (one at each exterior beam) should be able to enhance retainer yielding and fusing. Currently there is a retainer at the elastomeric bearing of every beam. As retainers fuse, there is a significant drop in the amount of load transferred from the superstructure to the piers. While a lack of retainer fusing does not necessarily indicate poor performance, the fusing of these components is likely more desirable than severe pier column damage.

The two IABs with enhanced designs are StC40EA and SlC15EA. These IABs were selected because steel superstructure IABs consistently experienced less retainer fusing than concrete superstructure IABs, owing to the lighter steel superstructures generating smaller inertial forces that must be transferred through the bearings during an earthquake. These IABs were also selected because they provide a good range of pier force demands including larger force demands (long-span IABs with short piers), and smaller force demands (taller piers).

StC40EA reduces the number of retainers from six per pier to two per pier. The number of retainers per pier in SlC15EA is reduced from eight to two. Additionally, SlC15EA is further modified by weakening the anchor bolts of the retainers in a separate subset of the study. This second enhanced design also includes only two retainers per pier, but the anchor bolts are then reduced from 2-in. diameter to 1.25-in. diameter in order to further encourage retainer fusing.

Transverse IDA results for the maximum pier concrete strain and retainer load of the original and enhanced StC40EA are presented in Figure 5.1. No difference can be found between the two designs in the longitudinal direction, as expected. In the transverse direction, it is found that there is still no retainer fusing (RF, red dashed line in Figure 5.1 (a)) occurring when the number of retainers is decreased, but there is an increase in the frequency of retainer yielding (RY, yellow dashed line in Figure 5.1 (a)). However, there is also a general increase in the force magnitude resisted by the retainers, as presented in the IDA curve of Figure 5.1 (a). In both bridges, Figure 5.1 (a) indicates that the retainer force reaches a maximum value, due to some other component acting as a fuse. This fusing component is the pier columns, whose peak resistance corresponds to the moderate pier column damage limit states (SM and CM). CM begins to occur at scale factors of 1.5 and larger, as shown in Figure 5.1 (b), corresponding to the vertical turn of the retainer behavior at a scale factor of 1.5 in Figure 5.1 (a).

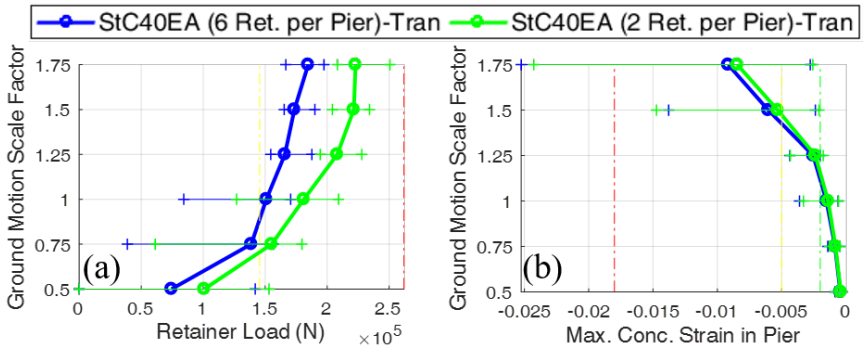

Figure 5.1: Transverse IDA results for the (a) maximum retainer load; and (b) maximum pier column concrete strain in the original and enhanced StC40EA. The dashed lines represent ideal (green), acceptable (yellow), and unacceptable (red) limit state values for the component.

Transverse IDA results for the maximum pier column concrete strain and retainer load for the original and enhanced SlC15EA are presented in Figure 5.2. The results indicate that retainer yielding (RY, yellow dashed line in Figure 5.2 (a)) always occurs and retainer fusing (RF, red dashed line in Figure 5.2 (a) never occurs when the number of retainers is reduced. This occurs despite significantly larger forces developing in the retainers, as shown in Figure 5.2 (a). It can also be noted from Figure 5.2 (a) that the retainer forces do not vary significantly from scale factor to scale factor. This is attributed to moderate pier column damage (SM and CM) occurring at the 0.5 scale factor, as shown in Figure 5.2 (b), which allows the piers to limit the force transferred through the bearings and retainers. The occurrence of SM and CM at low scale factors is due to the high demand placed on stiff piers in long span IABs.

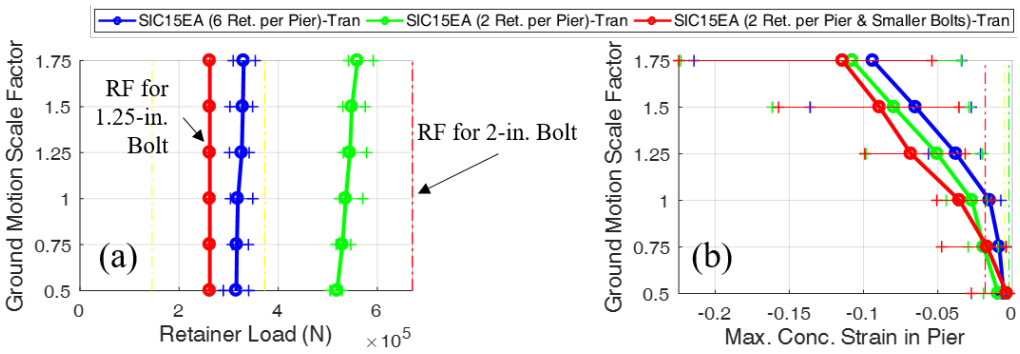

Figure 5.2: Transverse IDA results for the (a) maximum retainer load; and (b) maximum pier column concrete strain in the original and enhanced SIC15EA. The dashed lines represent ideal (green), acceptable (yellow), and unacceptable (red) limit state values for the component.

The lack of retainer fusing in SIC15EA is the motivation behind further weakening the retainers by decreasing the anchor bolt size. Transverse IDA results for SIC15EA with two retainers per pier and smaller anchor bolts are also presented in Figure 5.2. From Figure 5.2 (a), it can be seen that the goal of having the retainers fuse is accomplished with smaller anchor bolts. However, the demand on the piers is still so large that retainer fusing provides only mild relief for the pier column damage observed in SIC15EA, with only two retainers per pier. Nevertheless, it is an improvement. For the most part, the component behavior, aside from retainer behavior, is similar between the IAB with only two retainers per pier and the IAB with two retainers per pier and smaller anchor bolts.

5.2 REDUCTION IN FIXED BEARING RESISTANCE

The fixed bearings also do not fuse in many of the analyses. By reducing the size of the anchor bolts in the fixed bearings, they will become weaker. The goal in doing this is to weaken the fixed bearings such that they fracture and act as fuses, thereby limiting the force transferred to the piers and thus limiting pier column damage. The IABs with revised fixed bearing designs were selected to represent bridges that rarely encounter fixed bearing yielding or fusing under Cairo ground motions. The two IABs selected both have steel superstructures, due to the decreased load being transferred through the bearings when compared to concrete superstructure bridges. The two IABs with enhanced designs are StC40FA and SIC15FA.

The original design of the StC40FA fixed bearings has two 1.25-in. diameter anchor bolts. The enhanced design weakened the anchor bolts as much as allowed by IDOT, by reducing their diameter to 0.625 in. This reduces the ultimate resistance of each fixed bearing from 71 kips (314 kN) to 18 kips (79 kN). The original SIC15FA design has fixed bearings with two 2-in. diameter anchor bolts. The anchor bolt diameter is not reduced all the way to the minimum allowed by IDOT, as this would likely cause the fixed bearings to fuse too easily and encourage bearing unseating. Instead, the enhanced design had the fixed bearing anchor bolts be 1.625 in. in diameter, which reduces the ultimate resistance of each fixed bearing from 181 kips (805 kN) to 119 kips (531 kN).

The transverse IDA results for maximum pier column concrete strain and force transferred through the fixed bearings for the original and enhanced StC40FA are presented in Figure 5.3. The enhanced designs provide an increase in fixed bearing yielding (FY, yellow dashed lines in Figure 5.3 (a)) and fusing (FF, red dashed lines in Fig. 5.3 (a)). Also reflected in Figure 5.3 (a) is that the fixed bearing load in both cases is limited at scale factors of 1.25 and larger. In the original design, this is due to moderate pier column damage occurring at around this scale factor, as shown in Figure 5.3 (b). In the enhanced design, however, this limit is reached due to fixed bearing fusing. Having fixed bearing fusing occur before moderate pier damage allows for the piers to experience slightly less strain and limit state occurrences, as shown in Figure 5.3 (b). Aside from these differences, though, there are no other changes to the component behavior.

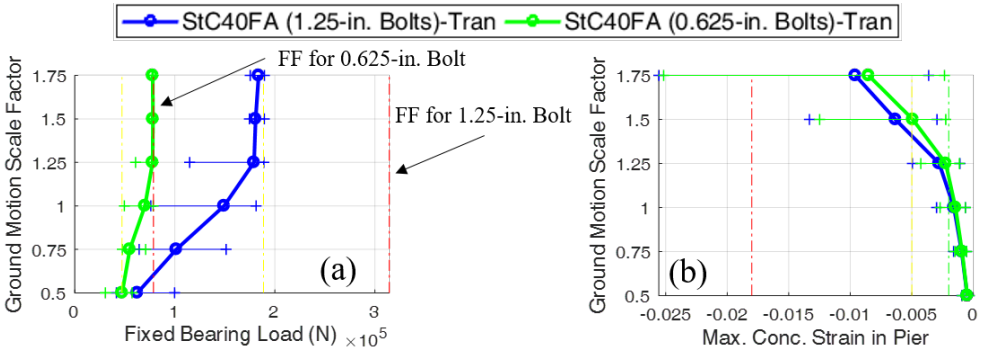

Figure 5.3: Transverse IDA results for the (a) maximum fixed bearing load; and (b) maximum pier column concrete strain in the original and enhanced StC40FA. The dashed lines represent ideal (green), acceptable (yellow), and unacceptable (red) limit state values for the component.

The StC40FA results indicate that there are only minimal changes in behavior despite the inclusion of fixed bearing fusing (FF). Fixed bearing yielding (FY) occurs at smaller scale factors, and severe pier column damage (SS/CS) occurs at slightly large scale factors. From this and the IDA results, it can be determined that IABs with lesser pier demands, such as bridges with taller piers, do show some improvement when the fixed bearing anchor bolt sizes are reduced. This happens by allowing the fixed bearing to fuse first and limit the forces in the columns. However, the minimum diameter of 0.625-in. is still too large to encounter any significant improvement in seismic performance.

The transverse IDA results for pier column concrete strain and force across the fixed bearings of the original and enhanced design of SIC15FA is presented in Figure 5.4. There are extremely minor to no changes in the results despite the fixed bearings being 62 kips (275 kN) weaker and having anchor bolts 0.375-in. smaller in diameter. Figure 5.4 (b) shows that the forces in the fixed bearings are very similar and do not vary much from scale factor to scale factor, leaving the fixed bearings well short of yielding in both designs. This lack of variation in fixed bearing load is due to the forces in the piers. The forces transferred through the bearings are limited by moderate pier column damage that occurs at scale factors as low as 0.5. This is caused by the large load demand in the piers from the short pier and long span characteristics of the IAB.

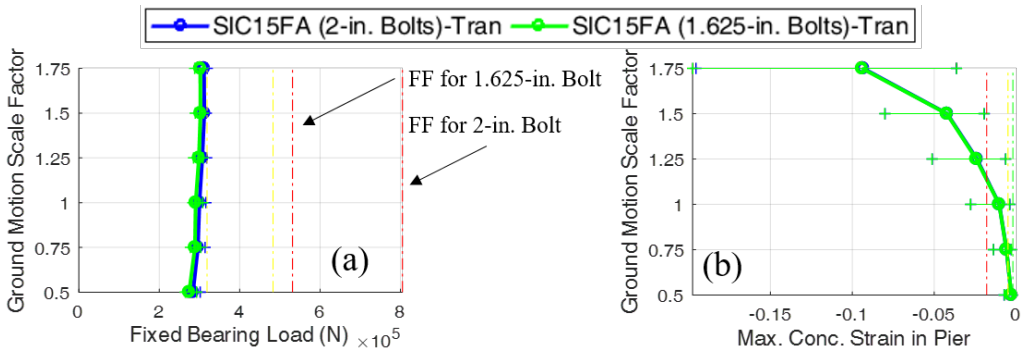

Figure 5.4: Transverse IDA results for the (a) maximum fixed bearing load; and (b) maximum pier column concrete strain in the original and enhanced SIC15FA. The dashed lines represent ideal (green), acceptable (yellow), and unacceptable (red) limit state values for the component.

5.3 STRENGTHENING OF PIER COLUMNS

The frequently expected severe damage to pier columns at moderate ground shaking intensity is of concern in IABs. The greatest damage to the pier columns is observed in concrete IABs with 15-ft tall piers. This is due to the shorter, stiffer piers creating more demand in the pier columns and the concrete superstructure creating more lateral inertia load in the bridge. A potential solution to this concern is to simply increase the size of the pier columns. By doing this, the pier columns will be strengthened and capable of accommodating the large demands without experiencing moderate or severe pier column damage. The original pier column designs for the IABs with 15-ft piers were 2.5-ft diameter concrete columns with (12) #10 reinforcing bars. The enhanced designs assessed in this section use 3-ft diameter concrete columns with (14) #10 bars. Although this reduces the reinforcement ratio in the columns from 2.1% to 1.7%, the overall strength is increased such that it is about twice as strong for the Extreme Event I load combination (AASHTO, 2011).

Both IABs whose designs are enhanced are concrete bridges with 15-ft tall piers. The first enhanced IAB is CtC15EA. In this bridge's original design, severe pier column concrete damage occurs under design-level shaking. The second enhanced IAB is ClC15EA. Due to the extreme flexibility of ClC15EA in the transverse direction, severe pier column concrete damage occurs at the lowest scale factor of 0.5 in the original design.

The longitudinal IDA results for CtC15EA indicate that there is a moderate decrease in pier column damage limit state occurrences, although severe pier column limit states (SS and CS) are still quite frequent at larger scale factors. Despite fewer pier column damage occurrences, there is no increase in abutment foundation damage (APY, APB, APR, and APS). However, the number of APY, APB, APR, and APS occurrences is already quite large in the original design. In the longitudinal IDA, it can be determined that for the most part there is no significant difference in the behavior of the individual components across the ground motion scale factors. The primary difference is in the total load on the IAB, as presented in Figure 5.5, which shows

that both designs reach a limit when the pier columns begin to experience moderate pier column damage at around the design-level scale factor of 1.0.

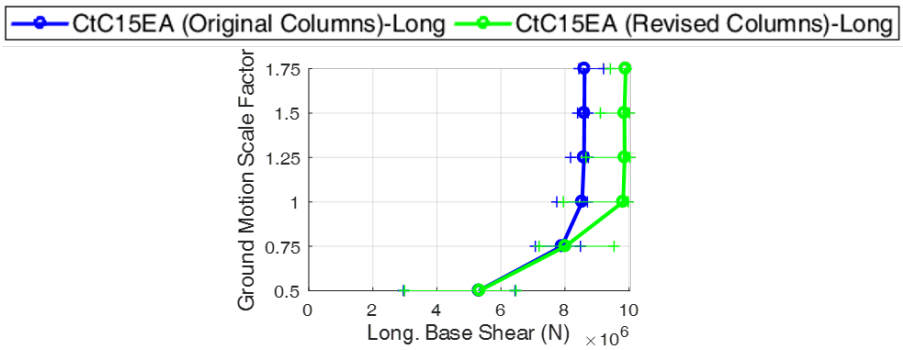

Figure 5.5: Longitudinal IDA results for the maximum base shear in the original and enhanced CtC15EA.

The transverse ClC15EA IDA results presented in Figure 5.6 demonstrate that there is much less pier column strain (Figure 5.6 (a)) and occurrence of pier column damage when the enhanced design is used. Severe pier column damage, as well as moderate pier column damage, is essentially eliminated in the enhanced designs. However, the stiffer piers of the enhanced design and the frequent occurrence of retainer fusing does lead to increased occurrences of bearing unseating. Loads in the enhanced design bridge are once again larger, as seen in Figure 5.6 (b), though a hard limit is not encountered due to the lack of moderate pier column damage as experienced in the original design.

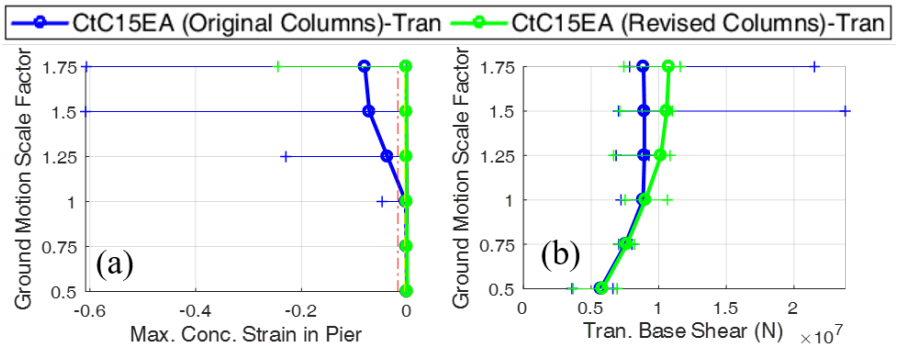

Figure 5.6: Transverse IDA results for the (a) maximum pier column concrete strain; and (b) maximum base shear in the original and enhanced CtC15EA. The dashed lines represent ideal (green), acceptable (yellow), and unacceptable (red) limit state values for the component.

The longitudinal IDA results for ClC15EA presented in Figure 5.7 indicate similar results to the CtC15EA longitudinal results. These results indicate moderate decreases in all three levels of pier column damage (see Fig. 5.7 (a)). APY and APS are once again consistently large as most of the longitudinal load is resisted by the abutments. APB and APR are also frequent at moderate to large scale factors but do increase slightly as the pier damage limit state occurrences decrease. This indicates a decrease in the abutment demand as pier demand increases. The

enhanced design IAB is also capable of obtaining larger loads in Figure 5.7 (b), but both designs reach caps set by moderate pier column damage.

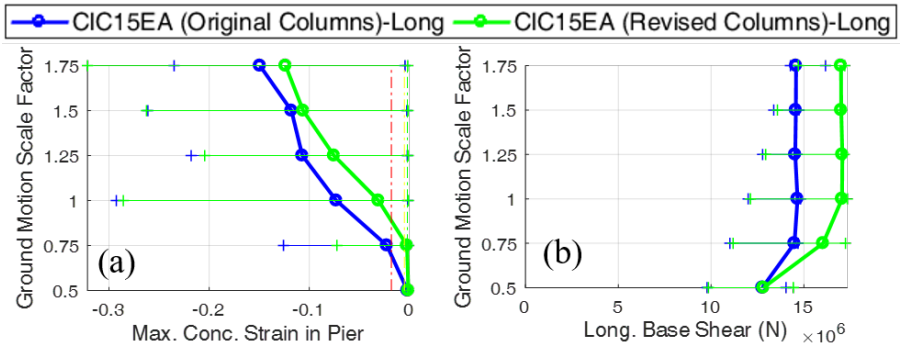

Figure 5.7: Longitudinal IDA results for the (a) maximum pier column concrete strain; and (b) maximum base shear in the original and enhanced ClC15EA. The dashed lines represent ideal (green), acceptable (yellow), and unacceptable (red) limit state values for the component.

The transverse IDA results for ClC15EA, presented in Figure 5.8, show that the stiffer revised pier columns lead to much more frequent occurrences of retainer fusing (see Figure 5.8 (a)). This in turn leads to larger deck displacements in the enhanced bridge. Unlike the three-span bridge observed above, the four-span ClC15EA does not experience a large drop in pier column damage. There are still significant amounts of moderate and severe limit state occurrences in the enhanced design, and any decrease in pier column damage is accompanied by increased abutment pile damage with larger APB and APR frequencies. This can be attributed to the long span bridge with short piers creating a demand too large for even the enhanced design's columns to accommodate. This can be observed in Figure 5.8 (b), where the enhanced design produces smaller pier concrete strains at the 0.75 scale factor, however the demand is so large that these smaller strains still exceed the severe damage limit state (dashed red line). The larger revised columns may even be a hindrance in this situation, as they cannot accommodate the extra force they demand, and so there is an increase in abutment foundation damage as well, as seen in Figure 5.8 (c).

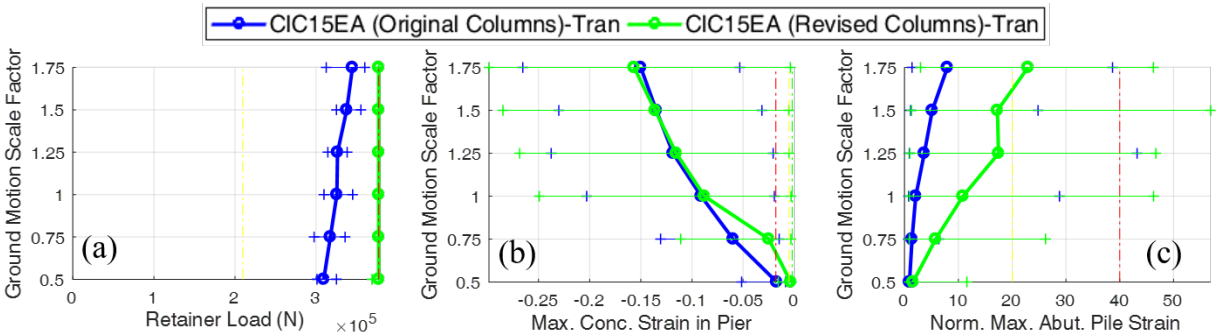

Figure 5.8: Transverse IDA results for the (a) maximum retainer load, (b) maximum pier column concrete strain, and (c) maximum abutment pile strain normalized to the yield strain in the original and enhanced ClC15EA. The dashed lines represent ideal (green), acceptable (yellow), and unacceptable (red) limit state values for the component.

5.4 INCREASED BACKFILL CONTRIBUTION

A common concern in many of the IAB analyses is the consistent yielding, local buckling, and even rupture of the abutment piles and mobilization of the soil surrounding the abutment piles at low intensities of ground shaking. While not necessarily unacceptable, these limit states are not desired either since they are difficult to identify and repair. The worst abutment foundation damage (either pile damage or mobilization of the soil surrounding the piles) occurs in IABs with concrete superstructures and tall piers. The concrete superstructures are heavier than the steel superstructures, which increases the total lateral force in the system during earthquakes. The use of tall piers creates larger abutment foundation damage, due to the relative flexibility of the piers decreasing the force in the piers and increasing the force demand that is resisted by the abutments.

Additionally, although abutment foundation damage frequently occurs, backfill mobilization rarely occurs in the longitudinal direction. The enhanced designs in this section look to increase the backfill contribution's force resistance in order to decrease the amount of force resisted by the abutment foundation. This is accomplished by increasing the height of the pile cap-backfill contact surface from 42 in. to 84 in., as shown schematically in Figure 5.9. The entire pile cap height is not increased, due to the desire not to increase the stiffness of the abutment piles.

The revised abutment pile cap design is applied to CtC40EA and ClC40EA, both of which have concrete superstructures and 40-ft tall piers. The implementation of the revised abutment pile cap design presented in Figure 5.9 is purely conceptual given the increased difficulty in constructability that it would pose. However, the concept of increasing backfill engagement by increasing the backfill-pile cap contact area is plausible. Thus, despite the unlikeliness of the revised design being used in actual IABs, the analyses can yield results that are important in understanding whether increasing the pile cap size aids in increasing backfill engagement.

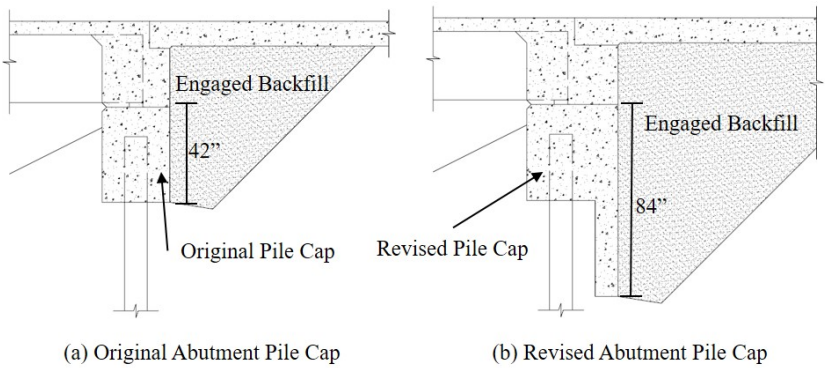

Figure 5.9: Original and revised abutment pile cap designs.

It should be noted that the lack of backfill mobilization may be less of a concern if temperature effects are considered prior to an earthquake occurring. Temperature changes will produce a ratcheting effect in the IAB abutments, by causing a gap behind the abutment which will be filled by loose backfill during cold temperatures. When temperatures rise, the backfill will

already be engaged and the loads in the backfill at a normal operating temperature will be larger than those determined in this study. This means that the backfill will be more likely to mobilize should the effects of temperature cycles also be considered.

By using the enhanced backwall design, it was determined that there are slight decreases in abutment pile strain. However, these decreases were fairly minimal considering that the abutment depth was increased by a factor of 2.

5.5 RECOMMENDATIONS

The potential design enhancements discussed in this chapter lead to recommendations for potentially ameliorating certain aspects of the seismic performance of IABs. As mentioned earlier, the design enhancements explored in this chapter were applied only to the site of Cairo, IL and immediate vicinity in seismic performance zone (SPZ) 4. SPZ 3 and SPZ 2 may require enhancements of the same manner, but to a lesser extent than those presented.

The first explored enhancement concerned a reduction in the number of elastomeric bearing side retainers used at each pier. It was found that in three-span IABs with tall bridges, there is a slight benefit to reducing the number of retainers. Unfortunately, even reducing the number of retainers to the minimum of two is not a viable method of ensuring that the retainers will fuse before pier column concrete spalling. The retainers may additionally be weakened by reducing the size of the anchor bolts, which further decreases the amount of damage in the piers. However, in some scenarios even this is insufficient at weakening the retainers such that they fuse before the columns. The main trend in these analyses revealed that the current pier column designs were too weak to allow for any retainer design changes to cause retainer fusing to occur before pier column concrete spalling (moderate pier column damage). This means that a retainer design change alone is not sufficient to mitigate damage in the piers.

Similar conclusions are reached when the fixed bearings are weakened by reducing anchor bolt sizes. It is found that the current pier column designs are once again too weak to allow for IAB behavior to be significantly affected by changes to fixed bearing design. It is shown that under ideal circumstances, for an IAB with low pier column load demands (three-span, tall pier) and the smallest allowable anchor bolts (5/8-in. diameter), fixed bearing fusing occurs slightly before concrete spalling in the columns. An improvement in pier column behavior is observed in this scenario, but it is not substantial. This leads to the conclusion that reducing fixed bearing anchor bolt size alone is not sufficient to ensure protection of the columns.

As noted in the scenarios involving retainers and fixed bearings, the weak columns are consistently an issue. Analyses on IABs with different pier column designs led to some useful conclusions. The first is that strengthening the columns does help the pier columns avoid moderate and severe damage. However, the damage is now in the retainers, which fracture easily and cause an increase in bearing unseating occurrences. Additionally, the piers are shown to require much stronger columns in longer-span bridges. This last point helps to address the increased flexibility in the transverse direction of four-span IABs.

Recommendations based on the first three enhancements (retainers, fixed bearings, and pier columns) go beyond just ensuring larger pier columns for longer span bridges in the future. It was shown that reducing the retainer or fixed bearing strength alone does not provide a viable solution. However, when used in conjunction with strengthened pier columns it may help. A key recommendation for the future would be to design the retainers / fixed bearings in conjunction with the pier columns. Preliminary investigation into enhanced designs with revised column and anchor bolt sizes has indicated that pier column damage can be mitigated by increased pier sizes, and that bearing unseating (which accompanies the stiffer piers) can be reduced through larger bearings. These conclusions can be observed in Table 5.1, which compares the original CtC15EA design with the revised column design and a revised column and bearing size design (13-b to 15-b Type I elastomeric bearings).

Finally, increasing the backfill contribution by increasing the size of the backfill-abutment contact area is shown to reduce forces in the abutment piles in three-span bridges. Unfortunately, an increase of the pile cap height by a factor of two is still insufficient to substantially reduce abutment foundation damage. A recommendation for future designs would be to increase the backfill contribution in another way in order to further reduce abutment foundation damage. This could perhaps be achieved through greater compaction of the backfill, causing it to be stiffer, or continuing to increase the backfill-abutment contact area through other means.

Table 5.1: Frequency of Transverse Limit State Occurrences Between Various CtC15EA Designs

Bridge	Revision	SF	Transverse Limit State Occurrences									
			Ideal					Acceptable		Unacceptable		
			SL	CL	RE	RY	RF	SM	CM	BU	SS	CS
CtC15EA	Original Pier Columns	0.50	0%	0%	100%	100%	5%	0%	0%	0%	0%	0%
		0.75	100%	25%	100%	100%	100%	0%	0%	0%	0%	0%
		1.00	100%	80%	100%	100%	100%	40%	40%	0%	5%	15%
		1.25	95%	85%	100%	100%	100%	80%	80%	0%	45%	65%
		1.50	95%	85%	100%	100%	100%	80%	80%	20%	75%	80%
		1.75	100%	95%	100%	100%	100%	80%	80%	20%	75%	80%
	Revised Pier Column Only	0.50	0%	0%	100%	100%	20%	0%	0%	0%	0%	0%
		0.75	0%	0%	100%	100%	100%	0%	0%	0%	0%	0%
		1.00	40%	0%	100%	100%	100%	0%	0%	0%	0%	0%
		1.25	80%	30%	100%	100%	100%	0%	0%	15%	0%	0%
		1.50	80%	45%	100%	100%	100%	0%	0%	55%	0%	0%
		1.75	85%	55%	100%	100%	100%	5%	5%	60%	5%	5%
	Revised Columns and Bearing Size	0.50	0%	0%	100%	35%	0%	0%	0%	0%	0%	0%
		0.75	0%	0%	100%	100%	0%	0%	0%	0%	0%	0%
		1.00	50%	0%	100%	100%	0%	0%	0%	0%	0%	0%
		1.25	80%	25%	100%	100%	0%	0%	0%	10%	0%	0%
		1.50	85%	50%	100%	100%	0%	5%	5%	45%	5%	5%
		1.75	85%	60%	100%	100%	0%	0%	0%	65%	0%	0%

CHAPTER 6: CONCLUSIONS

6.1 OVERVIEW

The conclusions from the dynamic analysis results presented in Chapters 3 and 4, including incremental dynamic analyses, are important contributions toward better understanding the seismic behavior of IABs. Unlike most past seismic IAB studies, the models in this study accounted for numerous components throughout the IAB and allowed for interactions between the components. In general, it was determined that the piers, abutment foundations, and bearings/retainers were the most important components with respect to seismic behavior. More detailed observations and conclusions are presented here below:

Moderate pier column damage, typically initiated by the onset of concrete spalling in pier column concrete, usually corresponds to the peak load capacity of a bridge. This is shown to often occur before the fusing of retainers or fixed bearings, leading to pier columns becoming the fusing elements in an IAB. Ideally, fracture of the retainers or fixed bearing anchor bolts would be the fusing elements, limiting the force transferred to the piers and saving the pier columns from severe damage. Retainers and fixed bearings are much easier and more economical to replace than entire piers. However, as indicated, current designs often have weak piers that allow for concrete spalling to occur before retainer or fixed bearing fusing. Even in analyses where retainer or fixed bearing fusing occurs, it is often accompanied by appreciable pier damage.

Abutment foundations almost always experience significant damage through pile yielding and mobilization of the soil surrounding the piles. Damage to these components occurs in almost all the analyses, including those with ground motion intensities half the magnitude of the design-level ground motions (scale factor of 0.5). The consistent occurrence of these limit states is not ideal due to the difficulty in identifying and repairing or replacing the abutment piles.

There is a small trade-off between abutment foundation damage and pier column damage. This is indicated through decreases in damage to abutment piles and soil when there is an increase in pier column damage, and vice versa. These changes are evident between IABs of different pier heights and different span configurations. Shorter piers are stiffer than taller piers, and this increased stiffness in the shorter piers increases force demand in the pier columns and leads to more damage. The increased proportion of lateral force that is carried by the piers decreases the force resisted by the abutments, which usually leads to small decreases in the frequency of damage. Similarly, four-span IABs excited in the transverse direction experience greater pier force demands than three-span IABs excited in the transverse direction. This is due to the flexibility of the four-span IABs in the transverse direction, which limits load redistribution to the abutments. Load redistribution is easier in the three-span IABs, as they are stiffer and have a shorter overall span, leading to less demand on the piers. The increased pier forces in four-span IABs lead to decreases in abutment force demands, while three-span IABs see more abutment force demand and less pier force demand. Increases in force demand typically correspond to increases in component damage, though this is often not observed in abutment

foundation components since they frequently incur damage regardless of other parameter variations.

Concrete superstructure IABs experience more damage than steel superstructure IABs. PPC girders weigh considerably more than steel plate girders, leading the overall girder/deck weight to be 60% larger in the concrete three-span IABs and 66% larger in the concrete four-span IABs. The increased mass of the concrete superstructures leads to larger lateral loads under the same ground accelerations. The increased lateral loads during seismic events means that there are increased forces and damage in most of the components. This leads to the conclusion that components in concrete IABs need to be more robust in order to accommodate the increased forces in the bridge.

6.2 DESIGN RECOMMENDATIONS

The design recommendations are based on conclusions from the dynamic analyses of existing Illinois IAB designs, along with assessment of potential revisions to current Illinois IAB designs as explored in Chapter 5. Three main design recommendations, which were formed based on the conclusions from these chapters, are listed below:

Recommendation 1: Longer span IABs require more robust columns than those with shorter spans.

The current IAB designs adopted from IDOT details had identical pier columns for both the three- and four-span IABs with matching pier heights. This was shown to be a concern, as the increased flexibility in the transverse direction of four-span IABs causes an increase in forces, and therefore damage, within the piers. It was also shown that by increasing pier column size by identical amounts in both three-span and four-span IABs, the damage to the three-span IABs is significantly reduced while damage to the four-span IAB is still frequent. While it is not ideal to have oversized columns in light of economy and unnecessary increases in bridge stiffness, the columns should accommodate the forces such that severe pier column damage is minimized. By this reasoning, increased pier forces in the longer span IABs require more robust columns to resist the increased forces.

Recommendation 2: Design the bearings, retainers, and piers as a system.

It was shown that reducing the number of side retainers per pier, as well as reducing the size of the retainer and fixed bearing anchor bolts, may allow for these components to fuse before pier column concrete spalling occurs. However, none of these revisions alone eliminates unacceptable limit state occurrences, and sometimes the revisions have insignificant effects. Similarly, strengthening pier columns allows for severe pier column damage to be reduced, but these changes alone are often not enough to completely eliminate unacceptable limit states. Two major issues that occur when pier columns are strengthened are the occurrence of pier column concrete spalling before retainer fusing, as well as bearing unseating after the retainers fuse. These issues can be remedied by either decreasing retainer strength such that the retainers fuse before column concrete spalling occurs, or by increasing the retainer strength or

bearing size such that bearing unseating is less likely. This formulates the recommendation that the piers, fixed bearings, elastomeric bearings, and retainers should be designed together such that the retainers and/or fixed bearings are weak enough to fuse before concrete spalling in the columns, yet strong enough to minimize bearing unseating.

Recommendation 3: Increase the backfill contribution to limit abutment foundation damage.

It was shown that increasing the backfill contribution (both strength and stiffness) increased the force resisted by the backfill and decreased the demand in the abutment foundation components. However, the studied method of achieving increased backfill contribution involved increasing the backfill-abutment contact area and demonstrated that this method alone is not sufficient to significantly reduce abutment foundation damage. To significantly decrease the amount of damage in the abutment foundations, increasing the strength and stiffness of the backfill through some other means would need to be achieved. In addition to further increasing the backfill-abutment contact area, increasing the compaction of the backfill soil or ensuring a backfill soil that is stronger and stiffer should also be implemented.

6.2.1 Recommendation Applicability

The recommendations provided above are not necessarily needed for IABs in all regions of Illinois. Sites in SPZ 3 or SPZ 2, which are further to the north of SPZ 4 that contains Cairo, do not necessarily need revisions as severe as those for SPZ 4. However, while the recommendations are based on analyses at Cairo, it is certainly reasonable to apply the recommendations to other similar sites within SPZ 4 as well.

Outside of SPZ 4, the recommendations are either needed to a lesser extent or not needed at all. In SPZ 3, which is just north of SPZ 4, it was shown that there are similar seismic behavior concerns in IABs to those in SPZ 4, yet the concerns are not as severe as those found in SPZ 4. For this reason, it is suggested that the recommendations provided above are applicable to a lesser extent. For example, the pier columns do need to be strengthened in SPZ 3, but not to the extent that they were strengthened for SPZ 4 IABs.

SPZ 2 is further north than SPZ 3, and IABs are found to have little unacceptable behavior during seismic events. This indicates that there is no need to apply any recommendations to SPZ 2 IABs, due to their designs already being acceptable. Taking these recommendation applicability suggestions into account is an economic method of ensuring IAB seismic performance while not overdesigning bridges in any particular SPZ.

6.3 RECOMMENDATIONS FOR FURTHER RESEARCH

The research described in this report expands the scope of knowledge concerning the seismic behavior of IABs and provides useful assessments of current Illinois IAB designs. Looking beyond the progress made as part of the ICT-R27-133 project, *Calibration and Refinement of Illinois' Earthquake Resisting System Bridge Design Methodology: Phase II*, future directions of research based on the results of the study presented in this report are provided below:

As mentioned, the majority of this study entailed the assessment of current Illinois IAB designs to design-level ground motions. While some recommendations were proposed and analyzed, a more detailed analysis of potential solutions to identified IAB seismic vulnerabilities is recommended for work in the future. This will allow for more detailed guidelines on how to design the bearings, retainers, and piers as a system. Further study of the recommended solutions and other damage mitigation techniques could also look into methods for increasing the backfill contribution in a feasible manner.

An expansion of the parametric study is also suggested as a topic for future work. While many parameters were evaluated in the study discussed in this report, there are still parameters which have not been investigated. Given the importance of the piers and abutment foundations, future parametric studies could include more options in terms of the pier configuration (i.e., wall or columns, number of columns), as well as the number of abutment piles and their orientation. The inclusion of various bridge skew angles and earthquake incident angles could also be included in future studies, as IABs are often skewed and only ground motions occurring in two orthogonal directions (bridge transverse and longitudinal) were explored in this study. Design modifications such as including the potential nonlinear behavior of superstructure elements could also be considered for inclusion in future parametric studies.

The seismic assessment of highway bridges in Illinois could also be expanded to include more types of bridges. Stub abutment bridges have been extensively studied by the ICT-R27-133 project and preceding projects (Steelman *et al.*, 2013; Filipov *et al.*, 2013a; Filipov *et al.*, 2013b; Steelman *et al.*, 2014; Steelman *et al.*, 2016; LaFave *et al.*, 2013a; LaFave *et al.*, 2013b; Luo *et al.*, 2016; Luo *et al.*, 2017). However, there are other bridge types that have not been considered. Chief among these unconsidered bridge types is the semi-integral abutment bridge. Semi-integral abutment bridges are similar to IABs in that the abutment and superstructure are cast in a single pour, but they differ in that semi-integral abutments have a defined joint between the abutment and pile cap, which can accommodate different movements of the abutment and its foundation. Given the concerns in IABs related to the abutment foundation, having the ability to separate the abutment foundation from the behavior of the rest of the abutment and superstructure is worth exploring further.

Beyond seismic assessments, the thermal effects of IABs could also be considered along with seismic effects in future studies. IAB thermal behavior has been studied extensively in Illinois. However, the resulting damage from thermal effects has not been applied to IABs before an earthquake analysis takes place. This study considers the IABs to be without damage before an earthquake occurs. This is not always the case, as cyclic temperature changes could have significant effects on bridge components, leaving the bridge already somewhat damaged before an earthquake. IAB component effects of special interest when considering thermal effects before earthquake analysis are yielding of the abutment piles and engagement of the backfill. The latter is interesting due to a ratcheting effect from the contraction of IABs in colder temperatures allowing the backfill to fill gaps created behind the abutment and increase the stress in the backfill when temperatures rise again. This would cause the backfill to be significantly closer to mobilization before an earthquake strikes.

REFERENCES

AASHTO (2011) *Guide Specifications for LRFD Seismic Bridge Design*, American Association of State Highway and Transportation Officials, Washington, DC, USA.

AISC (2017) *Steel Construction Manual, 15th Edition*. American Institute of Steel Construction, Chicago, IL, USA.

Al Atik, L. and Abrahamson, N. (2010) "An improved method for nonstationary spectral matching," *Earthquake Spectra* **26**(3), 601-617.

API (2002) *Recommended Practice for Planning, Designing and Constructing Fixed Offshore Platforms – Working Stress Design*, American Petroleum Institute, Washington, DC, USA.

Baker, J.W. (2011) "Conditional mean spectrum: Tool for ground motion selection," *Journal of Structural Engineering* **137**(3), 322-331.

Baker, J.W. and Cornell, C.A. (2006) "Spectral shape, epsilon and record selection," *Earthquake Engineering and Structural Dynamics* **35**(9), 1077-1095.

Boulanger, R.W., Curras, C.J., Kutter, B.L., Wilson, D.W. and Abghari, A. (1999) "Seismic Soil-Pile-Structure Interaction Experiments and Analyses," *Journal of Geotechnical and Geoenvironmental Engineering* **125**(9), 750-759.

Fernandez, J.A. and Rix, G.J. (2006) "Soil attenuation relationships and seismic hazard analyses in the upper Mississippi embayment," *Eighth U.S. National Conference on Earthquake Engineering*, San Francisco, CA, April.

Filipov, E.T., Fahnestock, L.A., Steelman, J.S., Hajjar, J.F., LaFave, J.M. and Foutch, D.A. (2013a) "Evaluation of quasi-isolated seismic bridge behavior using nonlinear bearing models," *Engineering Structures* **49**, 168-181.

Filipov, E.T., Revell, J.R., Fahnestock, L.A., LaFave, J.M., Hajjar, J.F., Foutch, D.A. and Steelman, J.S. (2013b) "Seismic performance of highway bridges with fusing bearing components for quasi-isolation," *Earthquake Engineering and Structural Dynamics* **42**, 1375-1394.

Franchin, P. and Pinto, P.E. (2014) "Performance-based seismic design of integral abutment bridges," *Bulletin of Earthquake Engineering* **12** 939-960.

Frosch, R.J., Kreger, M.E. and Talbott, A.M. (2009) *Earthquake Resistance of Integral Abutment Bridges*, Indiana Department of Transportation, West Lafayette, IN, USA.

Goulet, C.A., Kishida, T., Ancheta, T.D., Cramer, C.H., Darragh, R.B., Silva, W.J., Hashash, Y.M.A., Harmon, J., Stewart, J.P., Wooddell, K.E. and Youngs, R.R. (2014) *PEER Report No. 2014-17: PEER NGA-East Database*, Pacific Earthquake Engineering Research Center, University of California, Berkeley, CA, USA.

Hancock, J. Bommer, J.J. and Stafford, P.J. (2008) "Numbers of scaled and matched acceleragrams required for inelastic dynamic analyses," *Earthquake Engineering and Structural Dynamics* **37**(14), 1585-1607.

Hashash, Y. and Moon, S. (2011) *Site Amplification Factors for Deep Deposits and Their Application in Seismic Hazard Analysis for Central U.S.*, United States Geological Survey, Reston, VA, USA.

Hashash, Y.M.A., Musgrove, M.I., Harmon, J.A., Groholski, D.R., Phillips, C.A. and Park, D. (2015) *DEEPSOIL 6.0, User Manual*, University of Illinois, Urbana, IL, USA.

Herzog, B.L., Stiff, B.J., Chenoweth, C.A., Warner, K.L., Sievering, J.B. and Avery, C. (1994) *Buried Bedrock Surface of Illinois: ISGS GIS Database GISDB_BEDGEO. IL_Bedrock_Topography_1994_Ln*, Illinois State Geological Survey, Champaign, IL, USA.

IDOT (2012a) *Bridge Manual*, Illinois Department of Transportation, Springfield, IL, USA.

IDOT (2012b) *All Bridge Designers Memo 12.3: 2012 Integral Abutment Bridge Policies and Details*, Illinois Department of Transportation, Springfield, IL, USA.

IDOT (2014) *E-mail Communication 3/6/2014 to 6/13/2014*.

IDOT (2015) *All Bridge Designers Memo 15.2: New Precast Prestressed Concrete IL-Beam Section and Revisions to the I-Beams and Bulb T-Beams*, Illinois Department of Transportation, Springfield, IL, USA.

IDOT (2016) *IDOT Bridge Information System*, Illinois Department of Transportation, Springfield, IL, USA. Retrieved in 2016 from https://apps.dot.illinois.gov/bridgesinfosystem/search.aspx.

Itani, A.M. and Pekcan, G. (2011) *Seismic Performance of Steel Plate Girder Bridges with Integral Abutments*, Federal Highway Administration, Washington, DC, USA.

Kotsoglou, A.N. and Pantazopoulou, S.J. (2009) "Assessment and modeling of embankment participation in the seismic response of integral abutment bridges," *Bulletin of Earthquake Engineering* **7**, 343-361.

Kowalsky, M.J. (2000) "Deformation limit states for circular reinforced concrete bridge columns," *Journal of Structural Engineering* **126**(8), 869-878.

Kowalsky, M.J., Priestly, M.J.N. and Seible, F. (1999) "Shear and flexural behavior of lightweight concrete bridge columns in seismic regions," *ACI Structural Journal* **96**, 135-148.

Kozak, D.L., Luo, J., Olson, S.M., LaFave, J.M. and Fahnestock, L.A. (2017) "Modification of Ground Motions for Use in Central North America," *Journal of Earthquake Engineering,* dx.doi.org/10.1080/13632469.2017.1387190.

Kunin, J. and Alampalli, S. (1999) *Integral Abutment Bridges: Current practice in the United States and Canada*, New York State Department of Transportation, Albany, NY, USA.

LaFave, J., Fahnestock, L., Foutch, D., Steelman, J., Revell, J., Filipov, E. and Hajjar, J. (2013a) *Seismic Performance of Quasi-Isolated Highway Bridges in Illinois*, Illinois Department of Transportation, Springfield, IL, USA.

LaFave, J., Fahnestock, L., Foutch, D., Steelman, J., Revell, J., Filipov, E. and Hajjar, J. (2013b) *Experimental Investigation of the Seismic Response of Bridge Bearings*, Illinois Department of Transportation, Springfield, IL, USA.

LaFave, J.M., Riddle, J.K., Jarrett, M.W., Wright, B.A., Svatora, J.S., An, H. and Fahnestock, L.A. (2016) "Numerical Simulations of Steel Integral Abutment Bridges under Thermal Loading," *Journal of Bridge Engineering*, 04016061.

LaFave, J.M., Fahnestock, L.A., Brambila, G., Riddle, J.K., Jarrett, M.W., Svatora, J.S., Wright, B.A. and An, H. (2017) *Research Report No. FHWA-ICT-17-017: Integral Abutment Bridges under Thermal Loading: Field Monitoring and Analysis*, Illinois Center for Transportation, Rantoul, IL, USA.

Luo, J., Fahnestock, L.A., Kozak, D.L. and LaFave, J.M. (2016) "Seismic analysis incorporating detailed structure-abutment-foundation interaction for quasi-isolated highway bridges," *Structure and Infrastructure Engineering* **13**(5), 581-603.

Luo, J., Fahnestock, L.A. and LaFave, J.M. (2017) "Nonlinear static pushover and eigenvalue modal analyses of quasi-isolated highway bridges with seat-type abutments," *Structures* **12**, 145-167.

Matlock, H. (1970) "Correlation for Design of Laterally Loaded Piles in Soft Clay," *Offshore Technology Conference*, Houston, TX, April.

McGuire, R.K., Silva, W.J. and Costantino, C. (2001) *Report NUREG/CR-6728: Technical Basis for Revision of Regulatory Guidance on Design Ground Motions: Hazards- and Risk-Consistent Ground Motion Spectra Guidelines*, US Nuclear Regulatory Commission, Washington, DC, USA.

McKenna, F., Mazonni, S. and Fenves, G.L. (2006) *Open system for earthquake engineering simulation (OpenSees)*, Pacific Earthquake Engineering Research Center, University of California, Berkeley, CA, USA.

Olson, S.M., Long, J.H., Hansen, J.R., Renekis, D. and LaFave, J.M. (2009) *Modification of IDOT Integral Abutment Design Limitations and Details*, Illinois Department of Transportation, Springfield, IL, USA.

Olson, S.M., Holloway, K.P., Buenker, J.M., Long, J.H. and LaFave, J.M. (2013) *Thermal Behavior of IDOT Integral Abutment Bridges and Proposed Design Modifications*, Illinois Department of Transportation, Springfield, IL, USA.

Paraschos, A. and Amde, A.M. (2011) “A survey on the status of use, problems, and costs associated with Integral Abutment Bridges,” *Better Roads*, 1-20.

Scott, M.H. and Fenves, G.L. (2006) “Plastic Hinge Integration Methods for Force-Based Beam-Column Elements,” *Journal of Structural Engineering* **132**(2), 244-252.

Shamsabadi, A., Ashour, M. and Norris, G. (2005) “Bridge Abutment Nonlinear Force-Displacement-Capacity Prediction for Seismic Design,” *Journal of Geotechnical and Geoenvironmental Engineering* **131**(2), 151-161.

Shamsabadi, A., Rollins, K.M. and Kapuskar, M. (2007) “Nonlinear Soil-Abutment-Bridge Structure Interaction for Seismic Performance-Based Design,” *Journal of Geotechnical and Geoenvironmental Engineering* **133**(6), 707-720.

Spyrakos, C. and Ioannidis, G. (2003) “Seismic behavior of a post-tensioned integral bridge including soil-structure interaction (SSI),” *Soil Dynamics and Earthquake Engineering* **23**, 53-63.

Steelman, J.S., Fahnestock, L.A., Filipov, E.T., LaFave, J.M., Hajjar, J.F. and Foutch, D.A. (2013) “Shear and Friction Response of Non-Seismic Laminated Elastomeric Bridge Bearings Subject to Seismic Demands,” *Journal of Bridge Engineering* **18**(7), 612-623.

Steelman, J.S., Filipov, E.T., Fahnestock, L.A., Revell, J.R., LaFave, J.M., Hajjar, J.F. and Foutch, D.A. (2014) “Experimental Behavior of Steel Fixed Bearings and Implications for Seismic Bridge Response,” *Journal of Bridge Engineering* **19**(8), A4014007.

Steelman, J.S., Fahnestock, L.A., Hajjar, J.F. and LaFave, J.M. (2016) “Performance of Non-Seismic PTFE Sliding Bearings when Subjected to Seismic Demands,” *Journal of Bridge Engineering* **21**(1), 04015028.

Steelman, J.S., Fahnestock, L.A., Hajjar, J.F. and LaFave, J.M. (2018) “Cyclic Experimental Behavior of Nonseismic Elastomeric Bearings with Stiffened Angle Side Retainer Fuses for Quasi-Isolated Seismic Bridge Response," *Journa” of Bridge Engineering* **23**(1), 04017120.

Tassios, T.P. (1983) “Physical and mathematical models for re-design of damaged structures,” *Introductory Report, IABSE Symposium*, Venice, 29-77.

Teguh, M. Duffield, C.F., Mendis, P.A. and Hutchinson, G.L. (2006) “Seismic performance of pile-to-pile cap connections: An investigation of design issues,” *Electronic Journal of Structural Engineering* **6**, 8-18.

Terzaghi, K., Peck, R.B. and Mesri, G. (1996) *Soil Mechanics in Engineering Practice, Third Edition*. John Wiley & Sons, New York, NY, USA.

Toro, G.R., Abrahamson, N.A. and Schneider, J.F. (1997) “Model of strong ground motions from earthquakes in central and eastern North America: Best estimates and uncertainties,” *Seismological Research Letters* **68**(1), 41-57.

USGS (2008) *2008 Interactive Deaggregation*, United States Geological Survey, Reston, VA, USA. Retrieved from http://geohazards.usgs.gov/deaggint/2008/.

USGS (2014) *Hazard Curve Application*, United States Geological Survey, Reston, VA, USA. Retrieved from http://geohazards.usgs.gov/hazardtool/.

Vasheghani-Farahani, R., Zhao, Q. and Burdette, E.G. (2010) "Seismic Analysis of Integral Abutment Bridge in Tennessee, Including Soil-Structure Interaction," *Transportation Resource Records: Journal of the Transportation Research Board* **2201**, 70-79.

Vintzeleou, E.N. and Tassios, T.P. (1986) "Mathematical models for dowel action under monolithic and cyclic conditions," *Magazine of Concrete Research* **38**(134), 13-22.

Waldin, J., Jennings, J. and Routledge, P. (2012) "Critically, damaged bridges & concepts for earthquake recovery," *2012 New Zealand Society for Earthquake Engineering Conference*, Christchurch, NZ, January.

Wood, J.H. (2015) "Earthquake Design of Bridges With Integral Abutments," *6th International Conference on Earthquake Geotechnical Engineering*, Christchurch, NZ, November.

APPENDIX A: PROTOTYPE IAB SUPERSTRUCTURE PROPERTIES

The tables presented in this appendix describe the superstructure properties of the five basic prototype IABs. These table present the basic deck properties representing the appropriate deck and girder sections properties as well as the deck modeling properties which describe the concrete transformed section properties used for the transverse and longitudinal grillage elements. Table A.1 presents the detailed properties for the three steel girder prototype IABs. Table A.2 presents the details properties for the two concrete girder prototype IABs.

Table A.1: Detailed Steel Superstructure Information Used for Bridge Modeling

	Bridge Type		
Basic Deck Properties	**1-Span Steel**	**3-Span Steel**	**4-Span Steel**
Deck width - m (ft)	13.1572 (43.1667)	13.1572 (43.1667)	13.1572 (43.1667)
Deck thickness - cm (in)	20 (8)	20 (8)	20 (8)
Girder type	177.8cm PL Girder (70” PL Girder)	101.6cm PL Girder (40” PL Girder)	152.4cm PL Girder (60” PL Girder)
Span lengths - m (ft)	49 (160)	24-37-24 (80-120-80)	44-49-49-44 (145-160-160-145)
Shortest Span - m (ft)	49 (160)	24 (80)	44 (145)
Longest Span - m (ft)	49 (160)	37 (120)	49 (160)
Girder spacing - m (ft)	2.1 (7.0)	2.2 (7.25)	1.7 (5.5)
Girder Depth - cm (in)	186 (73.25)	109 (43)	157 (62)
Girder Area - cm^2 (in^2)	618 (95.75)	361 (56)	552 (85.5)
Girder I_{xx} - cm^4 (in^4)	3519986 (84568)	756459 (18174)	2326983 (55906)
Girder I_{yy} - cm^4 (in^4)	46235 (1110.8)	17998 (432.4)	95950 (2305.2)
Total Girder Weight - kN/m (kips/ft)	29 (1.9549)	17 (1.1433)	34 (2.3275)
Concrete Deck Weight - kN/m (kips/ft)	63 (4.3167)	63 (4.3167)	63 (4.3167)
Asphalt Topping Weight (1.5") - kN/m (kips/ft)	12 (0.8094)	12 (0.8094)	12 (0.8094)
Parapets Weight - kN/m (kips/ft)	11 (0.75)	11 (0.75)	11 (0.75)
Total deck weight - kN/m (kips/ft)	114 (7.8309)	102 (7.0194)	120 (8.2035)
Deck Modeling Properties (Based on concrete stiffness of 23.2 MPa / 3370 ksi)			
Transverse composite modulus I_{yy} - m^4 (ft^4)	81 (9374.8)	65 (7546.0)	95 (10963.6)
Vertical composite modulus I_{xx} - m^4 (ft^4)	3.37 (390.9)	0.86 (99.7)	2.85 (330.2)
Composite area - m^4 (ft^2)	0.54 (63.1)	0.42 (48.8)	0.60 (69.6)

Table A.2: Detailed Concrete Superstructure Information Used for Bridge Modeling

Basic Deck Properties	Bridge Type	
	3-Span Concrete	4-Span Concrete
Deck width - m (ft)	13.1572 (43.1667)	13.1572 (43.1667)
Deck thickness - cm (in)	20 (8)	20 (8)
Girder type	IL54-2438: 44B-2T-8db-4d Strand Pattern	IL72-3838: 58B-2T-8db-6d Strand Pattern
Span lengths - m (ft)	24-37-24 (80-120-80)	44-49-49-44 (145-160-160-145)
Shortest Span - m (ft)	24 (80)	44 (145)
Longest Span - m (ft)	37 (120)	49 (160)
Girder spacing - m (ft)	2.2 (7.25)	1.9 (6.1667)
Girder Depth - cm (in)	137 (54)	183 (72)
Girder Area - cm^2 (in^2)	5510 (854)	6822 (1057.4)
Girder I_{xx} - cm^4 (in^4)	12296600 (295427)	30727702 (738236)
Girder I_{yy} - cm^4 (in^4)	2139554 (51403)	2936887 (70559)
Total Girder Weight - kN/m (kips/ft)	78 (5.34)	113 (7.714)
Concrete Deck Weight - kN/m (kips/ft)	63 (4.3167)	63 (4.3167)
Asphalt Topping Weight (1.5") - kN/m (kips/ft)	12 (0.8094)	12 (0.8094)
Parapets Weight - kN/m (kips/ft)	11 (0.75)	11 (0.75)
Total deck weight - kN/m (kips/ft)	164 (11.2160)	198 (13.5900)
Deck Modeling Properties (Based on concrete stiffness of 23.2 MPa / 3370 ksi)		
Transverse composite modulus I_{yy} - m^4 (ft^4)	100 (11630.6)	127 (14736.9)
Vertical composite modulus I_{xx} - m^4 (ft^4)	2.00 (231.7)	4.76 (551.3)
Composite area - m^4 (ft^2)	0.65 (75.4)	0.83 (96.1)

APPENDIX B: GROUND MOTION DEVELOPMENT

This appendix provides a more detailed procedure concerning the development of ground motions in southern Illinois. The process involved the creation and matching of existing ground motions to conditional mean spectra (CMS) for 10 sites around southern Illinois which were then propagated through site-appropriate soil profiles to acquire surface ground motions. These surface ground motions are the motions used in the seismic analysis of IAB models. This appendix is originally presented as a chapter in Kozak (2018).

B.1 FORMATION OF SOIL PROFILES IN SOUTHERN ILLINOIS

B.1.1 Southern Illinois Sites

Ten sites were selected in southern Illinois to represent the different combinations of seismic risk and geologic setting that could be encountered in the region. The ten sites are: Anna, Benton, Cairo, Carbondale, East St. Louis, Eldorado, Elizabethtown, Mt. Carmel, Salem, and Sparta. The latitude and longitude of the sites, along with their approximate depth to bedrock (Herzog *et al.*, 1994) are presented in Table B.1. The sites were selected based on their general geologic setting, their location relative to each other, and the availability of nearby soil boring data.

Table B.1: Location of Sites in Southern Illinois

Site Name	Latitude (°)	Longitude (°)	Approximate Depth to Bedrock (m) (Herzog *et al.*, 1994)
Anna	37.461	-89.239	30
Benton	38.004	-88.916	15
Cairo	37.013	-89.180	60
Carbondale	37.726	-89.220	20
East St. Louis	38.617	-90.133	40
Eldorado	37.814	-88.441	20
Elizabethtown	37.449	-88.304	35
Mt. Carmel	38.415	-87.769	40
Salem	38.268	-88.948	10
Sparta	38.133	-89.700	20

The general geologic setting was based on the different quaternary deposits found throughout southern Illinois. A variety of geologic settings were considered when selecting the sites, as shown by their location on the quaternary (ice age) deposits map (ISGS, 2005) in Fig. B.1. Their geographic location was also important to consider ensuring that sites from across southern Illinois were included. A variety of geographic locations allows for different levels of ground motion shaking to be experienced due to the different hazard sources that affect different locations. Finally, the availability of soil boring data was important to account for site-specific soil effects through representative soil profiles. The representative soil profiles were used to propagate the developed bedrock ground motions to the surface, as well as for considering soil behavior in the IAB models. The soil boring data was acquired using information found in boring logs from IDOT bridge projects (IDOT, 2014).

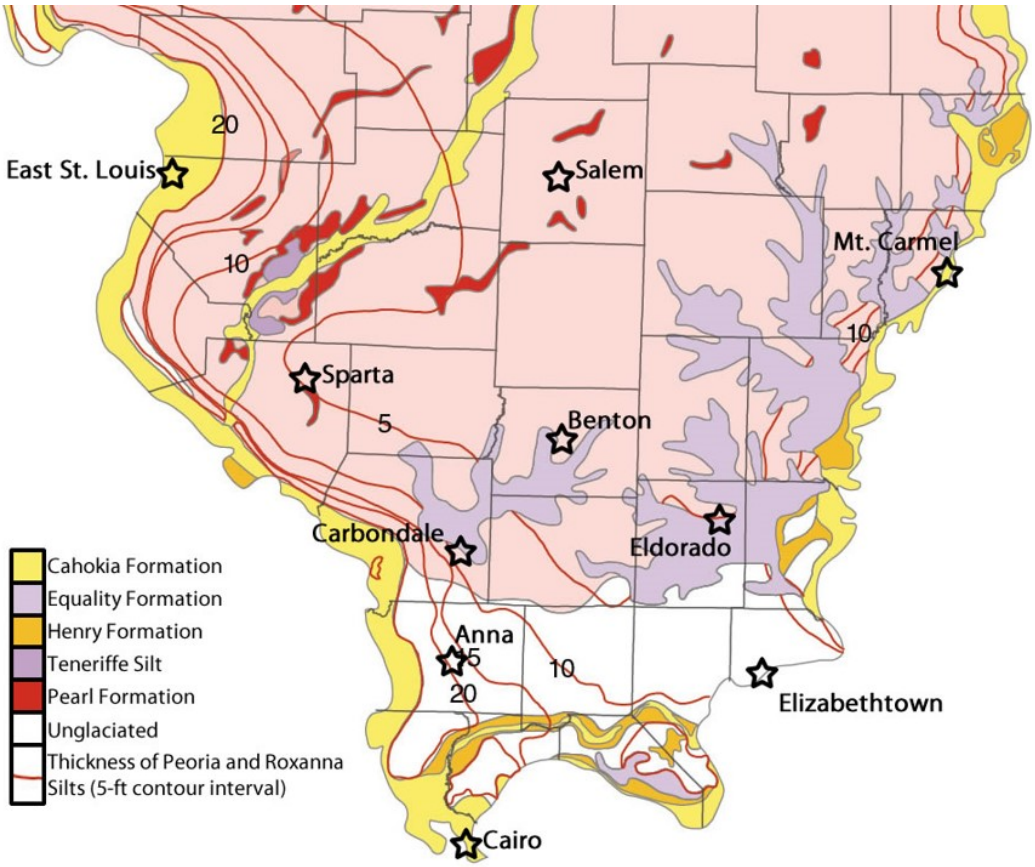

Figure B.1: Location of sites in southern Illinois overlaid on the Quaternary (ice age) deposits map for the region (ISGS, 2005).

B.1.2 Soil Profiles

The site-specific soil effects in the developed ground motions were accounted for by using site-representative soil profiles. The soil profiles were developed using 140 boring logs from bridge construction projects across southern Illinois (IDOT, 2014). The data acquired from the boring logs included the bore location, surface elevation, bedrock elevation, water table elevation, soil type for each soil layer, and standard penetration test (SPT) results for each soil layer. The soil type is described in terms of the AASHTO soil classification system, which is in turn used to estimate other key soil properties including liquid limit and median particle size. Some boring logs lack AASHTO soil classifications but do include soil descriptions. In these cases, an AASHTO soil classification is assigned based on the description. The data from the boring log and soil classification was used to create shear wave velocity (V_s) and coefficient of at-rest earth pressure (K_0) profiles for the 10 sites, which are necessary to propagate the ground motions from the bedrock to the surface.

As mentioned, the AASHTO soil classifications were used to make assumptions for soil properties such as the median particle size (D_{50}, in mm), the percent of soil passing a #200 sieve (P_{200}), the clay fraction (CF), and the liquid limit (w_L). These assumptions were made by placing

the values within the limits described in each AASHTO class, which can be found in many geotechnical engineering books, such as in Coduto *et al.* (2011).

To develop the V_s and K_0 profiles, the corrected SPT blow count (N_{60}), the effective vertical stress, and the effective friction angle (ϕ') must all be calculated using the boring and soil classification data. The N_{60} value was determined to be 1.25*N*, where *N* is the SPT blow count results from the boring logs (Coduto *et al.*, 2011; IDOT, 2014). The soil layer's unit weight (γ) and the effective vertical stress (σ'_z) in the layer could then be calculated using Eqs. (B.1)-(B.4). Eq. (B.1) describes the calculation of the SPT *N*-value corrected for field procedures and overburden stress, $N_{1,60}$ (Coduto *et al.*, 2011); Eq. (B.2) describes the relative density, D_r (Coduto *et al.*, 2011); Eq. (B.3) describes the unit weight, γ (Peck *et al.*, 1974); and Eq. (B.4) describes the effective vertical stress, σ'_z, where *H* is the height of each layer (Coduto *et al.*, 2011). As mentioned, these equations were used to solve iteratively, beginning with an assumption of σ'_z = 2000 psf and continuing until D_r converges.

$$N_{1,60} = N_{60}\sqrt{\frac{2000psf}{\sigma'_z}} \tag{3.1}$$

$$D_r = \sqrt{\frac{N_{1,60}}{C_p C_A C_{OCR}}} \; where \; C_p = 60 + 25\log(D_{50}),\; C_A \approx 1.2, C_{OCR} \approx 1.1329 \tag{3.2}$$

$$\gamma = \begin{Bmatrix} 124\ pcf\ for\ loose\ (D_r \le 0.35) AASHTO\ Class\ A-1, A-3 \\ 135\ pcf\ for\ dense\ (D_r > 0.35) AASHTO\ Class\ A-1, A-3 \\ 145\ pcf\ for\ AASHTO\ Class\ A-2 \\ 110\ pcf\ for\ soft\ (D_r \le 0.35) AASHTO\ Class\ A-4, A-5, A-6, A-7 \\ 129\ pcf\ for\ stiff\ (D_r > 0.35) AASHTO\ Class\ A-4, A-5, A-6, A-7 \end{Bmatrix} \tag{3.3}$$

$$\sigma'_z = \sum \gamma H - (62.4pcf)(depth\ from\ top\ of\ water\ table) \tag{3.4}$$

The V_s and K_0 values for each individual soil layer from each boring profile were then calculated using the corrected SPT blow count (N_{60}), effective vertical stress (σ'_v), and effective friction angle (ϕ') in each layer. In coarse-grained soils, ϕ' can be calculated from Eq. (B.5) below (Wolff, 1989; Hettiarachchi and Brown, 2009). The calculation of ϕ' in fine-grained soils is slightly more complex by first determining the residual friction angle (ϕ'_r) from the clay fraction and liquid limit of the soil, and then relating ϕ'_r to ϕ'. Both of these relationships involving ϕ'_r are described in plots in Terzaghi *et al.* (1996). Eq. (B.6) and (B.7) was then used to calculate the shear wave velocity (in m/s with the effective vertical stress, σ'_v, in in kPa) of coarse- and fine-grained soils, respectively, for Quaternary-age deposits (Wair *et al.*, 2012). The coefficient of at-rest earth pressure for each soil layer can be calculated from Eq. (B.8) with OCR estimated to be 2.0 (Coduto *et al.*, 2011).

$$\emptyset' = 27.1 + 0.3N_{60} - 0.00054N_{60}^2 \tag{B.5}$$

$$V_{s,coarse} = 30.0N_{60}^{0.23}\sigma'^{0.25}_v \tag{B.6}$$

$$V_{s,fine} = 26.0N_{60}^{0.17}\sigma'^{0.32}_v \tag{B.7}$$

$$K_0 = 1 - \sin(\emptyset')OCR^{\sin(\emptyset')} \tag{B.8}$$

The calculated shear wave velocity profiles were found to follow two trends and therefore provided two distinct geologies to consider: alluvial and non-alluvial. The alluvial sites consist of Benton, Cairo, East St. Louis, Mt. Carmel, Salem, and Sparta. The non-alluvial sites consist of Anna, Carbondale, Eldorado, and Elizabethtown. The calculated shear wave velocity profiles from each bore associated with the sites and their respective geology were combined to create the average shear wave velocity profiles for the alluvial and non-alluvial geologies. The individual shear wave velocity profiles from the bores and the average shear wave velocity profile for the upper 30 m of each geology is presented in Fig. B.2. It was found that the southern Illinois region does not have extremely large variations in shear wave velocity with respect to depth when considering the individual geologies. This is demonstrated by the relatively small dispersion found in the individual bore shear wave velocity profiles, shown in Fig. B.2 using the bounds formed by being one standard deviation from the average profile. These small variations allowed for the assumption that single shear wave velocity profiles are appropriate for representing each of the two geologies – the alluvial and non-alluvial.

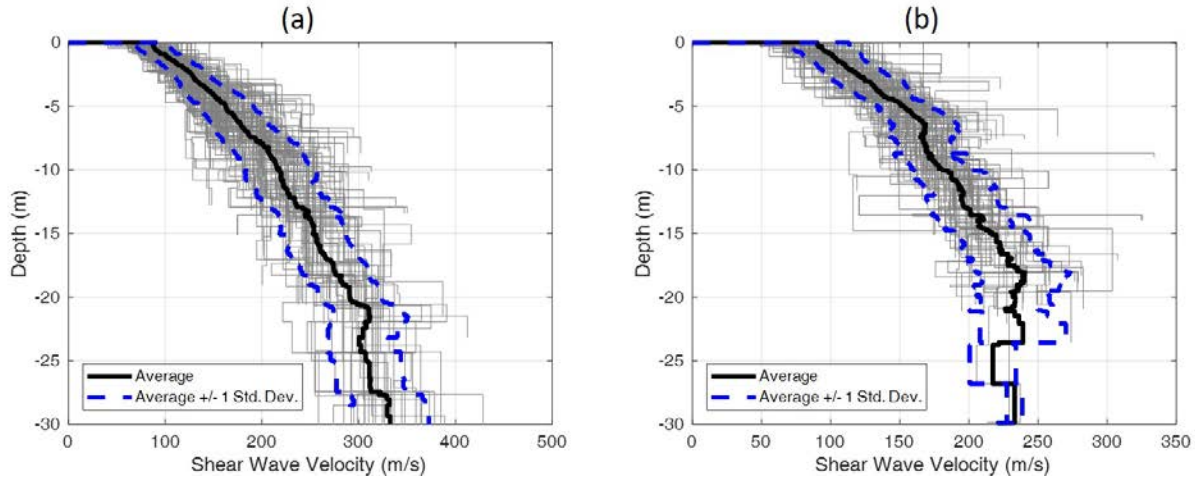

Figure B.2: Individual shear wave velocity profiles, average shear wave velocity profiles, and the bounds formed by being one standard deviation from the average for the upper 30 m of (a) the alluvial geology, and (b) the non-alluvial geology.

Many of the sites considered have a depth to bedrock deeper than the depths of the individual bores. This required a method of extending the average velocity profile to deeper depths. This was accomplished by using established Site Class D upland and lowland V_s reference profiles from Hashash and Moon (2011). The calculated shear wave velocity profiles were used for the upper 30 m of soil while the reference profiles were used for deeper depths. The upland and lowland V_s profiles were compared to the alluvial and non-alluvial V_s profiles to determine good matches based on minimizing any jumps in the profile at the 30 m depth. It was found that the alluvial and lowland profiles were comparable as well as the non-alluvial and upland profiles. These updated alluvial and non-alluvial profiles allow for site response to be dominated by the local geology condition while still maintaining a reasonable V_s profile to bedrock deeper than 30 m. Examples of the alluvial and non-alluvial profiles which contain both the calculated and

reference profiles are presented in Fig. B.3a for Cairo (alluvial) and Fig. B.3b for Anna (non-alluvial).

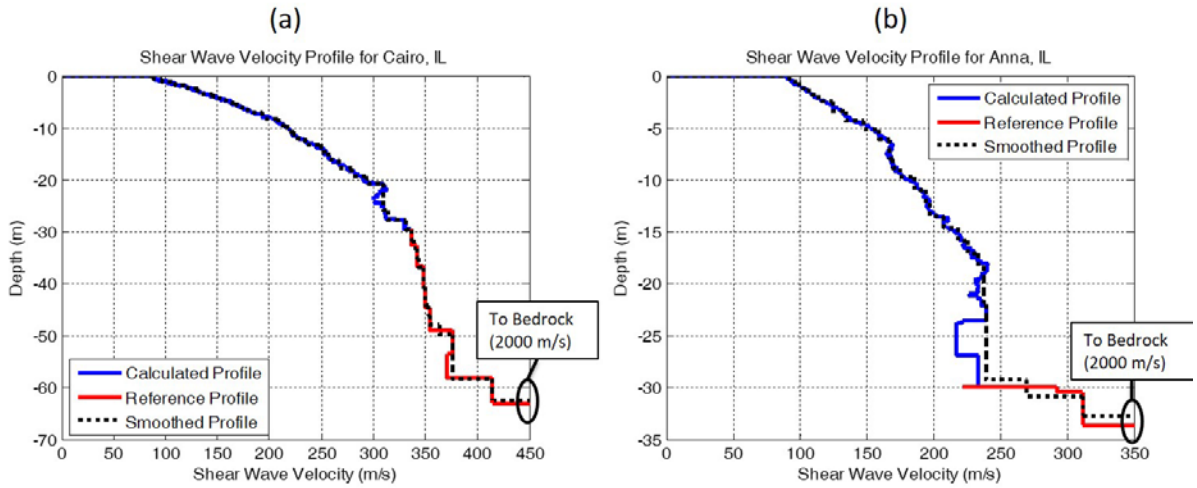

Figure B.3: Shear wave velocity profiles for (a) Cairo, which uses the alluvial profile for the top 30 m and the lowland profile for deeper than 30 m; and (b) Anna, which uses the non-alluvial profile for the top 30 m and the upland profile for deeper than 30 m.

Fig. B.3 also shows a smoothed profile for each geology along with the calculated and reference profile. These smoothed profiles were developed to allow for a more reasonable number of thicker soil layers as opposed to a larger number of thin layers in analysis. The smoothed profile also avoids any large impedance contrasts (particularly V_s inversions) within the profile. Another element to note from Fig. B.3 is that once the profile reaches the site's depth to bedrock (approximately 60 m for Cairo and 30 m for Anna, see Table B.1) the V_s value increases to the bedrock V_s value of 2000 m/s and no longer follows the alluvial or non-alluvial profiles. The final V_s profiles used in the development of ground motions for each site use this smoothed profile and account for the V_s jump at bedrock, as demonstrated in Fig. B.4. Note that due to all sites within the same geology (alluvial or non-alluvial) using the same calculated and reference (and therefore smoothed) V_s profiles, the only difference is the depth at which bedrock is encountered. The unit weight (γ) and effective friction angle (ϕ') profiles, which were used to calculate the coefficient of at-rest earth pressure (K_0), are similarly combined for the alluvial and non-alluvial geologies and smoothed to create thicker soil layers.

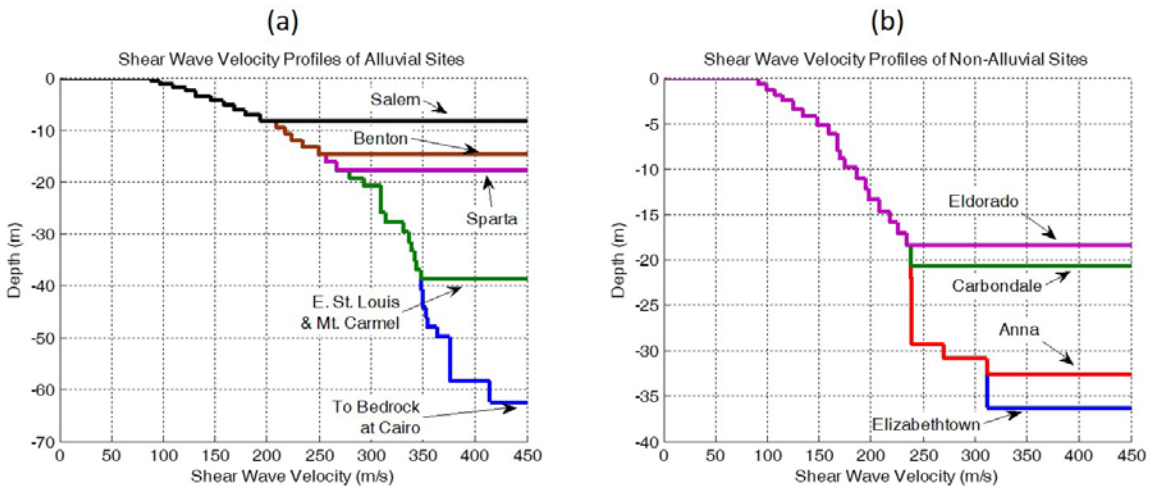

Figure B.4: Smoothed shear wave velocity profiles for (a) alluvial sites and (b) non-alluvial sites.

B.2 CONDITIONAL MEAN SPECTRUM DEVELOPMENT

B.2.1 Conditional Mean Spectrum and Uniform Hazard Spectrum Comparison

At the bedrock level existing ground motions are often modified such that their spectrum matches a target spectrum which accounts for the seismic hazard at a specific location. The target spectrum that has typically been used in the past is the uniform hazard spectrum (UHS) (Hancock *et al.*, 2008), which can be obtained from sources such as the United States Geological Survey (USGS) (2014). However, the conditional mean spectrum (CMS), originally developed by Baker and Cornell (2006), has been gaining popularity in its use as a target spectrum and is used in this project.

The motivation for using the CMS as opposed to the UHS lies with the unrealistic ground motion spectrum produced by matching to the UHS. The UHS is deemed unrealistic due to its large spectral acceleration values across all periods (Baker and Cornell, 2006). The UHS commonly integrates multiple earthquake sources at the same time, leading to the UHS being developed while considering both small magnitude, near-field earthquakes (which dominate short period behavior) and large magnitude, far-field earthquakes (which dominate long period behavior). Realistic ground motions would only consider one source, meaning that the UHS will be accurate around the period range dominated by the one source, but the UHS will be unrealistically large for any period outside this range (Baker and Cornell, 2006). This leads to the conclusion that the UHS would better serve as an intensity measure at a specific period during the ground motion development process (Baker and Cornell, 2006).

Deaggregated magnitude and source-to-site distance pairs (M, R) were acquired for each site and used to develop a median spectrum using an appropriate ground motion prediction equation (GMPE). The median spectrum and the UHS were then used to develop the CMS for the site (Baker, 2011). The shape of the CMS and its position between the median spectrum

and UHS is based on empirical data and such that the CMS matches the UHS at a specific period of interest called the conditional period, *T** (Baker and Jayaram, 2008). In general, the CMS and UHS are distinct from each other. However, in some cases where the seismic hazard is overwhelmingly dominated by a single source, the CMS and UHS tend to be similar. This is due to the UHS considering only one hazard source in its development, similar to how the CMS is meant to be developed. While there is a negligible advantage of the CMS in these situations, it is still not a disadvantage to use the CMS. These single source situations are rare, although they can occur in southern Illinois.

B.2.2 Conditional Mean Spectrum Creation

The conditional period, *T**, is typically taken as the fundamental period of the structure when developing a CMS. However, it is indicated that this approach is not always appropriate and if a range of periods is under investigation then a set of multiple *T** periods should be selected to induce different responses in structures by exciting different structural components (Baker, 2011). Selecting multiple *T** periods, and therefore making multiple CMS, was performed for the Illinois highway bridges studies in this project due to the variety of bridges under investigation. It was found that the initial fundamental period of Illinois highway bridges varies between 0.2-1.5 s (Revell, 2013). Additionally, damage to the bridges and their components could change the fundamental period of the bridge during dynamic or pushover analyses (Filipov *et al.*, 2013). A variety of *T** periods will allow the developed ground motions to be applicable to all the different bridges in the project throughout the analyses. For these reasons, the periods of 0.2, 0.3, 0.5, 1.0, and 2.0 s were selected as the five *T** periods for which to create CMS.

Four ground motions were developed for each of the five CMS at each site. This leads to 20 ground motions at each site and 200 ground motions for the entire southern Illinois region. All 20 ground motions will be applied to each bridge dynamic analysis for each site in this study. However, a main advantage of the CMS is its targeted nature, which means that if a fundamental period for a structure or component is known, then the use of fewer ground motions matched to CMS with a *T** matching that fundamental period is sufficient to obtain accurate seismic behavior (Baker, 2011). Unfortunately, as explained above, the varying fundamental period of the bridges during analysis in this study somewhat limits the use of this advantage of the CMS.

The hazard deaggregation results for each of the five *T** periods at each of the sites were then determined using the USGS Interactive Deaggregation application (USGS, 2008). The resulting mean (*M*, *R*) pairs for each of the sites and *T** periods were acquired at a 5% in 50-year probability of exceedance at a site class A rock boundary. The site class A rock boundary was used due to the CMS being developed for the bedrock level, with a shear wave velocity of 2000 m/s in the southern Illinois region (Hashash *et al.*, 2014), which corresponds to a site class A (hard rock) boundary (ASCE, 2016). Examples of the results for Cairo and East St. Louis at a period of 0.5 s are provided in Fig. B.5a and b, respectively. The results indicate that the mean (*M*, *R*) pair for Cairo is (7.65, 11.6 km) while it is (7.20, 152.1 km) for East St. Louis. These results

are logical given that East St. Louis is much further north than Cairo and the NMSZ, resulting in its mean source-to-site distance being much further than Cairo's.

Fig. B.5 also demonstrates the difference between single- and multi-source hazard sites that was mentioned earlier. Fig. B.5a shows that in Cairo the hazard is largely dominated by a single source (the NMSZ). In Fig. B.5b, it is shown that at East St. Louis the hazard does have a large contribution by a source around 200 km away (the NMSZ), but it also has many additional smaller contributions from much closer sources (less than 50 km). This is the reason why some southern Illinois sites, such as Cairo, do not benefit as much from using the CMS over the UHS, as they both end up only accounting for the single source. However, at multi-source sites such as East St. Louis, the UHS is developed using both the close sources and far sources while the CMS only considers one of the sources at a time.

Additionally, Fig. B.5a provides a mean epsilon parameter, ε_0, of -0.30. The epsilon parameter describes the number of standard deviations between the median spectrum and the UHS at a specific period (0.5 s for the cases in Fig. B.5). By being negative, Fig.B.5 is indicating that the median spectrum will be larger than the UHS at a period of 0.5 s for Cairo. This result is rare, with only Cairo and Anna experiencing negative epsilon values due to their single-source hazard characteristics.

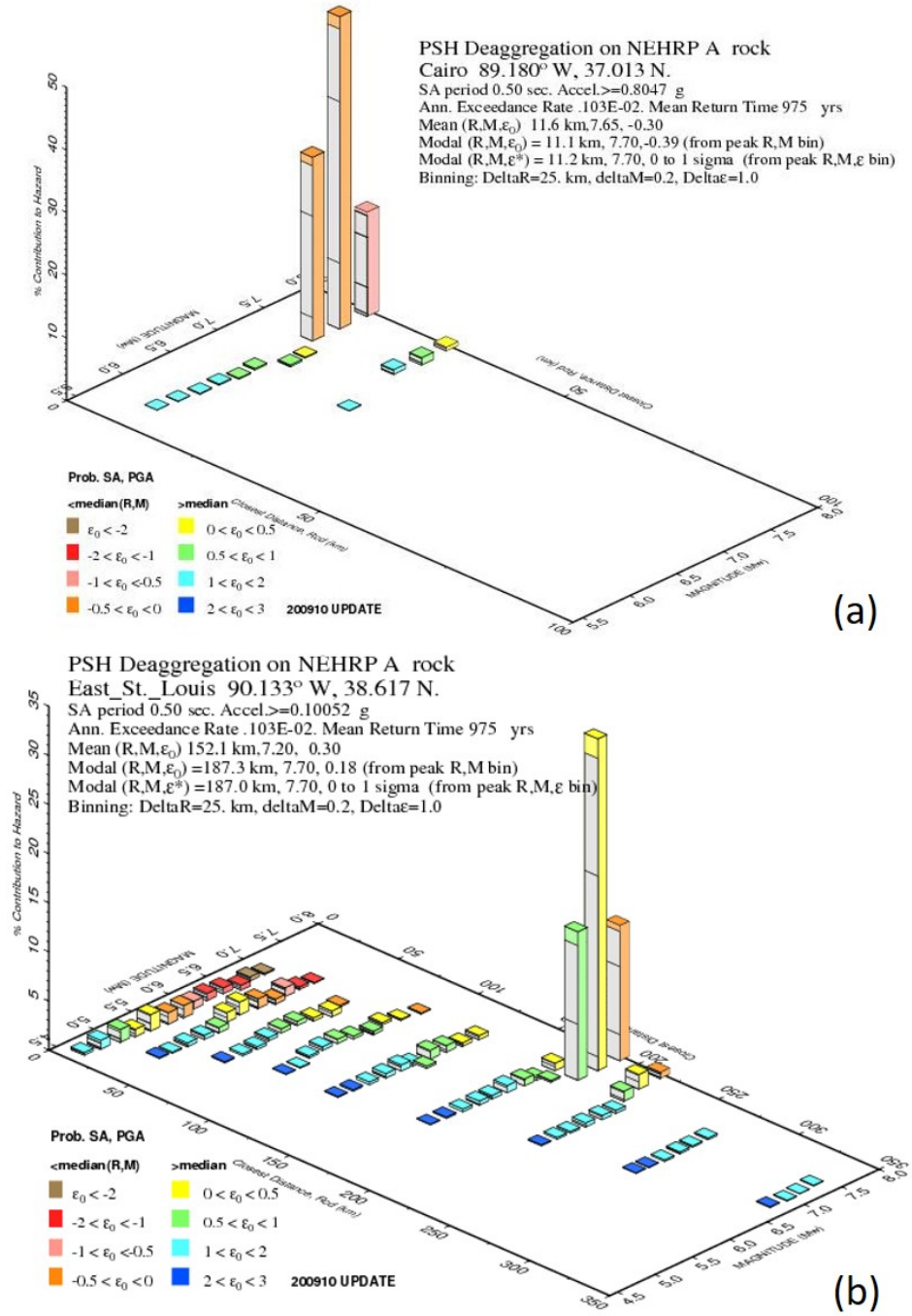

Figure B.5: Hazard deaggregation results for (a) Cairo, and (b) East St. Louis (USGS, 2008).

The hazard deaggregation results are used to develop median response spectra for each of the *T** periods. The median response spectrum, S_a, was determined using the Toro *et al.* (1997) GMPE. This GMPE was selected due to its use in the development of the USGS's UHS and hazard deaggregation results for central and eastern North America (Petersen *et al.*, 2008). To

better match the USGS procedure, spectral acceleration caps were applied to the Toro *et al.* (1997) GMPE as was performed by the USGS (Petersen *et al.*, 2008). The predicted mean and standard deviation of the natural logarithm of the median response spectrum ln(S_a) ($\mu_{\ln(Sa)}(M, R, T)$ and $\sigma_{\ln(Sa)}(T)$ respectively), are required for the calculation of the CMS. These values were determined by noting that in lognormal distributions the exponential of the mean of ln(S_a), $\mu_{\ln(Sa)}(M, R, T)$, is the same as the median response spectrum calculated using the GMPE (Baker, 2011). Examples of the CMS, UHS, and median spectrum are provided in Fig. B.6 for Cairo and East St. Louis with a T^* of 0.5 s. As discussed earlier, note that the Cairo median spectrum is larger than the UHS, as indicated by its negative epsilon value, while the East St. Louis median spectrum is smaller than the UHS.

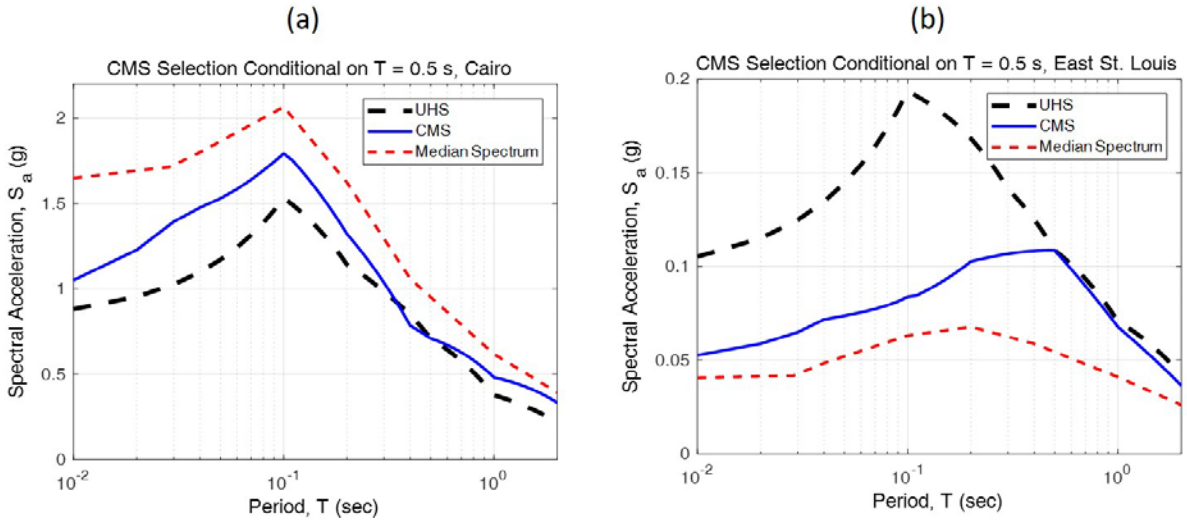

Figure B.6: UHS, CMS, and median spectra for a conditional period of 0.5 s at (a) Cairo, and (b) East St. Louis.

The procedure for developing the CMS using the predicted mean and standard deviation of ln(S_a) is provided in Baker (2011). The concept is to determine $\varepsilon(T^*)$ (the number of standard deviations between the ln($S_{a,CMS}$) and the $\mu_{\ln(Sa)}(M, R, T^*)$ curves at the conditional period T^*) such that the UHS and CMS match at T^*. The definition of $\varepsilon(T^*)$ is provided in Eq. (B.9); note that at the conditional period, T^*, $S_{a,CMS}(T^*) = S_{a,UHS}(T^*)$. Eq. (B.9) is specific to the conditional period, however once $\varepsilon(T^*)$ is determined the equation is rearranged into Eq. (B.10), which determines the natural logarithm of the CMS at all spectra ($S_{a,CMS}(T)$) using a correlation coefficient, $\rho(T, T^*)$, based on empirical data from Baker and Jayaram (2008).

$$\varepsilon(T^*) = \frac{\ln(S_{a,CMS}(T^*)) - \mu_{\ln(Sa)}(M,R,T^*)}{\sigma_{\ln(Sa)}(T^*)} \quad \text{(B.9)}$$

$$\ln\left(S_{a,CMS}(T)\right) = \mu_{\ln(Sa)}(M,R,T) + \rho(T,T^*)\varepsilon(T^*)\sigma_{\ln(Sa)}(T) \quad \text{(B.10)}$$

The CMS, $S_{a,CMS}$, was then simply calculated as a function of the period. These CMS were then used as the target spectra for the development of bedrock level ground motions. The

developed CMS for all five *T** periods along with the UHS are provided for all ten sites in southern Illinois in Fig. B.7 and Fig. B.8. Fig. B.7 provides the CMS for the alluvial sites, Fig. B.8 provides the CMS for the non-alluvial sites. Note that many look similar, however the scale of the y-axis (spectral acceleration) varies considerably from site to site depending on their location within southern Illinois.

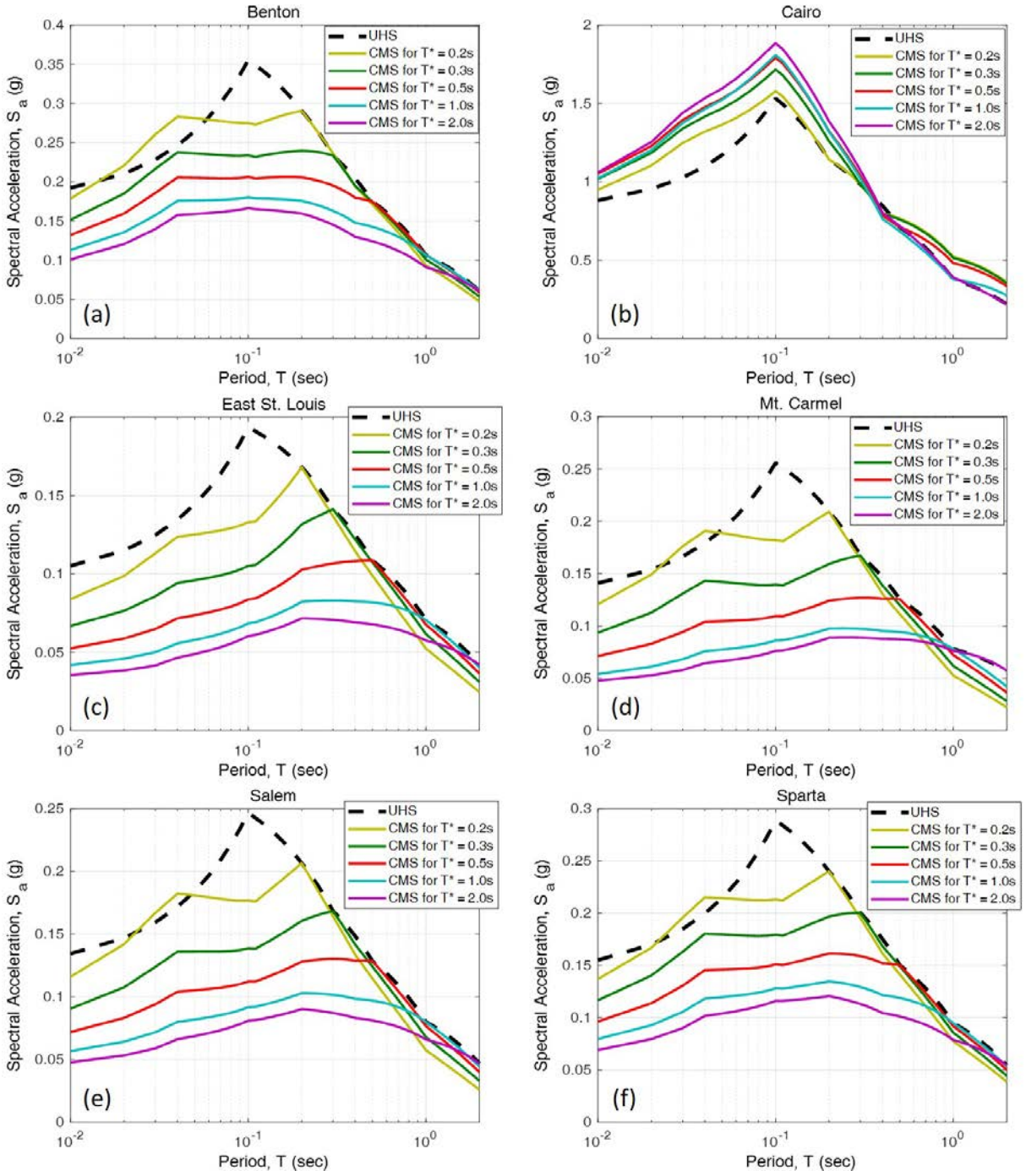

Figure B.7: CMS and UHS for alluvial sites (a) Benton, (b) Cairo, (c) East St. Louis, (d) Mt. Carmel, (e) Salem, and (f) Sparta.

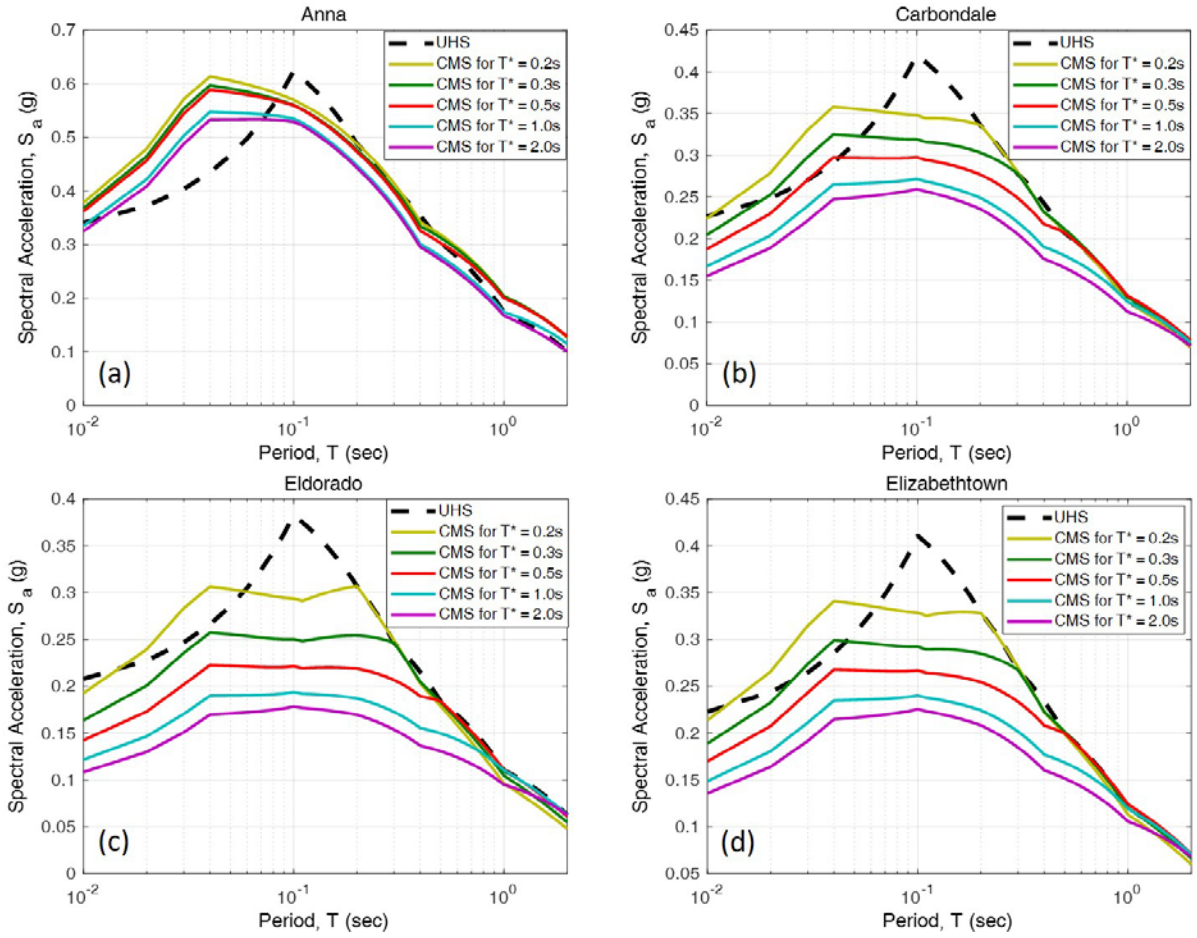

Figure B.8: CMS and UHS for non-alluvial sites (a) Anna, (b) Carbondale, (c) Eldorado, and (d) Elizabethtown.

B.3 MATCHING EXISTING GROUND MOTIONS TO THE CMS

B.3.1 Existing Ground Motions at the Bedrock Level

Existing ground motions for central and eastern North America (CENA) at the bedrock level were modified to match the CMS determined in section B.2 for the 10 southern Illinois sites. The existing ground motions are for the desired 1000-year return period event prescribed for AASHTO seismic design (AASHTO, 2011). Two main databases were used to act as the source ground motions that will be heavily modified in the following procedure: the NUREG/CR-6728 database (McGuire *et al.*, 2001), and the PEER NGA-East database (Goulet *et al.*, 2014).

The NUREG/CR-6728 database comprises 138 ground motion records for rock sites that are appropriate for use in CNA (McGuire *et al.*, 2001). The records originate from events worldwide and include many records from events in intraplate regions similar to CNA. The database is also supplemented with records from California and Japan which are modified to account for the seismic source and crustal properties of CNA (McGuire *et al.*, 2001).

The PEER NGA-East database contains ground motion records from 89 events within CENA (Goulet *et al.*, 2014). All of the records have magnitudes less than 6.0, limiting their use in the ground motion development, however they are considered in the process. This database contains many CENA ground motions not included in the NUREG/CR-6728 database, such as the 2008 Illinois earthquake whose epicenter was near Mt. Carmel, IL (Goulet *et al.*, 2014). However, many of the records, such as the records from the 1988 Saguenay earthquake in Quebec, are contained in both databases.

Both databases provide magnitude (*M*) and source-to-site distance (*R*) information for all the records. This information is important in determining which ground motions to use in matching to the CMS. Both databases also provide records for the combined 227 records in two orthogonal directions. Due to the limited amount of ground motion records in CNA the recordings in the two orthogonal directions are considered as individual records. This does present a bias in the overall set of ground motion records due to some records being related to others, however this bias is acknowledged and accepted. The acceptance of this bias can be justified by acknowledging that these source records are seed ground motions which will be heavily modified in the following procedure, so even minor differences in the bedrock source records allows for different surface ground motions to be developed. Additionally, there have been past studies which have determined that ground motion records from the same event at the same site but in orthogonal directions have sufficiently different spectral characteristics (Somerville *et al.*, 1997). The inclusion of both orthogonal directions allows for selection from among 454 individual records.

B.3.2 Selection of Source Records for Modification

Four source records were selected from the ground motion record databases provided above to match each of the five CMS developed for each southern Illinois site, leading to a suite of 20 ground motions for each site. The first step in selecting source records to match the CMS is to allocate the records into bins appropriate for each CMS based on magnitude and source-to-site distance. A source record was included in the bin of a CMS if the magnitude was within ±0.5 and the source-to-site distance was within ±30 km of the mean hazard deaggregation results for the appropriate site and period.

The source records within the bins were then evaluated for spectral similarity to the CMS. Similarity in spectral shape was assessed through the root-mean-squared values of the difference between the shape of the two spectra in terms of their ratio to the peak ground acceleration (Ambraseys *et al.*, 2004; Hancock *et al.*, 2008; Katsanos *et al.*, 2010). The root-mean-squared difference, D_{rms}, is calculated in Eq. (B.11), where *PSA* represents the pseudo-spectral acceleration at a period, *PGA* represents the peak ground acceleration, N_p represents the number of sampling periods, T_i represents the sampling period, and the subscripts *0* and *S* represent the record and target spectrum, respectively. The sampling points used to determine the spectral shape similarity were taken in a pseudo-logarithmic manner by sampling periods of 0.01, 0.02, 0.03, 0.04, 0.05, 0.06, 0.07, 0.08, 0.09, 0.1, 0.2, 0.3, 0.4, 0.5, 0.6, 0.7, 0.8, 0.9, 1.0, 2.0, 3.0, 4.0, and 5.0 s. The four source records with the smallest D_{rms} values which are within an average scale factor of 0.5-2.0 were then selected for modification to match to the CMS.

$$D_{rms} = \sqrt{\frac{1}{N_p}\sum_{i=1}^{N_p}\left(\frac{PSA_0(T_i)}{PGA_0} - \frac{PSA_S(T_i)}{PGA_S}\right)^2} \quad \text{(B.11)}$$

B.3.3 Modification of Source Records to Match the CMS

The four source records determined to be the best fit for spectral matching to a CMS were further modified through the software *RspMatch09* (Al Atik and Abrahamson, 2010). *RspMatch09* modifies the time history records by performing time-domain spectral matching between an input ground motion (the source records in this case) and a target spectrum (the CMS in this case) through the inclusion of improved tapered cosine wavelets to the time history. The improved tapered cosine wavelet is an improvement over other time-domain spectral matching software using other wavelets (like the reverse acceleration impulse response wavelet or the tapered cosine wavelet) due to its lack of velocity and displacement drift, and because it is more numerically efficient (Al Atik and Abrahamson, 2010).

The period range modified by *RspMatch09* is the 0.01-2.0 s period range. This range is too large for *RspMatch09* to modify in one pass, so modifications were made incrementally in 10-40 passes. The minimum period of every matching range is 0.01 s, however the maximum period considered in each pass varies. The maximum period in the initial pass was between 0.02125-0.055 s depending on if convergence is achieved, then the maximum period gradually increased with each subsequent pass until the entire 0.01-2.0 s range was included in the final pass.

The limited amount of source records that were included in many of the CMS bins unfortunately sometimes leads to poor spectral shape matches which cannot be completely corrected by *RspMatch09*. This often leads to poor spectral matches at the extremely short period range (periods less than or equal to 0.02s), as shown in Fig. B.9 which presents the initial (source) and unfiltered records compared to the CMS. This issue could be alleviated by more passes at the short period range in *RspMatch09*; however, this was deemed too computationally expensive, especially considering that it is extremely rare for a structure to be so stiff that the fundamental period is less than 0.02 s. The alternative solution, which was performed, was to filter the results such that none of the erroneous results in this extremely stiff period range affects the final ground motions. The filtering is performed using a fourth-order, low-pass Butterworth filter, which filters contributions from periods less than 0.02 s (frequencies greater than 50 Hz) after the wavelet modification has been completed.

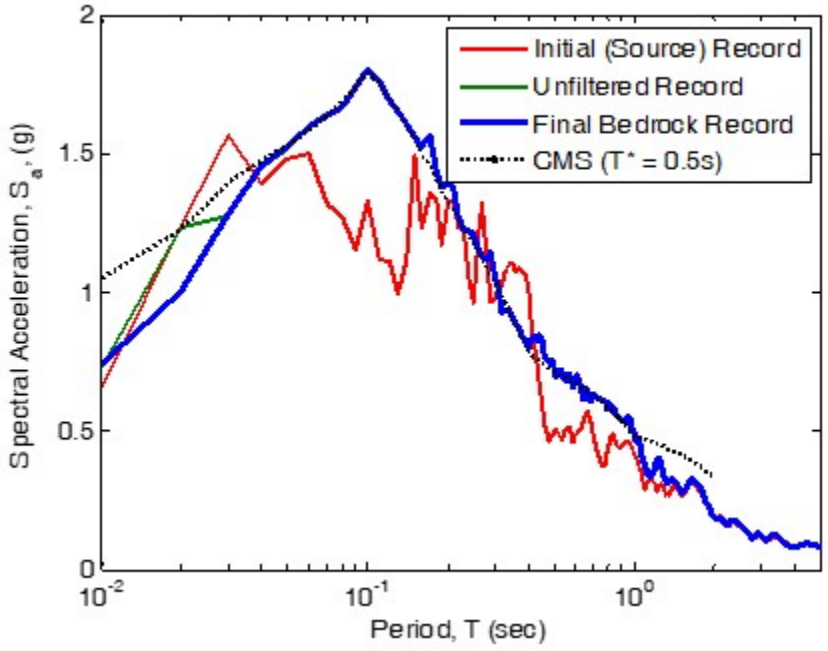

Figure B.9: Sample spectra for matching the TCU-089-W source record from the NUREG/CR6728 database (McGuire et al., 2001) to the T* = 0.5 s CMS for Cairo.

Additionally, the poor spectral matches may also cause velocity and displacement drifts in the time histories. The program *DEEPSOIL* (Hashash *et al.*, 2015) was used to baseline correct the time histories such that there is not any velocity or displacement drift. This process is performed by truncating the initial time history at the first and last zero-crossings, padding the ends with zeroes, applying a high-pass Butterworth filter (0.1 Hz cut-off frequency), and truncating the new time history at the first and last zero-crossings (Hashash *et al.*, 2015). The resulting time history has been spectrally matched, filtered, and baseline corrected. This time history represents the final bedrock ground motions which were used in the remaining ground motion development procedure. An example of the final bedrock ground motion record is also presented in Fig. B.9, in order to demonstrate the changes made throughout section B.3 to match the source records to the CMS.

As indicated previously, four ground motions are matched to each CMS at each site. Fig. B.10 presents the results for the five CMS developed at Cairo. While there is some variation of the individual ground motion spectra around the CMS they are matched to, the average of the four developed bedrock ground motion spectra tend to agree well with the CMS. The ground motions presented in Fig. B.10 are combined into a single plot for Cairo and presented alongside the final bedrock level ground motion spectra for the alluvial sites in Fig. B.11 and for the non-alluvial sites in Fig. B.12. Note how in single-source hazard sites, such as Cairo and Anna, the ground motion spectra from all the CMS are very close together, while in multi-source hazard sites such as East St. Louis there is a clear distinction between the bedrock level ground motions for each CMS, indicating the targeted nature of the CMS.

The suite size of 20 ground motions per site allows for each suite to be classified as large (FEMA, 2012). However, having only 4 ground motions matched to each CMS is below the industry standard of matching 7 ground motions to a target spectra to effectively account for the variability of the ground motions. In sites with single hazard sources (such as Cairo) this is not a large concern due to the CMS for all conditional periods being very similar leading to essentially 20 ground motions matched to a single target spectrum. Multiple hazard sites (such as East St. Louis), on the other hand, do have distinct CMS leading to the 4 ground motions matched to each CMS being insufficient in reaching the 7 ground motion per target spectra goal. This limitation is recognized and acknowledged.

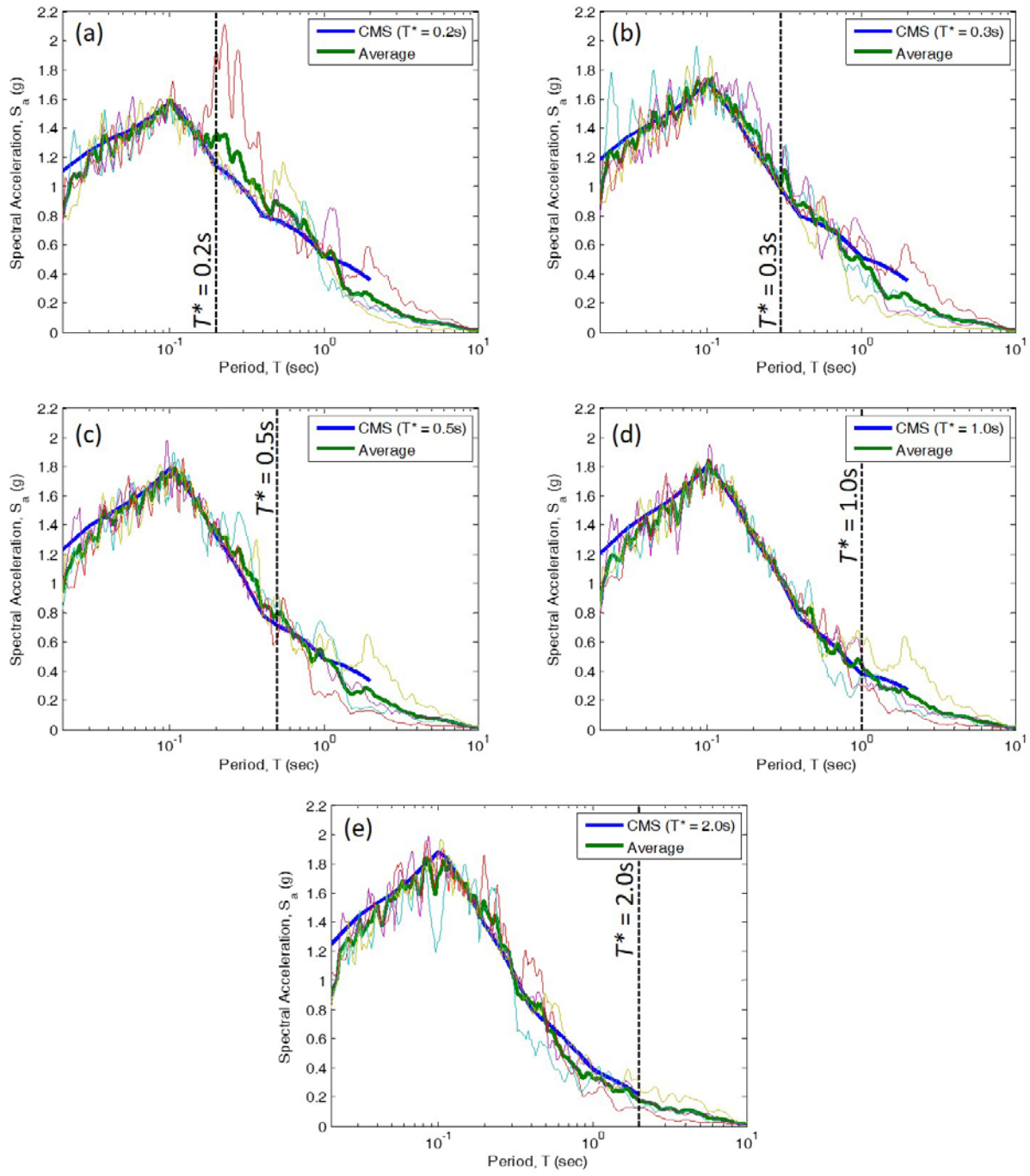

Figure B.10: Bedrock ground motion spectra for Cairo matched to the (a) T* = 0.2 s CMS, (b) T* = 0.3 s CMS, (c) T* = 0.5 s CMS, (d) T* = 1.0 s CMS, and (e) T* = 2.0 s CMS.

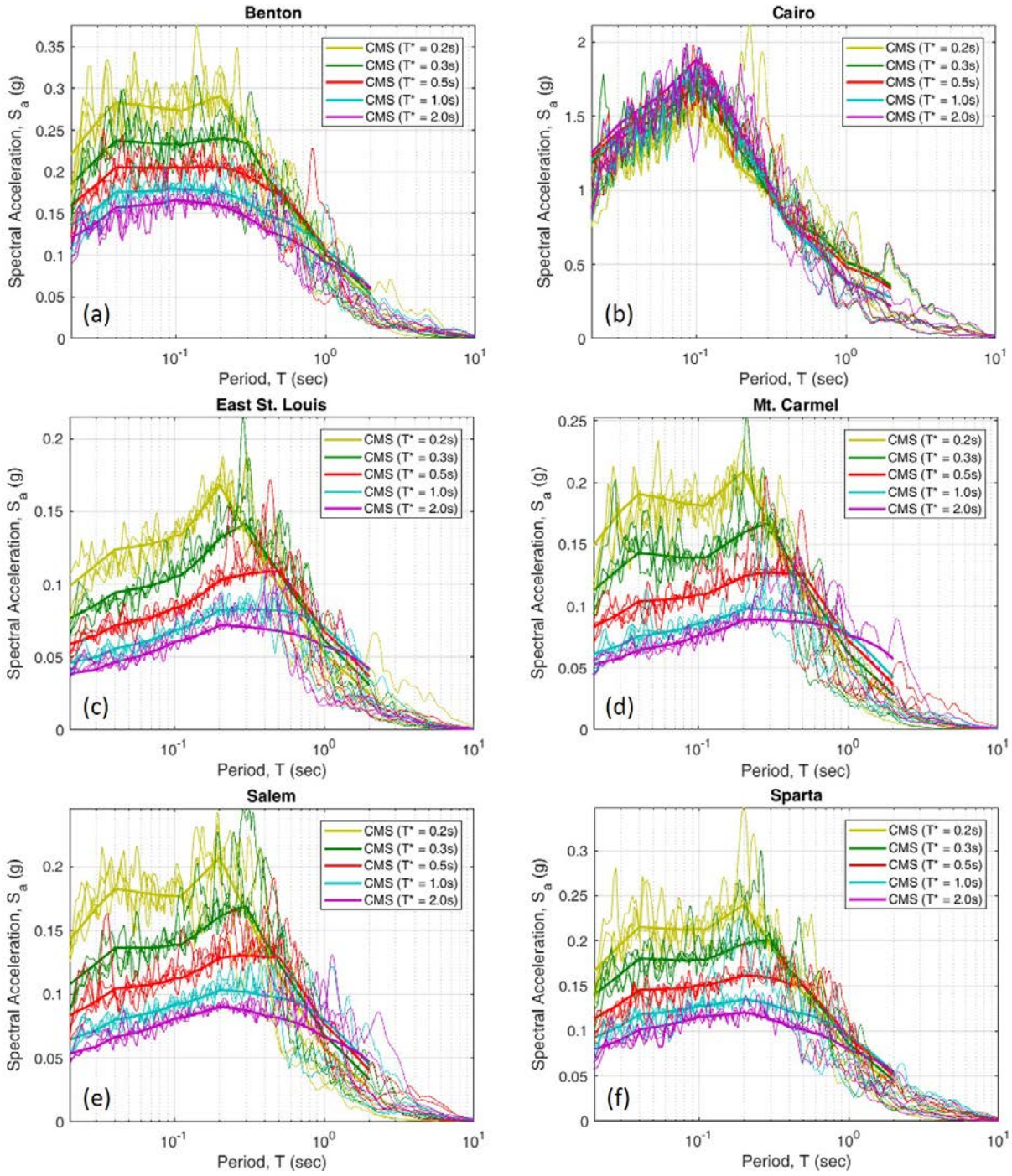

Figure B.11: Bedrock ground motion spectra for the alluvial sites (a) Benton, (b) Cairo, (c) East St. Louis, (d) Mt. Carmel, (e) Salem, and (f) Sparta.

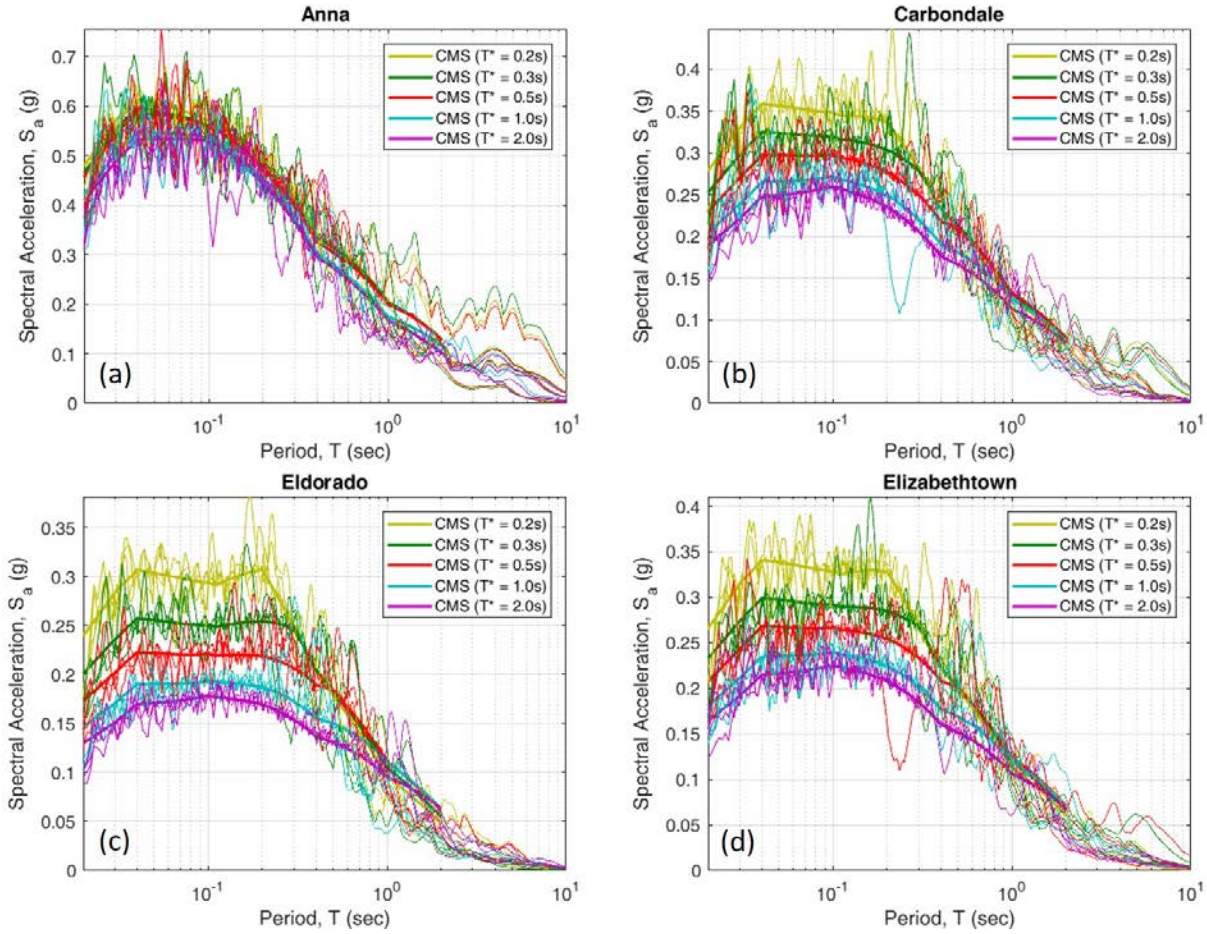

Figure B.12: Bedrock ground motion spectra for the non-alluvial sites (a) Anna, (b) Carbondale, (c) Eldorado, and (d) Elizabethtown.

B.4 SURFACE LEVEL GROUND MOTIONS

B.4.1 Propagation of Ground Motions from the Bedrock to the Surface

The soil property profiles developed in section B.1 were used to propagate the bedrock ground motions developed in section B.3 to the ground surface. The bedrock ground motions were propagated through each site's soil profile using the one-dimensional equivalent-linear frequency domain and nonlinear time domain analysis program *DEEPSOIL* (Hashash *et al.*, 2015). The nonlinear time domain analysis was used in this study, which uses the Newmark β method to solve the equations of motion in the time domain and accounts for the nonlinear properties of the soil. Equivalent-linear analyses were also performed for comparison to the nonlinear analyses in order to ensure that the soil is behaving reasonably in the nonlinear analyses.

As discussed earlier, soil property profiles were developed for the shear wave velocity, unit weight, and coefficient of at-rest earth pressure for all ten sites. In addition to this information, the layer thickness and ground water depth, as well as the modulus reduction ($G/G_{max} - \gamma$) and

damping ratio ($D - \gamma$) curves (where γ is shear strain), were also required at each soil layer in *DEEPSOIL*. *DEEPSOIL* provides a selection of soil models for use to describe the modulus reduction and damping ratio curves for both sand and clay soils. For this study the Darendeli (2001) models are used for both the sand and clay soil layers. The general Quadratic/Hyperbolic (GQ/H) (Groholski *et al.*, 2016) stress-strain constitutive model, which provides a small-strain shear modulus equal to the measured maximum shear modulus and a large-strain shear strength which asymptotically approaches the target shear strength, is used in this study through *DEEPSOIL*. The target shear strengths were defined as $\sigma'_{vo}tan(\phi')$ for coarse-grained soils and the undrained shear strength, s_u, for fine-grained soils. The effective friction angle, ϕ', was defined using the SPT results (as described earlier) and the undrained shear strength, s_u, was based on the soil layer description. The selected soil hysteretic behavior in *DEEPSOIL* was the non-Masing model described in Phillips and Hashash (2009).

Bedrock properties were also required in *DEEPSOIL* – the shear wave velocity and whether an elastic or rigid half-space is used. The shear wave velocity for bedrock in southern Illinois was taken as 2000 m/s (Hashash *et al.*, 2014), which is consistent with the site class A (hard rock) designation used in the creation of the CMS. The half-space of the bedrock describes whether an outcrop motion is being used in the analysis (elastic half-space) or a within motion is being used (rigid half-space). An elastic half-space was used in this study to represent that the ground motions were originating from the bedrock and not within the soil column.

The characteristics of the ground motion changes in both the time and spectral domains when propagated through the soil profile. An example demonstrating some of the changes that occur to a Cairo ground motion is presented in Fig. B.13. The differences in the time history and spectra at the bedrock and surface levels are clearly seen.

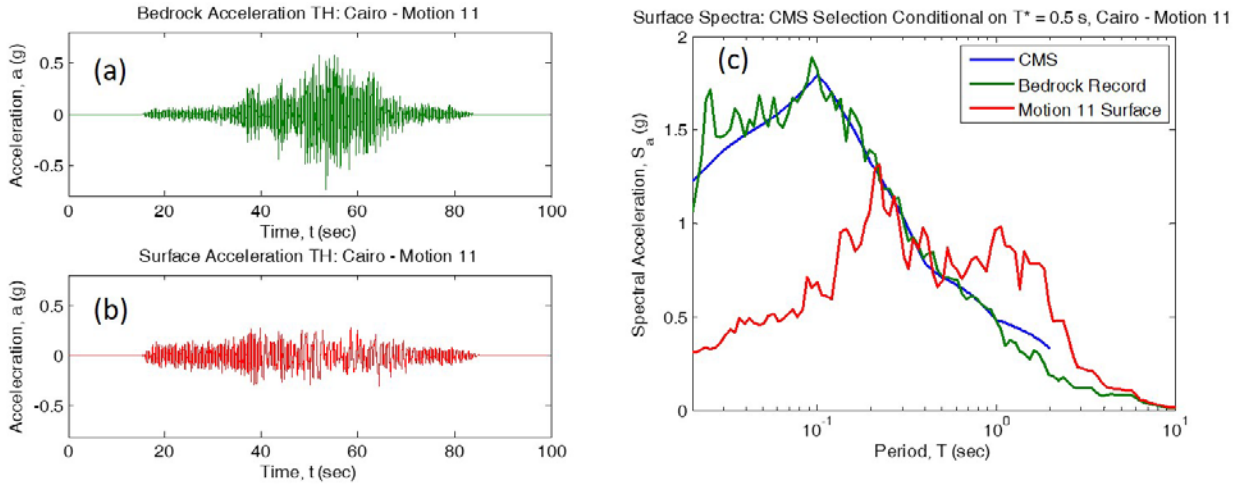

Figure B.13: Comparison of acceleration time histories of a ground motion developed for Cairo at the (a) bedrock level and (b) surface level. (c) The effect of ground motions propagation through the soil in the spectral domain.

B.4.2 Final Ground Motions

The surface ground motions acquired from the propagation of the bedrock ground motions through the soil property profiles in *DEEPSOIL* are the final ground motions for use in the study of seismic bridge behavior in Illinois. The final surface ground motion spectra are provided in Fig. B.14 for the alluvial sites and Fig. B.15 for the non-alluvial sites.

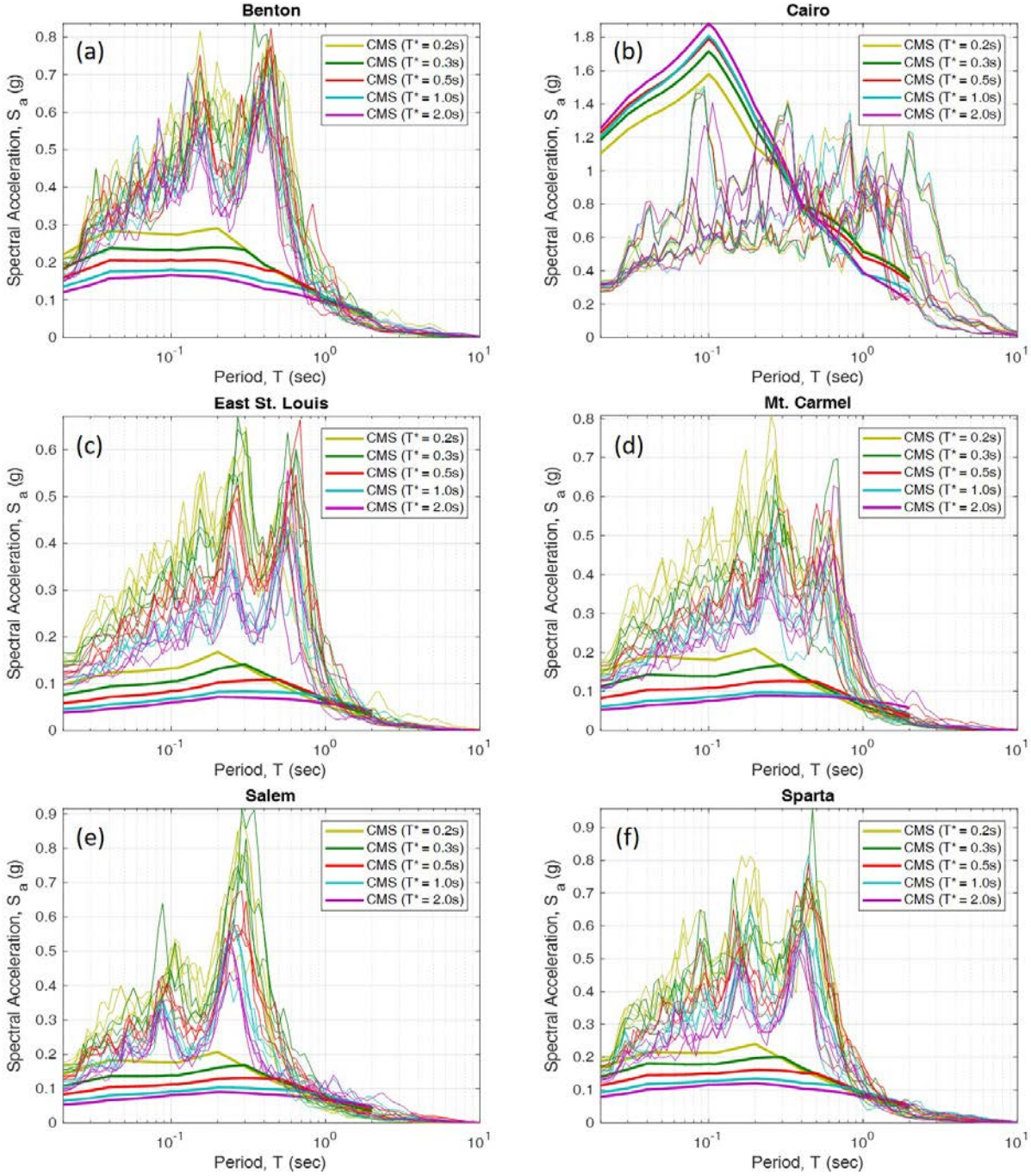

Figure B.14: Final ground motion spectra for the alluvial sites (a) Benton, (b) Cairo, (c) East St. Louis, (d) Mt. Carmel, (e) Salem, and (f) Sparta.

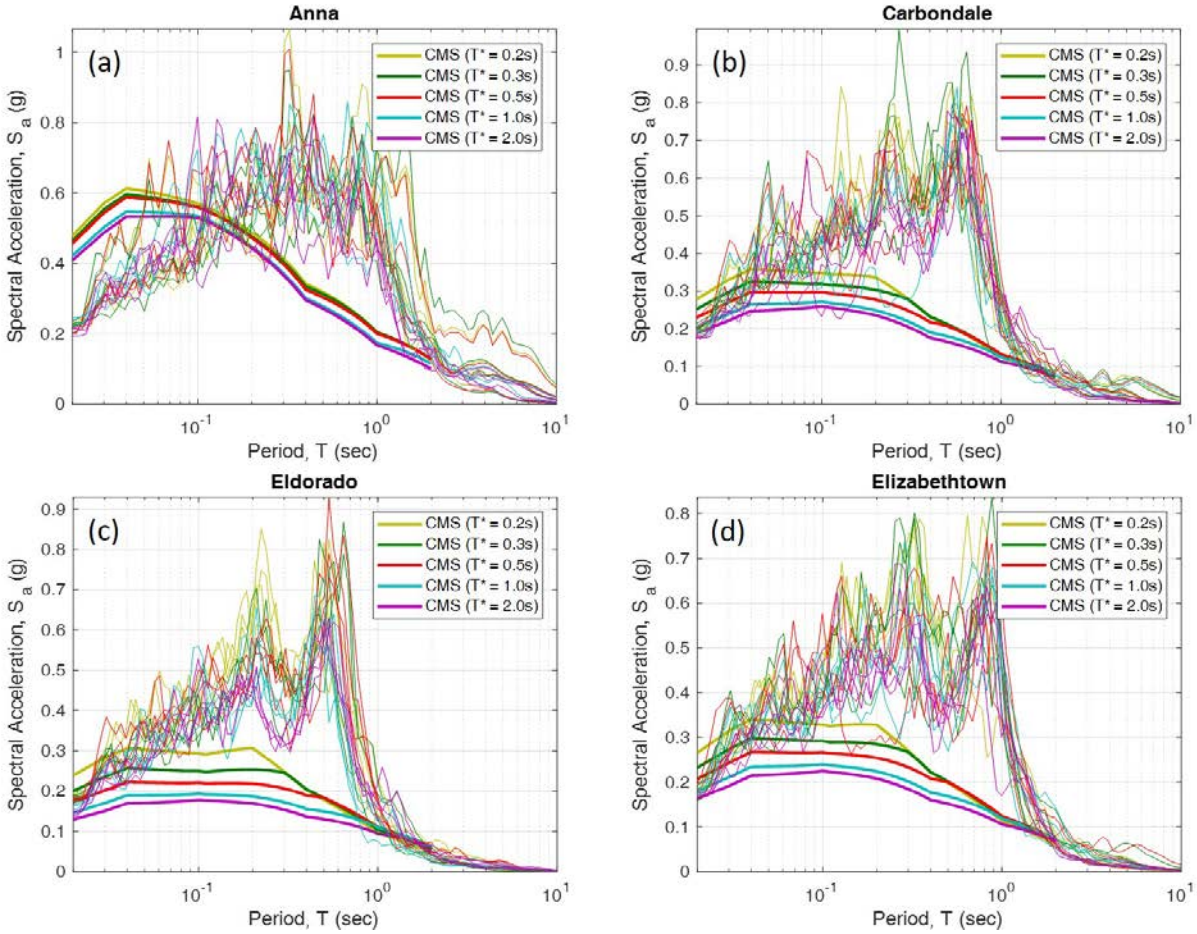

Figure B.15: Final ground motion spectra for the non-alluvial sites (a) Anna, (b) Carbondale, (c) Eldorado, and (d) Elizabethtown.

It can be noted in Fig. B.14 and Fig. B.15 that the soil properties tend to increase the spectral accelerations of some sites (as can be observed from their comparison to the CMS), such as at East St. Louis and Eldorado, while the spectra decrease in size at sites such as Cairo and Anna for some periods. Additionally, it can once again be observed that there are clear differences between the ground motion spectra produced at single- and multi-source hazard sites. Sites with a single hazard source, such as Cairo which is solely affected by the NMSZ, demonstrate that the spectra of the final ground motions produced when matching to all five CMS at the bedrock level are similar, as seen in Fig. B.14b. Sites with multiple hazard sources, such as East St. Louis which is affected by more than just the NMSZ, produce final ground motions that are separate from each other depending on the CMS they were matched to at the bedrock level. This is demonstrated in Fig. B.14c where clear distinctions in the color of the individual ground motions (which indicate which CMS they are matched to) are still discernable at the surface level. This difference is also made clear in Fig. B.16 where the average of the surface ground motions which were matched to the same CMS are plotted for Cairo and East St. Louis. As expected due to the difference in hazard sources, the average of Cairo's motions are all similar while East St. Louis' have a discernable difference, especially at short periods.

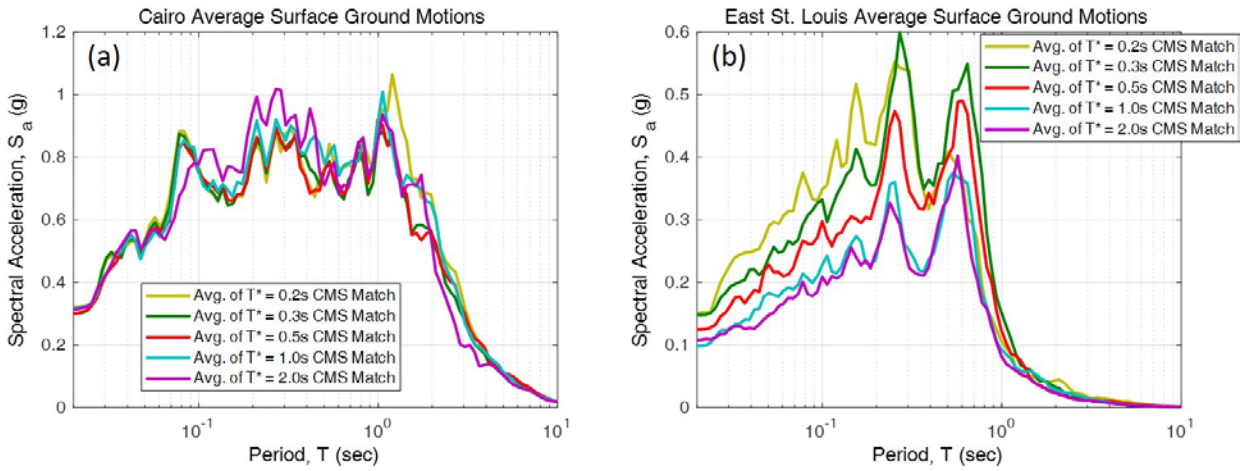

Figure B.16: Average of the surface level ground motions that were matched to each CMS at the bedrock level for (a) Cairo, and (b) East St. Louis.

It is important to acknowledge that this difference in surface ground motion spectral behavior between single- and multi-source hazard sites demonstrates how the CMS is less useful for a single-source hazard site. However, it is still just as useful as matching to the UHS in this case, which is essentially all that was performed for the Cairo site due to the similarity between the UHS and CMS. Advantages of the CMS are present in multi-source hazard sites such as East St. Louis, where a variety of fundamental periods are considered in analyses using these ground motions due to the multiple *T** periods considered in the development of the ground motions. As discussed earlier, the ability to consider multiple fundamental periods is important in this study due to the wide range of bridges investigated with these ground motions that have various fundamental periods which may change throughout analyses due to damage.

These developed ground motions are unique to southern Illinois in that they utilize the CMS, which has not previously been used for ground motion development in the region. The ground motions are also unique in their applicability to the study of highway bridges in Illinois due to the period range covered by the developed CMS. The ground motions for Cairo are generally used in the dynamic analyses of the studies in this project due to that site producing the most intense ground motions in the state. While the developed ground motions are used in this study to observe the seismic behavior of IABs, the Cairo ground motions have already also been used in published studies of the seismic behavior of stub abutment bridges in Luo *et al.* (2016; 2017) demonstrating their applicability and adequacy for use in the studies of this project. The ground motion time histories described in this chapter are also discussed in Kozak *et al.* (2017a) and a database containing the developed ground motion time histories can be accessed through Kozak *et al*. (2017b).

APPENDIX B REFERENCES

AASHTO (2011) *Guide Specifications for LRFD Seismic Bridge Design*, American Association of State Highway and Transportation Officials, Washington, DC, USA.

Al Atik, L. and Abrahamson, N. (2010) "An improved method for nonstationary spectral matching," *Earthquake Spectra* **26**(3), 601-617.

Ambraseys, N.N., Douglas, J., Rinaldis, D., Berge-Thierry, C., Suhadolc, P., Costa, G., Sigbjornsson, R. and Smit, P. (2004) *Dissemination of European Strong-Motion Data, Col. 2. CD-ROM Collection*, Engineering and Physical Sciences Research Council, Swindon, UK.

ASCE (2016) *ASCE 7-16: Minimum Design Loads for Buildings and Other Structures*, American Society of Civil Engineers, Reston, VA, USA.

Baker, J.W. (2011) "Conditional mean spectrum: Tool for ground motion selection," *Journal of Structural Engineering* **137**(3), 322-331.

Baker, J.W. and Cornell, C.A. (2006) "Spectral shape, epsilon and record selection," *Earthquake Engineering and Structural Dynamics* **35**(9), 1077-1095.

Baker, J.W. and Jayaram, N. (2008) "Correlation of spectral acceleration values from NGA ground motions models," *Earthquake Spectra* **24**(1), 299-317.

Coduto, D.P., Yeung, M.R. and Kitch, W.A. (2011) *Geotechnical Engineering: Principles and Practices*. Pearson Higher Education, Upper Saddle River, NJ, USA.

Darendeli, M. (2001) "Development of a new family of normalized modulus reduction and material damping curves," Ph.D. Dissertation, University of Texas, Austin, TX, USA.

FEMA (2012) *FEMA P-58-1: Seismic Performance Assessment of Buildings, Volume 1 – Methodology*, Federal Emergency Management Agency, Washington, DC, USA.

Filipov, E.T., Revell, J.R., Fahnestock, L.A., LaFave, J.M., Hajjar, J.F., Foutch, D.A. and Steelman, J.S. (2013) "Seismic performance of highway bridges with fusing bearing components for quasi-isolation," *Earthquake Engineering and Structural Dynamics* **42**, 1375-1394.

Goulet, C.A., Kishida, T., Ancheta, T.D., Cramer, C.H., Darragh, R.B., Silva, W.J., Hashash, Y.M.A., Harmon, J., Stewart, J.P., Wooddell, K.E. and Youngs, R.R. (2014) *PEER Report No. 2014-17: PEER NGA-East Database*, Pacific Earthquake Engineering Research Center, University of California, Berkeley, CA, USA.

Groholski, D.R., Hashash, Y.M.A., Kim, B. and Musgrove, M. (2016) "Simplified model for small-strain nonlinearity and strength in 1D seismic site response analysis," *Journal of Geotechnical and Geoenvironmental Engineering* **142**(9), 04016042-1-14.

Hancock, J. Bommer, J.J. and Stafford, P.J. (2008) "Numbers of scaled and matched acceleragrams required for inelastic dynamic analyses," *Earthquake Engineering and Structural Dynamics* **37**(14), 1585-1607.

Hashash, Y. and Moon, S. (2011) *Site Amplification Factors for Deep Deposits and Their Application in Seismic Hazard Analysis for Central U.S.*, United States Geological Survey, Reston, VA, USA.

Hashash, Y.M.A., Kottke, A.R., Stewart, J.P., Campbell, K.W., Kim, B., Rathje, E.M., Silva, W.J., Nikolaou, S. and Moss, C. (2014) *PEER Report No, 2013-08: Reference Rock Site Condition for Central and Eastern North America, Part I – Velocity Definition*, Pacific Earthquake Engineering Research Center, University of California, Berkeley, CA, USA.

Hashash, Y.M.A., Musgrove, M.I., Harmon, J.A., Groholski, D.R., Phillips, C.A. and Park, D. (2015) *DEEPSOIL 6.0, User Manual*, University of Illinois, Urbana, IL, USA.

Herzog, B.L., Stiff, B.J., Chenoweth, C.A., Warner, K.L., Sievering, J.B. and Avery, C. (1994) *Buried Bedrock Surface of Illinois: ISGS GIS Database GISDB_BEDGEO. IL_Bedrock_Topography_1994_Ln*, Illinois State Geological Survey, Champaign, IL, USA.

Hettiarachchi, H. and Brown, T. (2009) "Use of SPT blow count to estimate shear strength properties of soils: Energy balance approach," *Journal of Geotechnical and Geoenvironmental Engineering* **135**(6), 830-834.

IDOT (2014) *E-mail Communication 3/6/2014 to 6/13/2014*.

ISGS (2015) *Quaternary (Ice Age) Deposits Map*, Illinois State Geological Survey, Champaign, IL, USA.

Katsanos, E.I., Sextos, A.G. and Manolis, G.D. (2010) "Selection of earthquake ground motion records: A state-of-the-art review from a structural engineering perspective," *Soil Dynamics and Earthquake Engineering* **30**(4), 157-169.

Kozak D.L. (2018) "Seismic Behavior and Design of Integral Abutment Bridges in Southern Illinois," Ph.D. Dissertation, University of Illinois, Urbana, IL, USA.

Kozak, D.L., Luo, J., Olson, S.M., LaFave, J.M. and Fahnestock, L.A. (2017a) "Modification of Ground Motions for Use in Central North America," *Journal of Earthquake Engineering,* dx.doi.org/10.1080/13632469.2017.1387190.

Kozak, D.L., Luo, J., Olson, S.M., LaFave, J.M. and Fahnestock, L.A. (2017b) *Report No. NSEL-048: Modification of ground motions for use in Central North America: southern Illinois surface ground motions for structural analysis*, Newmark Structural Engineering Laboratory Report Series, University of Illinois, Urbana, IL, USA. hdl.handle.net/2142/98456.

Luo, J., Fahnestock, L.A., Kozak, D.L. and LaFave, J.M. (2016) "Seismic analysis incorporating detailed structure-abutment-foundation interaction for quasi-isolated highway bridges," *Structure and Infrastructure Engineering* **13**(5), 581-603.

Luo, J., Fahnestock, L.A. and LaFave, J.M. (2017) "Nonlinear static pushover and eigenvalue modal analyses of quasi-isolated highway bridges with seat-type abutments," *Structures* **12**, 145-167.

McGuire, R.K., Silva, W.J. and Costantino, C. (2001) *Report NUREG/CR-6728: Technical Basis for Revision of Regulatory Guidance on Design Ground Motions: Hazards- and Risk-Consistent Ground Motion Spectra Guidelines*, US Nuclear Regulatory Commission, Washington, DC, USA.

McKenna, F., Mazonni, S. and Fenves, G.L. (2006) *Open system for earthquake engineering simulation (OpenSees)*, Pacific Earthquake Engineering Research Center, University of California, Berkeley, CA, USA.

Peck, R.B., Hanson, W.E. and Thornburn, T.H. (1974) *Foundation Engineering*, John Wiley & Sons, New York, NY, USA.

Petersen, M.D., Frankel, A.D., Harmsen, S.C., Mueller, C.S., Haller, K.M., Wheeler, R.L., Wesson, R.L., Zeng, Y., Boyd, O.S., Perkins, D.M., Luco, N., Field, E.H., Wills, C.J. and Rukstales, K.S. (2008) *Documentation for the 2008 Update of the United States National Seismic Hazard Maps: U.S. Geological Survey Open-File Report 2008-1128*, U.S. Geological Survey, Reston, VA, USA.

Phillips, C. and Hashash, Y. (2009) "Damping formulation for non-linear 1D site response analyses," *Soil Dynamics and Earthquake Engineering* **29**, 1143-1158.

Revell, J. (2013) "Quasi-isolated highway bridges: Influence of bearing anchorage strength on seismic performance," M.S. Dissertation, University of Illinois, Urbana, IL, USA.

Somerville, P., Smith, N., Punyamurthula, S. and Sun, J. (1997) *Development of Ground Motion Time Histories for Phase 2 of the FEMA/SAC Steel Project*, SAC Joint Venture, Sacramento, CA, USA.

Terzaghi, K., Peck, R.B. and Mesri, G. (1996) *Soil Mechanics in Engineering Practice, Third Edition*. John Wiley & Sons, New York, NY, USA.

Toro, G.R., Abrahamson, N.A. and Schneider, J.F. (1997) "Model of strong ground motions from earthquakes in central and eastern North America: Best estimates and uncertainties," *Seismological Research Letters* **68**(1), 41-57.

USGS (2008) *2008 Interactive Deaggregation*, United States Geological Survey, Reston, VA, USA. Retrieved from http://geohazards.usgs.gov/deaggint/2008/.

USGS (2014) *Hazard Curve Application*, United States Geological Survey, Reston, VA, USA. Retrieved from http://geohazards.usgs.gov/hazardtool/.

Wair, B.R., DeJong, J.T. and Shantz, T. (2012) *PEER Report No. 2012/08: Guidelines for Estimation of Shear Wave Velocity Profiles*, Pacific Earthquake Engineering Research Center, University of California, Berkeley, CA, USA.

Wolff, T.E. (1989) “Pile capacity prediction using parameter functions,” *ASCE Geotechnical Special Publication* **23**, 96-107.

APPENDIX C: DESIGN-LEVEL DYNAMIC ANALYSIS DATA

Design-level dynamic analysis results for the 45 IABs of the parametric study are presented in this appendix. These results are used for the discussion in Chapter 4.

The IABs are separated into the 5 major types of prototype IABs: single-span steel, three-span steel, four-span steel, three-span concrete, and four-span concrete. The presented results in this appendix include the tables of frequency of limit state occurrences when the IABs are subjected to design-level ground motions in the bridge longitudinal and transverse direction in Cairo.

The design-level dynamic analysis frequency of limit state occurrence tables are presented for the other 9 southern Illinois sites as well. These tables are only for IABs with 15-foot tall piers, elastomeric bearings, and alluvial soil conditions. These results are used for the discussion in Chapter 4.6.

The design-level dynamic behavior of components in the IABs are also presented for a representative ground motion for each of the five IABs with 15-foot tall piers, elastomeric bearings, and alluvial soil conditions.

Table C.1 describes which tables and figures present data for each set of IABs.

Table C.1: Organization of Figures in Appendix C

	Bridge Type	Figure of Table
Frequency of Limit State Occurrence Table at Cairo	1-Span Steel	Table C.2
	3-Span Steel	Table C.3
	4-Span Steel	Table C.4
	3-Span Concrete	Table C.5
	4-Span Concrete	Table C.6
Frequency of Limit State Occurrence Table at All Southern Illinois Sites	1-Span Steel	Table C.7
	3-Span Steel	Table C.8
	4-Span Steel	Table C.9
	3-Span Concrete	Table C.10
	4-Span Concrete	Table C.11
Representative Design-Level Dynamic Analysis Behavior Plots at Cairo	1-Span Steel	Fig. C.1-C.2
	3-Span Steel	Fig. C.3-C.4
	4-Span Steel	Fig. C.5-C.6
	3-Span Concrete	Fig. C.7-C.8
	4-Span Concrete	Fig. C.9-C.10

Table C.2: Frequency of Limit State Occurrences for Single-Span Steel IABs Under Design-Level Ground Motion Suite

Bridge	Longitudinal Limit State Occurrence					
	Ideal	Acceptable				Unacceptable
	BF	APY	APB	APS	PA	APR
Ss____S	0%	65%	0%	30%	0%	0%
Ss____A	0%	80%	0%	0%	0%	0%
Ss____H	0%	30%	0%	0%	0%	0%
Bridge	**Transverse Limit State Occurrence**					
	Ideal	**Acceptable**				**Unacceptable**
	BF	**APY**	**APB**	**APS**	**PA**	**APR**
Ss____S	0%	80%	0%	65%	0%	0%
Ss____A	0%	10%	0%	5%	0%	0%
Ss____H	0%	0%	0%	0%	0%	0%

Table C.3: Frequency of Limit State Occurrences for Three-Span Steel IABs Under Design-Level Ground Motion Suite

Bridge	Longitudinal Limit State Occurrence																			
	Ideal								Acceptable								Unacceptable			
	BF	SL	CL	RE	RY	RF	FY	FF	APY	APB	APS	PA	PPY	PPS	SM	CM	BU	SS	CS	APR
StC15ES	0%	100%	100%	0%	0%	0%	-	-	100%	0%	100%	0%	20%	45%	50%	65%	0%	0%	0%	0%
StC15EA	0%	60%	35%	0%	0%	0%	-	-	100%	0%	70%	0%	0%	0%	0%	0%	0%	0%	0%	0%
StC15EH	0%	20%	5%	0%	0%	0%	-	-	100%	0%	30%	0%	0%	0%	0%	0%	0%	0%	0%	0%
StC40ES	0%	80%	25%	0%	0%	0%	-	-	100%	30%	100%	0%	0%	70%	10%	5%	0%	0%	0%	0%
StC40EA	0%	15%	0%	0%	0%	0%	-	-	100%	15%	100%	0%	0%	5%	0%	0%	0%	0%	0%	0%
StC40EH	0%	0%	0%	0%	0%	0%	-	-	100%	0%	60%	0%	0%	0%	0%	0%	0%	0%	0%	0%
StC15FS	0%	100%	90%	-	-	-	0%	0%	100%	0%	95%	0%	5%	20%	50%	60%	0%	0%	0%	0%
StC15FA	0%	80%	60%	-	-	-	0%	0%	100%	0%	55%	0%	0%	0%	10%	20%	0%	0%	0%	0%
StC15FH	0%	35%	25%	-	-	-	0%	0%	100%	0%	30%	0%	0%	0%	0%	0%	0%	0%	0%	0%
StC40FS	0%	70%	35%	-	-	-	0%	0%	100%	30%	100%	0%	0%	35%	10%	10%	0%	0%	0%	0%
StC40FA	0%	15%	0%	-	-	-	0%	0%	100%	15%	100%	0%	0%	0%	0%	0%	0%	0%	0%	0%
StC40FH	0%	0%	0%	-	-	-	0%	0%	100%	0%	55%	0%	0%	0%	0%	0%	0%	0%	0%	0%
Bridge	Transverse Limit State Occurrence																			
	Ideal								Acceptable								Unacceptable			
	BF	SL	CL	RE	RY	RF	FY	FF	APY	APB	APS	PA	PPY	PPS	SM	CM	BU	SS	CS	APR
StC15ES	0%	80%	40%	100%	100%	0%	-	-	80%	0%	75%	0%	75%	35%	0%	0%	0%	0%	0%	0%
StC15EA	0%	40%	10%	100%	100%	0%	-	-	100%	0%	30%	0%	0%	0%	0%	0%	0%	0%	0%	0%
StC15EH	0%	40%	0%	100%	100%	0%	-	-	100%	0%	10%	0%	0%	0%	0%	0%	0%	0%	0%	0%
StC40ES	0%	100%	85%	100%	100%	0%	-	-	100%	50%	100%	0%	0%	20%	10%	10%	0%	0%	0%	0%
StC40EA	0%	65%	20%	100%	80%	0%	-	-	100%	5%	70%	0%	0%	0%	0%	0%	0%	0%	0%	0%
StC40EH	0%	25%	0%	100%	55%	0%	-	-	100%	0%	35%	0%	0%	0%	0%	0%	0%	0%	0%	0%
StC15FS	0%	70%	30%	-	-	-	100%	0%	75%	0%	35%	0%	50%	30%	0%	0%	0%	0%	0%	0%
StC15FA	0%	60%	5%	-	-	-	80%	0%	60%	0%	10%	0%	0%	0%	0%	0%	0%	0%	0%	0%
StC15FH	0%	80%	0%	-	-	-	100%	0%	60%	0%	0%	0%	0%	0%	0%	0%	0%	0%	0%	0%
StC40FS	0%	100%	95%	-	-	-	15%	0%	100%	45%	100%	0%	0%	0%	10%	15%	0%	0%	0%	0%
StC40FA	0%	65%	35%	-	-	-	0%	0%	100%	5%	75%	0%	0%	0%	0%	0%	0%	0%	0%	0%
StC40FH	0%	35%	0%	-	-	-	0%	0%	100%	0%	30%	0%	0%	0%	0%	0%	0%	0%	0%	0%

Table C.4: Frequency of Limit State Occurrences for Four-Span Steel IABs Under Design-Level Ground Motion Suite

Bridge	Longitudinal Limit State Occurrence																			
	Ideal								Acceptable								Unacceptable			
	BF	SL	CL	RE	RY	RF	FY	FF	APY	APB	APS	PA	PPY	PPS	SM	CM	BU	SS	CS	APR
SIC15ES	0%	100%	100%	0%	0%	0%	-	-	100%	15%	100%	0%	0%	0%	85%	85%	0%	5%	45%	0%
SIC15EA	0%	100%	100%	0%	0%	0%	-	-	100%	0%	100%	0%	0%	5%	25%	35%	0%	0%	5%	0%
SIC15EH	0%	35%	25%	0%	0%	0%	-	-	100%	0%	30%	0%	0%	0%	0%	0%	0%	0%	0%	0%
SIC40ES	0%	80%	80%	0%	0%	0%	-	-	100%	35%	100%	0%	0%	25%	15%	20%	0%	0%	0%	0%
SIC40EA	0%	75%	50%	0%	0%	0%	-	-	100%	15%	100%	0%	0%	0%	0%	5%	0%	0%	0%	0%
SIC40EH	0%	5%	0%	0%	0%	0%	-	-	100%	0%	50%	0%	0%	0%	0%	0%	0%	0%	0%	0%
SIC15FS	0%	100%	100%	-	-	-	0%	0%	100%	15%	100%	0%	0%	0%	100%	100%	0%	5%	45%	0%
SIC15FA	0%	90%	85%	-	-	-	0%	0%	90%	0%	75%	0%	0%	0%	60%	80%	0%	0%	0%	0%
SIC15FH	0%	85%	80%	-	-	-	0%	0%	100%	0%	25%	0%	0%	0%	5%	25%	0%	0%	0%	0%
SIC40FS	0%	85%	80%	-	-	-	0%	0%	100%	35%	100%	0%	0%	35%	15%	20%	0%	0%	0%	0%
SIC40FA	0%	75%	50%	-	-	-	0%	0%	100%	15%	100%	0%	0%	5%	0%	0%	0%	0%	0%	0%
SIC40FH	0%	0%	0%	-	-	-	0%	0%	100%	0%	45%	0%	0%	0%	0%	0%	0%	0%	0%	0%
Bridge	**Transverse Limit State Occurrence**																			
	Ideal								Acceptable								Unacceptable			
	BF	SL	CL	RE	RY	RF	FY	FF	APY	APB	APS	PA	PPY	PPS	SM	CM	BU	SS	CS	APR
SIC15ES	0%	100%	100%	100%	0%	0%	-	-	15%	0%	0%	0%	0%	100%	100%	100%	0%	0%	50%	0%
SIC15EA	0%	100%	100%	100%	0%	0%	-	-	10%	0%	0%	0%	0%	0%	100%	100%	0%	0%	35%	0%
SIC15EH	0%	100%	100%	100%	0%	0%	-	-	20%	0%	0%	0%	0%	0%	100%	100%	0%	0%	35%	0%
SIC40ES	0%	100%	100%	100%	0%	0%	-	-	85%	15%	65%	0%	0%	0%	80%	85%	0%	0%	0%	0%
SIC40EA	0%	100%	100%	100%	0%	0%	-	-	100%	5%	80%	0%	0%	0%	85%	85%	0%	0%	0%	0%
SIC40EH	0%	100%	100%	100%	0%	0%	-	-	100%	0%	5%	0%	0%	0%	85%	90%	0%	0%	0%	0%
SIC15FS	0%	100%	100%	-	-	-	0%	0%	0%	0%	0%	0%	0%	100%	80%	85%	0%	0%	25%	0%
SIC15FA	0%	100%	100%	-	-	-	0%	0%	0%	0%	0%	0%	0%	0%	75%	90%	0%	0%	25%	0%
SIC15FH	0%	100%	100%	-	-	-	0%	0%	5%	0%	0%	0%	0%	0%	70%	90%	0%	0%	25%	0%
SIC40FS	0%	100%	100%	-	-	-	0%	0%	85%	15%	70%	0%	0%	0%	85%	90%	0%	0%	0%	0%
SIC40FA	0%	100%	100%	-	-	-	0%	0%	95%	0%	80%	0%	0%	0%	85%	95%	0%	0%	0%	0%
SIC40FH	0%	100%	100%	-	-	-	0%	0%	100%	0%	5%	0%	0%	0%	85%	95%	0%	0%	0%	0%

Table C.5: Frequency of Limit State Occurrences for Three-Span Concrete IABs Under Design-Level Ground Motion Suite

Bridge	Longitudinal Limit State Occurrence																			
	Ideal								Acceptable								Unacceptable			
	BF	SL	CL	RE	RY	RF	FY	FF	APY	APB	APS	PA	PPY	PPS	SM	CM	BU	SS	CS	APR
CtC15ES	0%	100%	100%	0%	0%	0%	-	-	100%	70%	100%	0%	0%	0%	85%	85%	0%	20%	75%	15%
CtC15EA	0%	100%	100%	0%	0%	0%	-	-	100%	75%	100%	0%	0%	0%	75%	85%	0%	5%	50%	20%
CtC15EH	0%	100%	80%	0%	0%	0%	-	-	100%	25%	100%	0%	0%	0%	25%	25%	0%	0%	0%	0%
CtC40ES	0%	75%	70%	0%	0%	0%	-	-	100%	65%	100%	0%	0%	10%	20%	30%	0%	0%	0%	15%
CtC40EA	0%	80%	75%	0%	0%	0%	-	-	100%	80%	100%	0%	0%	0%	20%	20%	0%	0%	0%	30%
CtC40EH	0%	55%	40%	0%	0%	0%	-	-	100%	75%	100%	0%	0%	10%	0%	5%	0%	0%	0%	20%
CtC40FS	0%	75%	70%	-	-	-	0%	0%	100%	70%	100%	0%	0%	15%	25%	30%	0%	0%	0%	15%
CtC40FA	0%	80%	65%	-	-	-	0%	0%	100%	80%	100%	0%	0%	15%	20%	20%	0%	0%	0%	30%
CtC40FH	0%	55%	35%	-	-	-	0%	0%	100%	75%	100%	0%	0%	0%	0%	5%	0%	0%	0%	20%
Bridge	**Transverse Limit State Occurrence**																			
	Ideal								Acceptable								Unacceptable			
	BF	SL	CL	RE	RY	RF	FY	FF	APY	APB	APS	PA	PPY	PPS	SM	CM	BU	SS	CS	APR
CtC15ES	0%	95%	80%	100%	100%	100%	-	-	100%	80%	100%	0%	0%	0%	65%	65%	0%	25%	50%	15%
CtC15EA	0%	100%	80%	100%	100%	100%	-	-	100%	90%	100%	0%	0%	0%	40%	40%	0%	5%	15%	10%
CtC15EH	0%	70%	45%	100%	100%	100%	-	-	100%	90%	90%	0%	0%	0%	0%	0%	0%	0%	0%	0%
CtC40ES	0%	85%	80%	100%	100%	60%	-	-	100%	75%	100%	0%	0%	0%	40%	50%	0%	0%	0%	15%
CtC40EA	0%	95%	80%	100%	100%	65%	-	-	100%	90%	100%	0%	0%	0%	25%	35%	0%	0%	0%	30%
CtC40EH	0%	90%	70%	100%	100%	20%	-	-	100%	100%	100%	0%	0%	0%	0%	5%	0%	0%	0%	45%
CtC40FS	0%	100%	100%	-	-	-	100%	0%	100%	80%	100%	0%	0%	0%	55%	60%	0%	0%	0%	15%
CtC40FA	0%	100%	95%	-	-	-	100%	0%	100%	90%	100%	0%	0%	0%	30%	55%	0%	0%	0%	25%
CtC40FH	0%	100%	100%	-	-	-	100%	0%	100%	100%	100%	0%	0%	0%	5%	10%	0%	0%	0%	20%

Table C.6: Frequency of Limit State Occurrences for Four-Span Concrete IABs Under Design-Level Ground Motion Suite

Bridge	Longitudinal Limit State Occurrence																			
	Ideal								Acceptable								Unacceptable			
	BF	SL	CL	RE	RY	RF	FY	FF	APY	APB	APS	PA	PPY	PPS	SM	CM	BU	SS	CS	APR
ClC15ES	0%	93%	93%	0%	0%	0%	-	-	100%	33%	100%	0%	0%	0%	67%	67%	0%	0%	67%	0%
ClC15EA	0%	94%	94%	0%	0%	0%	-	-	100%	59%	100%	0%	0%	0%	76%	76%	0%	6%	76%	6%
ClC15EH	0%	90%	90%	0%	0%	0%	-	-	100%	70%	100%	0%	0%	0%	75%	80%	0%	20%	70%	20%
ClC40ES	0%	75%	70%	0%	0%	0%	-	-	100%	60%	95%	0%	0%	0%	25%	35%	0%	0%	10%	15%
ClC40EA	0%	75%	70%	0%	0%	0%	-	-	100%	60%	100%	0%	0%	0%	20%	35%	0%	0%	0%	10%
ClC40EH	0%	80%	80%	0%	0%	0%	-	-	100%	80%	100%	0%	0%	0%	15%	25%	0%	0%	0%	20%
ClC40FS	0%	70%	70%	-	-	-	0%	0%	100%	60%	95%	0%	0%	0%	25%	45%	0%	0%	0%	15%
ClC40FA	0%	75%	70%	-	-	-	0%	0%	100%	65%	100%	0%	0%	0%	20%	35%	0%	0%	0%	10%
ClC40FH	0%	80%	70%	-	-	-	0%	0%	100%	80%	100%	0%	0%	0%	10%	20%	0%	0%	0%	25%
Bridge	Transverse Limit State Occurrence																			
	Ideal								Acceptable								Unacceptable			
	BF	SL	CL	RE	RY	RF	FY	FF	APY	APB	APS	PA	PPY	PPS	SM	CM	BU	SS	CS	APR
ClC15ES	0%	100%	100%	100%	100%	0%	-	-	75%	20%	40%	0%	0%	100%	100%	100%	0%	40%	95%	0%
ClC15EA	0%	100%	100%	100%	100%	0%	-	-	75%	15%	55%	0%	0%	0%	100%	100%	0%	35%	100%	0%
ClC15EH	0%	100%	100%	100%	100%	0%	-	-	80%	0%	25%	0%	0%	0%	100%	100%	0%	30%	95%	0%
ClC40ES	0%	100%	100%	100%	100%	0%	-	-	94%	22%	78%	0%	0%	0%	72%	89%	0%	6%	22%	11%
ClC40EA	0%	100%	100%	100%	100%	0%	-	-	100%	20%	85%	0%	0%	0%	75%	90%	0%	0%	25%	20%
ClC40EH	0%	100%	100%	100%	100%	0%	-	-	100%	20%	30%	0%	0%	0%	75%	90%	0%	0%	30%	20%
ClC40FS	0%	100%	100%	-	-	-	10%	0%	95%	25%	65%	0%	0%	0%	85%	100%	0%	10%	30%	20%
ClC40FA	0%	100%	100%	-	-	-	0%	0%	95%	20%	85%	0%	0%	0%	75%	100%	0%	0%	30%	15%
ClC40FH	0%	100%	100%	-	-	-	0%	0%	100%	20%	30%	0%	0%	0%	75%	100%	0%	0%	35%	10%

Table C.7: Frequency of Limit State Occurrences During Dynamic Analyses at the Design-Level for Single-Span Steel IABs Across the Southern Illinois Sites

SPZ	Site	Bridge	Longitudinal Limit State Occurrence					
			Ideal	Acceptable				Unacceptable
			BF	APY	APS	APB	PA	APR
4	Cairo	SsC15EA	0%	80%	0%	0%	0%	0%
3	Anna	SsC15EN	0%	0%	0%	0%	0%	0%
3	Elizabethtown	SsC15EN	0%	0%	0%	0%	0%	0%
3	Carbondale	SsC15EN	0%	0%	0%	0%	0%	0%
3	Eldorado	SsC15EN	0%	0%	0%	0%	0%	0%
3	Benton	SsC15EA	0%	0%	0%	0%	0%	0%
2	Sparta	SsC15EA	0%	0%	0%	0%	0%	0%
2	Mt. Carmel	SsC15EA	0%	0%	0%	0%	0%	0%
2	East St. Louis	SsC15EA	0%	0%	0%	0%	0%	0%
2	Salem	SsC15EA	0%	0%	0%	0%	0%	0%
SPZ	Site	Bridge	Transverse Limit State Occurrence					
			Ideal	Acceptable				Unacceptable
			BF	APY	APS	APB	PA	APR
4	Cairo	SsC15EA	0%	10%	5%	0%	0%	0%
3	Anna	SsC15EN	0%	0%	0%	0%	0%	0%
3	Elizabethtown	SsC15EN	0%	0%	0%	0%	0%	0%
3	Carbondale	SsC15EN	0%	0%	0%	0%	0%	0%
3	Eldorado	SsC15EN	0%	0%	0%	0%	0%	0%
3	Benton	SsC15EA	0%	0%	0%	0%	0%	0%
2	Sparta	SsC15EA	0%	0%	0%	0%	0%	0%
2	Mt. Carmel	SsC15EA	0%	0%	0%	0%	0%	0%
2	East St. Louis	SsC15EA	0%	0%	0%	0%	0%	0%
2	Salem	SsC15EA	0%	0%	0%	0%	0%	0%

Table C.8: Frequency of Limit State Occurrences During Dynamic Analyses at the Design-Level for Three-Span Steel Labs Across the Southern Illinois Sites

SPZ	Site	Bridge	Longitudinal Limit State Occurrence																	
			Ideal						Acceptable								Unacceptable			
			BF	SL	CL	RE	RY	RF	APY	APB	APS	PA	PPY	PPS	SM	CM	BU	SS	CS	APR
4	Cairo	StC15EA	0%	60%	35%	0%	0%	0%	100%	0%	70%	0%	0%	0%	0%	0%	0%	0%	0%	0%
3	Anna	StC15EN	0%	0%	0%	0%	0%	0%	100%	0%	80%	0%	0%	0%	0%	0%	0%	0%	0%	0%
3	Elizabethtown	StC15EN	0%	0%	0%	0%	0%	0%	90%	0%	0%	0%	0%	0%	0%	0%	0%	0%	0%	0%
3	Carbondale	StC15EN	0%	0%	0%	0%	0%	0%	100%	0%	15%	0%	0%	0%	0%	0%	0%	0%	0%	0%
3	Eldorado	StC15EN	0%	0%	0%	0%	0%	0%	100%	0%	5%	0%	0%	0%	0%	0%	0%	0%	0%	0%
3	Benton	StC15EA	0%	0%	0%	0%	0%	0%	45%	0%	0%	0%	0%	0%	0%	0%	0%	0%	0%	0%
2	Sparta	StC15EA	0%	0%	0%	0%	0%	0%	45%	0%	0%	0%	0%	0%	0%	0%	0%	0%	0%	0%
2	Mt. Carmel	StC15EA	0%	0%	0%	0%	0%	0%	55%	0%	0%	0%	0%	0%	0%	0%	0%	0%	0%	0%
2	East St. Louis	StC15EA	0%	0%	0%	0%	0%	0%	60%	0%	0%	0%	0%	0%	0%	0%	0%	0%	0%	0%
2	Salem	StC15EA	0%	0%	0%	0%	0%	0%	0%	0%	0%	0%	0%	0%	0%	0%	0%	0%	0%	0%
SPZ	Site	Bridge	Transverse Limit State Occurrence																	
			Ideal						Acceptable								Unacceptable			
			BF	SL	CL	RE	RY	RF	APY	APB	APS	PA	PPY	PPS	SM	CM	BU	SS	CS	APR
4	Cairo	StC15EA	0%	40%	10%	100%	100%	0%	100%	0%	30%	0%	0%	0%	0%	0%	0%	0%	0%	0%
3	Anna	StC15EN	0%	0%	0%	100%	95%	0%	75%	0%	0%	0%	0%	0%	0%	0%	0%	0%	0%	0%
3	Elizabethtown	StC15EN	0%	0%	0%	100%	40%	0%	20%	0%	0%	0%	0%	0%	0%	0%	0%	0%	0%	0%
3	Carbondale	StC15EN	0%	5%	0%	100%	100%	0%	75%	0%	0%	0%	0%	0%	0%	0%	0%	0%	0%	0%
3	Eldorado	StC15EN	0%	0%	0%	100%	90%	0%	45%	0%	0%	0%	0%	0%	0%	0%	0%	0%	0%	0%
3	Benton	StC15EA	0%	0%	0%	100%	30%	0%	10%	0%	0%	0%	0%	0%	0%	0%	0%	0%	0%	0%
2	Sparta	StC15EA	0%	0%	0%	100%	45%	0%	5%	0%	0%	0%	0%	0%	0%	0%	0%	0%	0%	0%
2	Mt. Carmel	StC15EA	0%	0%	0%	100%	20%	0%	5%	0%	0%	0%	0%	0%	0%	0%	0%	0%	0%	0%
2	East St. Louis	StC15EA	0%	0%	0%	100%	15%	0%	0%	0%	0%	0%	0%	0%	0%	0%	0%	0%	0%	0%
2	Salem	StC15EA	0%	0%	0%	65%	0%	0%	0%	0%	0%	0%	0%	0%	0%	0%	0%	0%	0%	0%

Table C.9: Frequency of Limit State Occurrences During Dynamic Analyses at the Design-Level for Four-Span Steel Labs Across the Southern Illinois Sites

SPZ	Site	Bridge	Longitudinal Limit State Occurrence																	
			Ideal						Acceptable								Unacceptable			
			BF	SL	CL	RE	RY	RF	APY	APB	APS	PA	PPY	PPS	SM	CM	BU	SS	CS	APR
4	Cairo	SIC15EA	0%	100%	100%	0%	0%	0%	100%	0%	100%	0%	0%	5%	25%	35%	0%	0%	5%	0%
3	Anna	SIC15EN	0%	10%	0%	0%	0%	0%	95%	0%	30%	0%	0%	0%	0%	0%	0%	0%	0%	0%
3	Elizabethtown	SIC15EN	0%	0%	0%	0%	0%	0%	70%	0%	10%	0%	0%	0%	0%	0%	0%	0%	0%	0%
3	Carbondale	SIC15EN	0%	0%	0%	0%	0%	0%	40%	0%	0%	0%	0%	0%	0%	0%	0%	0%	0%	0%
3	Eldorado	SIC15EN	0%	0%	0%	0%	0%	0%	10%	0%	0%	0%	0%	0%	0%	0%	0%	0%	0%	0%
3	Benton	SIC15EA	0%	0%	0%	0%	0%	0%	0%	0%	0%	0%	0%	0%	0%	0%	0%	0%	0%	0%
2	Sparta	SIC15EA	0%	0%	0%	0%	0%	0%	0%	0%	0%	0%	0%	0%	0%	0%	0%	0%	0%	0%
2	Mt. Carmel	SIC15EA	0%	0%	0%	0%	0%	0%	0%	0%	0%	0%	0%	0%	0%	0%	0%	0%	0%	0%
2	East St. Louis	SIC15EA	0%	0%	0%	0%	0%	0%	0%	0%	0%	0%	0%	0%	0%	0%	0%	0%	0%	0%
2	Salem	SIC15EA	0%	0%	0%	0%	0%	0%	0%	0%	0%	0%	0%	0%	0%	0%	0%	0%	0%	0%
SPZ	Site	Bridge	Transverse Limit State Occurrence																	
			Ideal						Acceptable								Unacceptable			
			BF	SL	CL	RE	RY	RF	APY	APB	APS	PA	PPY	PPS	SM	CM	BU	SS	CS	APR
4	Cairo	SIC15EA	0%	100%	100%	100%	0%	0%	10%	0%	0%	0%	0%	0%	100%	100%	0%	0%	35%	0%
3	Anna	SIC15EN	0%	100%	100%	100%	0%	0%	0%	0%	0%	0%	0%	10%	85%	100%	0%	0%	0%	0%
3	Elizabethtown	SIC15EN	0%	100%	100%	100%	0%	0%	0%	0%	0%	0%	0%	0%	70%	90%	0%	0%	0%	0%
3	Carbondale	SIC15EN	0%	95%	90%	100%	0%	0%	0%	0%	0%	0%	0%	0%	35%	65%	0%	0%	0%	0%
3	Eldorado	SIC15EN	0%	70%	65%	100%	0%	0%	0%	0%	0%	0%	0%	0%	0%	20%	0%	0%	0%	0%
3	Benton	SIC15EA	0%	65%	50%	100%	0%	0%	0%	0%	0%	0%	0%	0%	0%	0%	0%	0%	0%	0%
2	Sparta	SIC15EA	0%	45%	30%	100%	0%	0%	0%	0%	0%	0%	0%	0%	0%	0%	0%	0%	0%	0%
2	Mt. Carmel	SIC15EA	0%	60%	60%	100%	0%	0%	0%	0%	0%	0%	0%	0%	0%	0%	0%	0%	0%	0%
2	East St. Louis	SIC15EA	0%	60%	60%	100%	0%	0%	0%	0%	0%	0%	0%	0%	0%	5%	0%	0%	0%	0%
2	Salem	SIC15EA	0%	5%	0%	100%	0%	0%	0%	0%	0%	0%	0%	0%	0%	0%	0%	0%	0%	0%

Table C.10: Frequency of Limit State Occurrences During Dynamic Analyses at the Design-Level for Three-Span Concrete Labs Across the Southern Illinois Sites

SPZ	Site	Bridge	Longitudinal Limit State Occurrence																
			Ideal						Acceptable								Unacceptable			
			BF	SL	CL	RE	RY	RF	APY	APB	APS	PA	PPY	PPS	SM	CM	BU	SS	CS	APR
4	Cairo	CtC15EA	0%	100%	100%	0%	0%	0%	100%	75%	100%	0%	0%	0%	75%	85%	0%	5%	50%	20%
3	Anna	CtC15EN	0%	35%	20%	0%	0%	0%	100%	0%	80%	0%	0%	0%	0%	5%	0%	0%	0%	0%
3	Elizabethtown	CtC15EN	0%	0%	0%	0%	0%	0%	100%	0%	45%	0%	0%	0%	0%	0%	0%	0%	0%	0%
3	Carbondale	CtC15EN	0%	0%	0%	0%	0%	0%	100%	0%	25%	0%	0%	0%	0%	0%	0%	0%	0%	0%
3	Eldorado	CtC15EN	0%	0%	0%	0%	0%	0%	90%	0%	15%	0%	0%	0%	0%	0%	0%	0%	0%	0%
3	Benton	CtC15EA	0%	0%	0%	0%	0%	0%	60%	0%	0%	0%	0%	0%	0%	0%	0%	0%	0%	0%
2	Sparta	CtC15EA	0%	0%	0%	0%	0%	0%	60%	0%	0%	0%	0%	0%	0%	0%	0%	0%	0%	0%
2	Mt. Carmel	CtC15EA	0%	0%	0%	0%	0%	0%	80%	0%	10%	0%	0%	0%	0%	0%	0%	0%	0%	0%
2	East St. Louis	CtC15EA	0%	0%	0%	0%	0%	0%	75%	0%	0%	0%	0%	0%	0%	0%	0%	0%	0%	0%
2	Salem	CtC15EA	0%	0%	0%	0%	0%	0%	0%	0%	0%	0%	0%	0%	0%	0%	0%	0%	0%	0%
SPZ	Site	Bridge	Transverse Limit State Occurrence																
			Ideal						Acceptable								Unacceptable			
			BF	SL	CL	RE	RY	RF	APY	APB	APS	PA	PPY	PPS	SM	CM	BU	SS	CS	APR
4	Cairo	CtC15EA	0%	100%	80%	100%	100%	100%	100%	90%	100%	0%	0%	0%	40%	40%	0%	5%	15%	10%
3	Anna	CtC15EN	0%	45%	0%	100%	100%	70%	100%	15%	65%	0%	0%	0%	0%	0%	0%	0%	0%	0%
3	Elizabethtown	CtC15EN	0%	0%	0%	100%	100%	20%	100%	0%	30%	0%	0%	0%	0%	0%	0%	0%	0%	0%
3	Carbondale	CtC15EN	0%	0%	0%	100%	100%	0%	85%	0%	10%	0%	0%	0%	0%	0%	0%	0%	0%	0%
3	Eldorado	CtC15EN	0%	0%	0%	100%	100%	0%	40%	0%	0%	0%	0%	0%	0%	0%	0%	0%	0%	0%
3	Benton	CtC15EA	0%	0%	0%	100%	75%	0%	10%	0%	0%	0%	0%	0%	0%	0%	0%	0%	0%	0%
2	Sparta	CtC15EA	0%	0%	0%	100%	85%	0%	0%	0%	0%	0%	0%	0%	0%	0%	0%	0%	0%	0%
2	Mt. Carmel	CtC15EA	0%	0%	0%	100%	85%	0%	35%	0%	0%	0%	0%	0%	0%	0%	0%	0%	0%	0%
2	East St. Louis	CtC15EA	0%	0%	0%	100%	80%	0%	25%	0%	0%	0%	0%	0%	0%	0%	0%	0%	0%	0%
2	Salem	CtC15EA	0%	0%	0%	65%	5%	0%	0%	0%	0%	0%	0%	0%	0%	0%	0%	0%	0%	0%

Table C.11: Frequency of Limit State Occurrences During Dynamic Analyses at the Design-Level for Four-Span Concrete Labs Across the Southern Illinois Sites

SPZ	Site	Bridge	Longitudinal Limit State Occurrence																	
			Ideal						Acceptable								Unacceptable			
			BF	SL	CL	RE	RY	RF	APY	APB	APS	PA	PPY	PPS	SM	CM	BU	SS	CS	APR
4	Cairo	ClC15EA	0%	94%	94%	0%	0%	0%	100%	65%	100%	0%	0%	0%	76%	76%	0%	6%	76%	5%
3	Anna	ClC15EN	0%	25%	25%	0%	0%	0%	100%	0%	80%	0%	0%	0%	10%	15%	0%	0%	10%	0%
3	Elizabethtown	ClC15EN	0%	0%	0%	0%	0%	0%	100%	0%	25%	0%	0%	0%	0%	0%	0%	0%	0%	0%
3	Carbondale	ClC15EN	0%	0%	0%	0%	0%	0%	80%	0%	0%	0%	0%	0%	0%	0%	0%	0%	0%	0%
3	Eldorado	ClC15EN	0%	0%	0%	0%	0%	0%	15%	0%	0%	0%	0%	0%	0%	0%	0%	0%	0%	0%
3	Benton	ClC15EA	0%	0%	0%	0%	0%	0%	0%	0%	0%	0%	0%	0%	0%	0%	0%	0%	0%	0%
2	Sparta	ClC15EA	0%	0%	0%	0%	0%	0%	0%	0%	0%	0%	0%	0%	0%	0%	0%	0%	0%	0%
2	Mt. Carmel	ClC15EA	0%	0%	0%	0%	0%	0%	0%	0%	0%	0%	0%	0%	0%	0%	0%	0%	0%	0%
2	East St. Louis	ClC15EA	0%	0%	0%	0%	0%	0%	5%	0%	0%	0%	0%	0%	0%	0%	0%	0%	0%	0%
2	Salem	ClC15EA	0%	0%	0%	0%	0%	0%	0%	0%	0%	0%	0%	0%	0%	0%	0%	0%	0%	0%
SPZ	Site	Bridge	Transverse Limit State Occurrence																	
			Ideal						Acceptable								Unacceptable			
			BF	SL	CL	RE	RY	RF	APY	APB	APS	PA	PPY	PPS	SM	CM	BU	SS	CS	APR
4	Cairo	ClC15EA	0%	100%	100%	100%	100%	0%	75%	15%	55%	0%	0%	0%	100%	100%	0%	35%	100%	0%
3	Anna	ClC15EN	0%	100%	100%	100%	100%	0%	10%	0%	0%	0%	0%	0%	70%	90%	0%	0%	45%	0%
3	Elizabethtown	ClC15EN	0%	100%	100%	100%	100%	0%	0%	0%	0%	0%	0%	0%	5%	35%	0%	0%	0%	0%
3	Carbondale	ClC15EN	0%	80%	80%	100%	100%	0%	0%	0%	0%	0%	0%	0%	0%	0%	0%	0%	0%	0%
3	Eldorado	ClC15EN	0%	35%	40%	100%	90%	0%	0%	0%	0%	0%	0%	0%	0%	0%	0%	0%	0%	0%
3	Benton	ClC15EA	0%	20%	20%	100%	85%	0%	0%	0%	0%	0%	0%	0%	0%	0%	0%	0%	0%	0%
2	Sparta	ClC15EA	0%	0%	0%	100%	70%	0%	0%	0%	0%	0%	0%	0%	0%	0%	0%	0%	0%	0%
2	Mt. Carmel	ClC15EA	0%	5%	10%	100%	75%	0%	0%	0%	0%	0%	0%	0%	0%	0%	0%	0%	0%	0%
2	East St. Louis	ClC15EA	0%	15%	15%	100%	70%	0%	0%	0%	0%	0%	0%	0%	0%	0%	0%	0%	0%	0%
2	Salem	ClC15EA	0%	5%	5%	100%	35%	0%	0%	0%	0%	0%	0%	0%	0%	0%	0%	0%	0%	0%

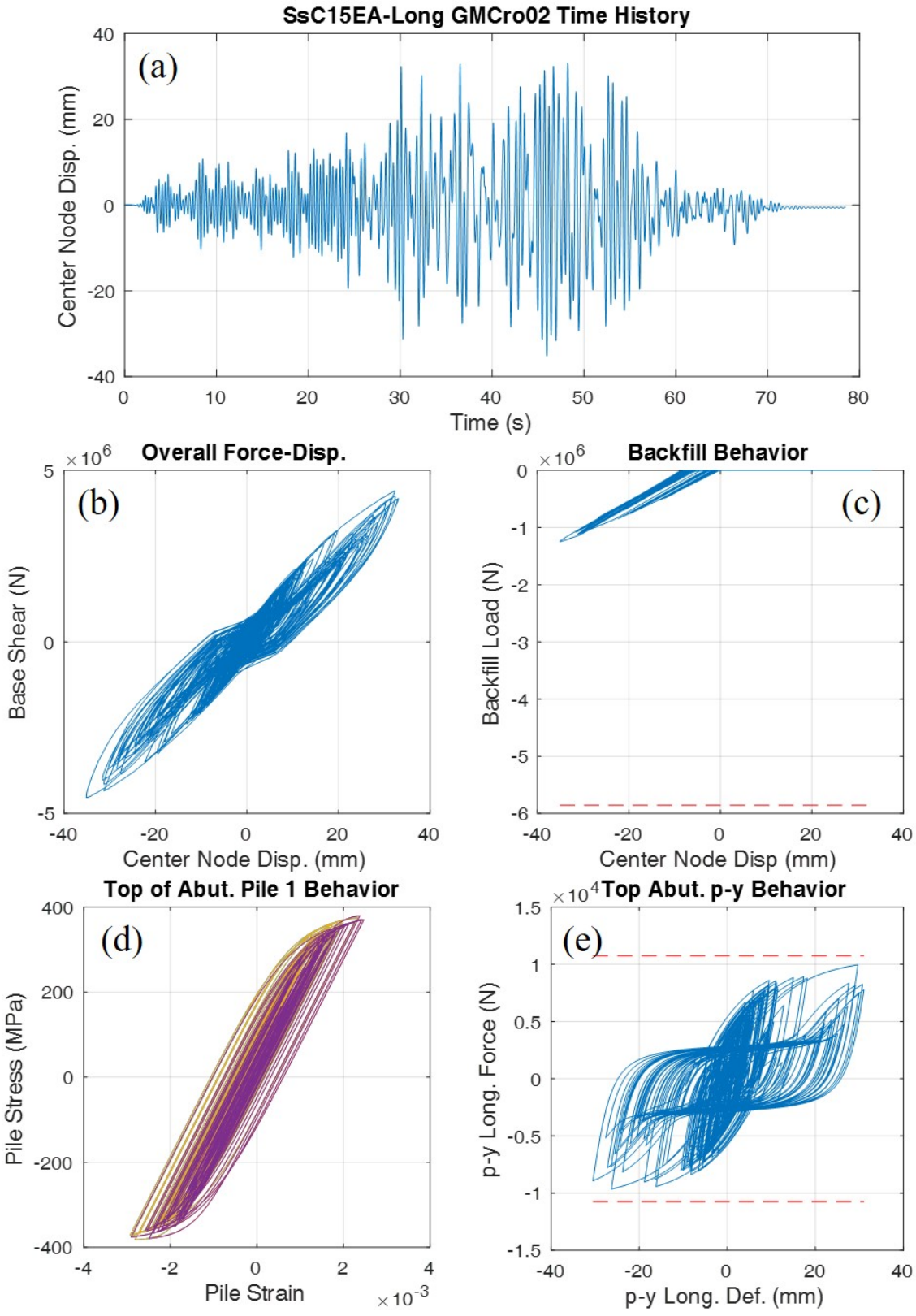

Figure C.1: Dynamic analysis results for Ss____A subjected to a design-level ground motion in the longitudinal direction.

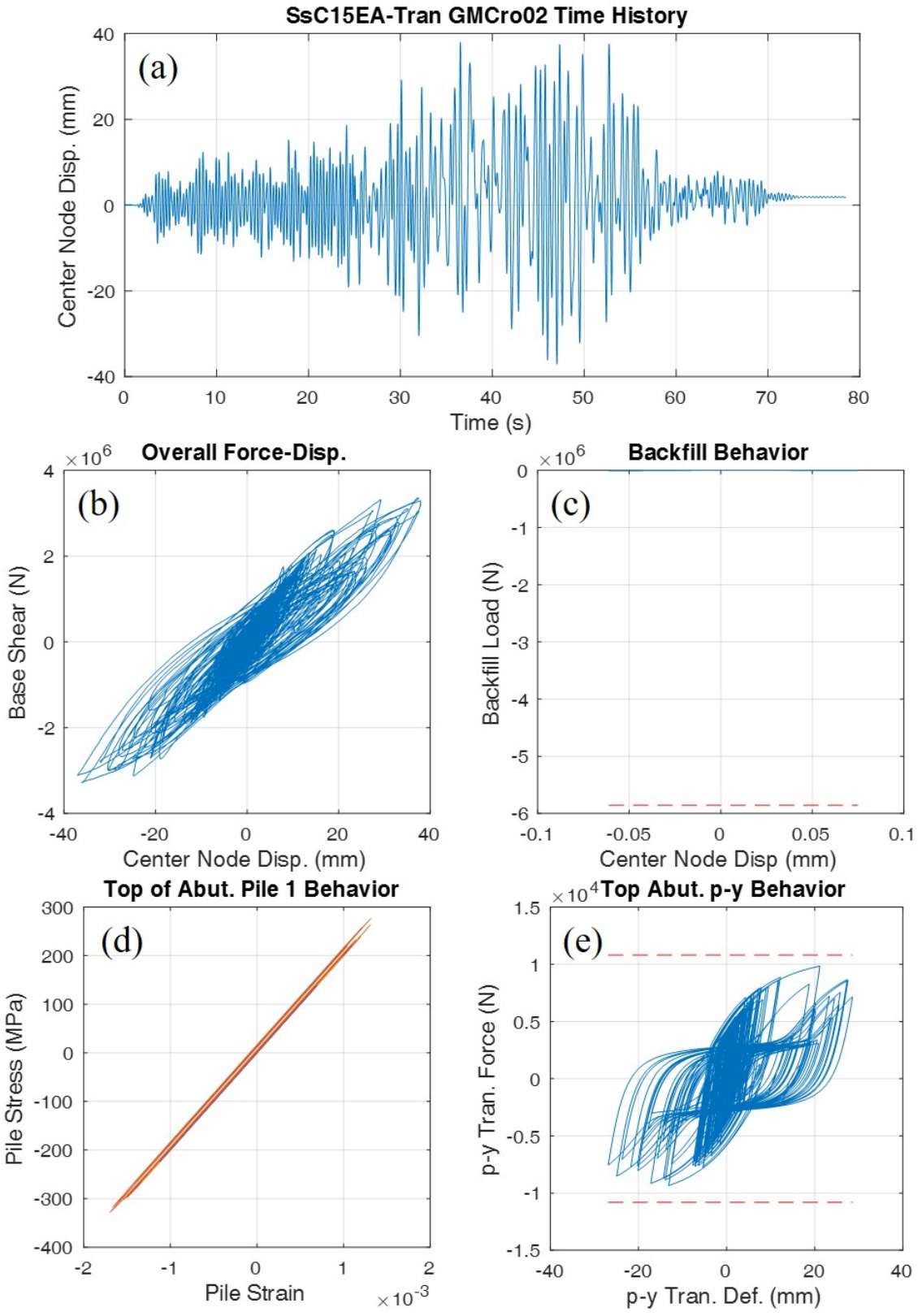

Figure C.2: Dynamic analysis results for Ss____A subjected to a design-level ground motion in the transverse direction.

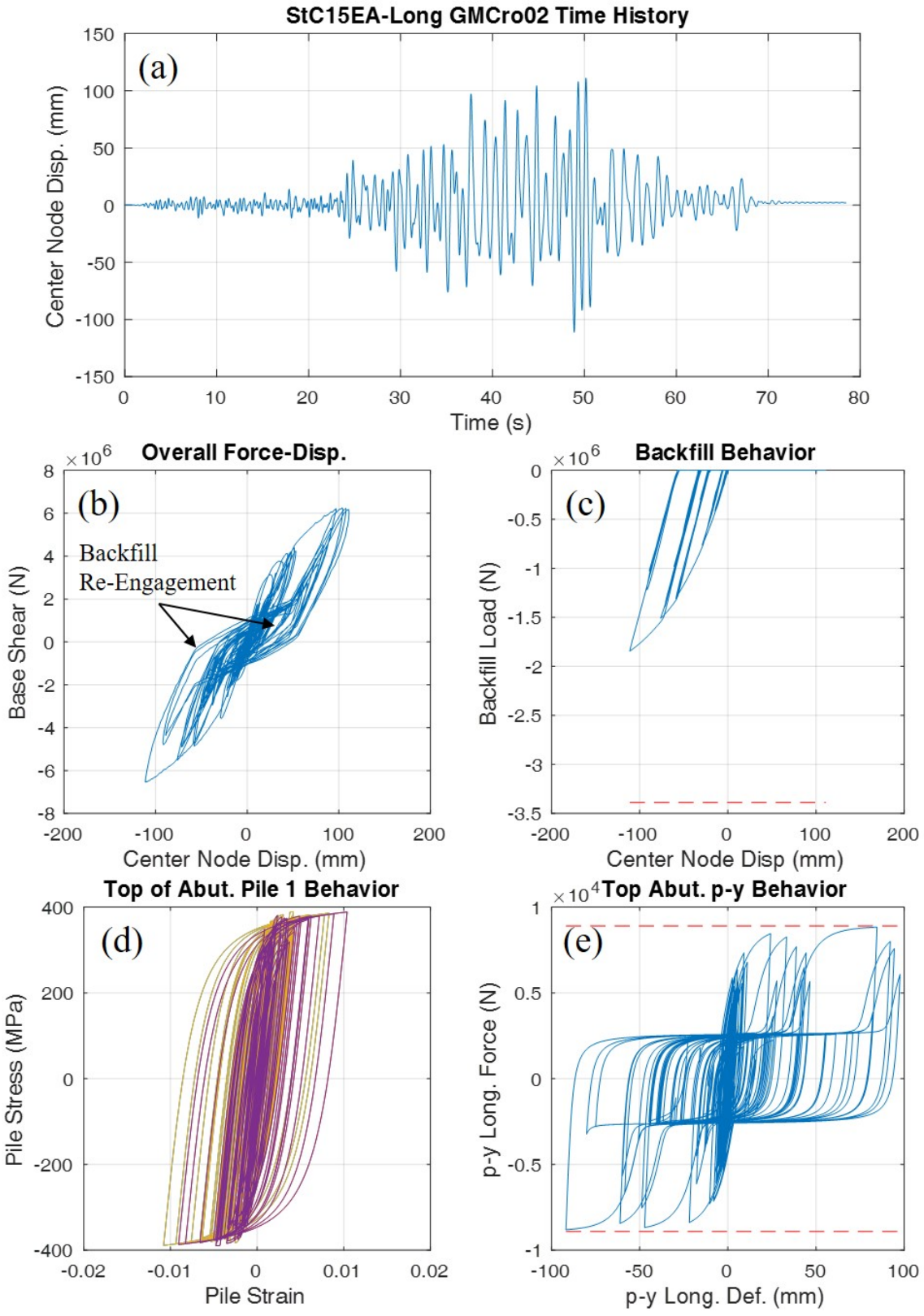

Figure C.3: Dynamic analysis results for StC15EA subjected to a design-level ground motion in the longitudinal direction.

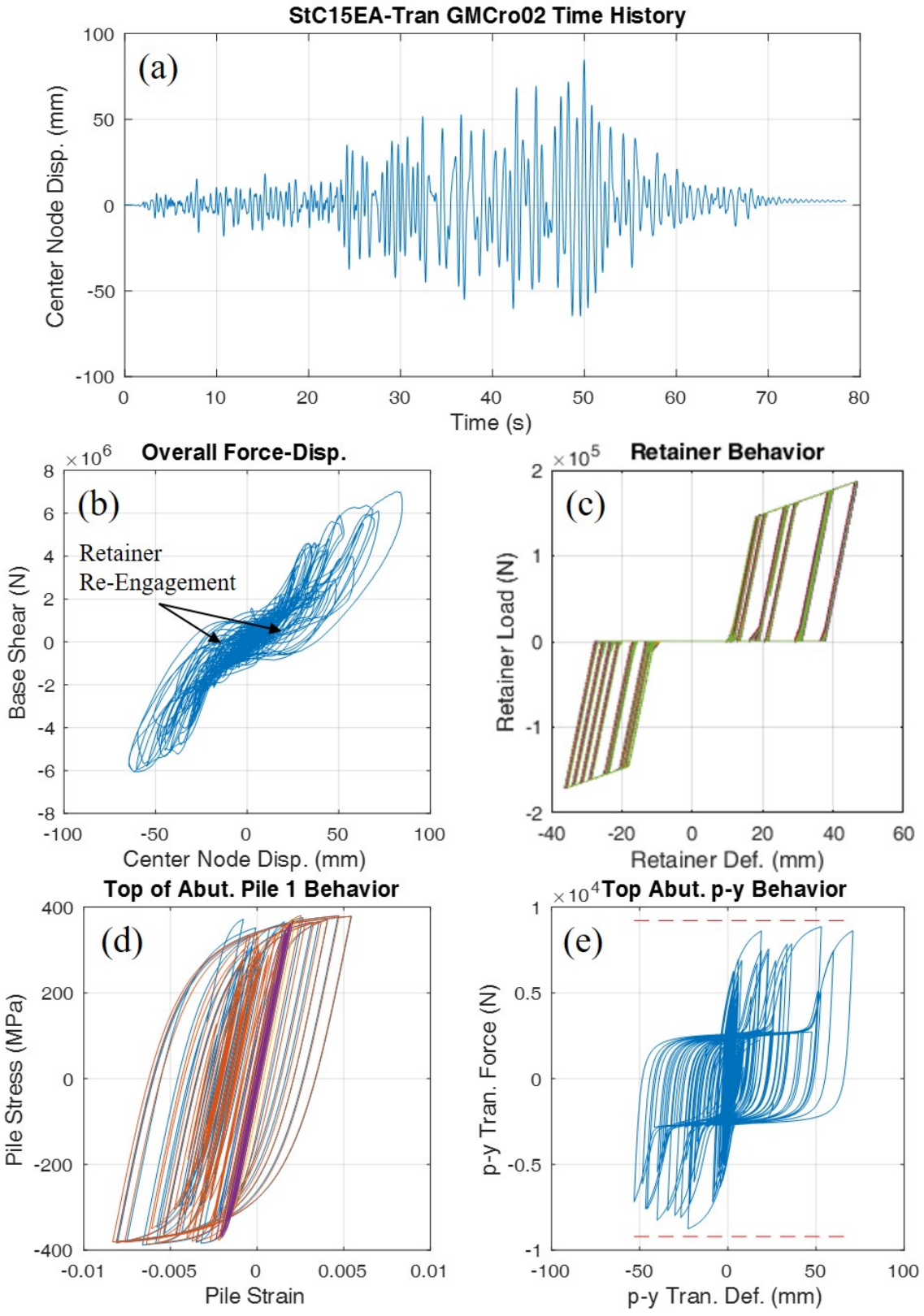

Figure C.4: Dynamic analysis results for StC15EA subjected to a design-level ground motion in the transverse direction.

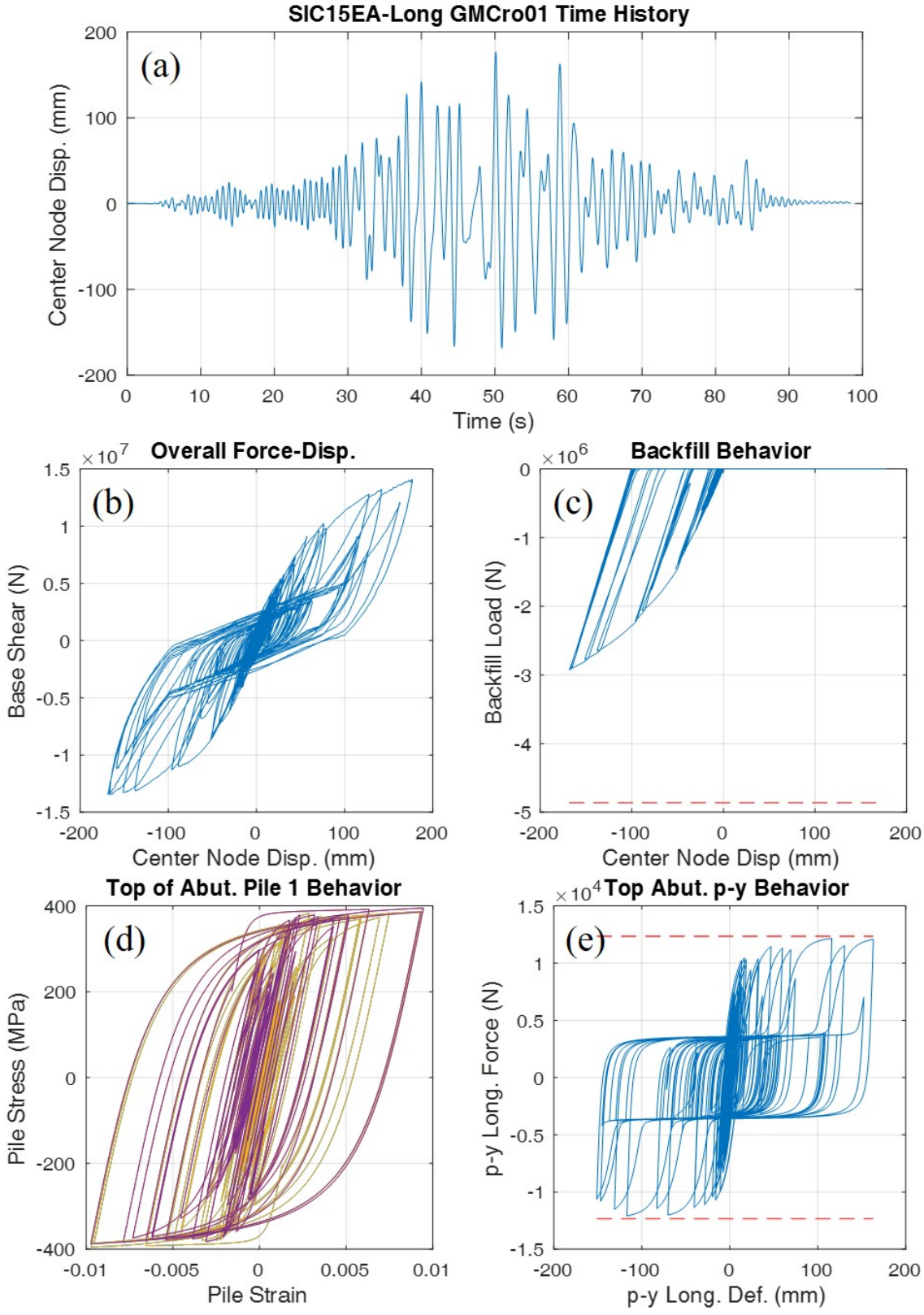

Figure C.5: Dynamic analysis results for SIC15EA subjected to a design-level ground motion in the longitudinal direction.

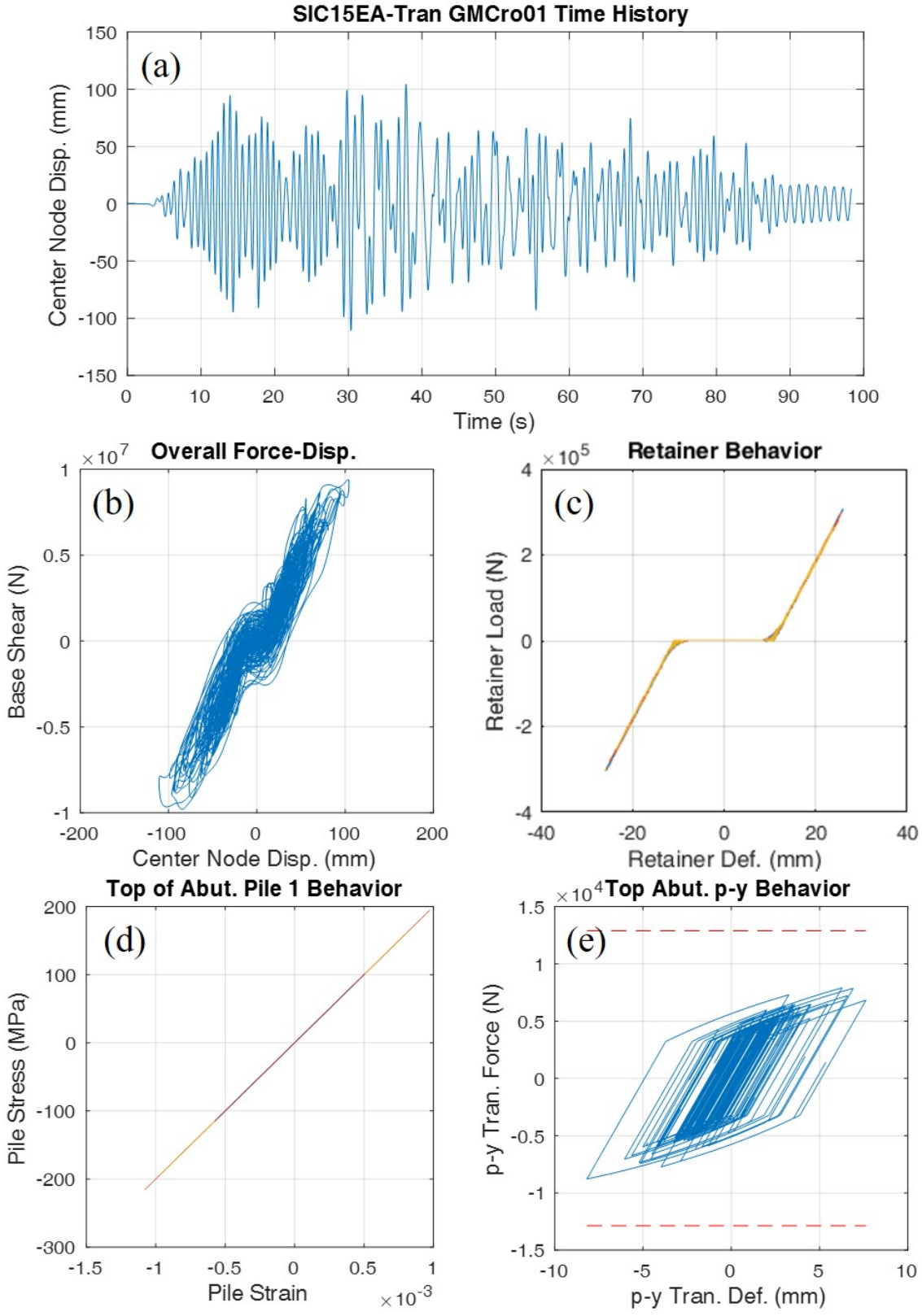

Figure C.6: Dynamic analysis results for SIC15EA subjected to a design-level ground motion in the transverse direction.

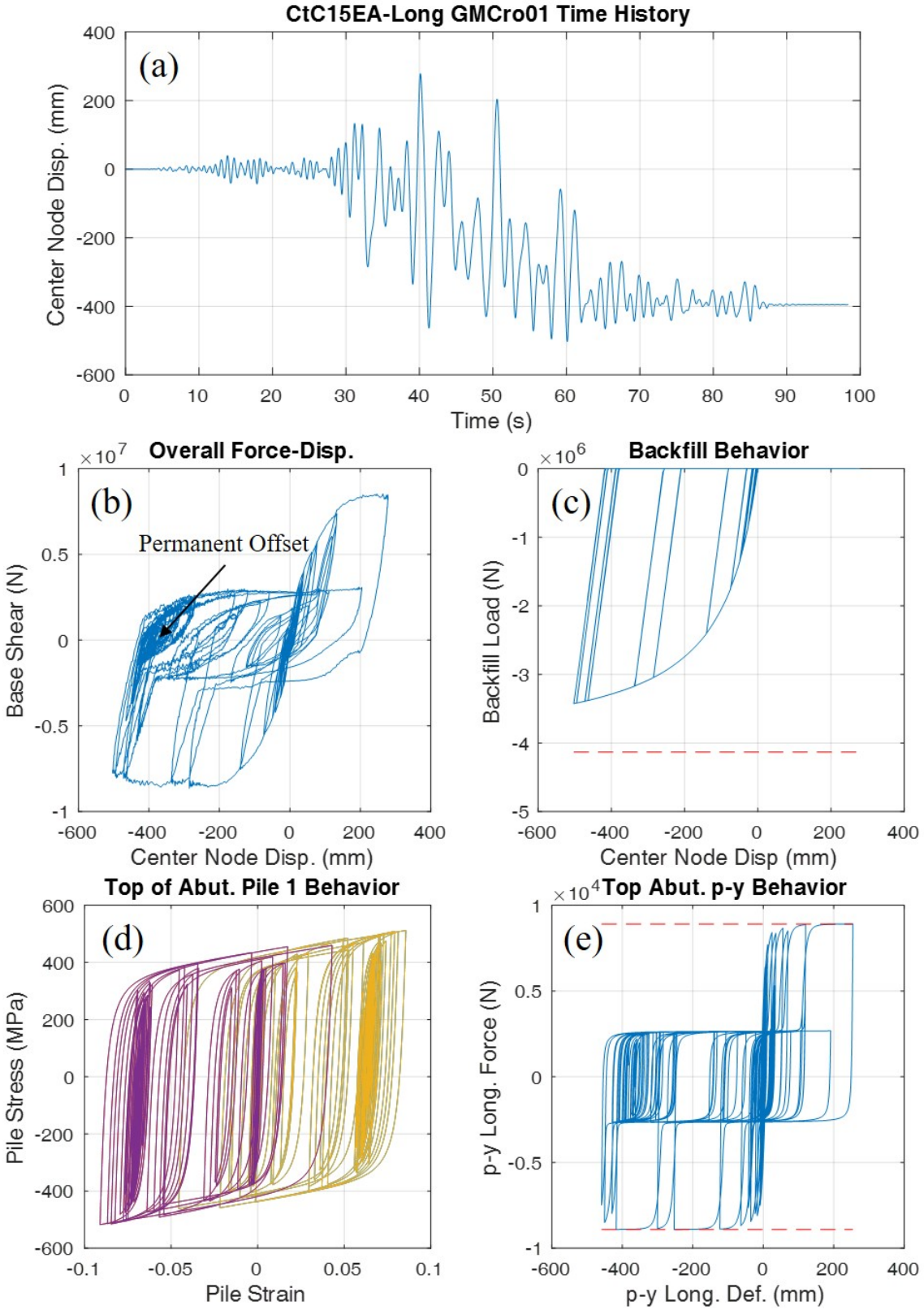

Figure C.7: Dynamic analysis results for CtC15EA subjected to a design-level ground motion in the longitudinal direction.

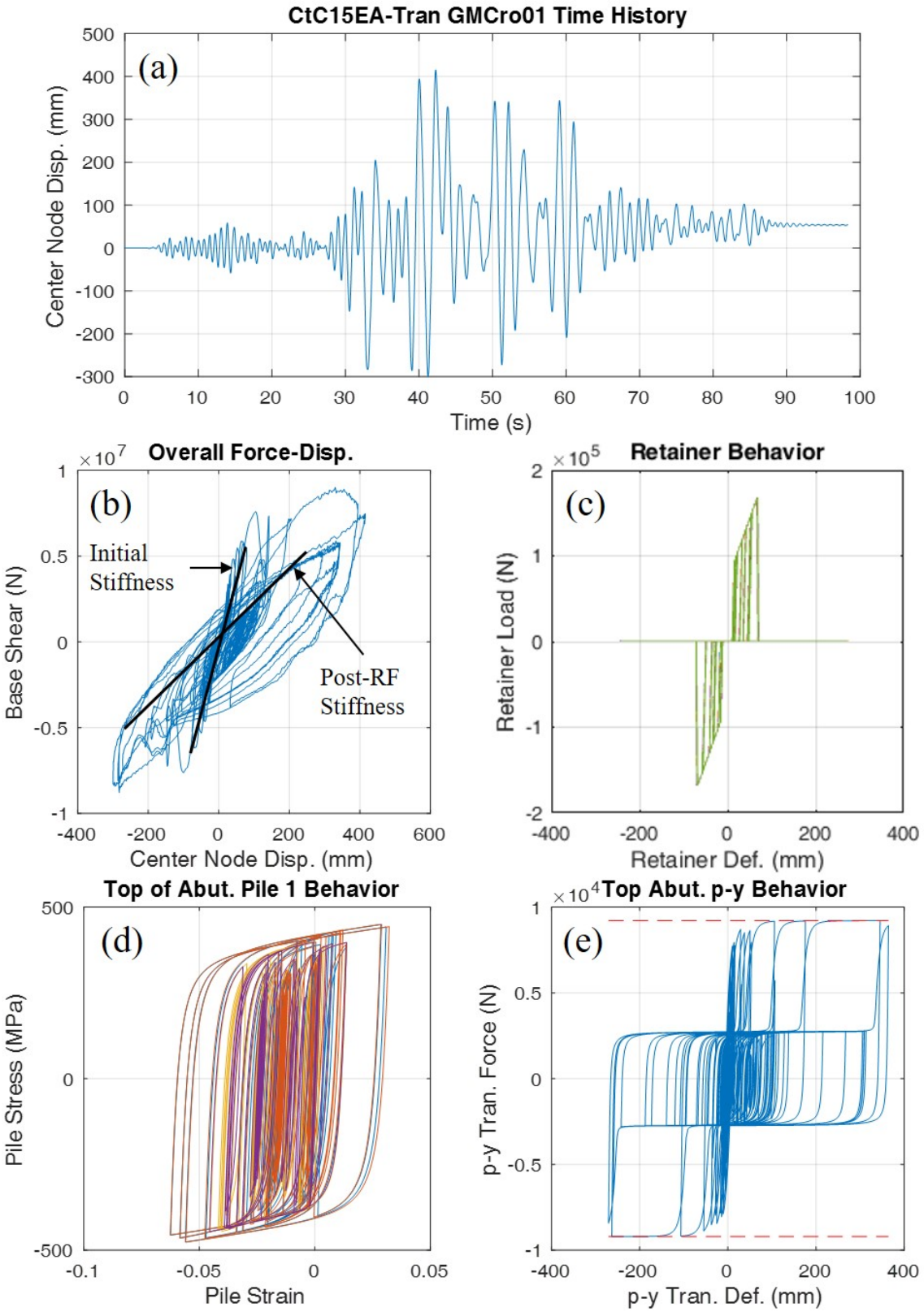

Figure C.8: Dynamic analysis results for CtC15EA subjected to a design-level ground motion in the transverse direction.

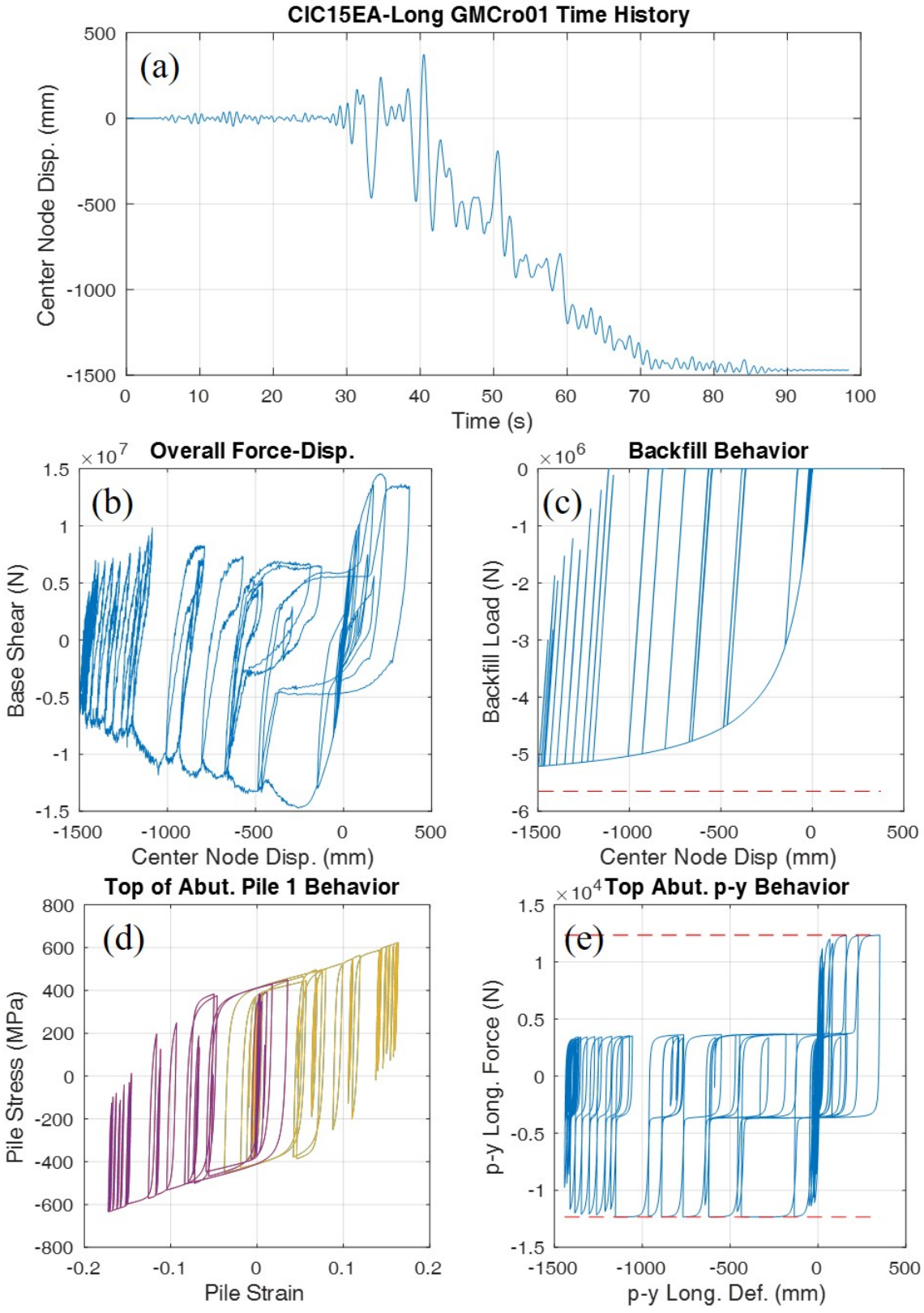

Figure C.9: Dynamic analysis results for ClC15EA subjected to a design-level ground motion in the longitudinal direction.

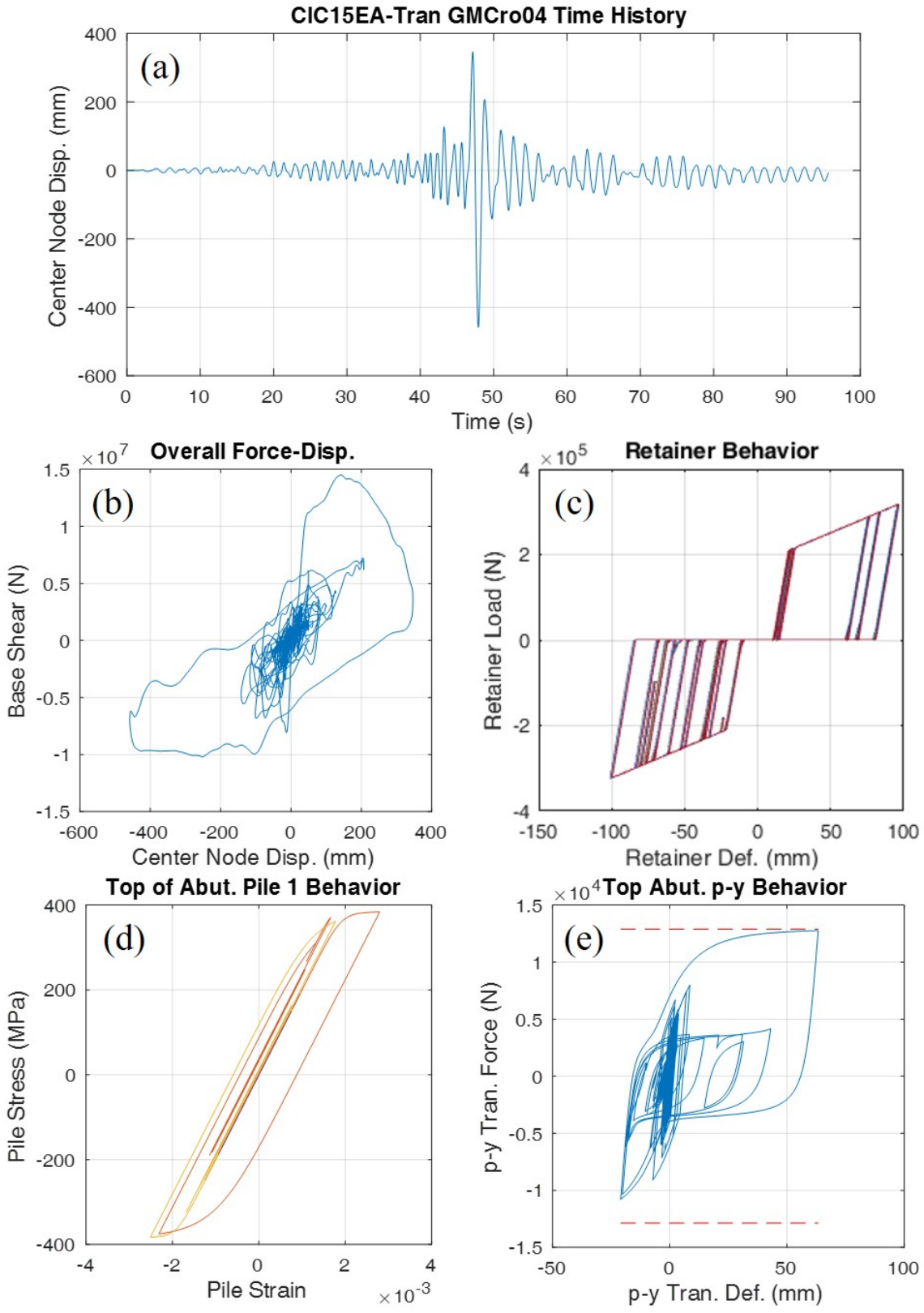

Figure C.10: Dynamic analysis results for ClC15EA subjected to a design-level ground motion in the transverse direction.

APPENDIX D: INCREMENTAL DYNAMIC ANALYSIS DATA

Incremental dynamic analysis results for the 14 IABs with alluvial soil conditions in the parametric study are presented in this appendix. These results are used for the discussion in Chapter 4.

The incremental dynamic analysis is presented with a scale factor of 1.0 being equivalent to the design-level response and the scale factor being approximately equivalent to the maximum considered earthquake-level. The data is presented through tables presenting the frequency of limit state occurrences when subjected to 20 ground motions developed for Cairo at various scale factors. IDA plots providing the median response of each component across the 20 ground motions at each scale factor along with the maximum and minimum values are also presented. The dashed vertical lines in the IDA plots represent limit states reached with green being an ideal limit stat, yellow an acceptable limit state, and red an unacceptable limit state. Finally, the sequence of damage for each IAB is presented with damage being indicated by the first occurrence of the limit state.

Desired sequences of damage were produced for the bridges and provided here, including ideal, acceptable, discouraged, and unacceptable occurrences. Ideal occurrences happen when a limit state begins to occur in the desired sequence. Acceptable is when a limit state begins to occur at larger scale factors than desired. Discouraged is when a limit state begins to occur at smaller scale factors than desired, and unacceptable is when the unacceptable limit states occur.

The desired sequence of damage for the single-span steel IAB includes having the backfill mobilization (BF) occur at scale factors of 1.0 or less, followed by initial damage to the abutment foundation (APY and APS), then failure of the pile cap-abutment connection (PA), and finally local buckling of the abutment piles (APB) occurring at scale factors of 1.0 or larger. The reason why the APY, APS, PA, and APB limit states are allowed at the design-level is due to the lack of other fuses in a single-span IAB.

The desired sequences of damage for the multi-span bridges are very similar to each other. However, there are a couple of exceptions. One of which is the fact that backfill mobilization (BF) only occurs in longitudinal sequences, while retainer engagement (RE), yielding (RY), and fusing (RF) only occur in transverse sequences. The other exception is that fixed bearing damage (FY and FF) only occurs in IABs with fixed bearings. In terms of the actual sequence, RE is expected to occur first at the 0.5 scale factor when it is present. Following that, any ideal limit state is intended to begin to occur at scale factors of 1.0 or less. These ideal limit states include light pier column damage (SL/CL), backfill mobilization (BF), fixed bearing damage (FY and FF), and retainer damage (RY and RF). These are desired to occur early due to their fusing capabilities and ease of access to repair after an event. Moderate pier column damage (SM/CM) follows and is desired to be at a scale factor of 1.0 or larger because of all the acceptable limit states, it is the easiest to identify and repair. All other acceptable limit states are desired to occur at a scale factor of 1.25 or larger. These limit states include initial

abutment foundation damage (APY/APS), pier foundation damage (PPY/PPS), pier cap-abutment connection failure (PA), and abutment pile local buckling (APB). Finally, unacceptable limit states such as severe pier column damage (SS/CS), bearing unseating (BU), and abutment pile rupture (APR) are unacceptable at all scale factors. It is necessary to note that some limit states are combined for the sequences of damage due to their close ties to each other. These limit states mostly comprise the pier column damage (SL/CL, SM/CM, SS/CS) and pile and p-y spring damage (APY/APS, PPY/PPS) structural behaviors.

Table D.1 describes which tables and figures present data for each set of IABs.

Table D.1: Organization of Figures in Appendix D

	Bridge Type	**Figure of Table**
Frequency of Limit State Occurrence Table at Cairo	1-Span Steel	Table D.2
	3-Span Steel	Table D.3-D.4
	4-Span Steel	Table D.5-D.6
	3-Span Concrete	Table D.7-D.8
	4-Span Concrete	Table D.9-D.10
IDA Plots	1-Span Steel	Fig. D.1-D.2
	3-Span Steel	Fig. D.4-D.5
	4-Span Steel	Fig. D.7-D.8
	3-Span Concrete	Fig. D.10-D.11
	4-Span Concrete	Fig. D.13-D.14
Sequence of Damage	1-Span Steel	Fig. D.3
	3-Span Steel	Fig. D.6
	4-Span Steel	Fig. D.9
	3-Span Concrete	Fig. D.12
	4-Span Concrete	Fig. D.15

Table D.2: Frequency of Limit State Occurrences for the Ida of Single-Span Steel IABs Where a Scale Factor of 1.00 Represents the Design-Level

Bridge	SF	Longitudinal Limit State Occurrence					
		Ideal	Acceptable				Unacc.
		BF	APY	APB	APS	PA	APR
Ss____A	0.50	0%	0%	0%	0%	0%	0%
	0.75	0%	5%	0%	0%	0%	0%
	1.00	0%	80%	0%	0%	0%	0%
	1.25	0%	80%	0%	10%	0%	0%
	1.50	0%	100%	0%	15%	0%	0%
	1.75	0%	100%	0%	45%	0%	0%
Bridge	**SF**	**Transverse Limit State Occurrence**					
		Ideal	**Acceptable**				**Unacc.**
		BF	**APY**	**APB**	**APS**	**PA**	**APR**
Ss____A	0.50	0%	0%	0%	0%	0%	0%
	0.75	0%	0%	0%	0%	0%	0%
	1.00	0%	10%	0%	5%	0%	0%
	1.25	0%	65%	0%	30%	0%	0%
	1.50	0%	100%	0%	65%	0%	0%
	1.75	0%	100%	45%	100%	0%	0%

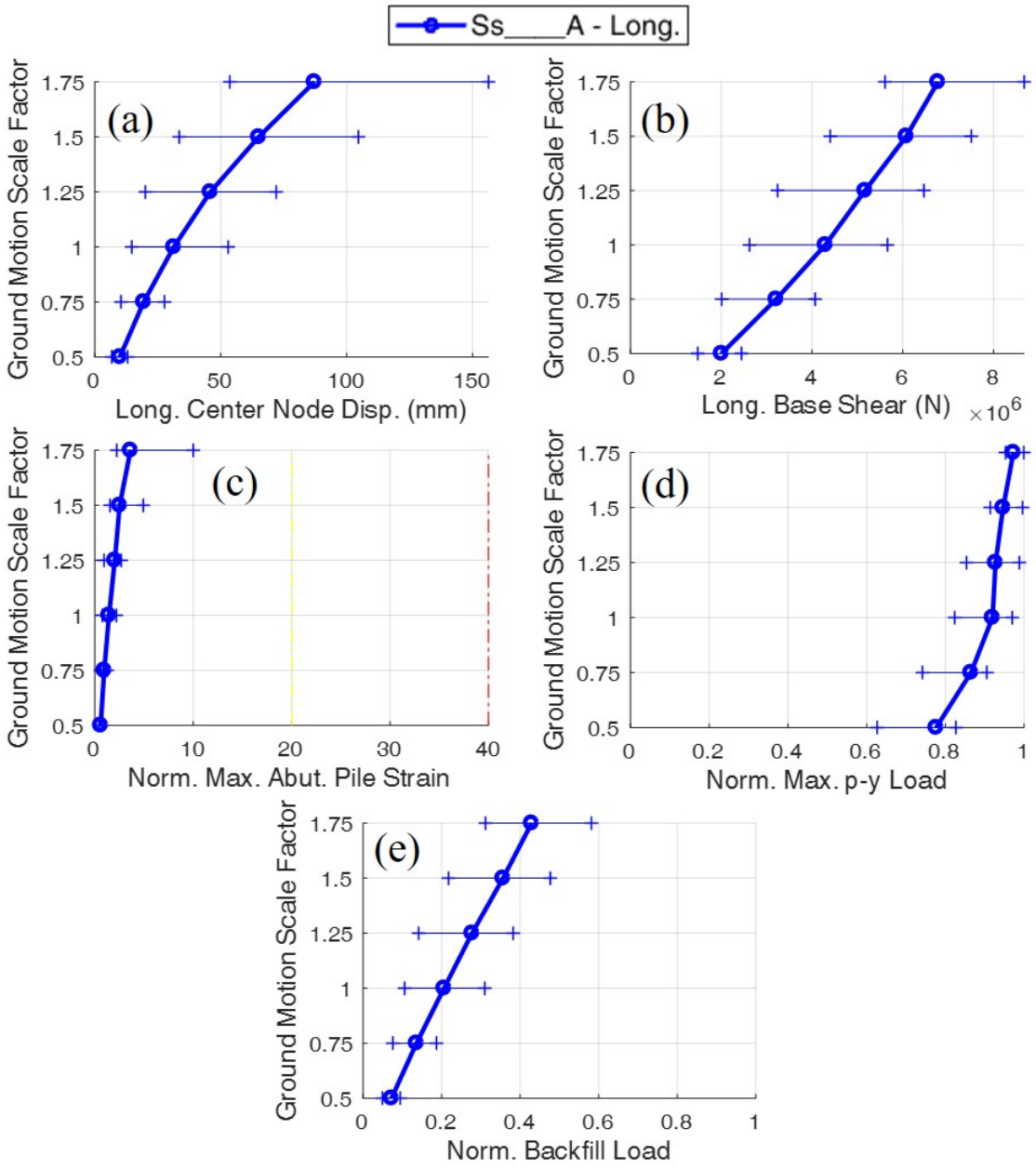

Figure D.1: IDA plots for single-span steel IABs in the longitudinal direction where a scale factor of 1.00 represents the design-level.

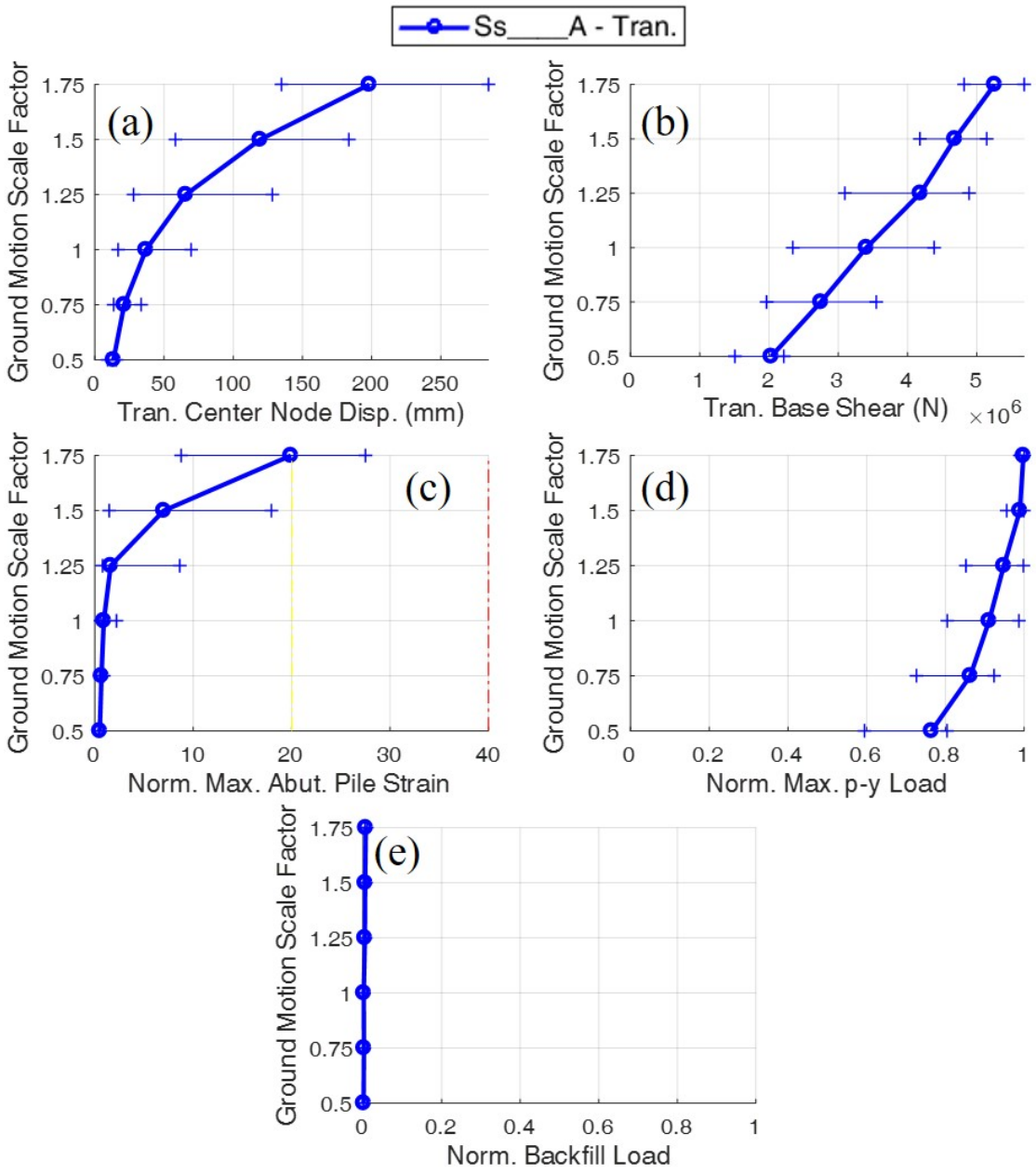

Figure D.2: IDA plots for single-span steel IABs in the transverse direction where a scale factor of 1.00 represents the design-level.

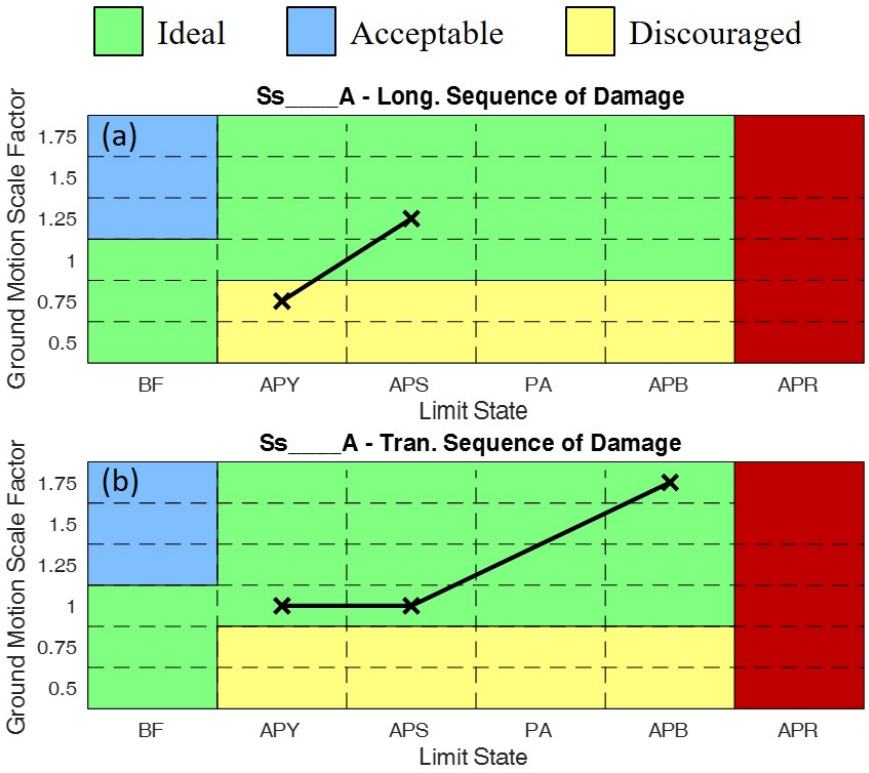

Figure D.3: Sequences of damage for single-span steel IABs where a scale factor of 1.00 represents the design-level.

Table D.3: Frequency of Limit State Occurrences for the Ida of Three-Span Steel IABs With 15-Ft Tall Piers Where a Scale Factor of 1.00 Represents the Design-Level

Bridge	SF	Longitudinal Limit State Occurrence																			
		Ideal								Acceptable								Unacceptable			
		BF	SL	CL	RE	RY	RF	FY	FF	APY	APB	APS	PA	PPY	PPS	SM	CM	BU	SS	CS	APR
StC15EA	0.50	0%	0%	0%	0%	0%	0%	-	-	55%	0%	10%	0%	0%	0%	0%	0%	0%	0%	0%	0%
	0.75	0%	15%	0%	0%	0%	0%	-	-	100%	0%	30%	0%	0%	0%	0%	0%	0%	0%	0%	0%
	1.00	0%	60%	35%	0%	0%	0%	-	-	100%	0%	70%	0%	0%	0%	0%	0%	0%	0%	0%	0%
	1.25	0%	80%	80%	0%	0%	0%	-	-	100%	15%	95%	0%	0%	20%	40%	50%	0%	0%	5%	0%
	1.50	0%	100%	100%	0%	0%	0%	-	-	100%	80%	100%	0%	0%	70%	95%	100%	0%	0%	25%	0%
	1.75	0%	100%	100%	0%	0%	0%	-	-	100%	100%	100%	0%	0%	85%	100%	100%	0%	40%	80%	55%
StC15FA	0.50	0%	0%	0%	-	-	-	0%	0%	55%	0%	10%	0%	0%	0%	0%	0%	0%	0%	0%	0%
	0.75	0%	35%	15%	-	-	-	0%	0%	100%	0%	30%	0%	0%	0%	0%	0%	0%	0%	0%	0%
	1.00	0%	80%	60%	-	-	-	0%	0%	100%	0%	55%	0%	0%	0%	10%	20%	0%	0%	0%	0%
	1.25	0%	85%	80%	-	-	-	0%	0%	100%	5%	80%	0%	0%	10%	55%	65%	0%	0%	5%	0%
	1.50	0%	100%	100%	-	-	-	0%	0%	100%	55%	100%	0%	0%	65%	80%	80%	0%	0%	20%	0%
	1.75	0%	100%	100%	-	-	-	0%	0%	100%	100%	100%	0%	0%	90%	100%	100%	0%	20%	75%	25%
Bridge	SF	Transverse Limit State Occurrence																			
		Ideal								Acceptable								Unacceptable			
		BF	SL	CL	RE	RY	RF	FY	FF	APY	APB	APS	PA	PPY	PPS	SM	CM	BU	SS	CS	APR
StC15EA	0.50	0%	0%	0%	100%	25%	0%	-	-	10%	0%	0%	0%	0%	0%	0%	0%	0%	0%	0%	0%
	0.75	0%	10%	0%	100%	95%	0%	-	-	70%	0%	10%	0%	0%	0%	0%	0%	0%	0%	0%	0%
	1.00	0%	40%	10%	100%	100%	0%	-	-	100%	0%	30%	0%	0%	0%	0%	0%	0%	0%	0%	0%
	1.25	0%	80%	50%	100%	100%	0%	-	-	100%	0%	35%	0%	0%	0%	0%	10%	0%	0%	0%	0%
	1.50	0%	100%	80%	100%	100%	0%	-	-	100%	25%	80%	0%	10%	10%	40%	50%	0%	0%	0%	0%
	1.75	0%	100%	100%	100%	100%	0%	-	-	100%	60%	90%	0%	15%	0%	80%	80%	0%	5%	20%	0%
StC15FA	0.50	0%	0%	0%	-	-	-	0%	0%	0%	0%	0%	0%	0%	0%	0%	0%	0%	0%	0%	0%
	0.75	0%	5%	0%	-	-	-	80%	0%	5%	0%	0%	0%	0%	0%	0%	0%	0%	0%	0%	0%
	1.00	0%	60%	5%	-	-	-	80%	0%	60%	0%	10%	0%	0%	0%	0%	0%	0%	0%	0%	0%
	1.25	0%	100%	35%	-	-	-	100%	0%	100%	0%	15%	0%	0%	0%	0%	5%	0%	0%	0%	0%
	1.50	0%	100%	95%	-	-	-	100%	0%	100%	0%	55%	0%	0%	0%	15%	25%	0%	0%	0%	0%
	1.75	0%	100%	100%	-	-	-	100%	0%	100%	10%	80%	0%	0%	0%	35%	50%	0%	0%	0%	0%

Table D.4: Frequency of Limit State Occurrences for the Ida of Three-Span Steel IABs With 40-Ft Tall Piers Where a Scale Factor of 1.00 Represents the Design-Level

Bridge	SF	Longitudinal Limit State Occurrence																			
		Ideal								Acceptable								Unacceptable			
		BF	SL	CL	RE	RY	RF	FY	FF	APY	APB	APS	PA	PPY	PPS	SM	CM	BU	SS	CS	APR
StC40EA	0.50	0%	0%	0%	0%	0%	0%	-	-	65%	0%	30%	0%	0%	0%	0%	0%	0%	0%	0%	0%
	0.75	0%	0%	0%	0%	0%	0%	-	-	100%	0%	60%	0%	0%	0%	0%	0%	0%	0%	0%	0%
	1.00	0%	15%	0%	0%	0%	0%	-	-	100%	15%	100%	0%	0%	5%	0%	0%	0%	0%	0%	0%
	1.25	0%	75%	45%	0%	0%	0%	-	-	100%	75%	100%	0%	0%	55%	0%	5%	0%	0%	0%	10%
	1.50	0%	90%	80%	0%	0%	0%	-	-	100%	90%	100%	0%	0%	90%	20%	25%	0%	0%	0%	55%
	1.75	0%	100%	80%	0%	0%	0%	-	-	100%	95%	100%	0%	0%	95%	40%	55%	0%	0%	15%	80%
StC40FA	0.50	0%	0%	0%	-	-	-	0%	0%	70%	0%	30%	0%	0%	0%	0%	0%	0%	0%	0%	0%
	0.75	0%	0%	0%	-	-	-	0%	0%	100%	0%	60%	0%	0%	0%	0%	0%	0%	0%	0%	0%
	1.00	0%	15%	0%	-	-	-	0%	0%	100%	15%	100%	0%	0%	0%	0%	0%	0%	0%	0%	0%
	1.25	0%	75%	40%	-	-	-	0%	0%	100%	75%	100%	0%	0%	5%	0%	0%	0%	0%	0%	5%
	1.50	0%	85%	75%	-	-	-	0%	0%	100%	90%	100%	0%	0%	50%	20%	25%	0%	0%	0%	55%
	1.75	0%	95%	85%	-	-	-	0%	0%	100%	95%	100%	0%	0%	55%	40%	60%	0%	0%	15%	80%
Bridge	**SF**	**Transverse Limit State Occurrence**																			
		Ideal								**Acceptable**								**Unacceptable**			
		BF	**SL**	**CL**	**RE**	**RY**	**RF**	**FY**	**FF**	**APY**	**APB**	**APS**	**PA**	**PPY**	**PPS**	**SM**	**CM**	**BU**	**SS**	**CS**	**APR**
StC40EA	0.50	0%	0%	0%	80%	0%	0%	-	-	45%	0%	10%	0%	0%	0%	0%	0%	0%	0%	0%	0%
	0.75	0%	20%	0%	100%	40%	0%	-	-	100%	0%	35%	0%	0%	0%	0%	0%	0%	0%	0%	0%
	1.00	0%	65%	20%	100%	80%	0%	-	-	100%	5%	70%	0%	0%	0%	0%	0%	0%	0%	0%	0%
	1.25	0%	100%	100%	100%	100%	0%	-	-	100%	70%	100%	0%	0%	5%	0%	0%	0%	0%	0%	0%
	1.50	0%	100%	100%	100%	100%	0%	-	-	100%	100%	100%	0%	0%	10%	45%	55%	0%	0%	0%	20%
	1.75	0%	100%	100%	100%	100%	0%	-	-	100%	100%	100%	0%	0%	25%	70%	75%	0%	0%	15%	60%
StC40FA	0.50	0%	0%	0%	-	-	-	0%	0%	45%	0%	10%	0%	0%	0%	0%	0%	0%	0%	0%	0%
	0.75	0%	20%	0%	-	-	-	0%	0%	100%	0%	30%	0%	0%	0%	0%	0%	0%	0%	0%	0%
	1.00	0%	65%	35%	-	-	-	0%	0%	100%	5%	75%	0%	0%	0%	0%	0%	0%	0%	0%	0%
	1.25	0%	85%	80%	-	-	-	10%	0%	100%	55%	100%	0%	0%	0%	5%	0%	0%	0%	0%	0%
	1.50	0%	100%	100%	-	-	-	15%	0%	100%	100%	100%	0%	0%	5%	55%	55%	0%	0%	0%	15%
	1.75	0%	100%	100%	-	-	-	15%	0%	100%	100%	100%	0%	0%	25%	70%	85%	0%	0%	20%	55%

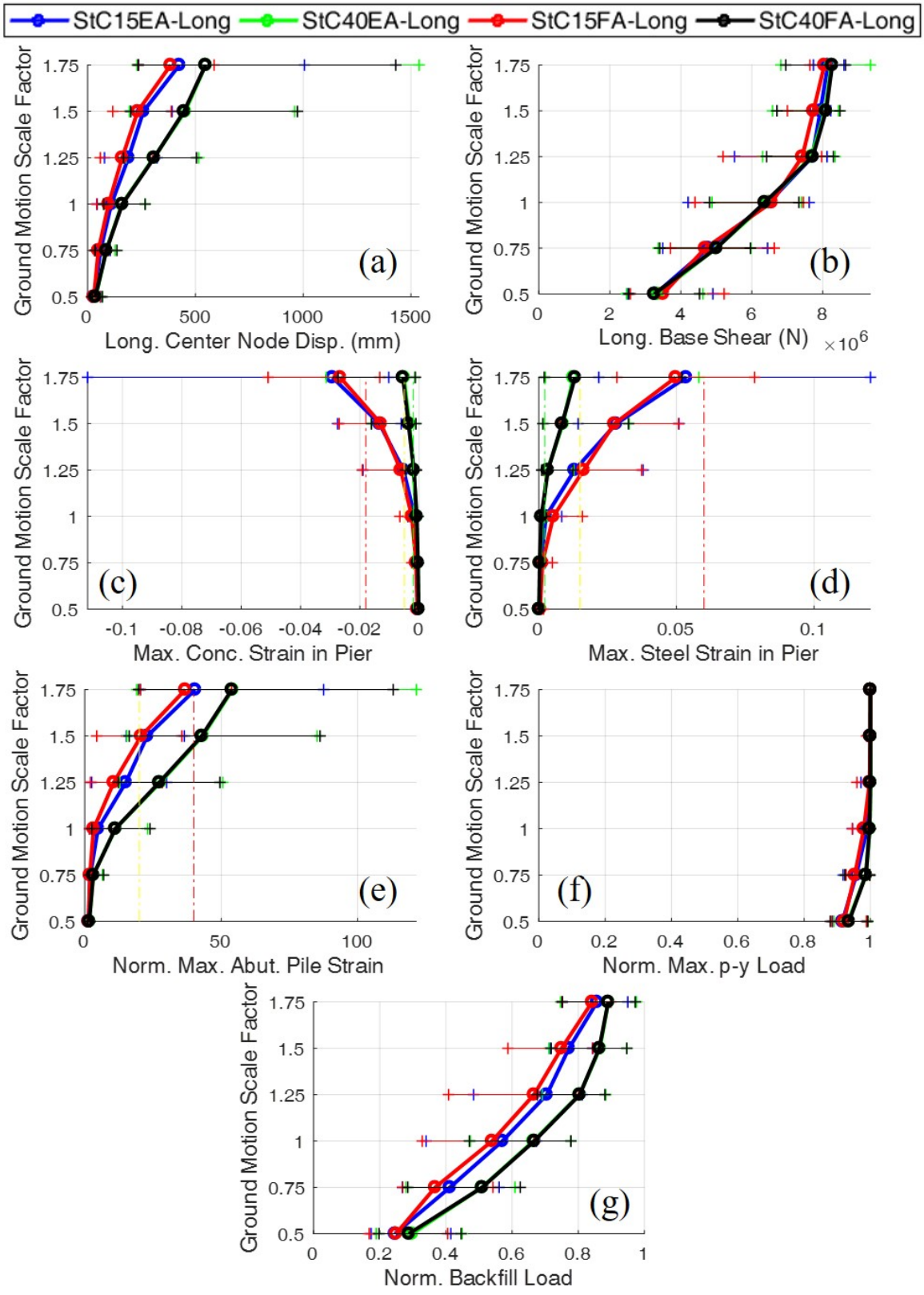

Figure D.4: IDA plots for three-span steel IABs in the longitudinal direction where a scale factor of 1.00 represents the design-level.

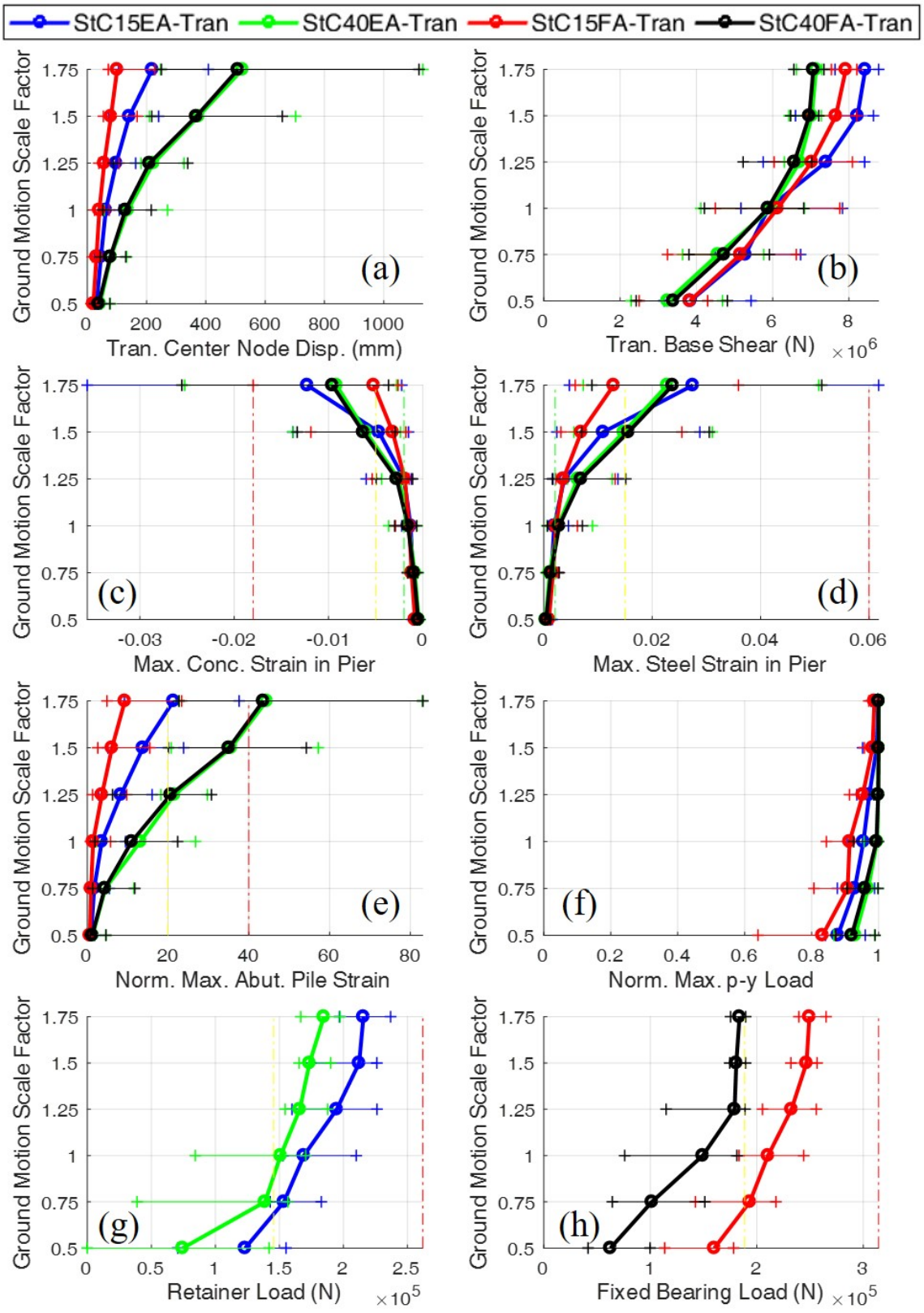

Figure D.5: IDA plots for three-span steel IABs in the transverse direction where a scale factor of 1.00 represents the design-level.

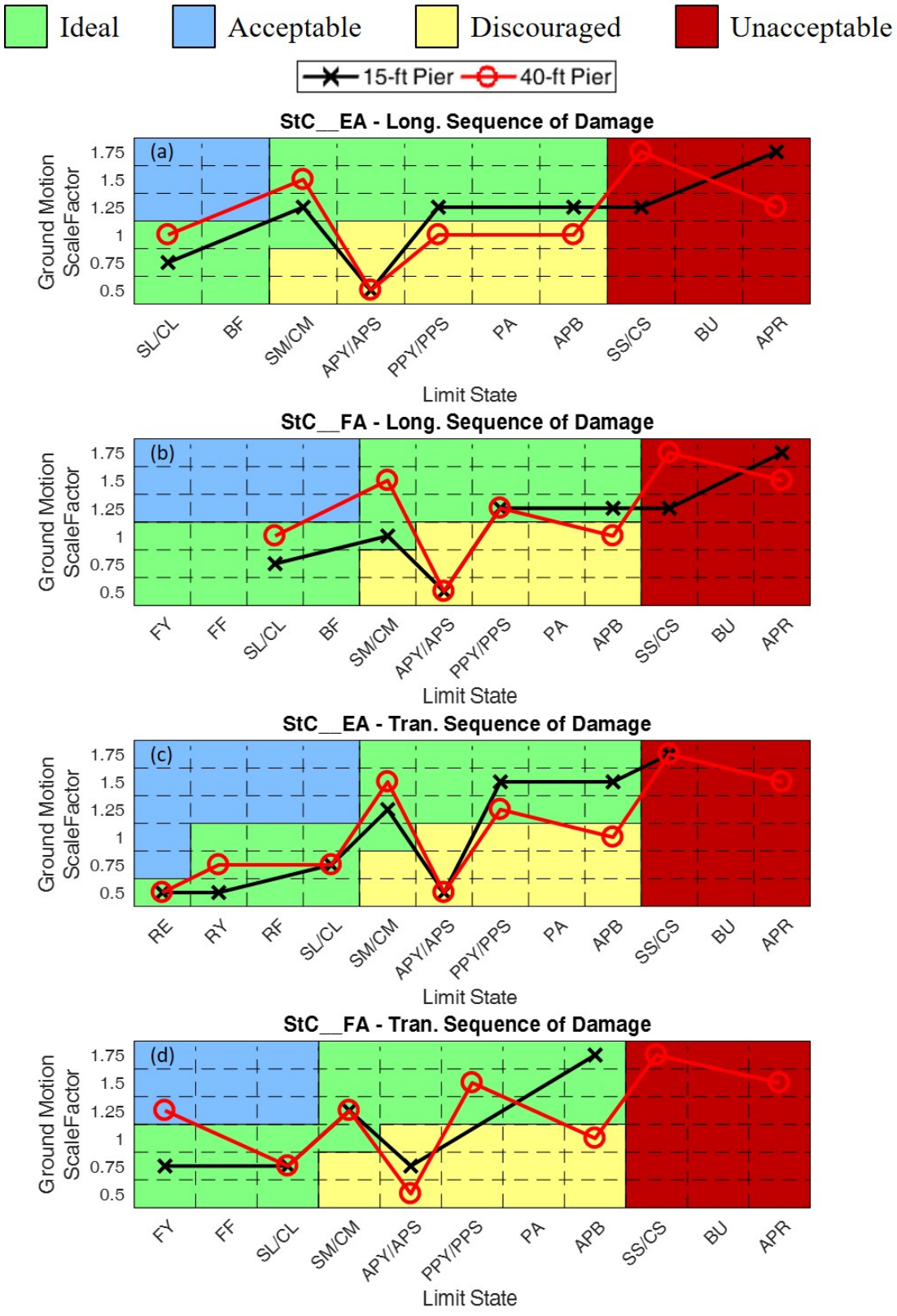

Figure D.6: Sequences of damage for three-span steel IABs where a scale factor of 1.00 represents the design-level.

Table D.5: Frequency of Limit State Occurrences for the Ida of Four-Span Steel IABs With 15-Ft Tall Piers Where a Scale Factor of 1.00 Represents the Design-Level

Bridge	SF	Longitudinal Limit State Occurrence																			
		Ideal								Acceptable								Unacceptable			
		BF	SL	CL	RE	RY	RF	FY	FF	APY	APB	APS	PA	PPY	PPS	SM	CM	BU	SS	CS	APR
SIC15EA	0.50	0%	0%	0%	0%	0%	0%	-	-	10%	0%	5%	0%	0%	0%	0%	0%	0%	0%	0%	0%
	0.75	0%	40%	10%	0%	0%	0%	-	-	80%	0%	40%	0%	0%	0%	0%	0%	0%	0%	0%	0%
	1.00	0%	100%	100%	0%	0%	0%	-	-	100%	0%	100%	0%	0%	5%	25%	35%	0%	0%	5%	0%
	1.25	0%	100%	100%	0%	0%	0%	-	-	100%	30%	100%	0%	0%	0%	85%	90%	0%	5%	60%	0%
	1.50	0%	100%	100%	0%	0%	0%	-	-	100%	60%	100%	0%	0%	0%	95%	100%	0%	35%	85%	20%
	1.75	0%	100%	100%	0%	0%	0%	-	-	100%	80%	100%	0%	0%	10%	100%	100%	0%	65%	90%	30%
SIC15FA	0.50	0%	20%	5%	-	-	-	0%	0%	5%	0%	0%	0%	0%	0%	0%	0%	0%	0%	0%	0%
	0.75	0%	80%	75%	-	-	-	0%	0%	75%	0%	30%	0%	0%	0%	0%	20%	0%	0%	0%	0%
	1.00	0%	90%	85%	-	-	-	0%	0%	90%	0%	75%	0%	0%	0%	60%	80%	0%	0%	0%	0%
	1.25	0%	100%	100%	-	-	-	0%	0%	100%	5%	100%	0%	0%	0%	100%	100%	0%	0%	55%	0%
	1.50	0%	100%	100%	-	-	-	0%	0%	100%	60%	100%	0%	0%	0%	100%	100%	0%	30%	85%	20%
	1.75	0%	100%	100%	-	-	-	0%	0%	100%	80%	100%	0%	0%	0%	100%	100%	0%	60%	95%	30%
Bridge	SF	Transverse Limit State Occurrence																			
		Ideal								Acceptable								Unacceptable			
		BF	SL	CL	RE	RY	RF	FY	FF	APY	APB	APS	PA	PPY	PPS	SM	CM	BU	SS	CS	APR
SIC15EA	0.50	0%	100%	100%	100%	0%	0%	-	-	0%	0%	0%	0%	0%	0%	30%	65%	0%	0%	0%	0%
	0.75	0%	100%	100%	100%	0%	0%	-	-	0%	0%	0%	0%	0%	0%	80%	85%	0%	0%	0%	0%
	1.00	0%	100%	100%	100%	0%	0%	-	-	10%	0%	0%	0%	0%	0%	100%	100%	0%	0%	35%	0%
	1.25	0%	100%	100%	100%	0%	0%	-	-	75%	0%	20%	0%	0%	0%	100%	100%	0%	30%	100%	0%
	1.50	0%	100%	100%	100%	0%	0%	-	-	90%	10%	50%	0%	0%	0%	100%	100%	0%	75%	100%	0%
	1.75	0%	100%	100%	100%	0%	0%	-	-	100%	20%	75%	0%	0%	0%	100%	100%	0%	85%	100%	15%
SIC15FA	0.50	0%	100%	100%	-	-	-	0%	0%	0%	0%	0%	0%	0%	0%	5%	10%	0%	0%	0%	0%
	0.75	0%	100%	100%	-	-	-	0%	0%	0%	0%	0%	0%	0%	0%	35%	75%	0%	0%	0%	0%
	1.00	0%	100%	100%	-	-	-	0%	0%	0%	0%	0%	0%	0%	0%	75%	90%	0%	0%	25%	0%
	1.25	0%	100%	100%	-	-	-	0%	0%	35%	0%	0%	0%	0%	0%	95%	100%	0%	10%	65%	0%
	1.50	0%	100%	100%	-	-	-	0%	0%	90%	0%	20%	0%	0%	0%	100%	100%	0%	60%	100%	0%
	1.75	0%	100%	100%	-	-	-	0%	0%	100%	15%	55%	0%	0%	0%	100%	100%	0%	85%	100%	5%

Table D.6: Frequency of Limit State Occurrences for the Ida of Four-Span Steel IABs With 40-Ft Tall Piers Where a Scale Factor Of 1.00 Represents the Design-Level

Bridge	SF	Longitudinal Limit State Occurrence																		
		Ideal								Acceptable								Unacceptable		
		BF	SL	CL	RE	RY	RF	FY	FF	APY	APB	APS	PA	PPY	PPS	SM	CM	BU	SS	CS	APR
SIC40EA	0.50	0%	0%	0%	0%	0%	0%	-	-	35%	0%	10%	0%	0%	0%	0%	0%	0%	0%	0%	0%
	0.75	0%	15%	0%	0%	0%	0%	-	-	100%	0%	70%	0%	0%	0%	0%	0%	0%	0%	0%	0%
	1.00	0%	75%	50%	0%	0%	0%	-	-	100%	15%	100%	0%	0%	0%	0%	5%	0%	0%	0%	0%
	1.25	0%	85%	80%	0%	0%	0%	-	-	100%	50%	100%	0%	0%	10%	20%	30%	0%	0%	0%	15%
	1.50	0%	95%	85%	0%	0%	0%	-	-	100%	80%	100%	0%	0%	20%	55%	80%	0%	0%	10%	30%
	1.75	0%	100%	85%	0%	0%	0%	-	-	100%	80%	100%	0%	0%	30%	75%	80%	0%	0%	20%	50%
SIC40FA	0.50	0%	0%	0%	-	-	-	0%	0%	35%	0%	10%	0%	0%	0%	0%	0%	0%	0%	0%	0%
	0.75	0%	0%	0%	-	-	-	0%	0%	100%	0%	70%	0%	0%	0%	0%	0%	0%	0%	0%	0%
	1.00	0%	75%	50%	-	-	-	0%	0%	100%	15%	100%	0%	0%	5%	0%	0%	0%	0%	0%	0%
	1.25	0%	85%	80%	-	-	-	0%	0%	100%	50%	100%	0%	0%	25%	20%	25%	0%	0%	0%	15%
	1.50	0%	95%	85%	-	-	-	0%	0%	100%	80%	100%	0%	0%	35%	40%	65%	0%	0%	5%	30%
	1.75	0%	100%	85%	-	-	-	0%	0%	100%	80%	100%	0%	0%	40%	70%	75%	0%	0%	20%	50%
Bridge	SF	Transverse Limit State Occurrence																		
		Ideal								Acceptable								Unacceptable		
		BF	SL	CL	RE	RY	RF	FY	FF	APY	APB	APS	PA	PPY	PPS	SM	CM	BU	SS	CS	APR
SIC40EA	0.50	0%	100%	100%	100%	0%	0%	-	-	35%	0%	0%	0%	0%	0%	0%	10%	0%	0%	0%	0%
	0.75	0%	100%	100%	100%	0%	0%	-	-	90%	0%	15%	0%	0%	0%	70%	75%	0%	0%	0%	0%
	1.00	0%	100%	100%	100%	0%	0%	-	-	100%	5%	80%	0%	0%	0%	85%	85%	0%	0%	0%	0%
	1.25	0%	100%	100%	100%	0%	0%	-	-	100%	25%	75%	0%	0%	0%	85%	100%	0%	0%	20%	0%

	1.50	0%	100%	100%	100%	0%	0%	-	-	100%	45%	75%	0%	0%	0%	100%	100%	0%	15%	50%	20%
	1.75	0%	100%	100%	100%	0%	0%	-	-	100%	65%	75%	0%	0%	5%	95%	100%	0%	15%	55%	25%
SIC40FA	0.50	0%	100%	100%	-	-	-	0%	0%	20%	0%	0%	0%	0%	0%	0%	15%	0%	0%	0%	0%
	0.75	0%	100%	100%	-	-	-	0%	0%	85%	0%	10%	0%	0%	0%	65%	65%	0%	0%	0%	0%
	1.00	0%	100%	100%	-	-	-	0%	0%	95%	0%	80%	0%	0%	0%	85%	95%	0%	0%	0%	0%
	1.25	0%	100%	100%	-	-	-	0%	0%	100%	25%	75%	0%	0%	0%	95%	100%	0%	0%	30%	0%
	1.50	0%	100%	100%	-	-	-	0%	0%	100%	45%	75%	0%	0%	0%	95%	100%	0%	15%	50%	20%
	1.75	0%	100%	100%	-	-	-	0%	0%	100%	60%	75%	0%	0%	0%	95%	95%	0%	15%	60%	25%

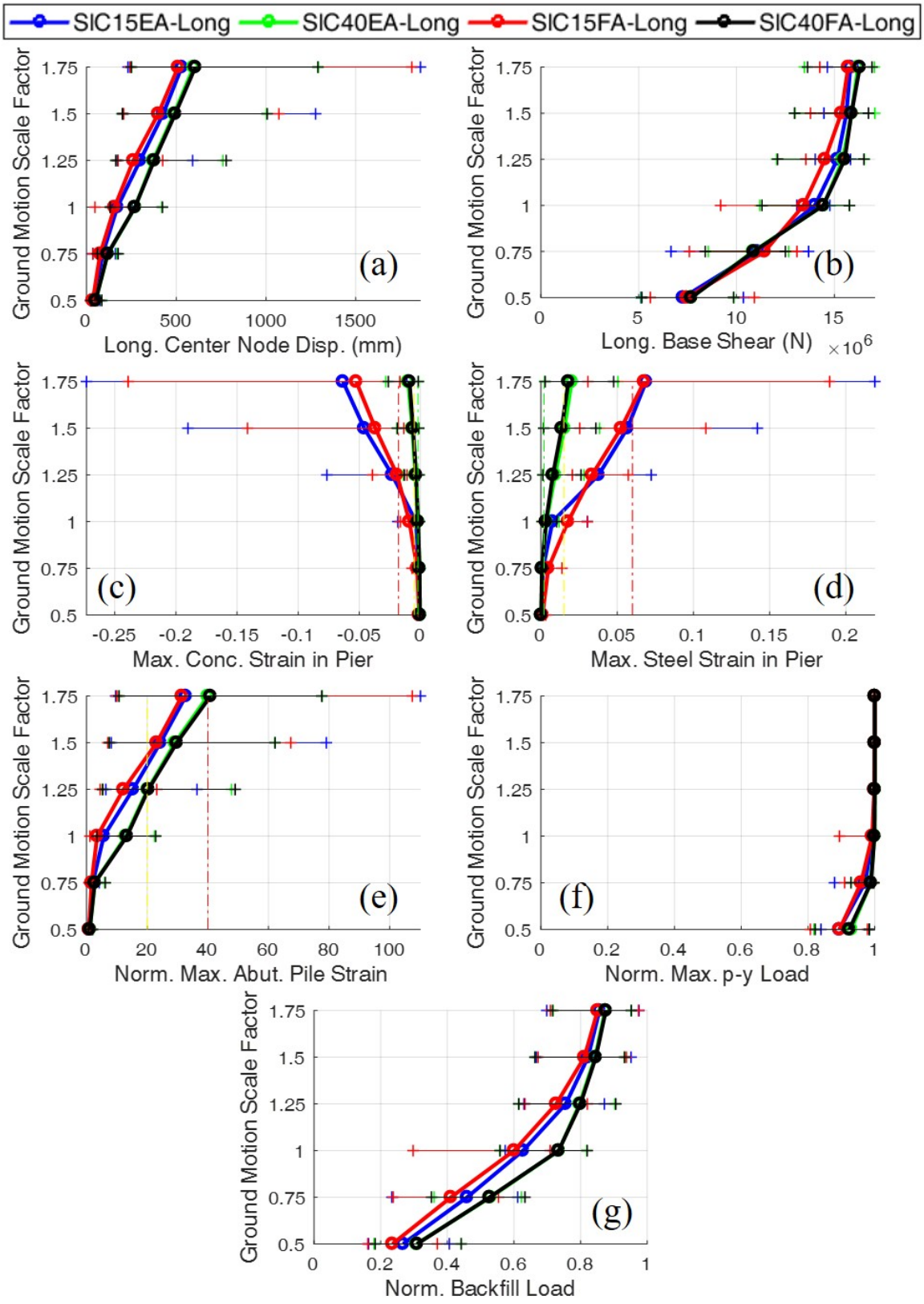

Figure D.7: IDA plots for four-span steel IABs in the longitudinal direction where a scale factor of 1.00 represents the design-level.

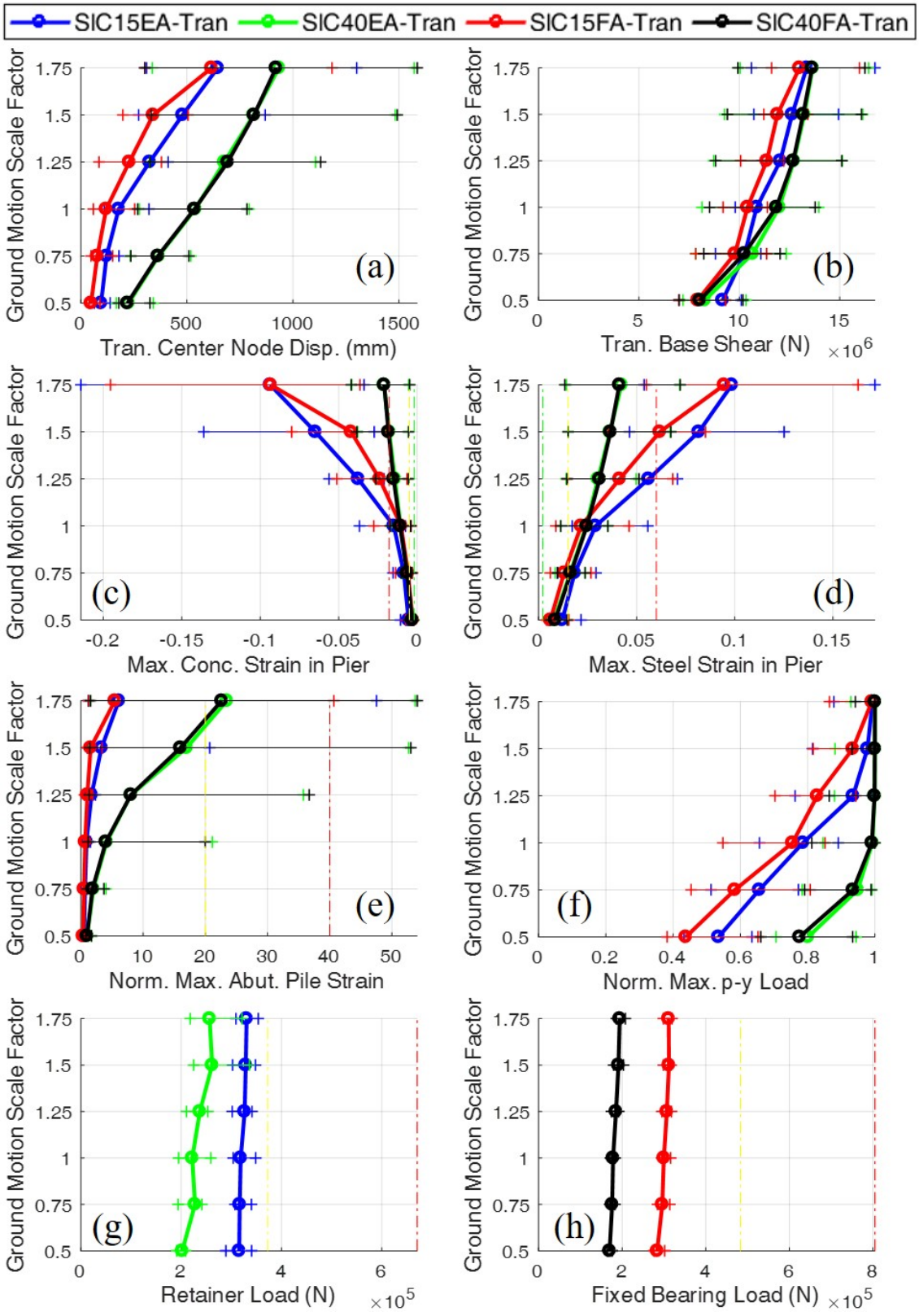

Figure D.8: IDA plots for four-span steel IABs in the transverse direction where a scale factor of 1.00 represents the design-level.

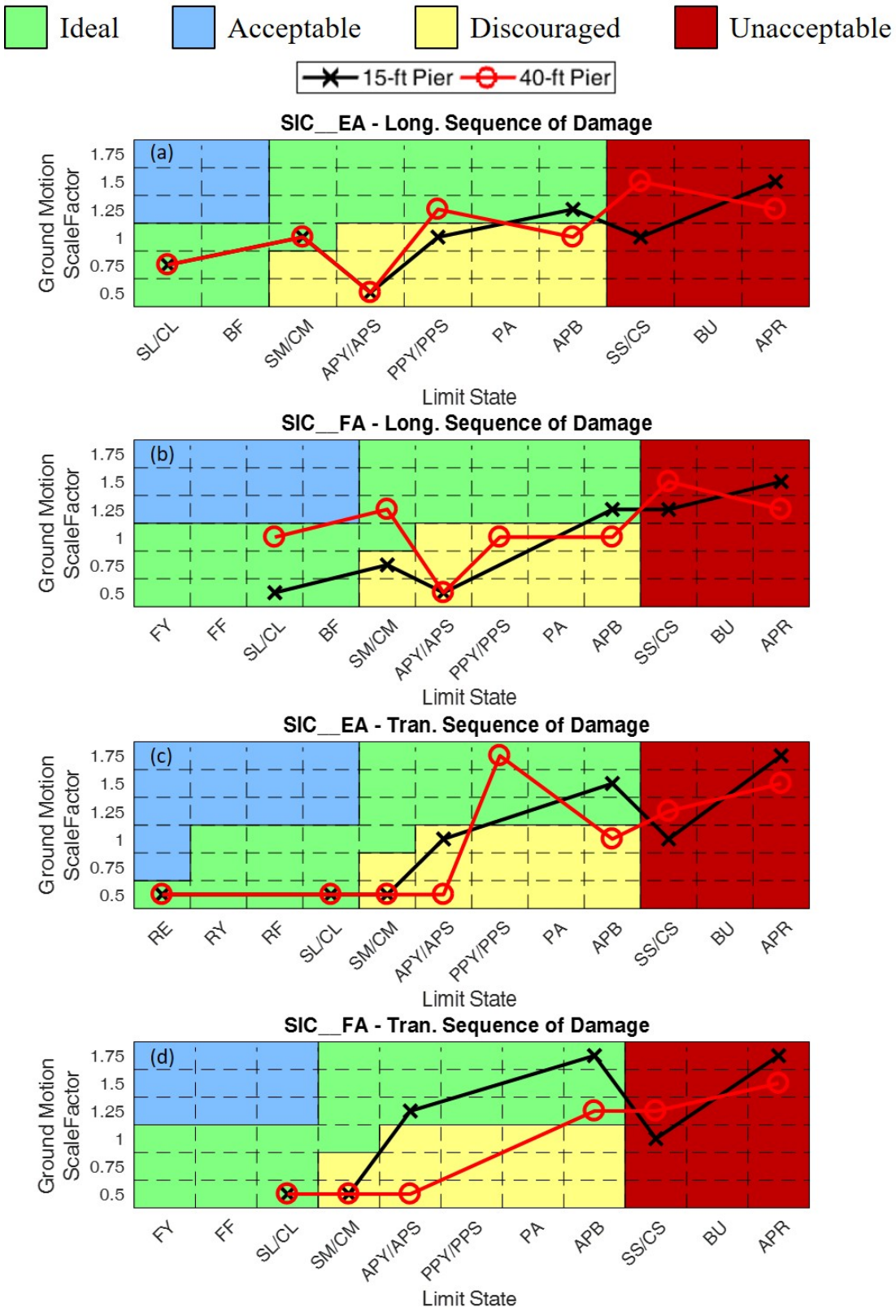

Figure D.9: Sequences of damage for four-span steel IABs where a scale factor of 1.00 represents the design-level.

Table D.7: Frequency of Limit State Occurrences for the Ida of Three-Span Concrete IABs With 15-Ft Tall Piers Where a Scale Factor of 1.00 Represents the Design-Level

Bridge	SF	Longitudinal Limit State Occurrence																				
		Ideal								Acceptable								Unacceptable			
		BF	SL	CL	RE	RY	RF	FY	FF	APY	APB	APS	PA	PPY	PPS	SM	CM	BU	SS	CS	APR
CtC15EA	0.50	0%	0%	0%	0%	0%	0%	-	-	100%	0%	55%	0%	0%	0%	0%	0%	0%	0%	0%	0%
	0.75	0%	95%	65%	0%	0%	0%	-	-	100%	5%	100%	0%	0%	0%	15%	20%	0%	0%	0%	0%
	1.00	0%	100%	100%	0%	0%	0%	-	-	100%	75%	100%	0%	0%	0%	75%	85%	0%	5%	50%	20%
	1.25	0%	100%	100%	0%	0%	0%	-	-	100%	85%	100%	0%	0%	0%	85%	90%	0%	35%	80%	60%
	1.50	10%	100%	100%	0%	0%	0%	-	-	100%	90%	100%	0%	10%	5%	90%	100%	0%	50%	75%	70%
	1.75	20%	100%	100%	5%	5%	0%	-	-	100%	100%	100%	0%	25%	15%	100%	100%	10%	70%	80%	70%
Bridge	SF	Transverse Limit State Occurrence																				
		Ideal								Acceptable								Unacceptable			
		BF	SL	CL	RE	RY	RF	FY	FF	APY	APB	APS	PA	PPY	PPS	SM	CM	BU	SS	CS	APR
CtC15EA	0.50	0%	0%	0%	100%	100%	5%	-	-	80%	0%	25%	0%	0%	0%	0%	0%	0%	0%	0%	0%
	0.75	0%	100%	25%	100%	100%	100%	-	-	100%	40%	100%	0%	0%	0%	0%	0%	0%	0%	0%	0%
	1.00	0%	100%	80%	100%	100%	100%	-	-	100%	90%	100%	0%	0%	0%	40%	40%	0%	5%	15%	10%
	1.25	0%	95%	85%	100%	100%	100%	-	-	100%	100%	100%	0%	0%	0%	80%	80%	0%	45%	65%	55%
	1.50	0%	95%	85%	100%	100%	100%	-	-	100%	100%	100%	0%	20%	20%	80%	80%	20%	75%	80%	80%
	1.75	0%	100%	95%	100%	100%	100%	-	-	100%	100%	100%	0%	20%	20%	80%	80%	20%	75%	80%	80%

Table D.8: Frequency of Limit State Occurrences for the Ida of Three-Span Concrete IABs With 40-Ft Tall Piers Where a Scale Factor of 1.00 Represents the Design-Level

Bridge	SF	Longitudinal Limit State Occurrence																			
		Ideal								Acceptable								Unacceptable			
		BF	SL	CL	RE	RY	RF	FY	FF	APY	APB	APS	PA	PPY	PPS	SM	CM	BU	SS	CS	APR
CtC40EA	0.50	0%	0%	0%	0%	0%	0%	-	-	100%	0%	75%	0%	0%	0%	0%	0%	0%	0%	0%	0%
	0.75	0%	55%	15%	0%	0%	0%	-	-	100%	45%	100%	0%	0%	5%	0%	0%	0%	0%	0%	0%
	1.00	0%	80%	75%	0%	0%	0%	-	-	100%	80%	100%	0%	0%	0%	20%	20%	0%	0%	0%	30%
	1.25	0%	85%	75%	0%	0%	0%	-	-	100%	85%	100%	0%	0%	20%	30%	50%	0%	0%	5%	70%
	1.50	10%	85%	75%	0%	0%	0%	-	-	100%	90%	100%	0%	5%	50%	50%	70%	0%	15%	20%	70%
	1.75	20%	90%	75%	0%	0%	0%	-	-	100%	90%	100%	0%	20%	30%	70%	70%	0%	20%	25%	70%
CtC40FA	0.50	0%	0%	0%	-	-	-	0%	0%	100%	0%	75%	0%	0%	0%	0%	0%	0%	0%	0%	0%
	0.75	0%	45%	20%	-	-	-	0%	0%	100%	45%	100%	0%	0%	0%	0%	0%	0%	0%	0%	0%
	1.00	0%	80%	65%	-	-	-	0%	0%	100%	80%	100%	0%	0%	15%	20%	20%	0%	0%	0%	30%
	1.25	0%	85%	75%	-	-	-	0%	0%	100%	85%	100%	0%	0%	5%	30%	45%	0%	0%	5%	70%
	1.50	10%	85%	75%	-	-	-	0%	0%	100%	90%	100%	0%	0%	20%	45%	70%	0%	10%	20%	70%
	1.75	20%	90%	85%	-	-	-	0%	0%	100%	90%	100%	0%	20%	15%	70%	70%	0%	20%	25%	70%
Bridge	SF	Transverse Limit State Occurrence																			
		Ideal								Acceptable								Unacceptable			
		BF	SL	CL	RE	RY	RF	FY	FF	APY	APB	APS	PA	PPY	PPS	SM	CM	BU	SS	CS	APR
CtC40EA	0.50	0%	5%	0%	100%	100%	0%	-	-	100%	5%	80%	0%	0%	0%	0%	0%	0%	0%	0%	0%
	0.75	0%	85%	60%	100%	100%	0%	-	-	100%	75%	100%	0%	0%	0%	0%	0%	0%	0%	0%	0%
	1.00	0%	95%	80%	100%	100%	65%	-	-	100%	90%	100%	0%	0%	0%	25%	35%	0%	0%	0%	30%
	1.25	0%	100%	85%	100%	100%	85%	-	-	100%	100%	100%	0%	0%	0%	55%	65%	0%	0%	10%	70%
	1.50	0%	100%	90%	100%	100%	100%	-	-	100%	100%	100%	0%	0%	0%	65%	70%	0%	20%	20%	70%
	1.75	0%	100%	95%	100%	100%	100%	-	-	100%	100%	100%	0%	0%	0%	70%	75%	0%	20%	30%	75%
CtC40FA	0.50	0%	15%	5%	-	-	-	80%	0%	100%	5%	70%	0%	0%	0%	0%	0%	0%	0%	0%	0%
	0.75	0%	100%	80%	-	-	-	100%	0%	100%	80%	100%	0%	0%	0%	0%	0%	0%	0%	0%	0%
	1.00	0%	100%	95%	-	-	-	100%	0%	100%	90%	100%	0%	0%	0%	30%	55%	0%	0%	0%	25%
	1.25	0%	100%	100%	-	-	-	100%	0%	100%	100%	100%	0%	0%	0%	70%	80%	0%	0%	15%	65%
	1.50	0%	100%	100%	-	-	-	100%	0%	100%	100%	100%	0%	0%	0%	75%	80%	0%	20%	20%	70%
	1.75	0%	100%	100%	-	-	-	100%	20%	100%	100%	100%	0%	0%	0%	80%	85%	5%	20%	30%	75%

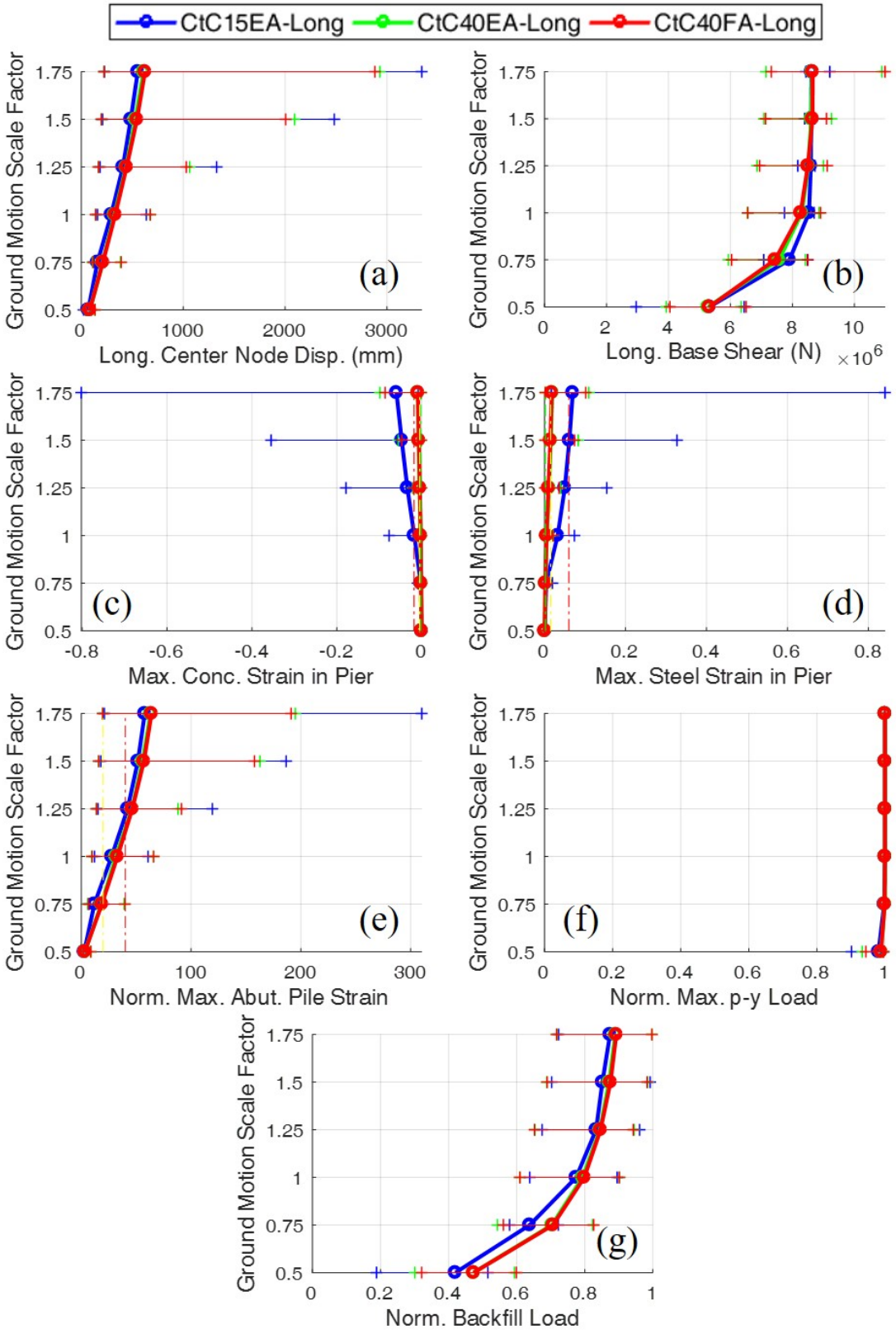

Figure D.10: IDA plots for three-span concrete IABs in the longitudinal direction where a scale factor of 1.00 represents the design-level.

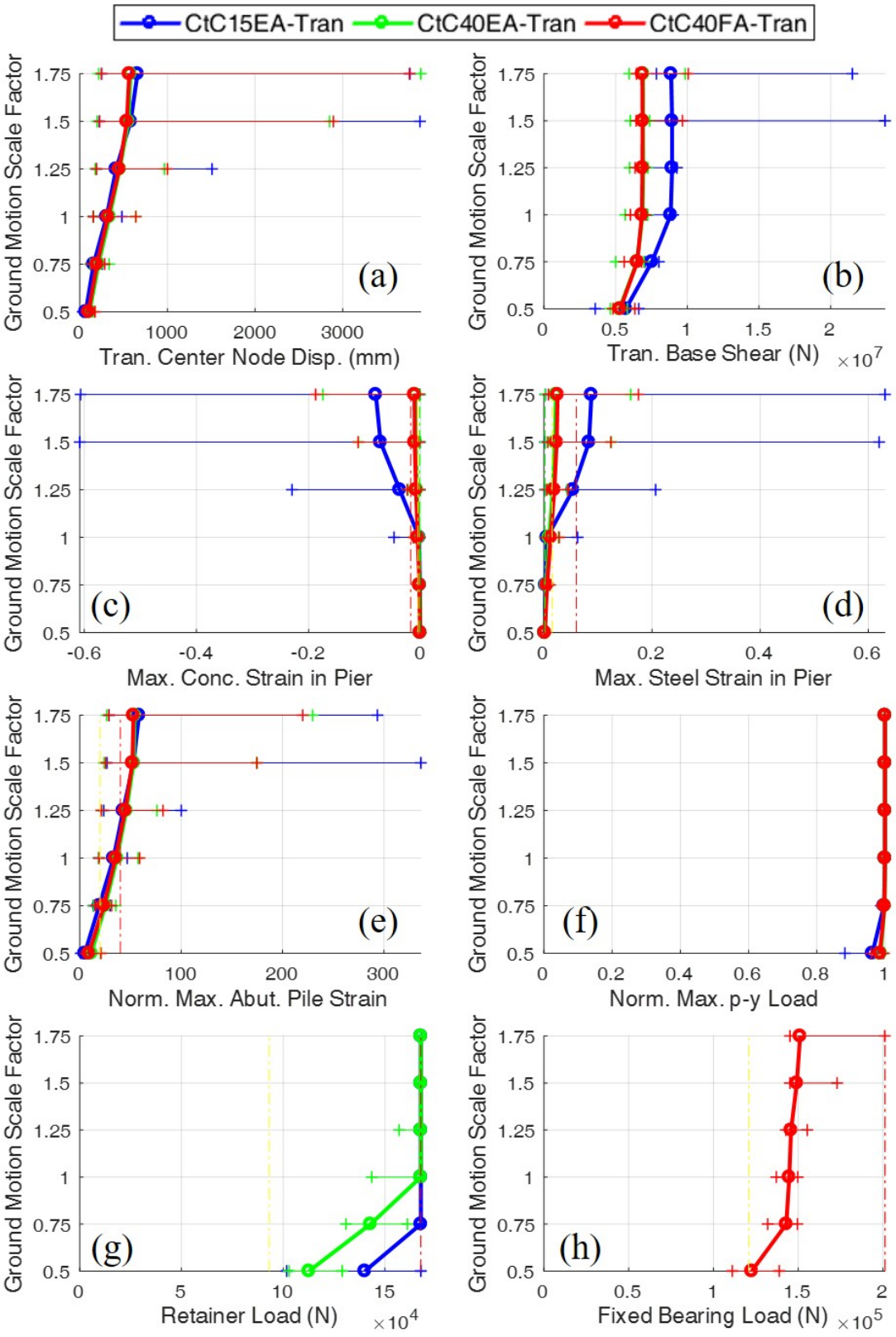

Figure D.11: IDA plots for three-span concrete IABs in the transverse direction where a scale factor of 1.00 represents the design-level.

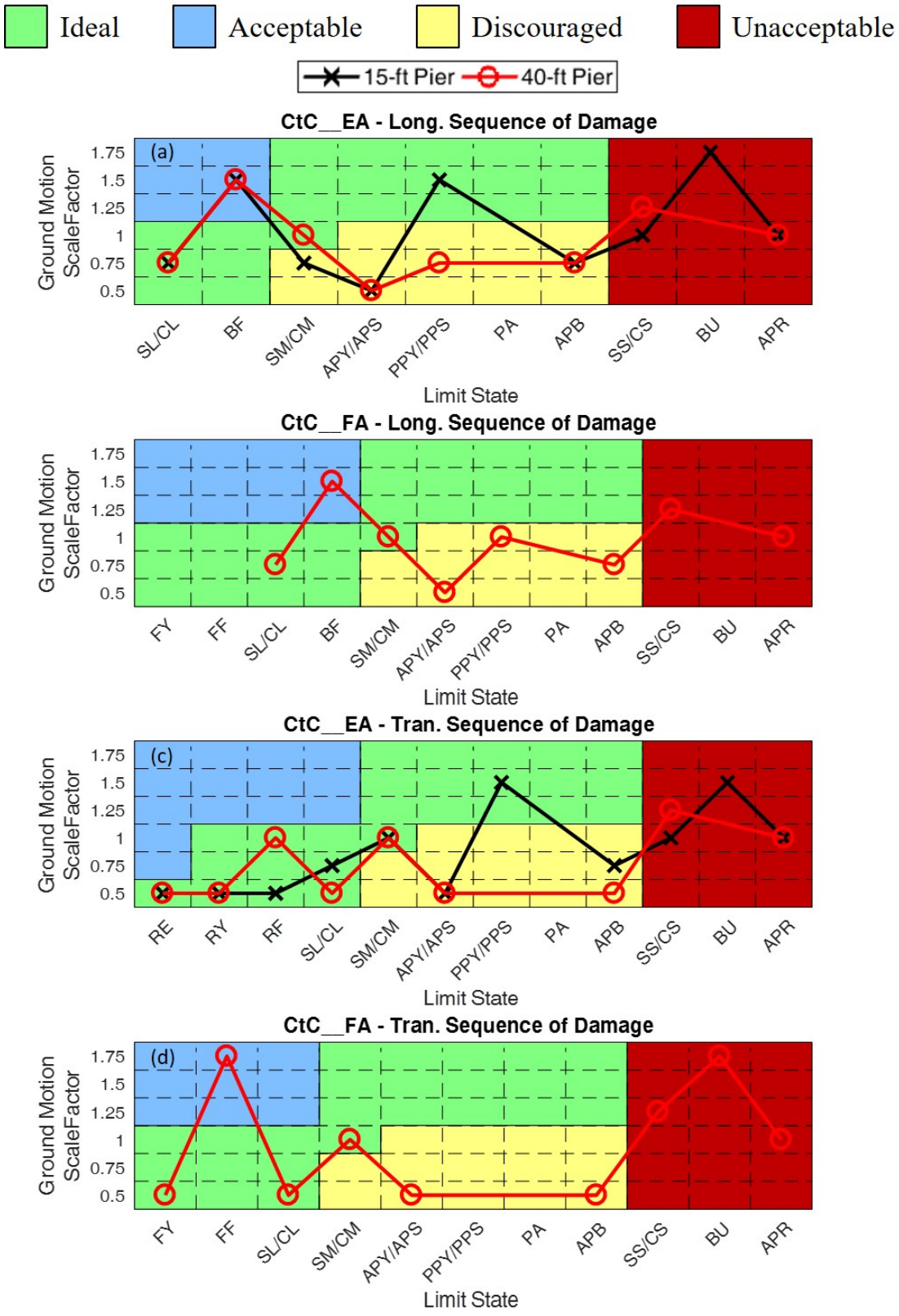

Figure D.12: Sequences of damage for three-span concrete IABs where a scale factor of 1.00 represents the design-level.

Table D.9: Frequency of Limit State Occurrences for the Ida of Four-Span Concrete IABs With 15-Ft Tall Piers Where a Scale Factor of 1.00 Represents the Design-Level

Bridge	SF	Longitudinal Limit State Occurrence																				
		Ideal								Acceptable								Unacceptable			
		BF	SL	CL	RE	RY	RF	FY	FF	APY	APB	APS	PA	PPY	PPS	SM	CM	BU	SS	CS	APR
ClC15EA	0.50	0%	50%	50%	0%	0%	0%	-	-	100%	0%	85%	0%	0%	0%	0%	0%	0%	0%	0%	0%
	0.75	0%	85%	85%	0%	0%	0%	-	-	100%	20%	100%	0%	0%	0%	70%	80%	0%	0%	50%	0%
	1.00	0%	95%	95%	0%	0%	0%	-	-	100%	65%	100%	0%	0%	0%	80%	80%	0%	5%	80%	5%
	1.25	0%	100%	100%	0%	0%	0%	-	-	100%	70%	100%	0%	0%	0%	85%	85%	0%	20%	75%	20%
	1.50	0%	100%	100%	0%	0%	0%	-	-	100%	70%	100%	0%	0%	0%	90%	95%	0%	20%	85%	25%
	1.75	5%	100%	100%	0%	0%	0%	-	-	100%	80%	100%	5%	0%	0%	95%	95%	0%	20%	95%	35%
Bridge	SF	Transverse Limit State Occurrence																				
		Ideal								Acceptable								Unacceptable			
		BF	SL	CL	RE	RY	RF	FY	FF	APY	APB	APS	PA	PPY	PPS	SM	CM	BU	SS	CS	APR
ClC15EA	0.50	0%	100%	100%	100%	100%	0%	-	-	5%	0%	0%	0%	0%	0%	95%	100%	0%	0%	45%	0%
	0.75	0%	100%	100%	100%	100%	0%	-	-	65%	0%	15%	0%	0%	0%	100%	100%	0%	5%	85%	0%
	1.00	0%	100%	100%	100%	100%	0%	-	-	75%	15%	55%	0%	0%	0%	100%	100%	0%	35%	100%	0%
	1.25	0%	100%	100%	100%	100%	0%	-	-	80%	15%	65%	0%	0%	0%	100%	100%	0%	30%	100%	5%
	1.50	0%	100%	100%	100%	100%	0%	-	-	100%	30%	75%	0%	0%	0%	100%	100%	0%	40%	100%	5%
	1.75	0%	100%	100%	100%	100%	0%	-	-	100%	35%	80%	0%	0%	0%	100%	100%	0%	45%	100%	5%

Table D.10: Frequency of Limit State Occurrences for the Ida of Four-Span Concrete IABs With 40-Ft Tall Piers Where a Scale Factor of 1.00 Represents the Design-Level

Bridge	SF	Longitudinal Limit State Occurrence																				
		Ideal								Acceptable								Unacceptable				
		BF	SL	CL	RE	RY	RF	FY	FF	APY	APB	APS	PA	PPY	PPS	SM	CM	BU	SS	CS	APR	
ClC40EA	0.50	0%	5%	0%	0%	0%	0%	-	-	100%	0%	90%	0%	0%	0%	0%	0%	0%	0%	0%	0%	
	0.75	0%	75%	60%	0%	0%	0%	-	-	100%	30%	100%	0%	0%	0%	10%	20%	0%	0%	0%	0%	
	1.00	0%	75%	70%	0%	0%	0%	-	-	100%	60%	100%	0%	0%	0%	20%	35%	0%	0%	0%	10%	
	1.25	10%	80%	75%	0%	0%	0%	-	-	100%	70%	100%	0%	0%	0%	35%	60%	0%	10%	20%	30%	
	1.50	15%	85%	80%	0%	0%	0%	-	-	100%	70%	100%	0%	5%	5%	45%	70%	0%	15%	30%	35%	
	1.75	15%	90%	90%	0%	0%	0%	-	-	100%	80%	100%	0%	5%	5%	50%	70%	0%	15%	30%	40%	
Bridge	SF	Transverse Limit State Occurrence																				
		Ideal								Acceptable								Unacceptable				
		BF	SL	CL	RE	RY	RF	FY	FF	APY	APB	APS	PA	PPY	PPS	SM	CM	BU	SS	CS	APR	
ClC40EA	0.50	0%	100%	90%	100%	100%	0%	-	-	55%	0%	20%	0%	0%	0%	40%	55%	0%	0%	5%	0%	
	0.75	0%	100%	100%	100%	100%	0%	-	-	75%	20%	55%	0%	0%	0%	65%	75%	0%	0%	10%	0%	
	1.00	0%	100%	100%	100%	100%	0%	-	-	100%	20%	85%	0%	0%	0%	75%	90%	0%	0%	25%	20%	
	1.25	0%	100%	100%	100%	100%	0%	-	-	100%	30%	90%	0%	0%	0%	95%	100%	0%	20%	35%	20%	
	1.50	0%	100%	100%	100%	100%	0%	-	-	100%	35%	95%	0%	0%	0%	100%	100%	0%	20%	50%	20%	
	1.75	0%	100%	100%	100%	100%	0%	-	-	100%	50%	100%	0%	0%	0%	100%	100%	0%	20%	60%	30%	

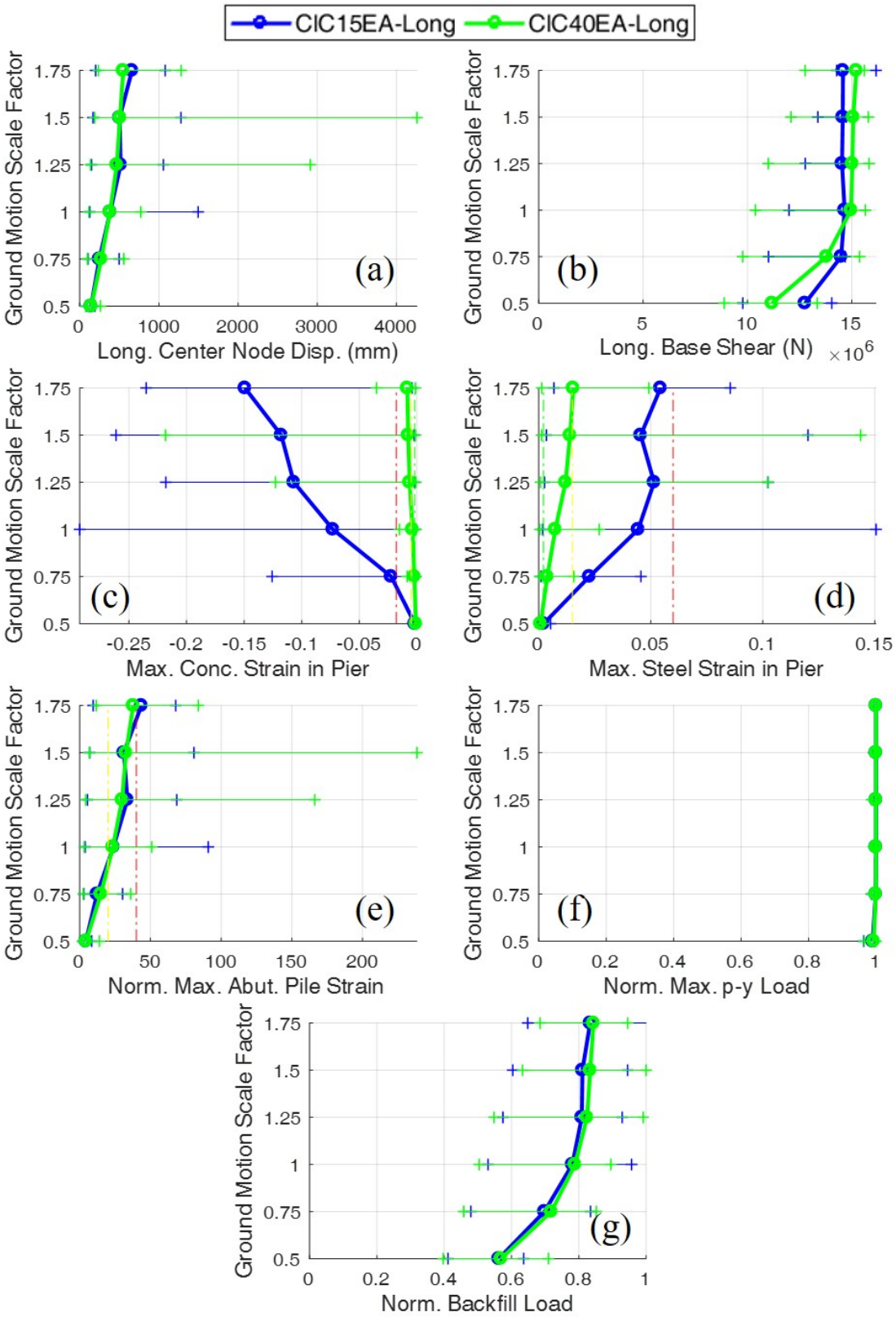

Figure D.13: IDA plots for four-span concrete IABs in the longitudinal direction where a scale factor of 1.00 represents the design-level.

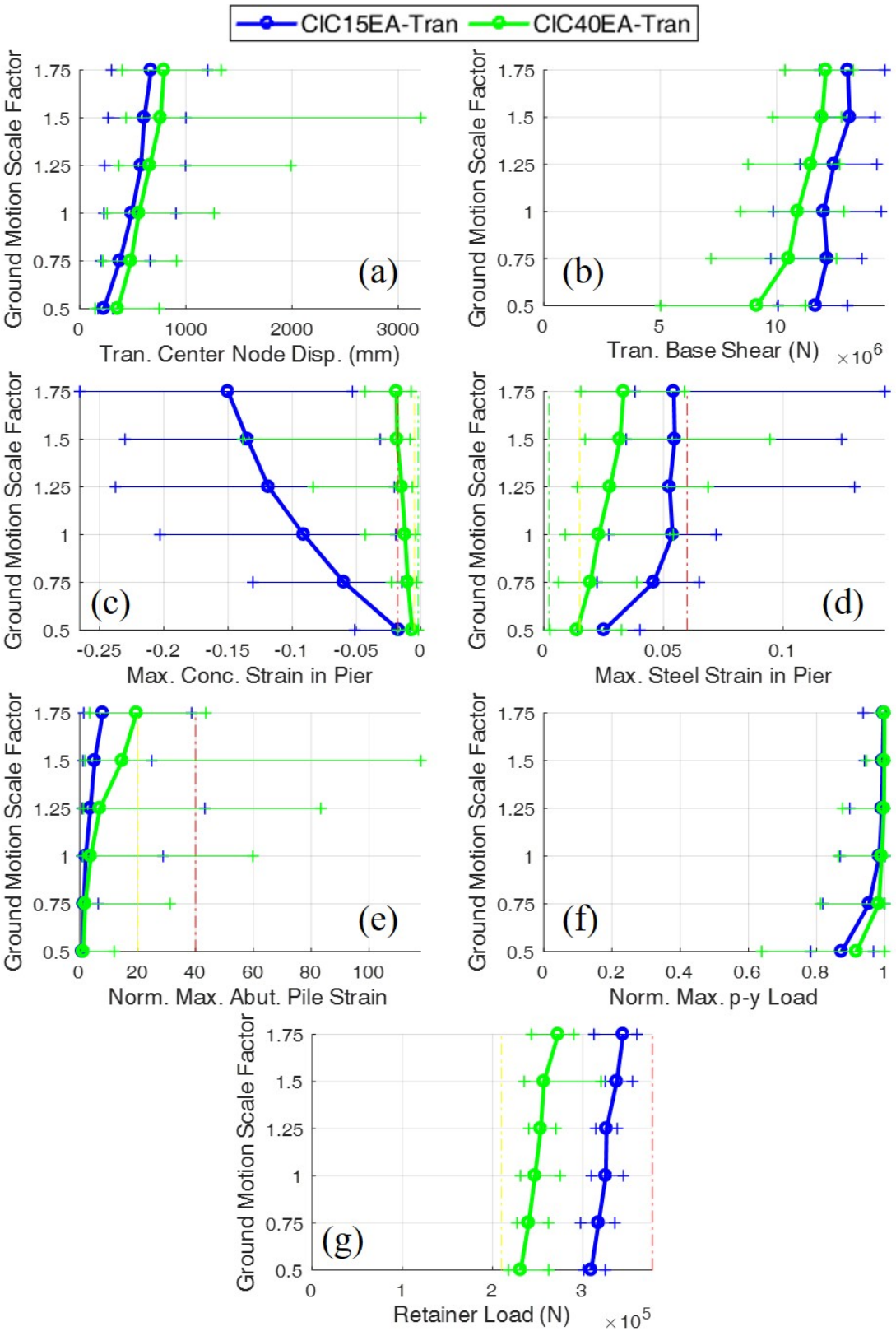

Figure D.14: IDA plots for four-span concrete IABs in the transverse direction where a scale factor of 1.00 represents the design-level.

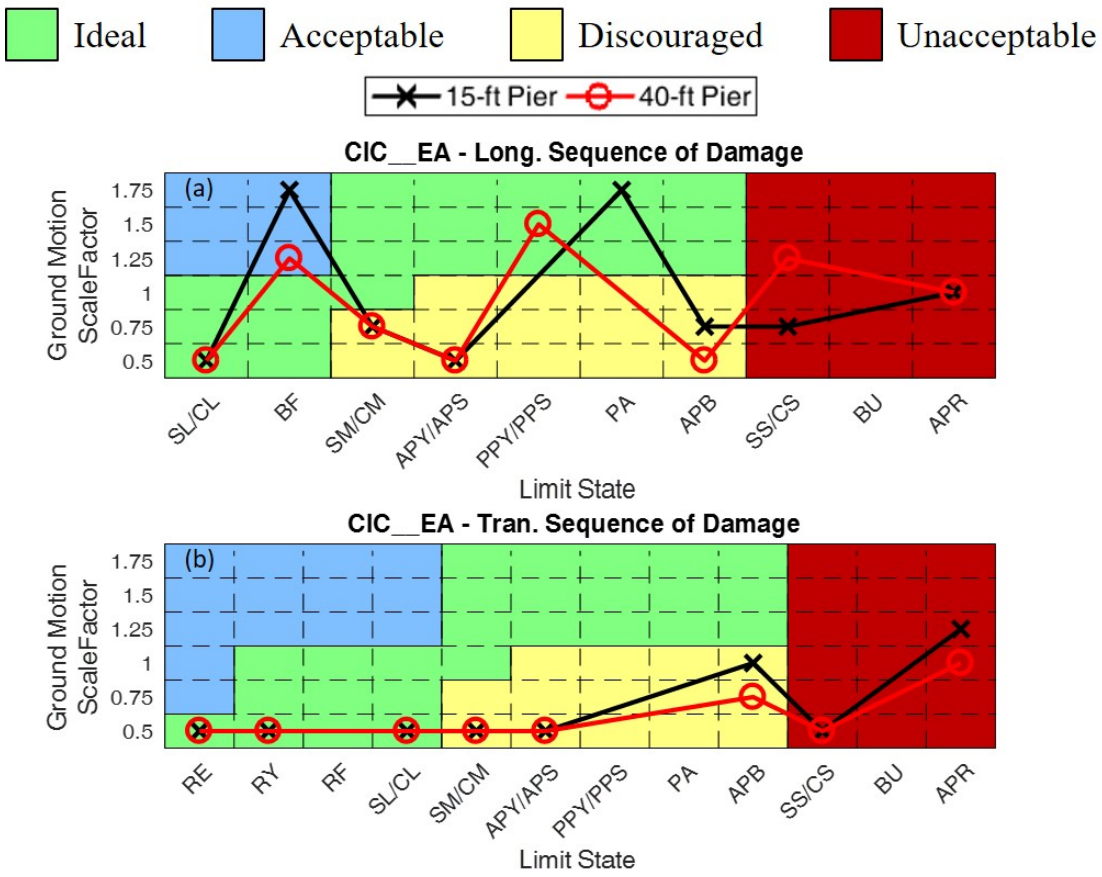

Figure D.15: Sequences of damage for four-span concrete IABs where a scale factor of 1.00 represents the design-level.

APPENDIX E: ENHANCED DESIGN IDA DATA

Incremental dynamic analysis results for the 8 IABs with design enhancements are presented in this appendix. These results are used for the discussion in Chapter 5.

The incremental dynamic analysis is presented with a scale factor of 1.0 being equivalent to the design-level response and the scale factor being approximately equivalent to the maximum considered earthquake-level. Four enhancements are studied: the reduction in retainer use, the reduction in fixed bearing strength, the strengthening of the pier columns, and increasing the backfill contribution. The data presented in the tables and figures is for both the original designs to the enhanced designs to facilitate comparisons. Only figures for relevant directions of excitation (bridge longitudinal or transverse) are presented.

The data is presented through tables presenting the frequency of limit state occurrences when subjected to 20 ground motions developed for Cairo at various scale factors. IDA plots providing the median response of each component across the 20 ground motions at each scale factor along with the maximum and minimum values are also presented. The dashed vertical lines in the IDA plots represent limit states reached with green being an ideal limit stat, yellow an acceptable limit state, and red an unacceptable limit state. Finally, the sequence of damage for each IAB is presented with damage being indicated by the first occurrence of the limit state.

Table E.1 describes which tables and figures present data for each set of enhanced design IABs.

Table E.1: Organization of Figures in Appendix E

	Enhancement	Figure or Table
Frequency of Limit State Occurrence Table at Cairo	Reduction in Retainer Use	Table E.2-E.4
	Reduction in Fixed Bearing Strength	Table E.5-E.6
	Strengthening of Pier Column	Table E.7-E.8
	Increased Backfill Contribution	Table E.9-E.10
IDA Plots	Reduction in Retainer Use	Fig. E.1-E.2
	Reduction in Fixed Bearing Strength	Fig. E.4-E.5
	Strengthening of Pier Column	Fig. E.7-E.10
	Increased Backfill Contribution	Fig. E.12-E.13
Sequence of Damage	Reduction in Retainer Use	Fig. E.3
	Reduction in Fixed Bearing Strength	Fig. E.6
	Strengthening of Pier Column	Fig. E.11
	Increased Backfill Contribution	Fig. E.14

Table E.2: Frequency of Limit State Occurrences for the Stc40ea Ida With Various Retainer Configurations Where a Scale Factor of 1.00 Represents the Design-Level

Bridge	Revision	SF	Longitudinal Limit State Occurrence																	
			Ideal						Acceptable								Unacceptable			
			BF	SL	CL	RE	RY	RF	APY	APB	APS	PA	PPY	PPS	SM	CM	BU	SS	CS	APR
StC40EA	6 Retainers per Pier	0.50	0%	0%	0%	0%	0%	0%	65%	0%	30%	0%	0%	0%	0%	0%	0%	0%	0%	0%
		0.75	0%	0%	0%	0%	0%	0%	100%	0%	60%	0%	0%	0%	0%	0%	0%	0%	0%	0%
		1.00	0%	15%	0%	0%	0%	0%	100%	15%	100%	0%	0%	5%	0%	0%	0%	0%	0%	0%
		1.25	0%	75%	45%	0%	0%	0%	100%	75%	100%	0%	0%	55%	0%	5%	0%	0%	0%	10%
		1.50	0%	90%	80%	0%	0%	0%	100%	90%	100%	0%	0%	90%	20%	25%	0%	0%	0%	55%
		1.75	0%	100%	80%	0%	0%	0%	100%	95%	100%	0%	0%	95%	40%	55%	0%	0%	15%	80%
	2 Retainers per Pier	0.50	0%	0%	0%	0%	0%	0%	65%	0%	30%	0%	0%	0%	0%	0%	0%	0%	0%	0%
		0.75	0%	0%	0%	0%	0%	0%	100%	0%	60%	0%	0%	0%	0%	0%	0%	0%	0%	0%
		1.00	0%	15%	0%	0%	0%	0%	100%	15%	100%	0%	0%	5%	0%	0%	0%	0%	0%	0%
		1.25	0%	75%	45%	0%	0%	0%	100%	75%	100%	0%	0%	55%	0%	5%	0%	0%	0%	10%
		1.50	0%	90%	80%	0%	0%	0%	100%	90%	100%	0%	0%	90%	20%	25%	0%	0%	0%	55%
		1.75	0%	100%	80%	0%	0%	0%	100%	95%	100%	0%	0%	95%	40%	55%	0%	0%	15%	80%
Bridge	**Revision**	**SF**	**Transverse Limit State Occurrence**																	
			Ideal						**Acceptable**								**Unacceptable**			
			BF	**SL**	**CL**	**RE**	**RY**	**RF**	**APY**	**APB**	**APS**	**PA**	**PPY**	**PPS**	**SM**	**CM**	**BU**	**SS**	**CS**	**APR**
StC40EA	6 Retainers per Pier	0.50	0%	0%	0%	80%	0%	0%	45%	0%	10%	0%	0%	0%	0%	0%	0%	0%	0%	0%
		0.75	0%	20%	0%	100%	40%	0%	100%	0%	35%	0%	0%	0%	0%	0%	0%	0%	0%	0%
		1.00	0%	65%	20%	100%	80%	0%	100%	5%	70%	0%	0%	0%	0%	0%	0%	0%	0%	0%

		1.25	0%	100%	100%	100%	100%	0%	100%	70%	100%	0%	0%	5%	0%	0%	0%	0%	0%	0%
		1.50	0%	100%	100%	100%	100%	0%	100%	100%	100%	0%	0%	10%	45%	55%	0%	0%	0%	20%
		1.75	0%	100%	100%	100%	100%	0%	100%	100%	100%	0%	0%	25%	70%	75%	0%	0%	15%	60%
	2 Retainers per Pier	0.50	0%	0%	0%	80%	35%	0%	45%	0%	15%	0%	0%	0%	0%	0%	0%	0%	0%	0%
		0.75	0%	0%	0%	100%	85%	0%	100%	0%	40%	0%	0%	0%	0%	0%	0%	0%	0%	0%
		1.00	0%	60%	5%	100%	95%	0%	100%	5%	80%	0%	0%	0%	0%	0%	0%	0%	0%	0%
		1.25	0%	100%	85%	100%	100%	0%	100%	80%	100%	0%	0%	0%	0%	0%	0%	0%	0%	0%
		1.50	0%	100%	100%	100%	100%	0%	100%	100%	100%	0%	0%	5%	45%	50%	0%	0%	0%	25%
		1.75	0%	100%	100%	100%	100%	0%	100%	100%	100%	0%	0%	5%	70%	75%	0%	0%	10%	60%

Table E.3: Frequency of Limit State Occurrences for the Slc15ea Ida With Various Retainer Configurations Where a Scale Factor of 1.00 Represents the Design-Level

Bridge	Revision	SF	Longitudinal Limit State Occurrence																	
			Ideal						Acceptable								Unacceptable			
			BF	SL	CL	RE	RY	RF	APY	APB	APS	PA	PPY	PPS	SM	CM	BU	SS	CS	APR
SlC15EA	8 Retainers per Pier	0.50	0%	0%	0%	0%	0%	0%	10%	0%	5%	0%	0%	0%	0%	0%	0%	0%	0%	0%
		0.75	0%	40%	10%	0%	0%	0%	80%	0%	40%	0%	0%	0%	0%	0%	0%	0%	0%	0%
		1.00	0%	100%	100%	0%	0%	0%	100%	0%	100%	0%	0%	5%	25%	35%	0%	0%	5%	0%
		1.25	0%	100%	100%	0%	0%	0%	100%	30%	100%	0%	0%	0%	85%	90%	0%	5%	60%	0%
		1.50	0%	100%	100%	0%	0%	0%	100%	60%	100%	0%	0%	0%	95%	100%	0%	35%	85%	20%
		1.75	0%	100%	100%	0%	0%	0%	100%	80%	100%	0%	0%	10%	100%	100%	0%	65%	90%	30%
	2 Retainers per Pier	0.50	0%	0%	0%	0%	0%	0%	10%	0%	5%	0%	0%	0%	0%	0%	0%	0%	0%	0%
		0.75	0%	40%	10%	0%	0%	0%	80%	0%	40%	0%	0%	0%	0%	0%	0%	0%	0%	0%
		1.00	0%	100%	100%	0%	0%	0%	100%	0%	100%	0%	0%	5%	25%	35%	0%	0%	5%	0%
		1.25	0%	100%	100%	0%	0%	0%	100%	30%	100%	0%	0%	0%	85%	90%	0%	5%	60%	0%
		1.50	0%	100%	100%	0%	0%	0%	100%	60%	100%	0%	0%	0%	95%	100%	0%	35%	85%	20%
		1.75	0%	100%	100%	0%	0%	0%	100%	80%	100%	0%	0%	10%	100%	100%	0%	65%	90%	30%
Bridge	**Revision**	**SF**	**Transverse Limit State Occurrence**																	
			Ideal						**Acceptable**								**Unacceptable**			
			BF	**SL**	**CL**	**RE**	**RY**	**RF**	**APY**	**APB**	**APS**	**PA**	**PPY**	**PPS**	**SM**	**CM**	**BU**	**SS**	**CS**	**APR**
SlC15EA	8 Retainers per Pier	0.50	0%	100%	100%	100%	0%	0%	0%	0%	0%	0%	0%	0%	30%	65%	0%	0%	0%	0%
		0.75	0%	100%	100%	100%	0%	0%	0%	0%	0%	0%	0%	0%	80%	85%	0%	0%	0%	0%
		1.00	0%	100%	100%	100%	0%	0%	10%	0%	0%	0%	0%	0%	100%	100%	0%	0%	35%	0%
		1.25	0%	100%	100%	100%	0%	0%	75%	0%	20%	0%	0%	0%	100%	100%	0%	30%	100%	0%
		1.50	0%	100%	100%	100%	0%	0%	90%	10%	50%	0%	0%	0%	100%	100%	0%	75%	100%	0%
		1.75	0%	100%	100%	100%	0%	0%	100%	20%	75%	0%	0%	0%	100%	100%	0%	85%	100%	15%
	2 Retainers per Pier	0.50	0%	100%	100%	100%	100%	0%	10%	0%	0%	0%	0%	0%	85%	90%	0%	0%	5%	0%
		0.75	0%	100%	100%	100%	100%	0%	75%	0%	0%	0%	0%	0%	100%	100%	0%	0%	65%	0%
		1.00	0%	100%	100%	100%	100%	0%	95%	0%	20%	0%	0%	0%	100%	100%	0%	20%	90%	0%
		1.25	0%	100%	100%	100%	100%	0%	100%	0%	50%	0%	0%	0%	100%	100%	0%	70%	100%	0%
		1.50	0%	100%	100%	100%	100%	0%	100%	15%	80%	0%	0%	0%	100%	100%	0%	80%	100%	0%
		1.75	0%	100%	100%	100%	100%	0%	100%	35%	85%	0%	0%	0%	100%	100%	0%	95%	100%	10%

Table E.4: Frequency of Limit State Occurrences for the Slc15ea Ida With 8 Retainers per Pier and 2 Weakened Retainers per Pier Where a Scale Factor of 1.00 Represents the Design-Level

Bridge	Revision	SF	Longitudinal Limit State Occurrence																	
			Ideal						Acceptable								Unacceptable			
			BF	SL	CL	RE	RY	RF	APY	APB	APS	PA	PPY	PPS	SM	CM	BU	SS	CS	APR
SlC15EA	8 Retainers per Pier	0.50	0%	0%	0%	0%	0%	0%	10%	0%	5%	0%	0%	0%	0%	0%	0%	0%	0%	0%
		0.75	0%	40%	10%	0%	0%	0%	80%	0%	40%	0%	0%	0%	0%	0%	0%	0%	0%	0%
		1.00	0%	100%	100%	0%	0%	0%	100%	0%	100%	0%	0%	5%	25%	35%	0%	0%	5%	0%
		1.25	0%	100%	100%	0%	0%	0%	100%	30%	100%	0%	0%	0%	85%	90%	0%	5%	60%	0%
		1.50	0%	100%	100%	0%	0%	0%	100%	60%	100%	0%	0%	0%	95%	100%	0%	35%	85%	20%
		1.75	0%	100%	100%	0%	0%	0%	100%	80%	100%	0%	0%	10%	100%	100%	0%	65%	90%	30%
	2 Retainers per Pier & Smaller Bolts	0.50	0%	0%	0%	0%	0%	0%	10%	0%	5%	0%	0%	0%	0%	0%	0%	0%	0%	0%
		0.75	0%	40%	10%	0%	0%	0%	80%	0%	40%	0%	0%	0%	0%	0%	0%	0%	0%	0%
		1.00	0%	100%	100%	0%	0%	0%	100%	0%	100%	0%	0%	5%	25%	35%	0%	0%	5%	0%
		1.25	0%	100%	100%	0%	0%	0%	100%	30%	100%	0%	0%	0%	85%	90%	0%	5%	60%	0%
		1.50	0%	100%	100%	0%	0%	0%	100%	60%	100%	0%	0%	0%	95%	100%	0%	35%	85%	20%
		1.75	0%	100%	100%	0%	0%	0%	100%	80%	100%	0%	0%	10%	100%	100%	0%	65%	90%	30%
Bridge	**Revision**	**SF**	**Transverse Limit State Occurrence**																	
			Ideal						**Acceptable**								**Unacceptable**			
			BF	**SL**	**CL**	**RE**	**RY**	**RF**	**APY**	**APB**	**APS**	**PA**	**PPY**	**PPS**	**SM**	**CM**	**BU**	**SS**	**CS**	**APR**
SlC15EA	8 Retainers per Pier	0.50	0%	100%	100%	100%	0%	0%	0%	0%	0%	0%	0%	0%	30%	65%	0%	0%	0%	0%
		0.75	0%	100%	100%	100%	0%	0%	0%	0%	0%	0%	0%	0%	80%	85%	0%	0%	0%	0%
		1.00	0%	100%	100%	100%	0%	0%	10%	0%	0%	0%	0%	0%	100%	100%	0%	0%	35%	0%
		1.25	0%	100%	100%	100%	0%	0%	75%	0%	20%	0%	0%	0%	100%	100%	0%	30%	100%	0%
		1.50	0%	100%	100%	100%	0%	0%	90%	10%	50%	0%	0%	0%	100%	100%	0%	75%	100%	0%
		1.75	0%	100%	100%	100%	0%	0%	100%	20%	75%	0%	0%	0%	100%	100%	0%	85%	100%	15%
	2 Retainers per Pier & Smaller Bolts	0.50	0%	100%	90%	100%	100%	100%	50%	0%	0%	0%	0%	0%	20%	35%	0%	0%	5%	0%
		0.75	0%	100%	100%	100%	100%	100%	95%	0%	15%	0%	0%	0%	85%	90%	0%	15%	35%	0%
		1.00	0%	100%	100%	100%	100%	100%	100%	0%	25%	0%	0%	0%	100%	100%	0%	40%	90%	0%
		1.25	0%	100%	100%	100%	100%	100%	100%	0%	75%	0%	0%	0%	100%	100%	0%	70%	100%	0%
		1.50	0%	100%	100%	100%	100%	100%	100%	25%	85%	0%	0%	0%	100%	100%	0%	95%	100%	0%
		1.75	0%	100%	100%	100%	100%	100%	100%	50%	95%	0%	0%	0%	100%	100%	0%	100%	100%	5%

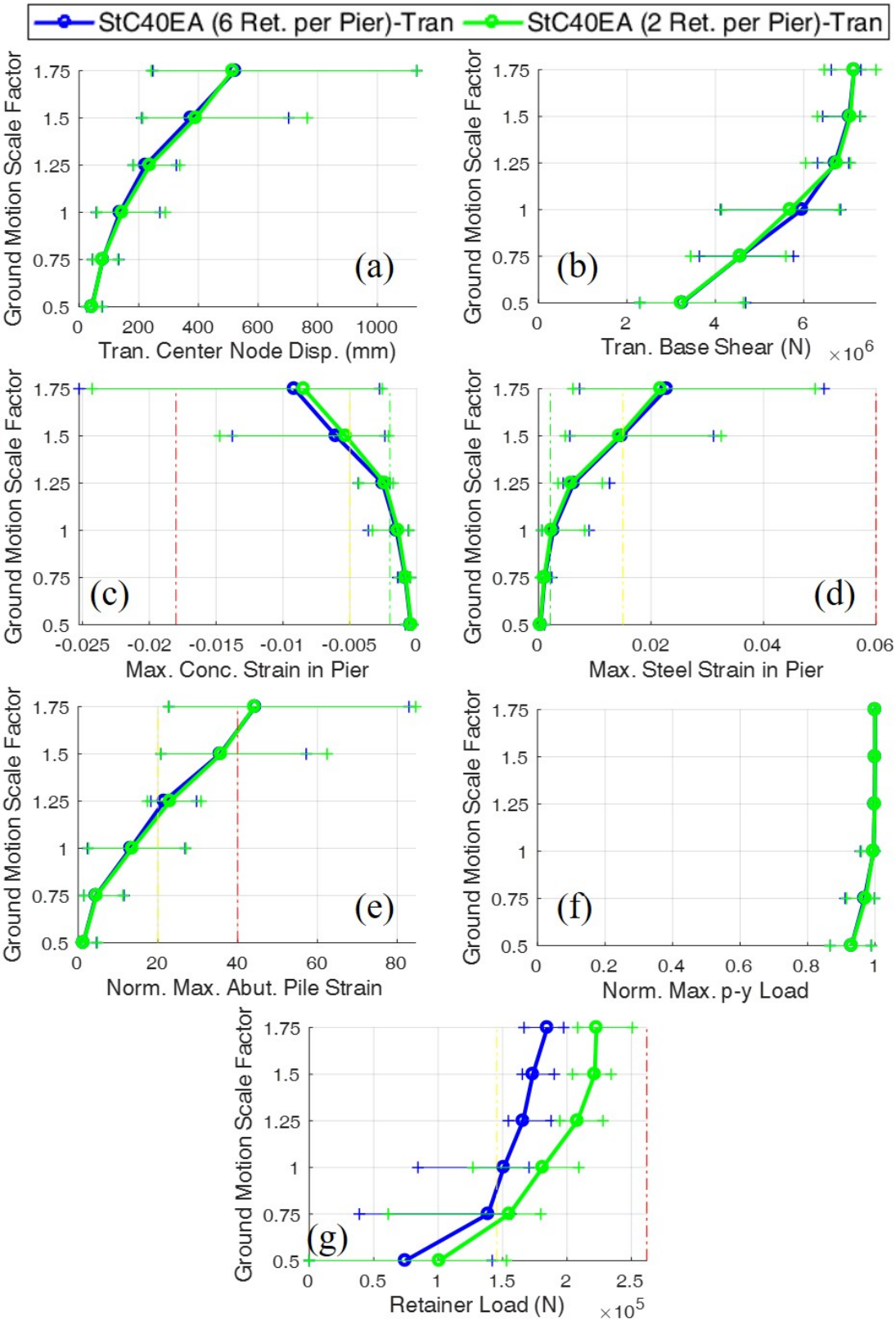

Figure E.1: IDA plots for the original and enhanced StC40EA in the transverse direction where a scale factor of 1.00 represents the design-level.

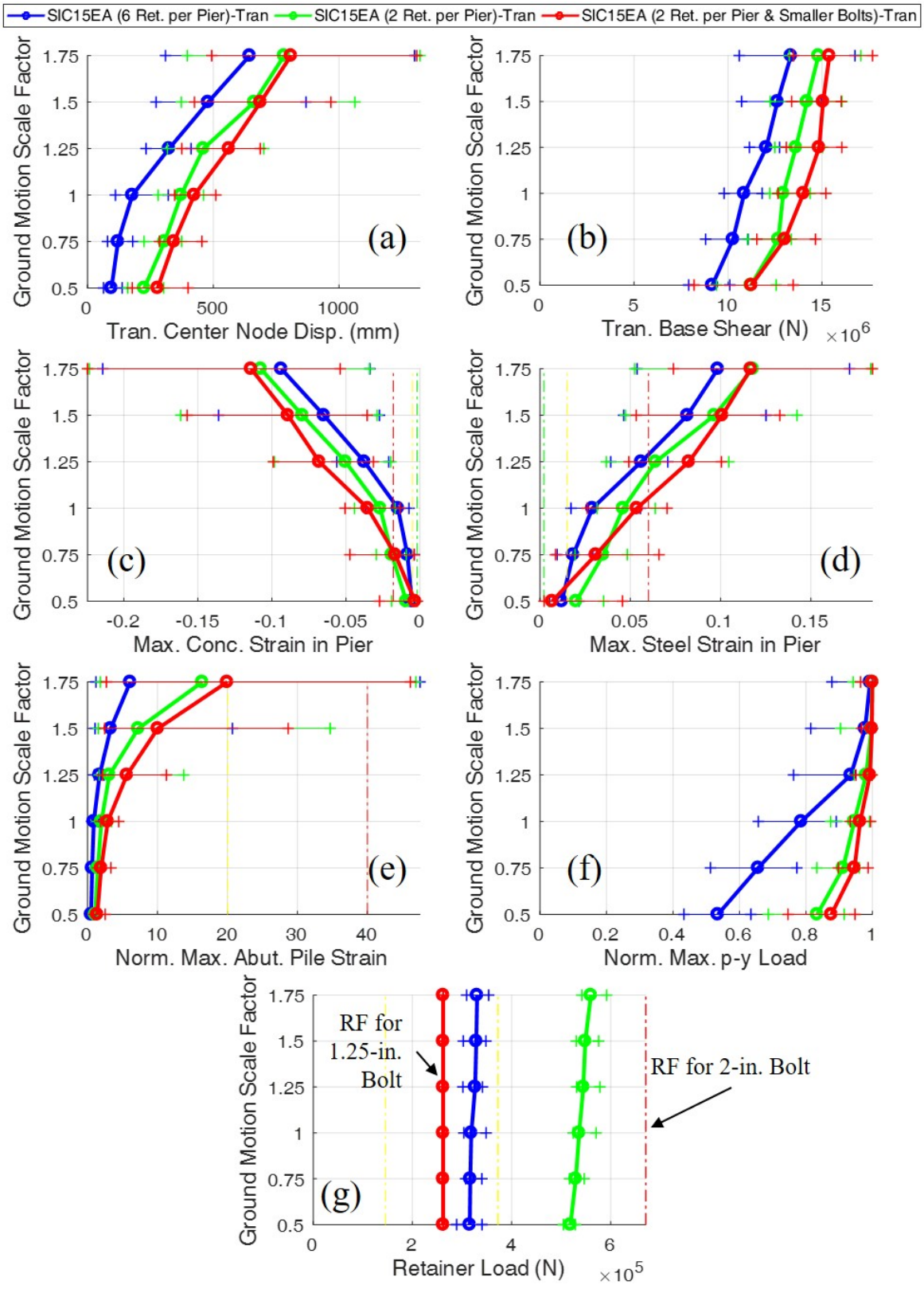

Figure E.2: IDA plots for the original and enhanced SIC15EA in the transverse direction where a scale factor of 1.00 represents the design-level.

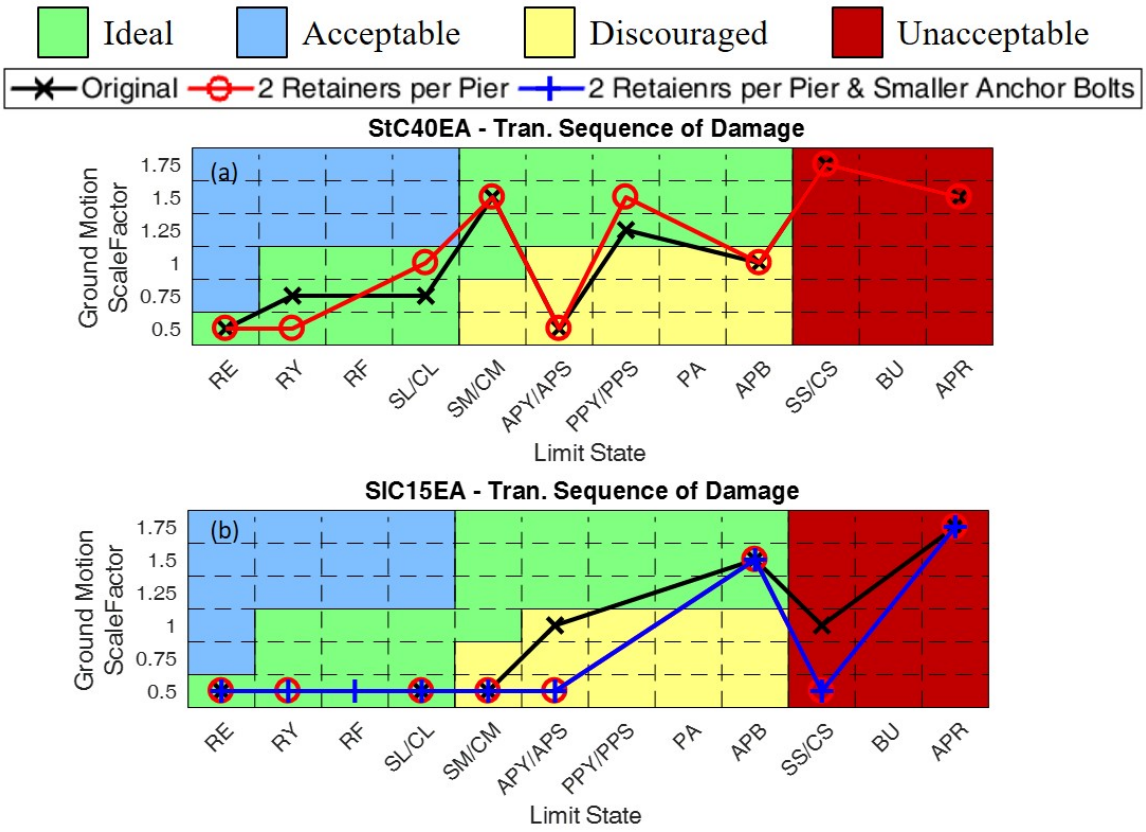

Figure E.3: Sequences of damage for the IABs with various retainer configurations where a scale factor of 1.00 represents the design-level.

Table E.5: Frequency of Limit State Occurrences for the Stc40fa Ida With Original and Weakened Fixed Bearing Anchor Bolts Where a Scale Factor of 1.00 Represents the Design-Level

Bridge	Revision	SF	Longitudinal Limit State Occurrence																
			Ideal					Acceptable								Unacceptable			
			BF	SL	CL	FY	FF	APY	APB	APS	PA	PPY	PPS	SM	CM	BU	SS	CS	APR
StC40FA	1.25-inch Diameter Anchor Bolts	0.50																	
		0.75																	
		1.00																	
		1.25	0%	75%	40%	0%	0%	100%	75%	100%	0%	0%	5%	0%	0%	0%	0%	0%	5%
		1.50	0%	85%	75%	0%	0%	100%	90%	100%	0%	0%	50%	20%	25%	0%	0%	0%	55%
		1.75	0%	95%	85%	0%	0%	100%	95%	100%	0%	0%	55%	40%	60%	0%	0%	15%	80%
	0.625-inch Diameter Anchor Bolts	0.50	0%	0%	0%	0%	0%	70%	0%	30%	0%	0%	0%	0%	0%	0%	0%	0%	0%
		0.75	0%	0%	0%	0%	0%	100%	0%	60%	0%	0%	0%	0%	0%	0%	0%	0%	0%
		1.00	0%	15%	0%	0%	0%	100%	15%	100%	0%	0%	0%	0%	0%	0%	0%	0%	0%
		1.25	0%	75%	40%	0%	0%	100%	75%	100%	0%	0%	15%	0%	0%	0%	0%	0%	5%
		1.50	0%	85%	75%	0%	0%	100%	90%	100%	0%	0%	45%	20%	25%	0%	0%	0%	55%
		1.75	0%	95%	85%	0%	0%	100%	95%	100%	0%	0%	55%	40%	60%	0%	0%	15%	80%
Bridge	**Revision**	**SF**	**Transverse Limit State Occurrence**																
			Ideal					**Acceptable**								**Unacceptable**			
			BF	**SL**	**CL**	**FY**	**FF**	**APY**		**APS**	**PA**	**PPY**	**PPS**	**SM**	**CM**	**BU**	**SS**	**CS**	**APR**
StC40FA	1.25-inch Diameter Anchor Bolts	0.50	0%	0%	0%	0%	0%	45%	0%	10%	0%	0%	0%	0%	0%	0%	0%	0%	0%
		0.75	0%	20%	0%	0%	0%	100%	0%	30%	0%	0%	0%	0%	0%	0%	0%	0%	0%
		1.00	0%	65%	35%	0%	0%	100%	5%	75%	0%	0%	0%	0%	0%	0%	0%	0%	0%
		1.25	0%	85%	80%	10%	0%	100%	55%	100%	0%	0%	0%	5%	0%	0%	0%	0%	0%
		1.50	0%	100%	100%	15%	0%	100%	100%	100%	0%	0%	5%	55%	55%	0%	0%	0%	15%
		1.75	0%	100%	100%	15%	0%	100%	100%	100%	0%	0%	25%	70%	85%	0%	0%	20%	55%
	0.625-inch Diameter Anchor Bolts	0.50	0%	0%	0%	50%	0%	45%	0%	10%	0%	0%	0%	0%	0%	0%	0%	0%	0%
		0.75	0%	20%	0%	100%	0%	100%	0%	30%	0%	0%	0%	0%	0%	0%	0%	0%	0%
		1.00	0%	60%	20%	100%	20%	100%	5%	70%	0%	0%	0%	0%	0%	0%	0%	0%	0%
		1.25	0%	95%	70%	100%	75%	100%	55%	100%	0%	0%	0%	0%	0%	0%	0%	0%	0%
		1.50	0%	100%	100%	100%	85%	100%	100%	100%	0%	0%	5%	40%	45%	0%	0%	0%	20%
		1.75	0%	100%	100%	100%	100%	100%	100%	100%	0%	0%	5%	70%	70%	0%	0%	10%	55%

Table E.6: Frequency of Limit State Occurrences for the Slc15fa Ida With Original and Weakened Fixed Bearing Anchor Bolts Where a Scale Factor of 1.00 Represents the Design-Level

Bridge	Revision	SF	Longitudinal Limit State Occurrence																
			Ideal					Acceptable								Unacceptable			
			BF	SL	CL	FY	FF	APY	APB	APS	PA	PPY	PPS	SM	CM	BU	SS	CS	APR
SlC15FA	2-inch Diameter Anchor Bolts	0.50	0%	20%	5%	0%	0%	5%	0%	0%	0%	0%	0%	0%	0%	0%	0%	0%	0%
		0.75	0%	80%	75%	0%	0%	75%	0%	30%	0%	0%	0%	0%	20%	0%	0%	0%	0%
		1.00	0%	90%	85%	0%	0%	90%	0%	75%	0%	0%	0%	60%	80%	0%	0%	0%	0%
		1.25	0%	100%	100%	0%	0%	100%	5%	100%	0%	0%	0%	100%	100%	0%	0%	55%	0%
		1.50	0%	100%	100%	0%	0%	100%	60%	100%	0%	0%	0%	100%	100%	0%	30%	85%	20%
		1.75	0%	100%	100%	0%	0%	100%	80%	100%	0%	0%	0%	100%	100%	0%	60%	95%	30%
	1.625-inch Diameter Anchor Bolts	0.50	0%	20%	5%	0%	0%	5%	0%	0%	0%	0%	0%	0%	0%	0%	0%	0%	0%
		0.75	0%	80%	75%	0%	0%	75%	0%	30%	0%	0%	0%	0%	20%	0%	0%	0%	0%
		1.00	0%	90%	85%	0%	0%	95%	0%	75%	0%	0%	0%	60%	80%	0%	0%	0%	0%
		1.25	0%	100%	100%	0%	0%	100%	5%	100%	0%	0%	0%	100%	100%	0%	0%	55%	0%
		1.50	0%	100%	100%	0%	0%	100%	60%	100%	0%	0%	0%	100%	100%	0%	30%	85%	20%
		1.75	0%	100%	100%	0%	0%	100%	80%	100%	0%	0%	0%	100%	100%	0%	60%	95%	30%
Bridge	Revision	SF	Transverse Limit State Occurrence																
			Ideal					Acceptable								Unacceptable			
			BF	SL	CL	FY	FF	APY	APB	APS	PA	PPY	PPS	SM	CM	BU	SS	CS	APR
SlC15FA	2-inch Diameter Anchor Bolts	0.50	0%	100%	100%	0%	0%	0%	0%	0%	0%	0%	0%	5%	10%	0%	0%	0%	0%
		0.75	0%	100%	100%	0%	0%	0%	0%	0%	0%	0%	0%	35%	75%	0%	0%	0%	0%
		1.00	0%	100%	100%	0%	0%	0%	0%	0%	0%	0%	0%	75%	90%	0%	0%	25%	0%
		1.25	0%	100%	100%	0%	0%	35%	0%	0%	0%	0%	0%	95%	100%	0%	10%	65%	0%
		1.50	0%	100%	100%	0%	0%	90%	0%	20%	0%	0%	0%	100%	100%	0%	60%	100%	0%
		1.75	0%	100%	100%	0%	0%	100%	15%	55%	0%	0%	0%	100%	100%	0%	85%	100%	5%
	1.625-inch Diameter Anchor Bolts	0.50	0%	100%	100%	0%	0%	0%	0%	0%	0%	0%	0%	5%	10%	0%	0%	0%	0%
		0.75	0%	100%	100%	0%	0%	0%	0%	0%	0%	0%	0%	35%	70%	0%	0%	0%	0%
		1.00	0%	100%	100%	0%	0%	0%	0%	0%	0%	0%	0%	75%	90%	0%	0%	25%	0%
		1.25	0%	100%	100%	0%	0%	35%	0%	0%	0%	0%	0%	95%	100%	0%	10%	65%	0%
		1.50	0%	100%	100%	0%	0%	90%	0%	25%	0%	0%	0%	100%	100%	0%	60%	100%	0%
		1.75	0%	100%	100%	0%	0%	100%	20%	60%	0%	0%	0%	100%	100%	0%	90%	100%	5%

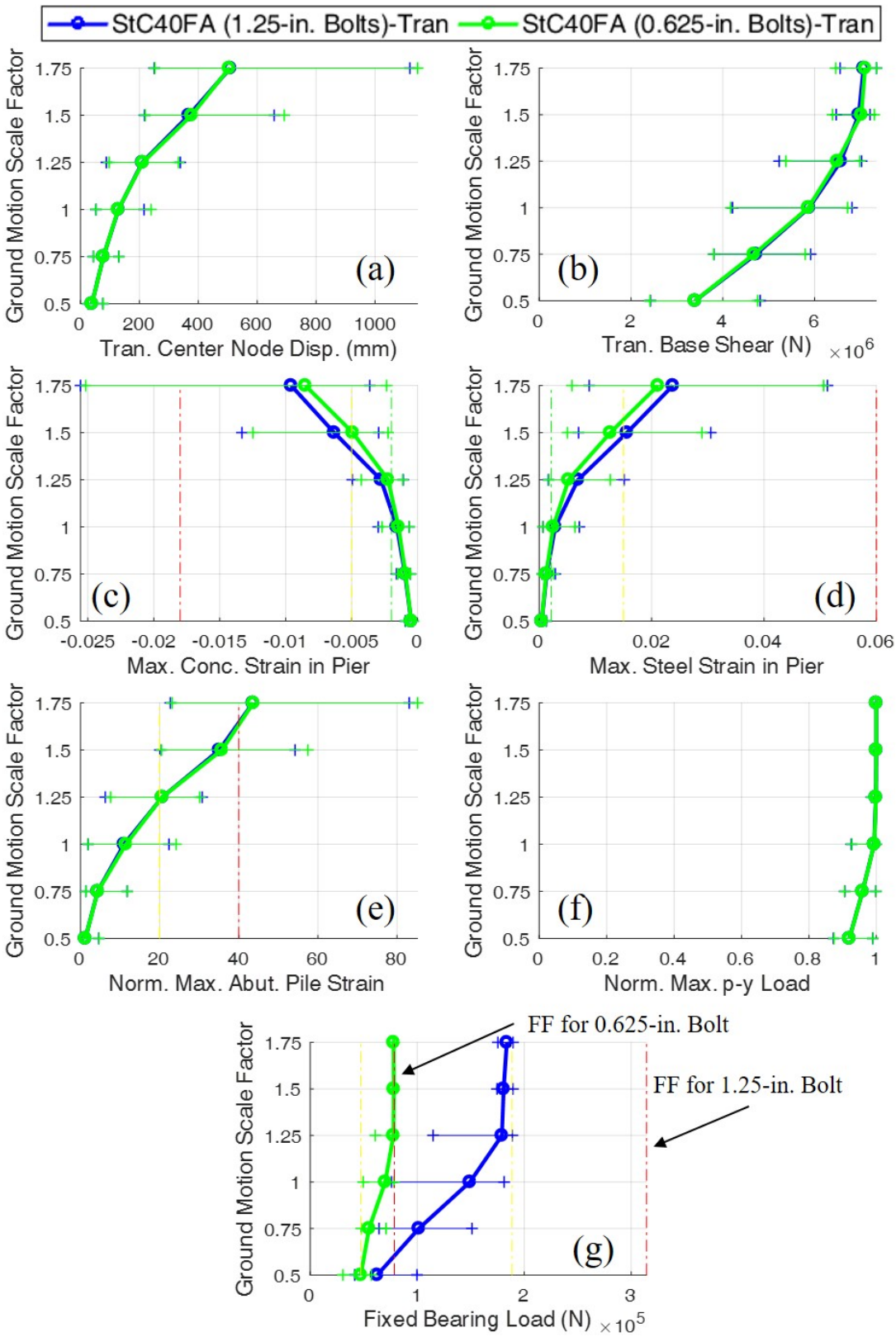

Figure E.4: IDA plots for the original and enhanced StC40FA in the transverse direction where a scale factor of 1.00 represents the design-level.

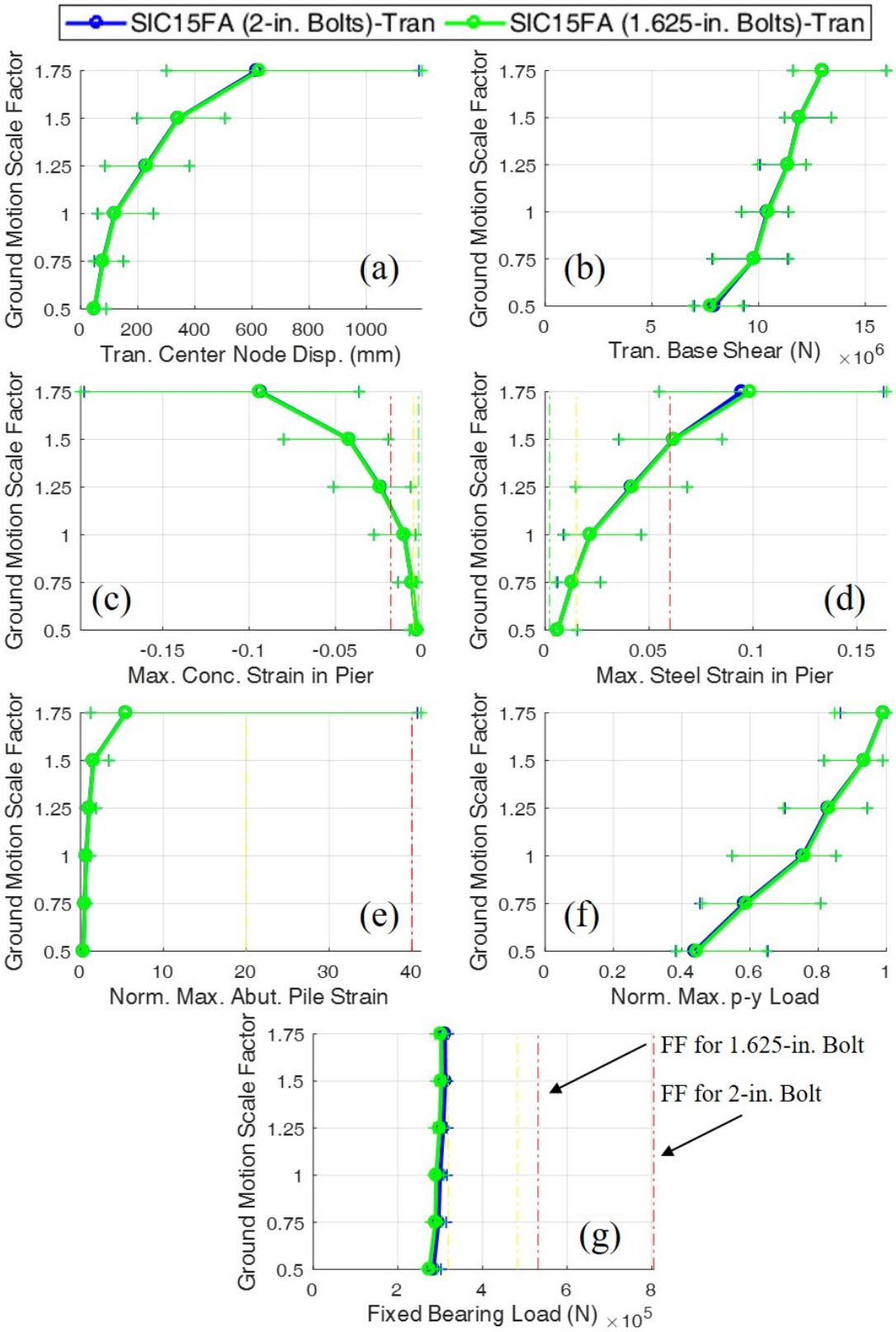

Figure E.5: IDA plots for the original and enhanced SIC15FA in the transverse direction where a scale factor of 1.00 represents the design-level.

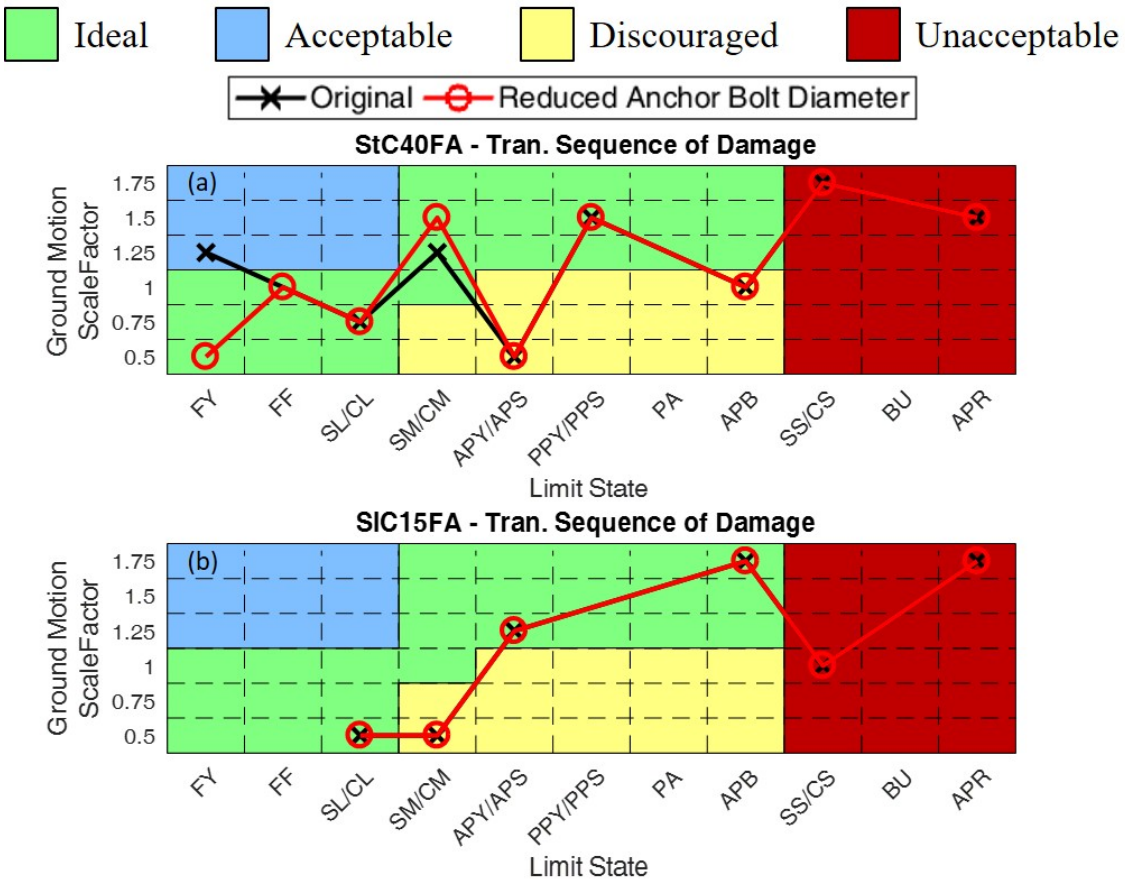

Figure E.6: Sequences of damage for the IABs with various fixed bearing anchor bolt sizes where a scale factor of 1.00 represents the design-level.

Table E.7: Frequency of Limit State Occurrences for The Ctc15ea Ida With Original and Revised Pier Column Designs Where a Scale Factor of 1.00 Represents the Design-Level

Bridge	Revision	SF	Longitudinal Limit State Occurrence																	
			Ideal						Acceptable								Unacceptable			
			BF	SL	CL	RE	RY	RF	APY	APB	APS	PA	PPY	PPS	SM	CM	BU	SS	CS	APR
CtC15EA	Original Pier Columns	0.50	0%	0%	0%	0%	0%	0%	100%	0%	55%	0%	0%	0%	0%	0%	0%	0%	0%	0%
		0.75	0%	95%	65%	0%	0%	0%	100%	5%	100%	0%	0%	0%	15%	20%	0%	0%	0%	0%
		1.00	0%	100%	100%	0%	0%	0%	100%	75%	100%	0%	0%	0%	75%	85%	0%	5%	50%	20%
		1.25	0%	100%	100%	0%	0%	0%	100%	85%	100%	0%	0%	0%	85%	90%	0%	35%	80%	60%
		1.50	10%	100%	100%	0%	0%	0%	100%	90%	100%	0%	10%	5%	90%	100%	0%	50%	75%	70%
		1.75	20%	100%	100%	5%	5%	0%	100%	100%	100%	0%	25%	15%	100%	100%	10%	70%	80%	70%
	Revised Pier Columns	0.50	0%	0%	0%	0%	0%	0%	100%	0%	55%	0%	0%	0%	0%	0%	0%	0%	0%	0%
		0.75	0%	40%	15%	0%	0%	0%	100%	5%	100%	0%	0%	0%	0%	0%	0%	0%	0%	0%
		1.00	0%	95%	80%	0%	0%	0%	100%	75%	100%	0%	0%	15%	55%	55%	0%	5%	35%	15%
		1.25	0%	100%	90%	0%	0%	0%	100%	85%	100%	0%	0%	40%	80%	80%	0%	45%	75%	55%
		1.50	0%	100%	100%	0%	0%	0%	100%	95%	100%	0%	10%	35%	85%	85%	0%	75%	80%	75%
		1.75	20%	100%	100%	0%	0%	0%	100%	100%	100%	0%	20%	20%	85%	90%	0%	70%	80%	70%
Bridge	**Revision**	**SF**	**Transverse Limit State Occurrence**																	
			Ideal						**Acceptable**								**Unacceptable**			
			BF	**SL**	**CL**	**RE**	**RY**	**RF**	**APY**	**APB**	**APS**	**PA**	**PPY**	**PPS**	**SM**	**CM**	**BU**	**SS**	**CS**	**APR**
CtC15EA	Original Pier Columns	0.50	0%	0%	0%	100%	100%	5%	80%	0%	25%	0%	0%	0%	0%	0%	0%	0%	0%	0%
		0.75	0%	100%	25%	100%	100%	100%	100%	40%	100%	0%	0%	0%	0%	0%	0%	0%	0%	0%
		1.00	0%	100%	80%	100%	100%	100%	100%	90%	100%	0%	0%	0%	40%	40%	0%	5%	15%	10%
		1.25	0%	95%	85%	100%	100%	100%	100%	100%	100%	0%	0%	0%	80%	80%	0%	45%	65%	55%
		1.50	0%	95%	85%	100%	100%	100%	100%	100%	100%	0%	20%	20%	80%	80%	20%	75%	80%	80%
		1.75	0%	100%	95%	100%	100%	100%	100%	100%	100%	0%	20%	20%	80%	80%	20%	75%	80%	80%
	Revised Pier Columns	0.50	0%	0%	0%	100%	100%	20%	85%	0%	25%	0%	0%	0%	0%	0%	0%	0%	0%	0%
		0.75	0%	0%	0%	100%	100%	100%	100%	35%	100%	0%	0%	0%	0%	0%	0%	0%	0%	0%
		1.00	0%	40%	0%	100%	100%	100%	100%	90%	100%	0%	0%	0%	0%	0%	0%	0%	0%	15%
		1.25	0%	80%	30%	100%	100%	100%	100%	100%	100%	0%	0%	0%	0%	0%	15%	0%	0%	55%
		1.50	0%	80%	45%	100%	100%	100%	100%	100%	100%	0%	0%	0%	0%	0%	55%	0%	0%	80%
		1.75	0%	85%	55%	100%	100%	100%	100%	100%	100%	0%	0%	0%	5%	5%	60%	5%	5%	80%

Table E.8: Frequency of Limit State Occurrences for The Clc15ea Ida With Original and Revised Pier Column Designs Where a Scale Factor of 1.00 Represents the Design-Level

Bridge	Revision	SF	Longitudinal Limit State Occurrence																	
			Ideal						Acceptable								Unacceptable			
			BF	SL	CL	RE	RY	RF	APY	APB	APS	PA	PPY	PPS	SM	CM	BU	SS	CS	APR
ClC15EA	Original Pier Columns	0.50	0%	50%	50%	0%	0%	0%	100%	0%	85%	0%	0%	0%	0%	0%	0%	0%	0%	0%
		0.75	0%	85%	85%	0%	0%	0%	100%	20%	100%	0%	0%	0%	70%	80%	0%	0%	50%	0%
		1.00	0%	95%	95%	0%	0%	0%	100%	65%	100%	0%	0%	0%	80%	80%	0%	5%	80%	5%
		1.25	0%	100%	100%	0%	0%	0%	100%	70%	100%	0%	0%	0%	85%	85%	0%	20%	75%	20%
		1.50	0%	100%	100%	0%	0%	0%	100%	70%	100%	0%	0%	0%	90%	95%	0%	20%	85%	25%
		1.75	5%	100%	100%	0%	0%	0%	100%	80%	100%	5%	0%	0%	95%	95%	0%	20%	95%	35%
	Revised Pier Columns	0.50	0%	0%	0%	0%	0%	0%	100%	0%	85%	0%	0%	0%	0%	0%	0%	0%	0%	0%
		0.75	0%	80%	70%	0%	0%	0%	100%	20%	100%	0%	0%	10%	35%	40%	0%	10%	25%	0%
		1.00	0%	85%	80%	0%	0%	0%	100%	65%	100%	0%	0%	30%	70%	70%	0%	40%	70%	15%
		1.25	0%	85%	85%	0%	0%	0%	100%	70%	100%	0%	0%	25%	75%	75%	0%	70%	70%	30%
		1.50	0%	95%	95%	0%	0%	0%	100%	75%	100%	0%	0%	45%	75%	80%	0%	70%	75%	45%
		1.75	0%	95%	95%	0%	0%	0%	100%	80%	100%	0%	0%	45%	85%	90%	0%	70%	80%	50%
Bridge	**Revision**	**SF**	**Transverse Limit State Occurrence**																	
			Ideal						**Acceptable**								**Unacceptable**			
			BF	**SL**	**CL**	**RE**	**RY**	**RF**	**APY**	**APB**	**APS**	**PA**	**PPY**	**PPS**	**SM**	**CM**	**BU**	**SS**	**CS**	**APR**
ClC15EA	Original Pier Columns	0.50	0%	100%	100%	100%	100%	0%	5%	0%	0%	0%	0%	0%	95%	100%	0%	0%	45%	0%
		0.75	0%	100%	100%	100%	100%	0%	65%	0%	15%	0%	0%	0%	100%	100%	0%	5%	85%	0%
		1.00	0%	100%	100%	100%	100%	0%	75%	15%	55%	0%	0%	0%	100%	100%	0%	35%	100%	0%
		1.25	0%	100%	100%	100%	100%	0%	80%	15%	65%	0%	0%	0%	100%	100%	0%	30%	100%	5%
		1.50	0%	100%	100%	100%	100%	0%	100%	30%	75%	0%	0%	0%	100%	100%	0%	40%	100%	5%
		1.75	0%	100%	100%	100%	100%	0%	100%	35%	80%	0%	0%	0%	100%	100%	0%	45%	100%	5%
	Revised Pier Columns	0.50	0%	100%	100%	100%	100%	95%	65%	0%	35%	0%	0%	0%	5%	10%	0%	0%	0%	0%
		0.75	0%	100%	100%	100%	100%	100%	85%	20%	65%	0%	0%	0%	55%	60%	0%	40%	55%	0%
		1.00	0%	100%	100%	100%	100%	100%	85%	35%	75%	0%	0%	0%	80%	90%	0%	60%	60%	10%
		1.25	0%	100%	100%	100%	100%	100%	90%	50%	80%	0%	0%	0%	90%	100%	0%	70%	80%	10%
		1.50	0%	100%	100%	100%	100%	100%	100%	45%	90%	0%	0%	0%	95%	100%	0%	75%	85%	15%
		1.75	0%	100%	100%	100%	100%	100%	100%	65%	100%	0%	0%	0%	85%	95%	0%	80%	85%	20%

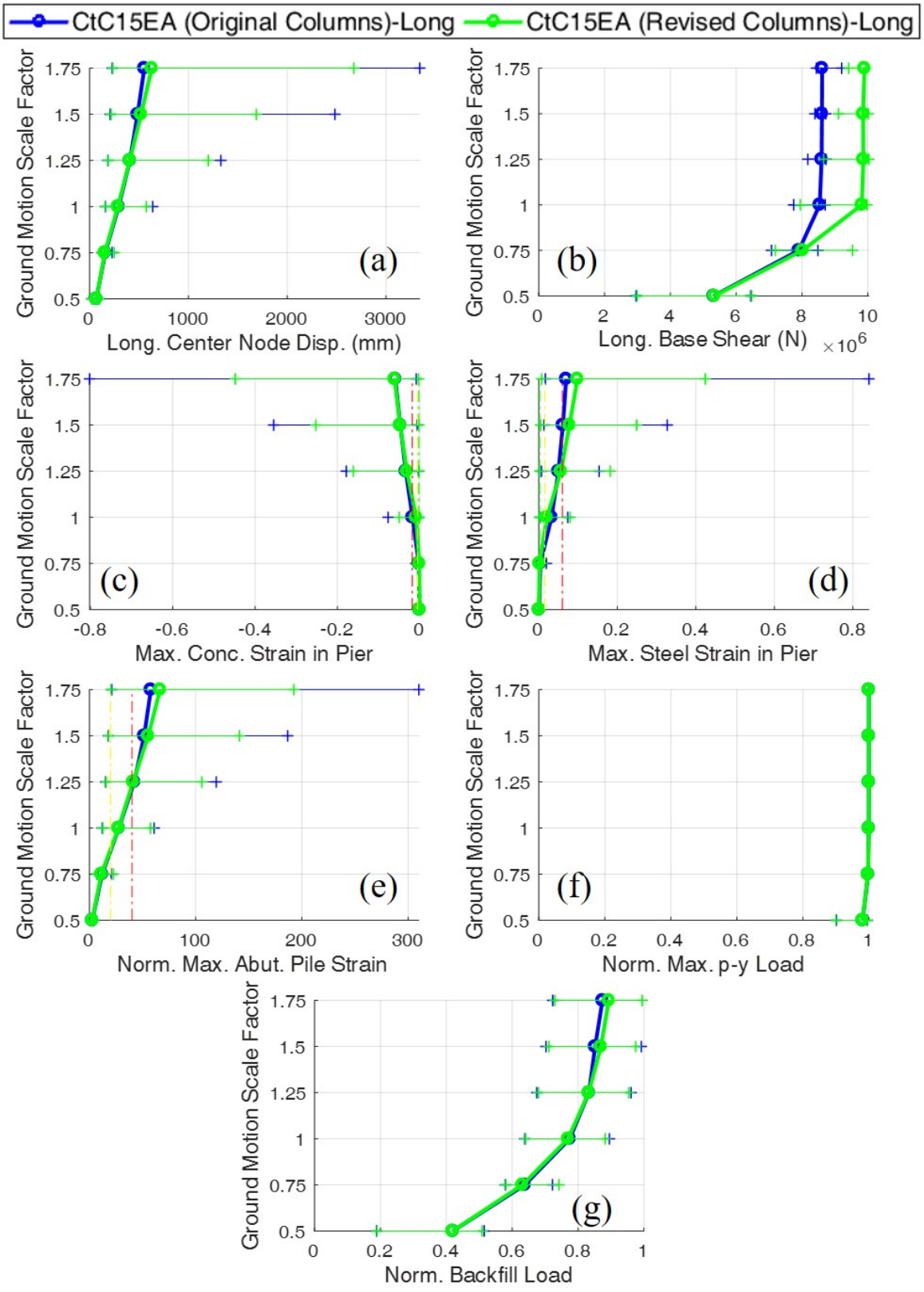

Figure E.7: IDA plots for the original and enhanced CtC15EA in the longitudinal direction where a scale factor of 1.00 represents the design-level.

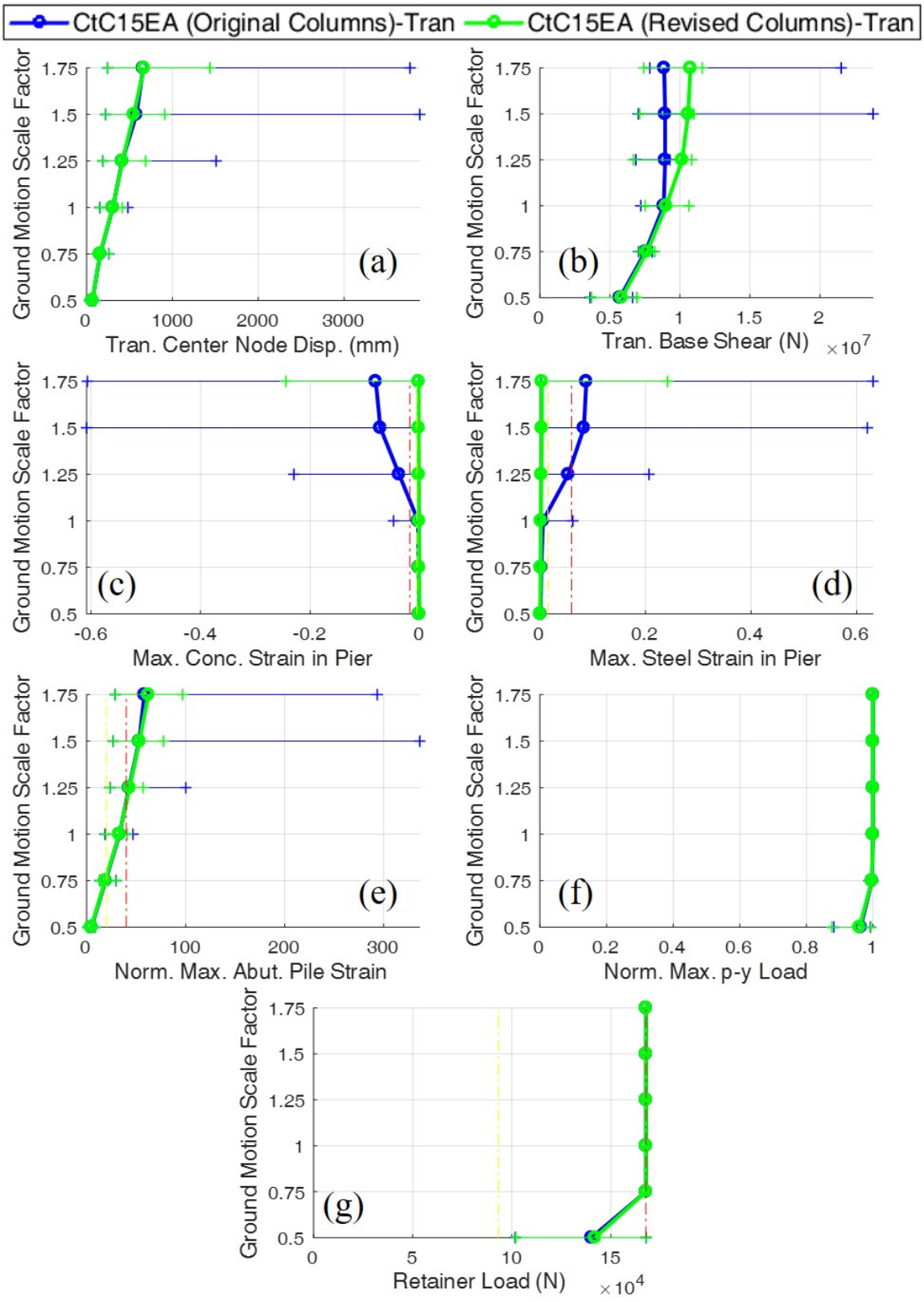

Figure E.8: IDA plots for the original and enhanced CtC15EA in the transverse direction where a scale factor of 1.00 represents the design-level.

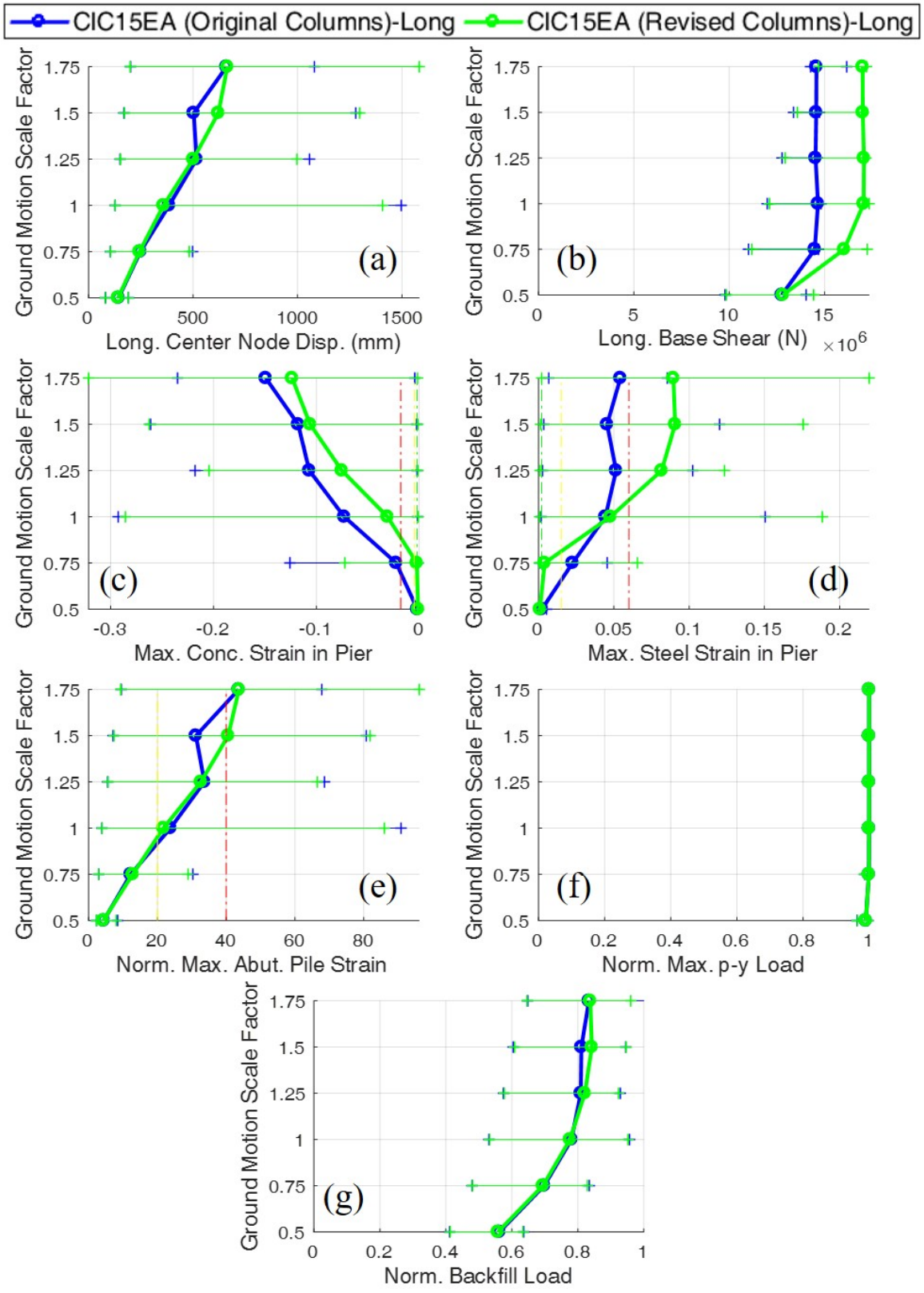

Figure E.9: IDA plots for the original and enhanced ClC15EA in the longitudinal direction where a scale factor of 1.00 represents the design-level.

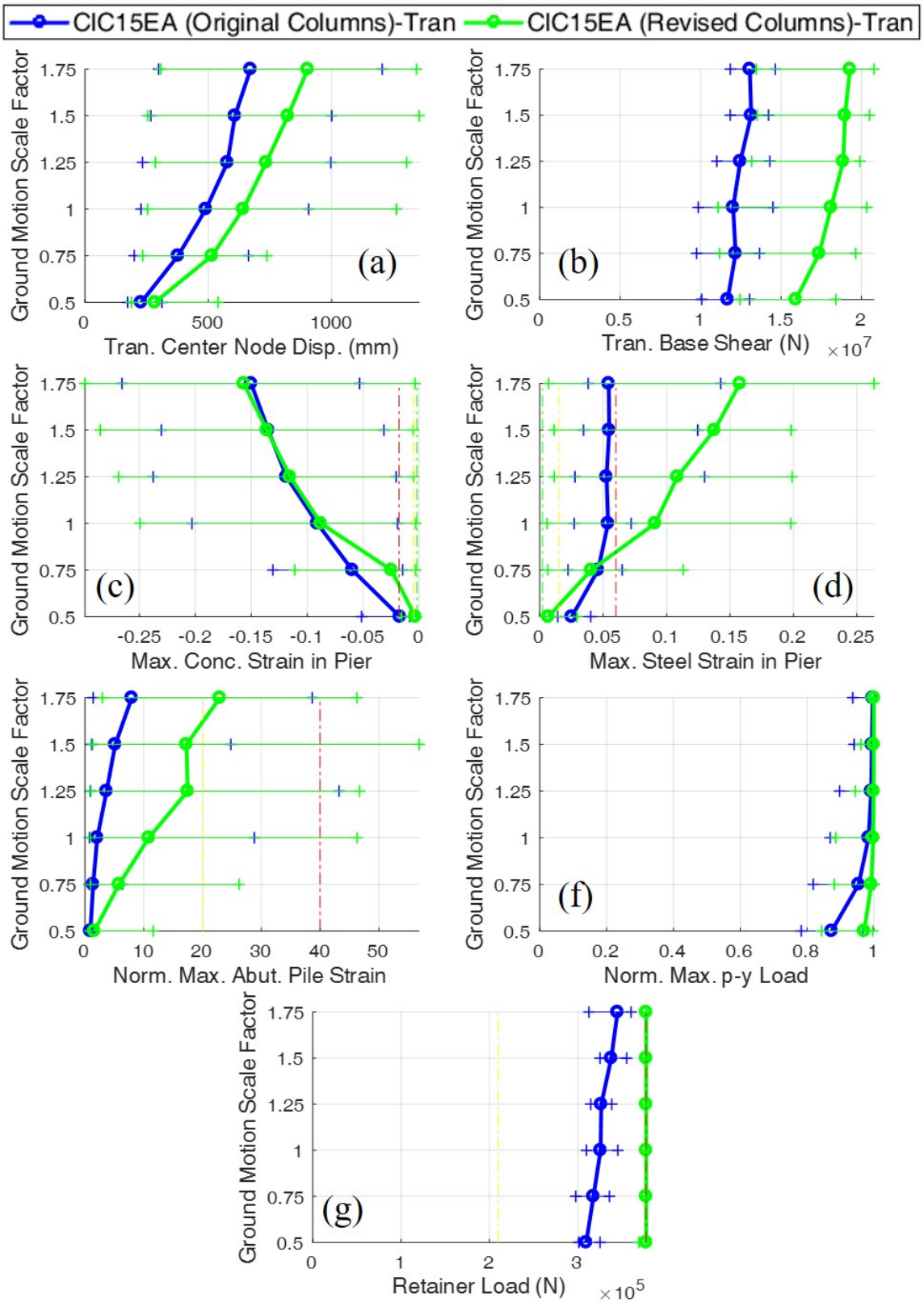

Figure E.10: IDA plots for the original and enhanced ClC15EA in the transverse direction where a scale factor of 1.00 represents the design-level.

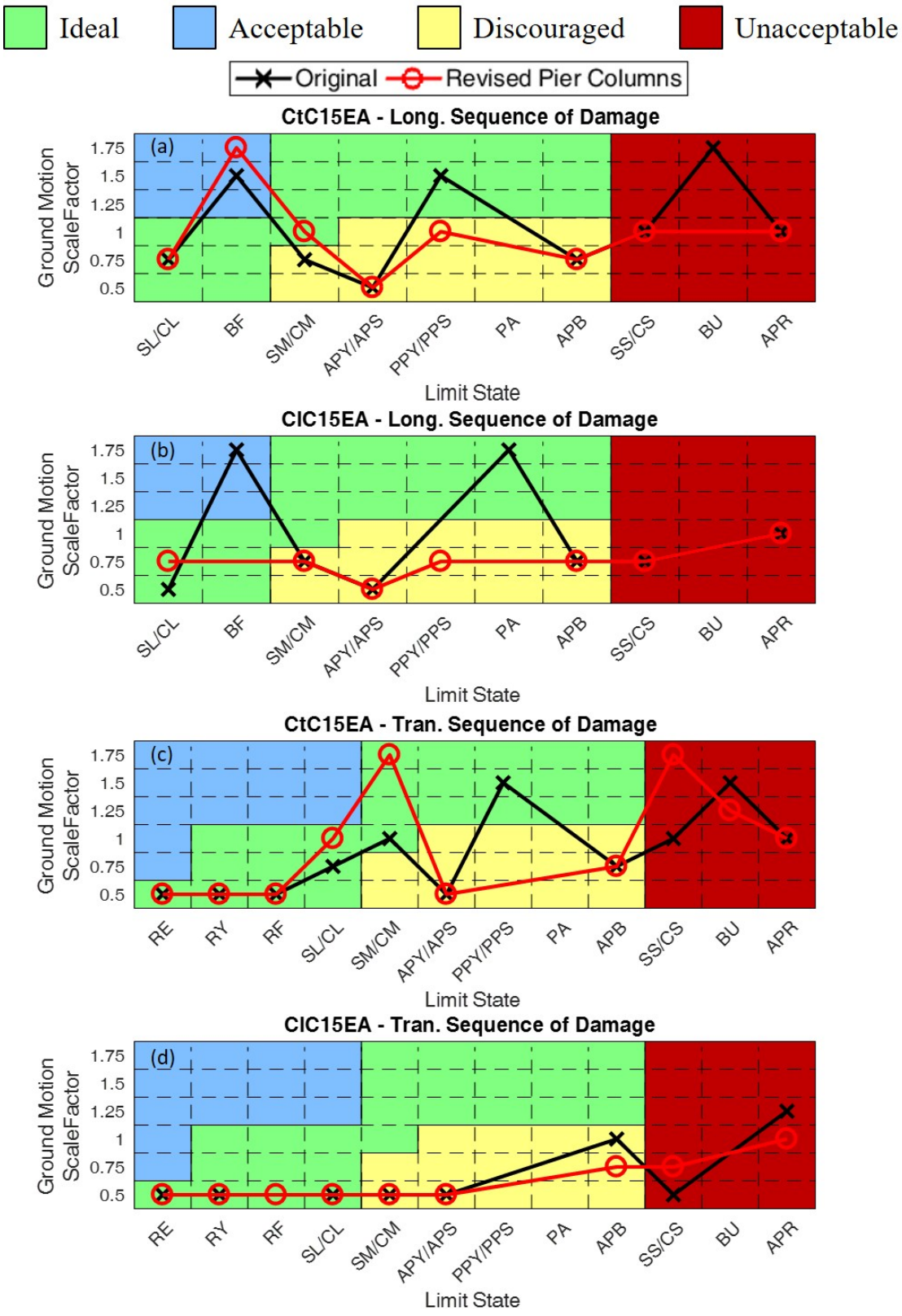

Figure E.11: Sequences of damage for the IABs with various pier column designs where a scale factor of 1.00 represents the design-level.

Table E.9: Frequency of Limit State Occurrences for The Ctc40ea Ida With Original and Revised Abutment Pile Cap Designs Where a Scale Factor of 1.00 Represents the Design-Level

Bridge	Revision	SF	Longitudinal Limit State Occurrence																	
			Ideal						Acceptable								Unacceptable			
			BF	SL	CL	RE	RY	RF	APY	APB	APS	PA	PPY	PPS	SM	CM	BU	SS	CS	APR
CtC40EA	Original Abutment Pile Cap	0.50	0%	0%	0%	0%	0%	0%	100%	0%	75%	0%	0%	0%	0%	0%	0%	0%	0%	0%
		0.75	0%	55%	15%	0%	0%	0%	100%	45%	100%	0%	0%	5%	0%	0%	0%	0%	0%	0%
		1.00	0%	80%	75%	0%	0%	0%	100%	80%	100%	0%	0%	0%	20%	20%	0%	0%	0%	30%
		1.25	0%	85%	75%	0%	0%	0%	100%	85%	100%	0%	0%	20%	30%	50%	0%	0%	5%	70%
		1.50	10%	85%	75%	0%	0%	0%	100%	90%	100%	0%	5%	50%	50%	70%	0%	15%	20%	70%
		1.75	20%	90%	75%	0%	0%	0%	100%	90%	100%	0%	20%	30%	70%	70%	0%	20%	25%	70%
	Revised Abutment Pile Cap	0.50	0%	0%	0%	0%	0%	0%	100%	0%	45%	0%	0%	0%	0%	0%	0%	0%	0%	0%
		0.75	0%	20%	15%	0%	0%	0%	100%	0%	100%	0%	0%	0%	0%	0%	0%	0%	0%	0%
		1.00	0%	80%	55%	0%	0%	0%	100%	70%	100%	0%	0%	10%	0%	0%	0%	0%	0%	10%
		1.25	0%	95%	85%	0%	0%	0%	100%	90%	100%	0%	0%	35%	20%	35%	0%	0%	0%	35%
		1.50	0%	100%	85%	0%	0%	0%	100%	95%	100%	0%	0%	45%	65%	75%	0%	0%	15%	80%
		1.75	0%	100%	95%	0%	0%	0%	100%	100%	100%	0%	0%	60%	75%	80%	0%	5%	15%	80%
Bridge	**Revision**	**SF**	**Transverse Limit State Occurrence**																	
			Ideal						**Acceptable**								**Unacceptable**			
			BF	**SL**	**CL**	**RE**	**RY**	**RF**	**APY**	**APB**	**APS**	**PA**	**PPY**	**PPS**	**SM**	**CM**	**BU**	**SS**	**CS**	**APR**
CtC40EA	Original Abutment Pile Cap	0.50	0%	5%	0%	100%	100%	0%	100%	5%	80%	0%	0%	0%	0%	0%	0%	0%	0%	0%
		0.75	0%	85%	60%	100%	100%	0%	100%	75%	100%	0%	0%	0%	0%	0%	0%	0%	0%	0%
		1.00	0%	95%	80%	100%	100%	65%	100%	90%	100%	0%	0%	0%	25%	35%	0%	0%	0%	30%
		1.25	0%	100%	85%	100%	100%	85%	100%	100%	100%	0%	0%	0%	55%	65%	0%	0%	10%	70%
		1.50	0%	100%	90%	100%	100%	100%	100%	100%	100%	0%	0%	0%	65%	70%	0%	20%	20%	70%
		1.75	0%	100%	95%	100%	100%	100%	100%	100%	100%	0%	0%	0%	70%	75%	0%	20%	30%	75%
	Revised Abutment Pile Cap	0.50	0%	5%	0%	100%	100%	0%	100%	5%	80%	0%	0%	0%	0%	0%	0%	0%	0%	0%
		0.75	0%	85%	60%	100%	100%	0%	100%	75%	100%	0%	0%	0%	0%	0%	0%	0%	0%	0%
		1.00	0%	95%	80%	100%	100%	65%	100%	90%	100%	0%	0%	0%	25%	35%	0%	0%	0%	30%
		1.25	0%	100%	85%	100%	100%	85%	100%	100%	100%	0%	0%	0%	55%	65%	0%	0%	10%	70%
		1.50	0%	100%	90%	100%	100%	100%	100%	100%	100%	0%	0%	0%	65%	70%	0%	20%	20%	70%
		1.75	0%	100%	95%	100%	100%	100%	100%	100%	100%	0%	0%	0%	75%	75%	0%	20%	30%	75%

Table E.10: Frequency of Limit State Occurrences for the Clc40ea Ida With Original and Revised Abutment Pile Cap Designs Where a Scale Factor of 1.00 Represents the Design-Level

Bridge	Revision	SF	Longitudinal Limit State Occurrence																	
			Ideal						Acceptable								Unacceptable			
			BF	SL	CL	RE	RY	RF	APY	APB	APS	PA	PPY	PPS	SM	CM	BU	SS	CS	APR
ClC40EA	Original Abutment Pile Cap	0.50	0%	5%	0%	0%	0%	0%	100%	0%	90%	0%	0%	0%	0%	0%	0%	0%	0%	0%
		0.75	0%	75%	60%	0%	0%	0%	100%	30%	100%	0%	0%	0%	10%	20%	0%	0%	0%	0%
		1.00	0%	75%	70%	0%	0%	0%	100%	60%	100%	0%	0%	0%	20%	35%	0%	0%	0%	10%
		1.25	10%	80%	75%	0%	0%	0%	100%	70%	100%	0%	0%	0%	35%	60%	0%	10%	20%	30%
		1.50	15%	85%	80%	0%	0%	0%	100%	70%	100%	0%	5%	5%	45%	70%	0%	15%	30%	35%
		1.75	15%	90%	90%	0%	0%	0%	100%	80%	100%	0%	5%	5%	50%	70%	0%	15%	30%	40%
	Revised Abutment Pile Cap	0.50	0%	0%	0%	0%	0%	0%	100%	0%	80%	0%	0%	0%	0%	0%	0%	0%	0%	0%
		0.75	0%	65%	50%	0%	0%	0%	100%	25%	100%	0%	0%	0%	0%	15%	0%	0%	0%	0%
		1.00	0%	80%	80%	0%	0%	0%	100%	70%	100%	0%	0%	0%	30%	40%	0%	0%	0%	15%
		1.25	0%	80%	80%	0%	0%	0%	100%	70%	100%	0%	0%	0%	45%	70%	0%	0%	5%	30%
		1.50	0%	90%	80%	0%	0%	0%	100%	70%	100%	0%	0%	0%	60%	70%	0%	10%	25%	50%
		1.75	10%	90%	90%	0%	0%	0%	100%	80%	100%	10%	10%	5%	70%	70%	0%	20%	35%	60%
Bridge	**Revision**	**SF**	**Transverse Limit State Occurrence**																	
			Ideal						Acceptable								Unacceptable			
			BF	SL	CL	RE	RY	RF	APY	APB	APS	PA	PPY	PPS	SM	CM	BU	SS	CS	APR
ClC40EA	Original Abutment Pile Cap	0.50	0%	100%	90%	100%	100%	0%	55%	0%	20%	0%	0%	0%	40%	55%	0%	0%	5%	0%
		0.75	0%	100%	100%	100%	100%	0%	75%	20%	55%	0%	0%	0%	65%	75%	0%	0%	10%	0%
		1.00	0%	100%	100%	100%	100%	0%	100%	20%	85%	0%	0%	0%	75%	90%	0%	0%	25%	20%
		1.25	0%	100%	100%	100%	100%	0%	100%	30%	90%	0%	0%	0%	95%	100%	0%	20%	35%	20%
		1.50	0%	100%	100%	100%	100%	0%	100%	35%	95%	0%	0%	0%	100%	100%	0%	20%	50%	20%
		1.75	0%	100%	100%	100%	100%	0%	100%	50%	100%	0%	0%	0%	100%	100%	0%	20%	60%	30%
	Revised Abutment Pile Cap	0.50	0%	100%	90%	100%	100%	0%	55%	0%	20%	0%	0%	0%	40%	55%	0%	0%	5%	0%
		0.75	0%	100%	100%	100%	100%	0%	75%	20%	55%	0%	0%	0%	65%	75%	0%	0%	10%	0%
		1.00	0%	100%	100%	100%	100%	0%	95%	20%	85%	0%	0%	0%	75%	90%	0%	0%	25%	20%
		1.25	0%	100%	100%	100%	100%	0%	100%	30%	90%	0%	0%	0%	95%	100%	0%	20%	40%	20%
		1.50	0%	100%	100%	100%	100%	0%	100%	35%	95%	0%	0%	0%	100%	100%	0%	20%	50%	20%
		1.75	0%	100%	100%	100%	100%	0%	100%	50%	100%	0%	0%	0%	100%	100%	0%	20%	60%	30%

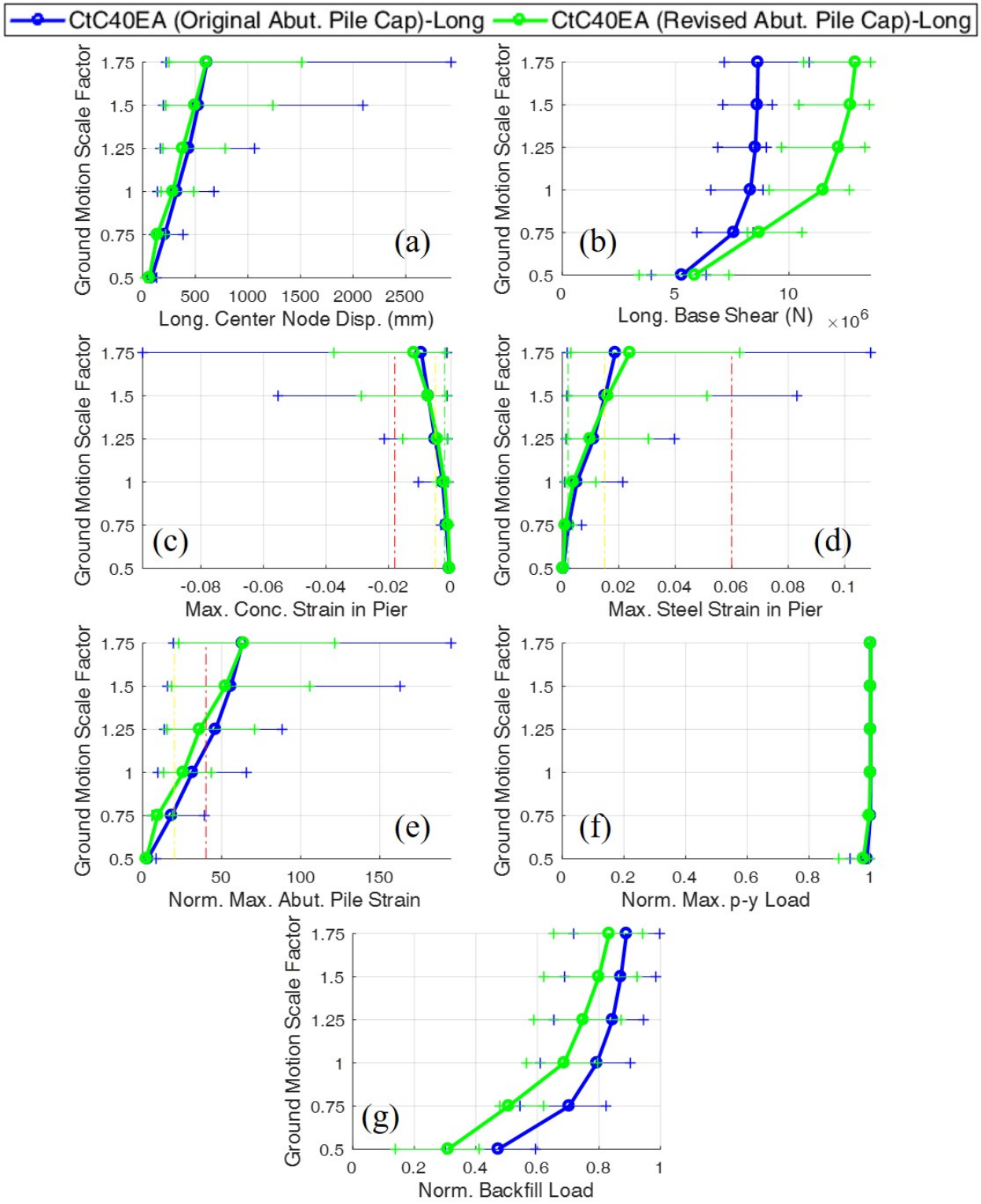

Figure E.12: IDA plots for the original and enhanced CtC40EA in the longitudinal direction where a scale factor of 1.00 represents the design-level.

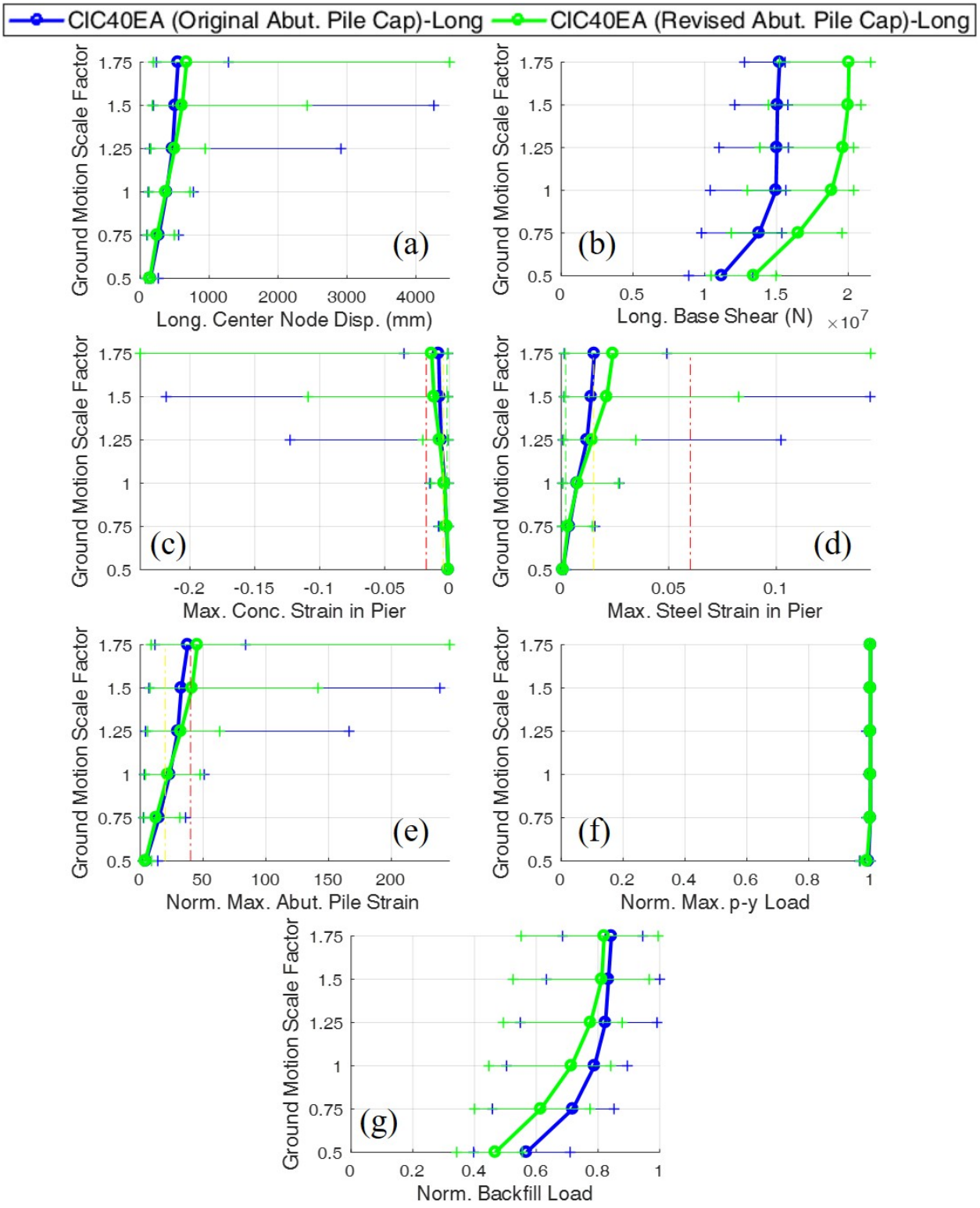

Figure E.13: IDA plots for the original and enhanced ClC40EA in the longitudinal direction where a scale factor of 1.00 represents the design-level.

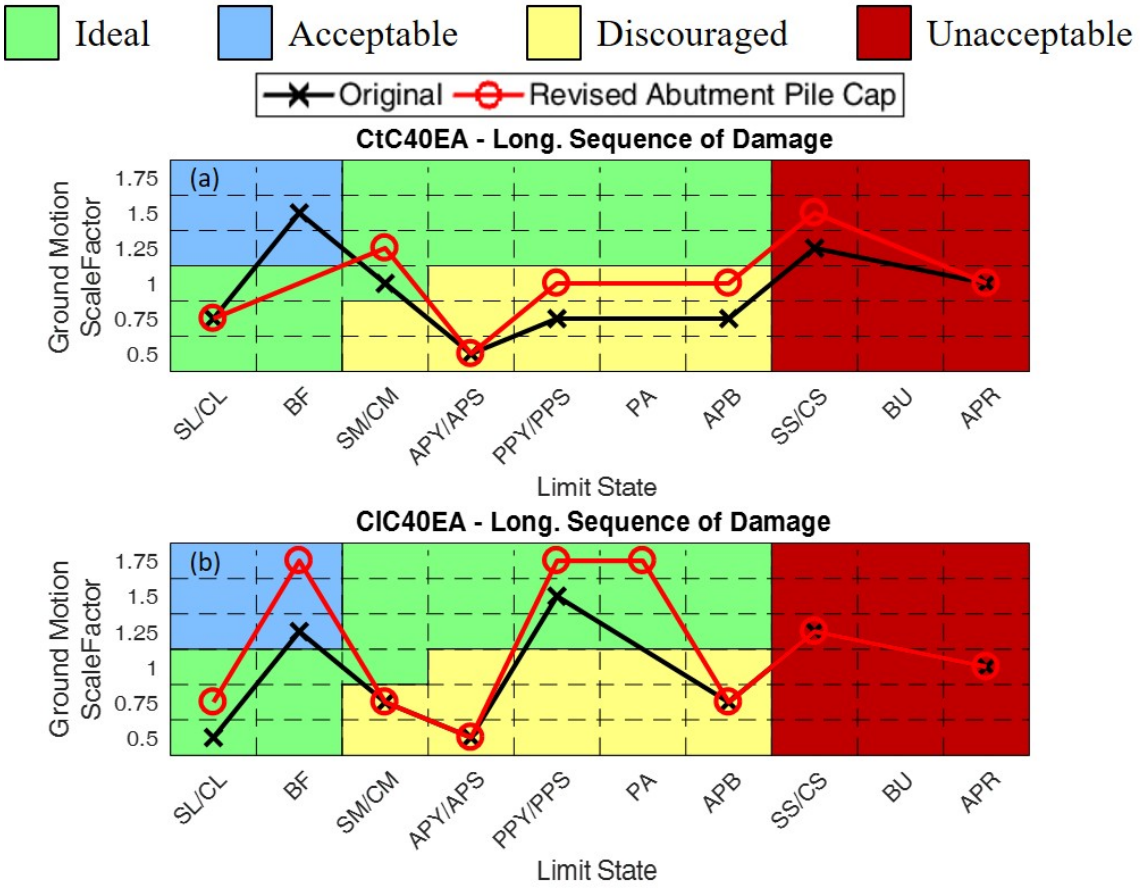

Figure E.14: Sequences of damage for the IABs with various abutment pile cap designs where a scale factor of 1.00 represents the design-level.


Illinois Department
of Transportation


ILLINOIS